

**Solubilities and diffusivities of metals (Platinum, Tin) and  
metal-oxide (Cassiterite) in silicate melts: The effect of  
halogens (Cl, F).**

**Löslichkeit und Diffusion von Metallen (Platin, Zinn) und  
Metalloxid (Cassiterit) in Silikatschmelzen in Gegenwart von  
Halogenen (Cl, F).**

Vom Fachbereich Geowissenschaften and Geographie

Der Universität Hannover

Zur Erlangung des Grades

**DOKTOR DER NATURWISSENSCHAFTEN**

**Dr. rer. nat.**

genehmigte Dissertation

von

**M.Sc. (H.S.) Geology Paras Bhalla**

**geboren am 25.05.1977 in Sundernagar**

**2005**

**Solubilities and diffusivities of metals (Platinum, Tin) and  
metal-oxide (Cassiterite) in silicate melts: The effect of  
halogens (Cl, F).**

**Löslichkeit und Diffusion von Metallen (Platin, Zinn) und  
Metalloxid (Cassiterit) in Silikatschmelzen in Gegenwart von  
Halogenen (Cl, F).**

Vom Fachbereich Geowissenschaften and Geographie

Der Universität Hannover

Zur Erlangung des Grades

**DOKTOR DER NATURWISSENSCHAFTEN**

**Dr. rer. nat.**

genehmigte Dissertation

von

**M.Sc. (H.S.) Geology Paras Bhalla**

**geboren am 25.05.1977 in Sundernagar**

**2005**

Referent: Prof. Dr. F. Holtz

Korreferenten: PD Dr. H. Behrens  
Assoc. Prof. R.L. Linnen

Tag der Promotion: 04. Februar 2005

*D*edicated to my Grandmother,  
Late Smt. Lajwanti Bhalla,

## Preface

Numerous people helped to make this text a reality. Prof. Dr. François Holtz contributed countless hours of discussion and guidance and set me on the right track with his persistent questions, e.g., “Why is it important? “Why does this happen?” PD Dr. Harald Behrens and Assoc. Prof. Dr. Robert L. Linnen reviewed individual chapters. I owe a particular debt to my supervisor, Prof. Dr. François Holtz (University of Hannover, Germany), for his pains in cheerfully reading the text and making numerous suggestions for improvement despite other heavy claims on his time.

*I* would like to thank in the context of this work to my supervisor, PD Dr. Harald Behrens, for his valuable and constructive reviews to this work. I pay my cordial thanks to Dr. Behrens, for his interesting and applicable ideas, which helped me to solve some experimental problems in this work. His straight-forwardness to the critical remarks and reviews to this work is greatly appreciated.

*I* would like to pay my hearties thanks to my other supervisor, Assoc. Prof. Dr. Robert L. Linnen from Department of Earth Sciences, University of Waterloo, Canada, for his patience to do hours-long discussions. His critical and valuable reviews, which have provided this work with numerous ideas and great help. I would also like to thank Dr. Linnen, for his kind and technical support during my research stay at his department. I also pay my heartily thanks to him for his comments on improvements of the English text.

*I* should say that without patience and goodwill of all of my supervisors, the undertaking of this work would have been immeasurably more difficult; as it is, the text inadequately reflects the thought and time generously given it by these critics.

*I* would also appreciate help of Prof. Dr. Brüggemann, under his guidance I could able to perform my analytical work at geochemical laboratories of Max Planck Institute of Chemistry, Mainz (Germany).

*I* have also had the benefit of inspiration, comments and suggestions from Dr. Naveen Chaudhri, who showed me the path of research, and he has also given me a lot of courage to accomplish this work with complete dedication.

*I* should like to acknowledge PD Dr. Jürgen Koepke, Dipl.-Geol. Annette Schimrosczyk, Magnus Johansson, for their support during Electron Microprobe analyses. I gratefully acknowledge Otto Diedrich, for his technical and masterful work in preparing

the samples for my experiments. I would also like to appreciate technical help from Mr. Willi Hurkuck and Ms. Bettina Aichinger in the workshop at Hannover.

*I* gratefully acknowledge the help and friendly understanding of Prof. Dr. Josef-Christian Buhl, Prof. Dr. Peter Behrens, and Prof. Dr. Thomas Bredow, in tackling official matters with scholarship holders in this Graduate Program. I would also pay my thanks to my all colleagues in Graduate Program, who gave me an encouragement and assisted me to complete this work.

*A*mong colleagues at Institute of Mineralogy I should like to thank PD Dr. Marcus Nowak, Dr. Ingo Horn, Dr. Marc Memberti, Dr. Fleurice Parat, Dr. Roman E. Botcharnikov, Dr. Marcus Freise, Dr. Kevin Klimm, M.Sc. Francesco Vetere, M.Sc. Piero Del Gaudio, Dipl.-Geol. Matthias Hahn, Dipl.-Geow. Kai Spickenbom, Dipl.- Min. Holger Strauß and Dipl.-Geow. Sandrin T. Feig, for their cooperation and kind help during this work. I would also like to thank Ms. Heidi Hoffmann for her kind help.

*I* am also indebted to my parents B.A. B.Ed. Asha Bhalla and A.E.E. Om Parkash Bhalla, as both of them helped me to achieve this goal of my life, and finally, made this dream a reality. I would also like to appreciate my brother, M.B.B.S. Dr. Rahul Bhalla, as without his moral support and his way of encouraging me towards my work and daily-life duties, helped me to stick to my goal and kept me tuned to it. In addition, all of my relatives who helped to me achieve this milestone. I have been inspired a lot from my grandparents Raj Rani and Rattan Lal Kapoor, and my Grandfather Karam Chand Bhalla. I pay my heartiest thanks to my Grandmother Late Lajwanti Bhalla, who was always there for me and also gave me the warmth of her care and love. Everybody of them has motivated me and encouraged me, "Never-ever give up in your life, before you do not achieve your goals!". All my relatives provided me a bunch of moral support in terms of encouragement, love, punctuality, and to pay respect to others.

*I*t is my pleasure to thank Dipl.-Bio. Dok. Katrin Müller who helped me in various aspects, by providing me a gift of motivation and a package of encouragement while accomplishing this task. I am also indebted to her for her help to improve my German language as well as skills in Computers.

*I* also pay my heartiest thanks to Bundesanstalt für Geowissenschaften und Rohstoffe (BGR), Hanover for its financial support from Project No. - 75, and I am also indebted to Georg-Lichtenberg Fellowship from Ministry of Science and Culture, Lower Saxony, Germany, regarding financial support for this Ph.D.

## Vorwort

Die vorliegende Arbeit ist während meiner Tätigkeit an der Universität Hannover im Fachbereich Geowissenschaften entstanden.

Besonders danken möchte ich Herrn Prof. Dr. François Holtz. Er hat mich in jeder Phase der Arbeit wirkungsvoll durch seine Anregungen und Erklärungen unterstützt und deutlich zum Gelingen der Arbeit beigetragen. Er hat meine Selbstständigkeit gefördert durch häufige Aufforderung zum Überdenken jedes Schrittes.

Herrn Pd. Dr. Harald Behrens möchte ich für sein freundliches Entgegenkommen und seine raschen und aufrichtigen Kommentare bei der Betreuung der Arbeit sehr danken.

Herrn Dr. Robert L. Linnen möchte ich für die Möglichkeit des Aufenthaltes im Department of Earth Sciences sehr danken. Dadurch konnte ich meine Arbeit schneller fortsetzen. Für seine Mühe der Korrektur der englischen Sprache möchte ich mehrfach danken.

Die Arbeit hat sich durch die Anregungen und Ideen aller Begutachter zu einer komplexen und dadurch sinnvollen Arbeit entwickelt.

Mein Dank gilt auch Herrn Dr. Naveen Chaudhri, der mich auf die Idee brachte diese Promotionsarbeit zu verfassen. Mit seinem fachlichen Wissen konnte er meine Arbeit wirkungsvoll unterstützen.

Danke ich auch Herrn Prof. Dr. Gerhard E. Brüggemann, der mich beim experimente in Geochemielabor der Max Planck Institut für Chemie, Mainz (Deutschland) geholfen hat. Dadurch konnte ich auch meine Arbeit schneller fortsetzen.

Auch meinen Kollegen und Freunden danke ich für die Unterstützung und Motivation mein Ziel zu erreichen.

Besonders möchte ich Herrn Otto Diedrich danken, dessen perfekte Künste in der Schliffpräparation und der persönlichen Betreuung mich sehr unterstützt haben.

Für das seelische und zeitliche Entgegenkommen möchte ich meiner Familie sehr danken. For allem möchte ich meiner Mutter B.A. B.Ed. Asha Bhalla und meinem Vater A.E.E. Om Parkash Bhalla danken. Meinem Bruder Dr. Rahul Bhalla möchte ich danken, mich aufzufordern weiterzumachen, mich aufzubauen und mich in allen Lebenslagen zu unterstützen. Für Ihre persönliche Wärme, die sie mir vermittelt haben, möchte ich vielmals danken.

© *M*einem Großeltern Raj Rani und Rattan Lal Kapoor und meinem Großvater Karam Chand Bhalla möchte ich danken für die vielen netten aufmunternden Gespräche.  
An meine Großmutter Lajwanti Bhalla möchte ich hier erinnern, die sich immer liebevoll um mich gekümmert hat und auch sehr zum Gelingen meiner Person beigetragen hat.

© *M*einem Verwandten danke ich besonders für Ihre freundliche Unterstützung und Motivation.

*B*esonders möchte ich Katrin Müller danken, mich seelisch aufzubauen und mich in allen Lebenslagen zu unterstützen. Ihre Fähigkeiten in der Computerbenutzung haben mir sehr geholfen. Für ihre Mühe der Korrektur der deutsche Sprache möchte ich mehrfach danken.



## Abstract

Noble metal ore deposits are mostly dependent on the ability of metals to dissolve in fluids or silicate melts. These phases can act as transport media and lead to concentrations of the metals in other environments (usually at lower temperatures). The knowledge of the solubility of metals/metal-oxides in fluids and their dissolution kinetics represent key information to understand ore deposits. One of the most important observations in the 1970's was that hydrothermal fluids in nature are not composed of pure water, but that they may contain high amounts of halogens (some of these fluids are in fact brines). Thus, most of the previous experimental data on metal solubilities in pure water need to be reconsidered. This is particularly important for metals of economic interest such as Pt, Pd, Au and Sn, because these elements can form chlorine-bearing complexes in fluids and silicate melts.

This experimental study is aimed to understand the solubility of metals in fluids coexisting with geologically-relevant systems from lower temperatures up to magmatic temperatures. Thus, experimental investigations of the behavior of metals (e.g., tin and platinum) in melts coexisting with supercritical fluids have been undertaken, in an attempt to evaluate the physical and chemical constraints on the mobilization of Sn and Pt in silicate melts. In both metals, solution-remobilisation mechanisms play an important role in the concentrations of metals. Thus, the experiments were designed to determine: (1) the dissolution kinetics of the metals; (2) the effect of temperature, oxygen fugacity and Cl<sup>-</sup> and/or F-concentrations on the metal solubility in silicate melt; (3) the effect of various compositional parameters (e.g., corundum content, alumina saturation index). The pressure and temperature range varied from 1000 to 2000 bars and 600-1250 °C, respectively. For both metals, different systems have been modelled experimentally.

In the case of tin, particular attention has been given to the solubility of cassiterite (SnO<sub>2</sub>), one of the main minerals used as source of Sn. Cassiterite can be observed in both magmatic and hydrothermal environments. The solubility and dissolution kinetics of cassiterite was investigated in Chlorine- and Fluorine-bearing melts. Experiments were performed at a temperature range (600-850 °C) and pressure of 2 kbar, on F-bearing natural peraluminous melt and also on F-free and F-bearing synthetic granitic melts (peralkaline – peraluminous compositions) as well as on pegmatites. The main parameters, which have been varied, were: time, temperature, F- and Cl-concentrations,  $fO_2$  and various compositional parameters. Concentration of tin in the products (silicate melt or glass) was determined by electron microprobe (EMP). Bulk composition, Cl and F were also measured by EMP and Inductively Coupled Plasma-Atomic Emission Spectroscopy (ICP-AES). Experiments were also designed to examine diffusion behaviour of tin in various granitic and pegmatitic melts to investigate the effect of halogens (Cl, F) and  $fO_2$  on tin diffusivity in these kinds of melts. Various diffusion profiles were analyzed from glass-crystal (SnO<sub>2</sub>) interface towards glass boundary. The SnO<sub>2</sub> concentration calculated at the SnO<sub>2</sub>-glass interface is interpreted as SnO<sub>2</sub> solubility. At a log  $fO_2$  of Ni-NiO, SnO<sub>2</sub> solubility in a subaluminous melt (with 2.4 wt.% F in melt) can be predicted as  $\log C_{SnO_2} = 6.09 - 6.26 \cdot 10^3/T$ , respectively, where  $C_{SnO_2}$  is concentration of SnO<sub>2</sub> (wt.%) and T (K). SnO<sub>2</sub> solubility increases with an increase in excess alumina and F.

In the case of platinum, main consideration has been given to the solubility of Pt in Cl-free and Cl-bearing haplobasaltic melts, whereas, concentration of chloride and its partitioning in silicate melt has also been investigated. The experiments have mainly been performed at high temperatures (~1200 °C). The products, Cl-bearing free fluid and a haplobasaltic melt (glass) containing platinum concentration, were analyzed by a titrator and isotope-dilution-multi-collector inductively coupled mass spectroscopy (ID-MC-ICPMS), respectively. The main parameters, which have been varied in these series of experiments, were: time, temperature, chloride concentration and pressure. The present study shows that H<sub>2</sub>O solubility is higher when Cl<sup>-</sup> is present in the melt. Combined with data in a Cl-free system from study of Blaine et al. (2004), an effect of Cl<sup>-</sup> on Pt solubility in H<sub>2</sub>O-saturated melts (~5–6 wt.% H<sub>2</sub>O) at ~1200 °C can be predicted as:  $C_{Pt} = 57.30 + 260.24 \cdot Cl$ , where  $C_{Pt}$  and Cl are concentration of platinum (ppb) and amount of chloride content (wt.%) in the melt, respectively.

**Keywords:** Platinum; Silicate melts; Tin.

## Zusammenfassung

Die Bildung von Erzlagerstätten ist abhängig von der Fähigkeit der Metalle, sich in Fluiden oder Silikatschmelzen zu lösen. Das Wissen der Löslichkeit von Metallen oder Metalloxiden in diesen Phasen und ihre Auflösungskinetik ist ein wesentlicher Bestandteil, um die Entstehung von Erzlagerstätten zu verstehen. Eine wichtige Beobachtung in den 1970-igern war, dass natürliche hydrothermale Fluide nicht aus reinem Wasser bestehen, sondern auch einen wesentlichen Anteil an Halogenen enthalten. Dadurch sind viele der vorhergegangenen experimentellen Daten über Löslichkeiten von Metallen in reinem Wasser nur bedingt anwendbar. Dies ist besonders wichtig für Metalle mit ökonomischer Bedeutung, wie z.B. Pt, Pd, Au und Sn, weil diese Elemente Chlorid-Komplexe in Fluiden und Silikatschmelzen bilden können.

Ziel dieser Arbeit ist die Quantifizierung der Löslichkeit von Metallen in Fluiden und silikatischen Schmelzen bei geologisch relevanten Bedingungen und Systemen. Deshalb wurden experimentelle Untersuchungen des Verhaltens von Metall-Oxiden und Metallen (z.B. Cassiterit und Platin) in superkritischen fluidhaltigen Schmelzen durchgeführt, um die physikalischen und chemischen Zusammenhänge der Mobilisation von Sn und Pt in Silikatschmelzen zu evaluieren. Für beide Metalle spielen Löslichkeits-Remobilisierungs-Mechanismen eine wichtige Rolle bei der Bildung von Lagerstätten. Gezielte Experimente wurden durchgeführt, um folgende Sachverhalte zu ermitteln: (1) die Auflösungskinetik von Metallen, (2) den Einfluss der Temperatur, Sauerstoff fugazität und Cl- und/oder F-Konzentrationen auf die Metalllöslichkeit in Silikatschmelzen, (3) den Einfluss der Zusammensetzung der Schmelze, i.B. des Aluminiumgehaltes (ausgedrückt durch den Alumina Saturation Index, ASI). Die Untersuchungen wurden im Druck- und Temperaturbereich 1000 bis 2000 bar und 600 bis 1250 °C durchgeführt.

Bei Zinn wurde besonders die Löslichkeit von Cassiterit ( $\text{SnO}_2$ ) untersucht, eins der Hauptminerale, die benutzt werden als Zinnquelle. Cassiterit kann sowohl unter magmatischen als auch unter hydrothermalen entstehen. Die Löslichkeit und kinetische Auflösung von Cassiterit wurde in Cl- und F-führenden Schmelzen untersucht. Die Experimente wurden im Temperaturbereich 600-850 °C bei einem Druck von 2 kbar durchgeführt. Natürliche und synthetische Systeme (Rhyolith bis Pegmatit) wurden benutzt, um den Einfluss von Aluminium und Alkalien, F und Cl auf die Löslichkeit und Diffusion von Sn in silikatischen Schmelzen zu ermitteln. Zusätzlich wurden folgende Parameter variiert: Zeit, Temperatur, F- und Cl-Konzentrationen und  $f\text{O}_2$ . Die Konzentration von Zinn in den Produkten (Silikatschmelzen oder Glas) wurden mit der Mikrosonde ermittelt. Alle Hauptelemente, Cl und F wurden auch mit der Mikrosonde und Inductively Coupled Plasma-Atomic Emission Spectroscopy (ICP-AES) gemessen. Ortsaufgelöste Diffusionsprofile wurden von der Grenzfläche Kristall/Glas aus ins Innere des Glases hinein aufgenommen. Die  $\text{SnO}_2$ -Konzentration an der  $\text{SnO}_2$ -Glasgrenzfläche wird interpretiert als die  $\text{SnO}_2$ -Löslichkeit in der Schmelze. Bei einem durch den Ni-NiO Sauerstoffpuffer definierten  $\log f\text{O}_2$  kann die  $\text{SnO}_2$ -Löslichkeit in einer subaluminischen Schmelze (mit 2.4 Gew% F in der Schmelze) als  $\log C_{\text{SnO}_2} = 6.09 - 6.26 \cdot 10^3/T$  beschrieben werden, wobei  $C_{\text{SnO}_2}$  die Konzentration von  $\text{SnO}_2$  (Gew%) und T (K) ist. Die  $\text{SnO}_2$ -Löslichkeit nimmt mit zunehmendem Al- und F-Gehalt in der Schmelze zu.

Bei Platin war die Löslichkeit von Pt in Cl-freien und Cl-führenden haplobasaltischen Schmelzen Schwerpunkt der Untersuchung, wobei insbesondere der Einfluss der Konzentration von Chloriden und ihre Verteilung zwischen Silikatschmelzen und Fluiden erforscht wurden. Die Experimente wurden hauptsächlich bei hohen Temperaturen (~1200 °C) durchgeführt. Die Produkte, Cl-enthaltende Fluide und eine Pt-führende haplobasaltische Schmelze, wurden mit einem Titrator und mit Isotope-Dilution-Multi-Collector Inductively Coupled Mass Spectroscopy (ID-MC-ICPMS) analysiert. Die Hauptparameter, welche in diesen Experimenten variiert wurden, waren: Zeit, Temperatur, Chloridkonzentration und Druck. Die Ergebnisse zeigen, dass die  $\text{H}_2\text{O}$ -Löslichkeit höher ist, wenn Cl<sup>-</sup> in den Schmelzen vorhanden ist. Kombiniert mit den Daten von Blaine et al. (2004) für ein Cl-freies System kann der Einfluss von Cl<sup>-</sup> auf die Pt-Löslichkeit in  $\text{H}_2\text{O}$ -gesättigten Schmelzen (~5–6 Gew%  $\text{H}_2\text{O}$ ) bei ~1200 °C mit folgender Gleichung beschrieben werden:  $C_{\text{Pt}} = 57.30 + 260.24 \cdot \text{Cl}$ , wobei  $C_{\text{Pt}}$  und Cl<sup>-</sup> die Konzentration von Platin in ppb und den Cl-Gehalt in der Schmelze (Gew% Cl) entsprechen.

**Schlagwörter:** Platin; Silikatschmelzen; Zinn.

---

**Table of contents**

<b>1. Cassiterite solubility in peraluminous melts; effect of T, <math>fO_2</math>, corundum content and halogens (Cl, F) .....</b>	<b>1</b>
<b>Abstract .....</b>	<b>1</b>
<b>1.1. Introduction .....</b>	<b>2</b>
<b>1.2. Experimental and analytical methods .....</b>	<b>5</b>
1.2.1. Starting materials.....	5
1.2.2. Experimental method.....	6
1.2.3. Analytical techniques .....	8
<i>1.2.3.1. Electron microprobe .....</i>	<i>8</i>
<b>1.3. Results.....</b>	<b>11</b>
1.3.1. Attainment of saturation values and diffusion problems .....	11
<i>1.3.1.1. Run duration .....</i>	<i>11</i>
<i>1.3.1.2. Interdiffusion of major elements .....</i>	<i>11</i>
<i>1.3.1.3. Reproducibility of experiments .....</i>	<i>12</i>
1.3.2. Effect of temperature and $fO_2$ on $SnO_2$ solubility in natural granitic melts .....	14
1.3.3. Effect of fluorine on $SnO_2$ solubility.....	16
1.3.4. Effect of corundum content on $SnO_2$ solubility .....	18
1.3.5. Effect of chlorine on $SnO_2$ solubility .....	20
<b>1.4. Discussion .....</b>	<b>23</b>
 <b>2. Tin diffusivity and cassiterite solubility in granites and pegmatites;</b>	

---

<b>effect of T, <math>fO_2</math>, halogens and melt composition</b> .....	<b>27</b>
<b>Abstract</b> .....	<b>27</b>
<b>2.1. Introduction</b> .....	<b>30</b>
<b>2.2. Experimental and analytical methods</b> .....	<b>37</b>
<b>2.2.1. Starting materials</b> .....	37
<b>2.2.2. Experimental method</b> .....	40
<b>2.2.3. Experimental technique</b> .....	41
<b>2.2.3.1. Equipment</b> .....	42
<b>2.2.3.2. Experimental configuration</b> .....	44
<b>2.2.4. Analytical techniques</b> .....	45
<b>2.2.4.1. Electron microprobe</b> .....	45
<b>2.2.4.2. Inductively Coupled Plasma-Atomic Emission Spectroscopy</b> .....	46
<b>2.2.4.3. Karl Fischer titration</b> .....	46
<b>2.2.4.4. Preparation of samples and orientation of <math>SnO_2</math> crystals</b> <b>in melt</b> .....	49
<b>2.2.5. Determination of cassiterite solubility and diffusivity of tin</b> .....	57
<b>2.2.5.1. General equations for transport of tin in melts</b> .....	57
<b>2.2.5.2. An evaluation of <math>SnO_2</math> solubility and tin diffusivity</b> .....	58
<b>2.2.5.3. Attainment of equilibrium</b> .....	61
<b>2.2.6. Calculation of systematic error</b> .....	62
<b>2.3. Results</b> .....	<b>67</b>
<b>2.3.1. Fluorine-bearing peraluminous (A.S.I. <math>\geq 1.2</math>) melts</b> .....	67

---

2.3.1.1. Interdiffusion of major elements .....	67
2.3.1.2. Effect of $T$ and $fO_2$ on cassiterite solubility in peraluminous melts.....	72
2.3.1.3. Effect of fluorine on the solubility of cassiterite in peraluminous melts .....	74
2.3.2.4. Effect of $F$ on tin diffusivity in peraluminous melt compositions .....	78
2.3.2. Chlorine-bearing peraluminous compositions .....	79
2.3.2.1. Effect of $Cl$ on tin diffusivity .....	79
2.3.3. Behavior of $SnO_2$ in subaluminous (A.S.I. = 1.0) melts .....	83
2.3.3.1. Interdiffusion of major elements .....	83
2.3.3.2. Effect of fluorine as a $f(T)$ on cassiterite solubility in subaluminous melts .....	84
2.3.3.3. Effect of $fO_2$ on cassiterite solubility in subaluminous melts.....	86
2.3.3.4. Effect of fluorine on tin diffusivity in subaluminous melt compositions .....	86
2.3.4. F-bearing peralkaline (A.S.I. $\leq 0.6$ ) melts .....	90
2.3.4.1. Interdiffusion of major elements .....	90
2.3.4.2. Effect of $T$ and $fO_2$ on cassiterite solubility in peralkaline melts.....	90
2.3.4.3. Effect of $F$ on cassiterite solubility in peralkaline melts .....	90
2.3.4.4. Effect of $F$ on diffusivity of tin in peralkaline melt compositions.....	93

---

2.3.4.5. <i>Apparent equilibrium experiments</i> .....	93
2.3.5. Behavior of SnO <sub>2</sub> in Pegmatite melt composition .....	95
2.3.5.1. <i>Interdiffusion of major elements</i> .....	95
2.3.5.2. <i>Effect of T and fO<sub>2</sub> on cassiterite solubility in pegmatitic melt</i> .....	96
2.3.5.3. <i>Diffusivity of tin in pegmatitic melt composition</i> .....	97
2.4. Discussion .....	100
2.4.1. This study versus natural systems .....	100
2.4.1.1. <i>Effect of T, fO<sub>2</sub> and fluorine on the transport of cassiterite in silicate melts</i> .....	100
2.4.2. Effect of F on cassiterite solubility in subaluminous and peraluminous melts .....	103
2.4.3. Comparison with other studies using synthetic melts .....	109
2.5. Implications .....	113
2.6. Appendix .....	116
3. Solubility of chlorine and effect of chloride on platinum solubility in haplobasaltic melts .....	121
Abstract .....	121
3.1. Introduction .....	123
3.2. Experimental and analytical methods .....	126
3.2.1. Experimental method .....	126

---

3.2.1.1. <i>Starting material</i> .....	126
3.2.2. <b>Experimental procedure</b> .....	127
3.2.3. <b>Analytical methods</b> .....	127
3.2.3.1. <i>Determination of chloride content</i> .....	127
3.2.3.1.1. <i>Titration method</i> .....	128
3.2.3.1.2. <i>Electron microprobe</i> .....	128
3.2.3.2. <i>Determination of H<sub>2</sub>O solubility</i> .....	129
3.2.3.2.1. <i>Karl Fischer Titration (KFT)</i> .....	129
3.2.3.2.2. <i>IR-spectroscopy</i> .....	129
3.2.3.2.3. <i>Electron microprobe</i> .....	130
3.2.3.3. <i>Determination of platinum in haplobasalts</i> .....	130
3.2.3.3.1. <i>Cleaning of glass samples</i> .....	131
3.2.3.3.2. <i>Column technique and analysis</i> .....	131
<b>3.3. Results and discussion</b> .....	<b>133</b>
3.3.1. <b>Compositional Variation of glasses after experiment</b> .....	133
3.3.2. <b>Effect of Cl<sup>-</sup> on H<sub>2</sub>O solubility in Haplobasaltic melt</b> .....	135
3.3.3. <b>Distribution coefficient of chloride (D<sub>Cl</sub>)</b> .....	140
3.3.4. <b>Platinum concentrations in glasses</b> .....	141
3.3.4.1. <i>Pt concentrations in glasses synthesized in Pt crucible: The</i> <i>Pt-micronugget problem</i> .....	141
3.3.4.2. <i>Effect of chloride on Pt solubility</i> .....	145
<b>4. References</b> .....	<b>149</b>

## 1. Cassiterite solubility in peraluminous melts; effect of T, *f*O<sub>2</sub>, corundum content and halogens (Cl, F)

### Abstract

The aim of this experimental study was to determine the solubility of cassiterite in natural topaz- and cassiterite-bearing granite melts at temperatures close to the solidus. Profiles of Sn concentrations at glass-crystal (SnO<sub>2</sub>) interface were determined following the method of Harrison and Watson (1983). The cassiterite concentration calculated at the SnO<sub>2</sub>-glass interface is the SnO<sub>2</sub> solubility. Experiments were performed at 700-850 °C and 2 kbar using a natural fluorine-bearing peraluminous granitic melt with 2.8 wt.% normative corundum. Slightly H<sub>2</sub>O-undersaturated to H<sub>2</sub>O-saturated melt compositions were chosen, in order to minimize the loss of tin to the noble metal capsule walls. At the Ni-NiO oxygen fugacity buffer, the solubility of cassiterite in melts containing 1.12 wt.% fluorine increases from 0.32 wt.% SnO<sub>2</sub> to 1.20 wt.% SnO<sub>2</sub> with an increasing temperature from 700-850 °C. At the Ni-NiO buffer and a given corundum content, SnO<sub>2</sub> solubility increases by 10-20% relative to increase of fluorine from 0 to 1.12 wt.%. SnO<sub>2</sub> solubility increases by ~20% relative to increasing chlorine content from 0 to 0.37 wt.% in synthetic granitic melts at 850 °C. This study shows that chlorine is at least as important as fluorine in controlling SnO<sub>2</sub> solubility in evolved peraluminous melts at oxygen fugacities close to the Ni-NiO buffer. In addition to the strong effects of temperature and *f*O<sub>2</sub> on SnO<sub>2</sub> solubility, an additional controlling parameter is the amount of excess alumina (corundum content). At Ni-NiO and 850 °C, SnO<sub>2</sub> solubility increases from 0.47 to 1.10 wt.% SnO<sub>2</sub> as the normative corundum content increases from 0.1 to 2.8 wt.%. At oxidizing conditions (Ni-NiO +2 to +3), tin is mainly incorporated as Sn<sup>4+</sup> and the effect of excess alumina seems to be significantly weaker than at reducing conditions.

**Keywords:** Cassiterite; Cl; Concentration; F; Granite; SnO<sub>2</sub> solubility.



## 1.1 Introduction

Tin deposits display a wide range of structural and mineralogical types (Taylor, 1979a) and are generally spatially related to evolved granite intrusions. Tin and associated rare-element mineralisation (W, Be, Nb, Ta) are frequently associated with chemically specialized granites, with high contents of SiO<sub>2</sub>, alkalis, Sn, W, Mo, Be, B, Li and F, and low contents of CaO, MgO, Ba and Sr (Tischendorf, 1977). The deposits themselves contain characteristically fluorite, topaz, tourmaline and Li-micas (Pollard et al., 1987). In a number of natural processes, F and B contribute to the magmatic and post-magmatic evolution of the tin systems, including fractionation/crystallization, fluid phase evolution, wall-rock alterations, metal transportation and deposition (Pollard et al., 1987).

A fundamental concept in understanding the relationship between tin mineralisation and magmatism is that variations in the basicity of a melt (i.e., the activity of free oxygens) play an important role (Taylor, 1988). Peralkaline magmas display high melt basicities, and consequently will generate fluids during resurgent boiling that are markedly less acid than fluids associated with peraluminous melt systems (Taylor, 1988). Hence, peralkaline magmas have the capacity to store a far greater concentration of Sn than peraluminous magmas and Sn would be less prone to remobilization in peralkaline magmas by a fluid phase. Tin will be most effectively partitioned from reduced, high temperature, potassium-rich, aluminous magmas (Taylor, 1988). These characteristics describe a major portion of the Sn-mineralized granitoids (see also Štemprok, 1971; Štemprok and Skvor, 1974). Bivalent tin is a relatively large cation and is considered to behave as an incompatible element during the evolution of granitoid suites (Taylor, 1979a; Taylor 1979b; Eugster, 1985). Crystal fractionation, crystallochemical dispersion, magma mixing, and assimilation are the main processes that account for the generally systematic trends in Sn distribution in natural granitoid systems (Barsukov and Durasova, 1966; Kovalenko et al., 1968; Tauson, 1968; Groves, 1972; Groves, 1974; Tauson, 1974; Groves and McCarthy, 1978; Taylor, 1979a; Lehmann, 1982; Taylor and Wall, 1992).

Taylor (1988) concluded that across a broad range of physical and chemical

conditions, resurgent boiling is a viable mechanism for mobilizing substantial amounts of Sn that can be readily accommodated in many granitoid magmas. Taylor (1988) suggested that large quantities of Sn can be efficiently extracted from the magmas by relatively dilute, supercritical Cl solutions, and transported as a complex series of Cl-bearing stannous species. However, if the chlorinity of the fluid coexisting with melt is low, less Sn will be partitioned into the fluid. This may be an important parameter influencing the formation of magmatic cassiterite (Linnen, 1998a). Without a good understanding of the solubility systematics of Sn in natural granitic magmas, and a knowledge of the solubility of tin in Cl-bearing melts (+ Cl-bearing fluid), it is difficult to predict the influence of these or other mechanisms that control the distribution of tin in granitic rocks. In this respect, the solubility behavior of Sn in natural granitic systems containing halogens (Cl, F), has received little systematic attention.

Studies on ongonites (subvolcanic analogues of Li-F granites) show that tin accumulates in the residual magma and may reach concentrations high enough to promote SnO<sub>2</sub> precipitation. Other examples of this level of accumulation include the Beauvoir Granite (Cuney et al., 1992), which is an example of a Li-F granite containing disseminated SnO<sub>2</sub>, and the Macusani glasses (Pichavant et al., 1987). The presence of B and F in granite magmas results in the reorganisation of melt structure (Manning, 1981) by promoting depolymerisation and the creation of new complex species in the melt. In this process, the number of structurally favorable sites for incorporation of lithophile elements such as Sn increases, which may result in enhanced solubility of these elements (Manning, 1981; Pollard et al., 1987).

Ryabchikov et al. (1978a, 1978b) were the first to study the solubility of SnO<sub>2</sub> in a synthetic granitic system under geologically relevant conditions. They determined that at 750 °C, 1.5 kbar, and *f*O<sub>2</sub> buffered by the nickel-nickel oxide assemblage (Ni-NiO), a haplogranite melt saturated with SnO<sub>2</sub>, fluorite and topaz, and in equilibrium with a 4.0-m chloride solution contained 1100 (± 500) ppm SnO<sub>2</sub>. Štemprok and Voldán (1978) determined the concentration of Sn in SnO<sub>2</sub>-saturated natural granite and sodium disilicate glass at 1300 and 1600 °C, at oxygen fugacities controlled by atmospheric pressure. They found that the Sn concentration in equilibrium with cassiterite ranged from 5 to 7 wt.%

SnO<sub>2</sub> at 1300 °C, up to 20 wt.% at 1600 °C, and was directly proportional to the sodium content of the peralkaline glasses. Equal concentrations of stannic and stannous ions in basaltic liquids (hawaiite) at 1200 °C and at oxygen fugacity conditions close to the fayalite-magnetite-quartz buffer (FMQ) were found by Durasova et al. (1984). They observed also an increase in SnO<sub>2</sub> solubility in melts under reducing conditions. To examine the effect of melt composition and *f*O<sub>2</sub> on SnO<sub>2</sub> solubility, Linnen et al. (1995, 1996) investigated the solubility of cassiterite in peralkaline and peraluminous melts. In addition, Linnen et al. (1996) confirmed a significant increase in the solubility of SnO<sub>2</sub> with decreasing *f*O<sub>2</sub>.

The effect of *f*O<sub>2</sub> and melt composition on the solubility of cassiterite in granitic melts were modeled by Taylor and Wall (1992) and Linnen et al. (1995, 1996). On the other hand, the effect of temperature and F and Cl content of the melt to cassiterite solubility has received less attention Štemprok (1990a, 1990b). In partitioning experiments between haplogranitic melts and aqueous fluids Keppler and Wyllie (1991) observed a strong increase of the fluid/melt partition coefficient of Sn with increasing Cl concentration in the fluid while F content had no effect. This can be explained by the formation of Cl complexes of Sn and by F complexes being less stable. Dissolution experiments with various minerals in haplogranitic melts show that dissolved F can strongly enhance the solubility of the high field strength elements (HFSE) in the melt (Keppler, 1993). Keppler (1993) suggested that this behaviour is due to the formation of HFSE complexes with non-bridging oxygen atoms, which are expelled from coordination with Al by reaction with F (Keppler found that the solubility of TiO<sub>2</sub> increased from 0.26 ± 0.01 to 0.33 ± 0.01 wt.% TiO<sub>2</sub> when 2 wt.% of F was added into a water saturated haplogranite melt). In the present study, a series of experiments has been performed to investigate the effects of temperature, F and to some extent Cl on the solubility of SnO<sub>2</sub> in natural granitic melts.

## 1.2 Experimental and analytical methods

### 1.2.1 Starting materials

Five starting glass compositions were used. One was a re-melted natural topaz- and cassiterite-bearing granite from Kymi (Finland) containing 1.12 wt.% fluorine and approximately 200 ppm SnO<sub>2</sub> (Glass 1, Table 1.1), provided by Ilmari Haapala. A second composition (Glass 2) was prepared by adding Na<sub>3</sub>AlF<sub>6</sub> and AlF<sub>3</sub> to Glass 1 so as to obtain a F-content of 2.12 wt.%. In this glass, F was introduced so that F replaced a stoichiometrically equivalent amount of O (2F = O) while the molar Al/(Na + K) ratio was kept constant. The starting glass 3 was prepared with a mixture of oxides of Si, Al, Ca, Na, K and Fe, and is nearly same as glass 1, but F-free. The starting material was placed in an open platinum crucible and melted at 1600 °C / 1 atm for 2 to 3 hours in a furnace. The obtained glass was crushed and melted again at 1600 °C / 1 atm for 1-2 hours to obtain a homogeneous glass. These dry starting glasses were hydrated at high pressure and temperature to obtain water-bearing glasses, which were subsequently used as starting materials. The two additional Cl-bearing glasses (glass 4 and glass 5) were also synthesized at high pressure and temperature by adding diluted HCl-H<sub>2</sub>O fluid (slightly water undersaturated) to glass 3. The glasses were synthesized in cold seal pressure vessels at 850 °C and 2 kbar for 6-7 days. The *f*O<sub>2</sub> conditions were buffered by a Ni-NiO assemblage. For these experiments, deionised H<sub>2</sub>O or dilute HCl (33.5 wt.%) was loaded in gold capsules (inner diameter 5.0 mm, outer diameter 5.4 mm, length 45 mm), together with the dry starting glasses (Glass 1 and 3). The samples were sealed in gold capsules by arc welding. Water contents in the hydrous starting materials were determined by Karl Fischer Titration (KFT; cf. Behrens et al. 1996). For each synthesis, two KFT analyses were done. The variation of the duplicate analyses was less than 0.03 wt.%. The water content of the hydrous glasses varied between 5.1 and 6.2 wt.% and the glasses were either slightly water-undersaturated or water-saturated.

## 1.2.2 Experimental method

The experimental technique used was similar to that of Linnen et al. (1995), which was modified from Harrison and Watson (1983). The experiments produced a

**Table 1.1: Microprobe analysis of starting material (natural granitic melt and synthetic granitic melt)**

Starting					
Materials	Glass 1*	Glass 2*	Glass 3	Glass 4	Glass 5
SiO <sub>2</sub> (wt.%)	73.87	72.57	75.79	75.06	77.10
Al <sub>2</sub> O <sub>3</sub>	15.46	15.88	14.66	15.06	13.95
Σ FeO	0.99	0.95	0.99	1.06	0.38
CaO	0.80	0.79	0.73	0.80	0.69
Na <sub>2</sub> O	4.03	4.33	3.65	3.64	3.56
K <sub>2</sub> O	4.30	4.24	4.18	4.18	3.95
SnO <sub>2</sub>	0.02	0.02	0.00	0.00	0.00
F	1.12	2.12	0.00	0.00	0.00
F=O	0.47	0.88	0.00	0.00	0.00
Cl	0.00	0.00	0.00	0.20	0.37
Total	100.17	100.06	100.00	100.00	100.00
Quartz	35.2	32.3	37.9	37.2	41.0
Orthoclase	27.7	27.5	25.9	26.1	24.2
Albite	37.1	40.2	36.2	36.7	34.8
Corundum	2.8	2.8	2.8	3.1	2.6
A/CNK	1.21	1.21	1.24	1.26	1.23

\*Data from Lukkari and Holtz (2000). Glass compositions 3, 4 and 5 are normalized to 100%. The concentration of TiO<sub>2</sub>, MgO and MnO are lower than 0.02, 0.01 and 0.03 wt.%, respectively in the natural glasses (glass 1 and 2). P<sub>2</sub>O<sub>5</sub> is below detection limit. Glasses 3, 4 and 5 are synthetic and free of these oxides.

concentration gradient of SnO<sub>2</sub> in a melt adjacent to a SnO<sub>2</sub> crystal. Care was taken that the crystal was surrounded by the melt to avoid any contact between cassiterite and the noble metal capsule. This minimizes the formation of Au-Sn alloy, which may result in experimental problems. Hydrous starting glasses were crushed and inserted in a ~15-mm long gold capsule that was closed at the base by arc welding. A natural tabular SnO<sub>2</sub> crystal (~1x1x2 mm) was placed in the center of the capsule. The top end of the capsule was crimped and welded shut. The experiments were performed in a horizontal cold seal pressure vessel (CSPVs) at 2 kbar and in the temperature range of 700-850 °C for 5-22 hours, except for one experiment, which was conducted for 145 hours.

The CSPVs used for the experiments were made of a Ni-rich alloy. The temperature was controlled by type K-thermocouple placed outside of the vessel close to the hot-spot zone. The vessels were calibrated periodically and the temperature was known within  $\pm 10$  °C. The experiments were quenched by removing the vessel from the furnace and blowing compressed air around the vessel—the temperature inside the vessel dropped to  $\sim 200$  °C after 5 minutes. Pressure was measured with a strain-gauge manometer (accuracy  $\pm 0.03$  kbar), using two pressure media that allowed different *f*O<sub>2</sub> ranges. In one case, water was used as pressure medium and the buffer was close to that of the Ni-NiO assemblage. In these experiments, the Ni-NiO powder was placed around the sample capsules. Because of the Ni-rich composition of the vessel, this buffer had a long life time and the buffer assemblage comprised Ni-NiO after the experiment (the intrinsic *f*O<sub>2</sub> of the vessel was close to that of the Ni-NiO buffer). In other experiments, vessels were pressurized with argon and the oxygen fugacity was significantly higher. At 800-840 °C and 2 kbar, the oxygen fugacity measured by sensor capsules (Taylor et al., 1992) was Ni-NiO + 2.3 log units (Berndt et al., 2001). Hereafter, the runs buffered by the Ni-NiO assemblage will be referred to as “NNO experiments” or runs under reducing conditions, and the experiments with argon as the pressure medium will be referred to as “NNO+2.3 experiments” or runs under oxidizing conditions.

After quenching, the capsules were weighed and cut perpendicular to the base of the SnO<sub>2</sub> crystal. The experimental products were always glass + cassiterite, except in run GGC 11 in which quench crystals (feldspar) were formed near the cassiterite due to slow cooling rate. Because the exact orientation of the SnO<sub>2</sub> crystal in the capsule was not known, the studied sections were not always strictly perpendicular to the SnO<sub>2</sub> crystal. This may have influenced the calculation of diffusivity of SnO<sub>2</sub>, but is not expected to have influenced the solubility of SnO<sub>2</sub>, which corresponds to the concentration of SnO<sub>2</sub> at the crystal-melt interface. In three experiments (GGC 3, GGC 4, GGC 5) two sections were prepared, one longitudinally and one transversely relative to the axis of the capsule. This procedure allowed us to investigate concentration profiles of tin along three orthogonal directions.

### 1.2.3 Analytical techniques

#### 1.2.3.1 *Electron microprobe*

The compositions of the glasses were determined with a Cameca SX-100 electron microprobe with analytical conditions of 15 kV and 6 nA. Counting time for Na and K was 2 seconds for all starting glasses and run products and 5 seconds for other elements. The beam was defocused at least 10 μm for starting glasses and run products. To measure Cl in the two starting glasses, profiles of more than 40 analyses were performed. Peak count time for each analysis of Cl in the melt was 30 seconds for the starting glasses. The Cl content was homogeneous in the run product glasses (samples containing SnO<sub>2</sub>) this was confirmed by traverses across the final run products. The fluorine content of the starting glasses was also analyzed by electron microprobe (see Lukkari and Holtz, 2000).

All the analyses of tin in the glasses were conducted with an electron beam (2 μm in diameter) and the peak counting time for determining SnO<sub>2</sub> was 120 seconds. Concentration profiles were determined at a 90° angle to the SnO<sub>2</sub>-glass interface. To avoid fluorescence from the SnO<sub>2</sub> crystal, the first analysis was done at a distance of 10-15 μm from the SnO<sub>2</sub>-crystal boundary. One to four profiles with 35-50 analytical points each were determined per sample. In most of the samples, the length of the profiles was 900 μm to 1400 μm. A typical concentration profile obtained from the experiment at 843 °C, 16 hours and NNO is shown in Fig. 1.1.

This profile fits well with the solution of Fick's second law

$$C = C_0 (1 - \text{erf } x/(4 Dt)^{1/2}) \quad (1)$$

assuming infinite one dimensional diffusion, a concentration independent diffusivity *D* of Sn and a constant concentration *C*<sub>0</sub> of SnO<sub>2</sub> at the surface of the crystal. *x* is the distance to the surface and *t* is the run duration. The solubility of SnO<sub>2</sub> in the melt can be calculated by

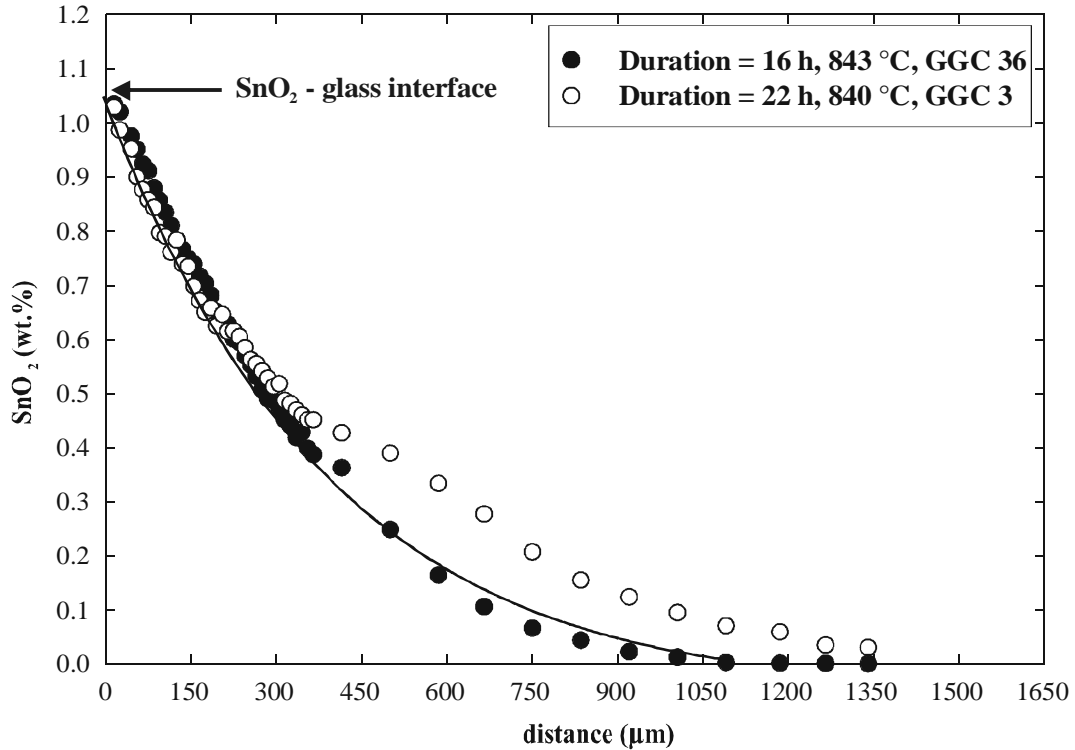


**Figure 1.1: Typical concentration profiles of SnO<sub>2</sub> for experiments with run durations of 16 and 22 hours. The solubility of SnO<sub>2</sub> is defined by the intercept between the concentration profiles and Y-axis. The two profiles obtained at ~840 °C show that the concentration of SnO<sub>2</sub> at the interface is not time dependent. A typical concentration profile of SnO<sub>2</sub> fitted from the error function (solid line, see text) is also shown (experiment GGC 36).**

extrapolating the error function to the SnO<sub>2</sub>-glass interface. Not all concentration profiles could be fitted accurately by an error function, however. In these cases the run duration may have been too long and concentration of SnO<sub>2</sub> along the profile never reached a value close to zero, or the profile may have been longer than the half-size of the crystal so that the source cannot be considered as an infinite plane. Furthermore, the SnO<sub>2</sub> crystal may have descended in the melt during the experiment and the experimental section may not have been cut perpendicular to the SnO<sub>2</sub> surface.

In any case, even if the concentration profiles had different shapes, the maximum SnO<sub>2</sub> concentration in the glass at the interface, corresponding to the equilibrium solubility value, should still be discernable. This is illustrated in Fig. 1.1, in which two profiles



obtained at the same temperature in two different experiments have been plotted.

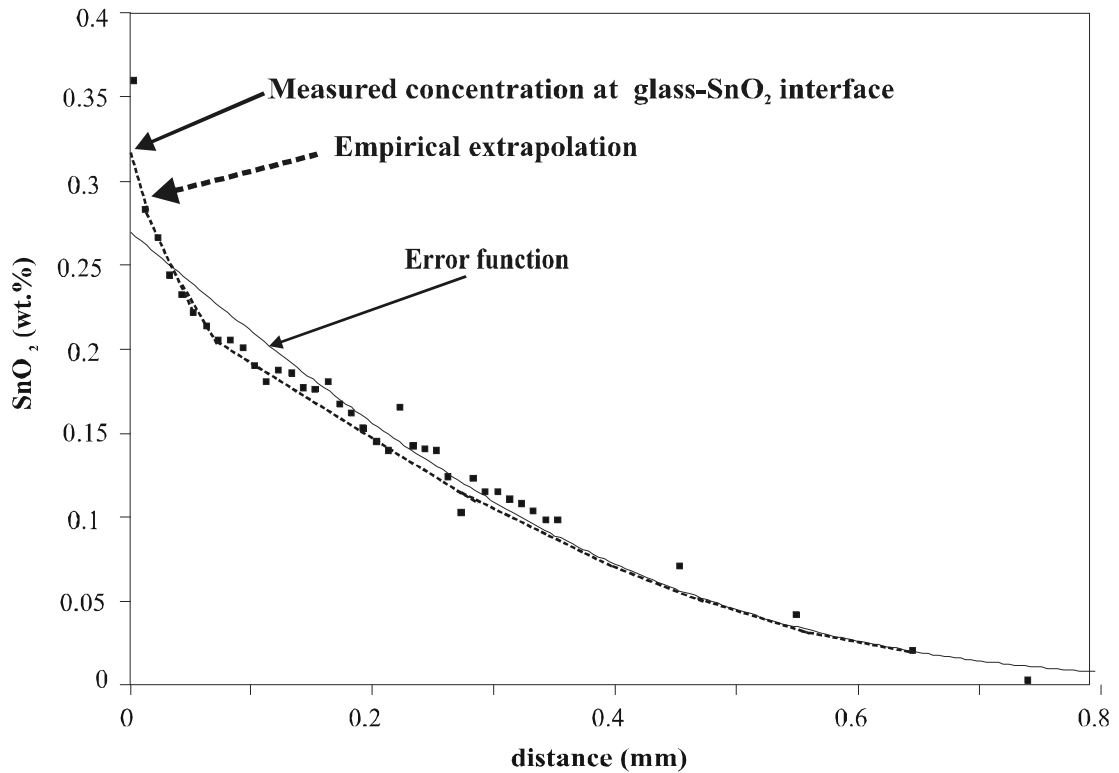


**Figure 1.2: Concentration profile of SnO<sub>2</sub> in experiment GGC 14. The concentration at the interface was extrapolated empirically from the data points close to SnO<sub>2</sub>-glass interface.**

The profile of sample GGC 36 can be fitted successfully by an error function. The profile of sample GGC 3 does not have the typical shape of a concentration profile (in fine planar diffusion), especially at 300-750  $\mu\text{m}$  from the interface (Fig. 1.1). However, the concentration at the interface is identical within error [ $1.05 \pm 0.05$  wt.% SnO<sub>2</sub> (GGC 36) and  $1.03 \pm 0.05$  wt.% SnO<sub>2</sub> (GGC 3)]. For concentration profiles that could not be fitted with an error function, the concentration at the interface was extrapolated by fitting data points close to the interface empirically. Such an empirical fit is shown in Fig. 1.2.

## 1.3 Results

### 1.3.1 Attainment of saturation values and diffusion problems

#### 1.3.1.1 Run duration

To know the effect of time on the SnO<sub>2</sub> concentration profile, experiments were performed at different run durations. Experiments conducted for 145 and 22 hours at identical P, T and *f*O<sub>2</sub>, also yielded identical SnO<sub>2</sub> solubility within error [compare GGC 11 and GGC 5 at NNO; see also GGC 16 and GGC 6 at NNO+2.3 (Table 1.2)]. This also implies that the concentration of SnO<sub>2</sub> at the SnO<sub>2</sub>-melt interface corresponds to the solubility of SnO<sub>2</sub>. This study confirmed the results of Linnen et al. (1995) who suggested that the extrapolated concentration at the SnO<sub>2</sub>-melt interface is identical within error independently on the run duration (cf. Fig. 1.1).

#### 1.3.1.2 Interdiffusion of major elements

Dissolution of SnO<sub>2</sub> in the melt is a complex multi-component diffusion process and the concentration of other melt components may change relative to each other along the SnO<sub>2</sub> diffusion profiles. Such compositional variations in the melt were observed by Linnen et al. (1995, 1996) especially at reducing conditions when the solubility of SnO<sub>2</sub> is high. In this case, alkalis were depleted near the surface of the crystal. Solubility of SnO<sub>2</sub> varies with the alkali/Al ratio of the melt (Taylor and Wall, 1992; Linnen et al., 1995, 1996; Ellison et al., 1998) and, hence, the measured concentration of SnO<sub>2</sub> at the surface is not representative of the initial melt but for a more peraluminous composition. In this study, the SnO<sub>2</sub> concentration was at most 1.20 wt.%. Major-element concentrations along the profiles were analyzed on selected samples with the highest SnO<sub>2</sub> concentrations. Typical results for run product GGC 19 are shown in Fig. 1.3. There is no significant variation in alkalis and Al, thus coupled diffusion would not be considered a problem in this study.

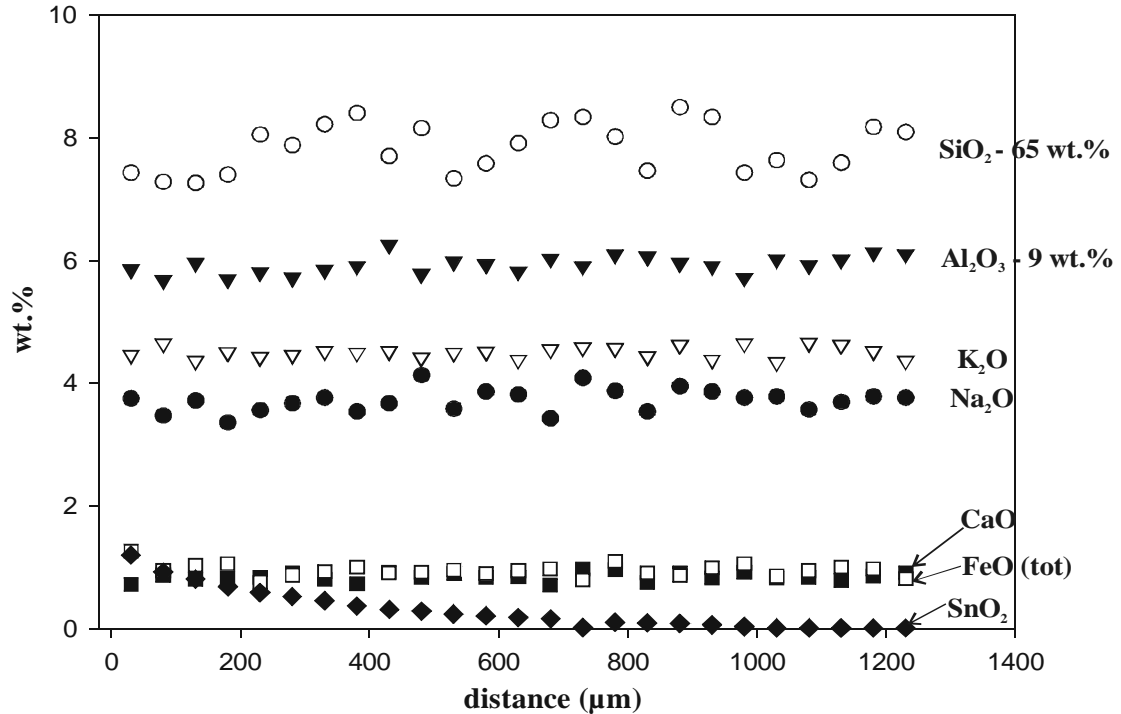


**Figure 1.3: Representative electron microprobe analyses of major elements as a function of distance from SnO<sub>2</sub> crystal in experiment GGC 19. All analyses are normalized to 100%. SnO<sub>2</sub> concentration at the interface is 1.2 wt.%. To report the SiO<sub>2</sub> and Al<sub>2</sub>O<sub>3</sub> contents on the same scale, 65 wt.% and 9 wt.% have been subtracted from the analyzed SiO<sub>2</sub> and Al<sub>2</sub>O<sub>3</sub> contents, respectively.**

### 1.3.1.3 Reproducibility of experiments

The diffusion profile method used in this study is well suited to investigate SnO<sub>2</sub> solubility and to minimize problems related to interaction of tin and noble metal capsules. However, several factors may influence the concentration of SnO<sub>2</sub> at the SnO<sub>2</sub>-melt interface. Concentration profiles cannot always be fitted by an error function, making it difficult to extrapolate SnO<sub>2</sub> concentration at the crystal-melt interface. Beside analytical errors, the scatter of the solubility data may be due to variations in water concentration and temperature. Several experiments were conducted at identical conditions (P, T, *f*O<sub>2</sub> and run duration) to establish the reproducibility of the results from this study. The calculated SnO<sub>2</sub> solubilities for the nine experiments performed at NNO and at 840 °C vary by up to ±15% relative, and are independent of the run duration (Fig. 1.4).

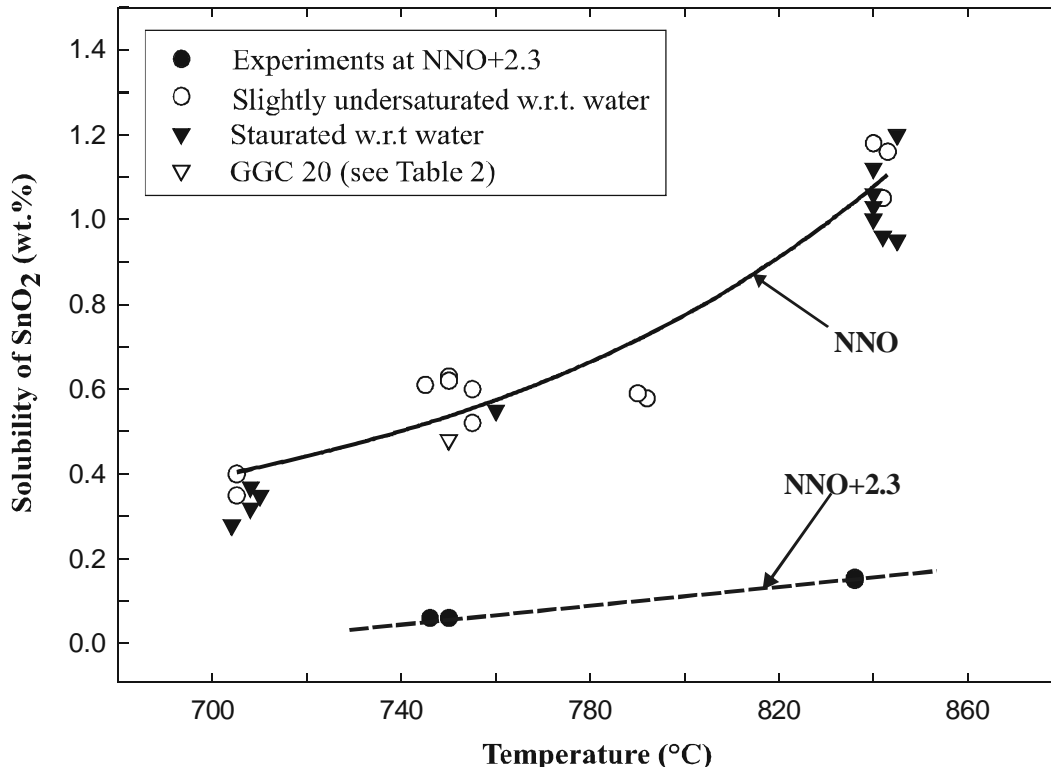


**Figure 1.4: Solubility of SnO<sub>2</sub> as a function of temperature in a natural F-bearing composition in reduced (NNO) and oxidized (NNO +2.3) conditions. Experiment GGC 20 was performed using glass 2, all other with glass 1.**

However, for seven of these experiments the relative variation is less than  $\pm 10\%$ . Long run durations and resulting interaction with gold capsule may explain the low solubility values of the experiments GGC 11 and GGC 5. Furthermore, crystals were observed in the product of run GGC 11, probably as a result of slow quench (diminished air flux around the vessel), and this may have affected the solubility determination. This study considers that a variation of  $\pm 10\%$  relative corresponds to the precision of the solubility data from the present study at  $840 \pm 10$  °C. At 700 and 750 °C, the relative variation in SnO<sub>2</sub> solubility is larger due to lower absolute concentration of SnO<sub>2</sub> ( $\pm 20\%$  at 750 °C,  $\pm 18\%$  at 700 °C). The error bars shown in Fig. 1.5 correspond to this variation.

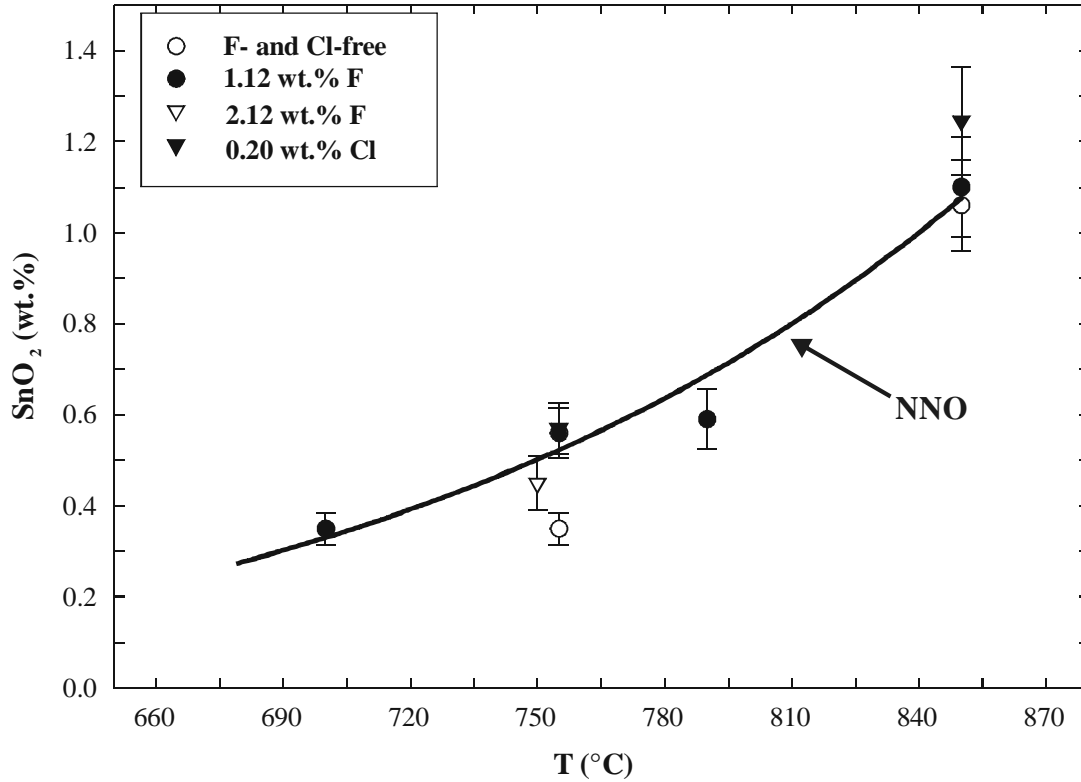


**Figure 1.5: Effect of F and Cl content on SnO<sub>2</sub> solubility as a function of temperature in reduced conditions (NNO). Experiments performed with glasses 1, 2, 3, 4 and 5. Average solubility values are shown (see Table 1.2).**

### 1.3.2 Effect of temperature and fO<sub>2</sub> on SnO<sub>2</sub> solubility in natural granitic melts

The experimental results on the solubility of SnO<sub>2</sub> in the melt with composition of glass 1 are shown in Table 1.2 and Fig. 1.4. At NNO, the solubility of SnO<sub>2</sub> increases from 0.28 wt.% SnO<sub>2</sub> at 700 ± 10 °C to 1.20 wt.% SnO<sub>2</sub> at 850 ± 10 °C (corresponding to GGC 16 and GGC 19, respectively). At NNO+2.3, the solubility of SnO<sub>2</sub> is significantly lower (see also Linnen et al., 1995) and varies from 0.06 wt.% SnO<sub>2</sub> at 750 ± 10 °C to 0.14 wt.% SnO<sub>2</sub> at 840 ± 10 °C. However, the effect of temperature is of the same order of magnitude as at NNO. When plotted in a diagram log C<sub>SnO<sub>2</sub></sub> vs. 1/T · 10<sup>3</sup> (Fig. 1.6), the slope of the linear regression between 700 and 840 °C at NNO is -3.51. At NNO+2.3, the slope

between 736 and 836 °C is -4.25 (not shown on Fig. 1.6). Thus the slopes are similar at both oxygen fugacities. The effect of temperature can also be estimated from experiments with glass 3—the same trend as with glass 1 is observed.

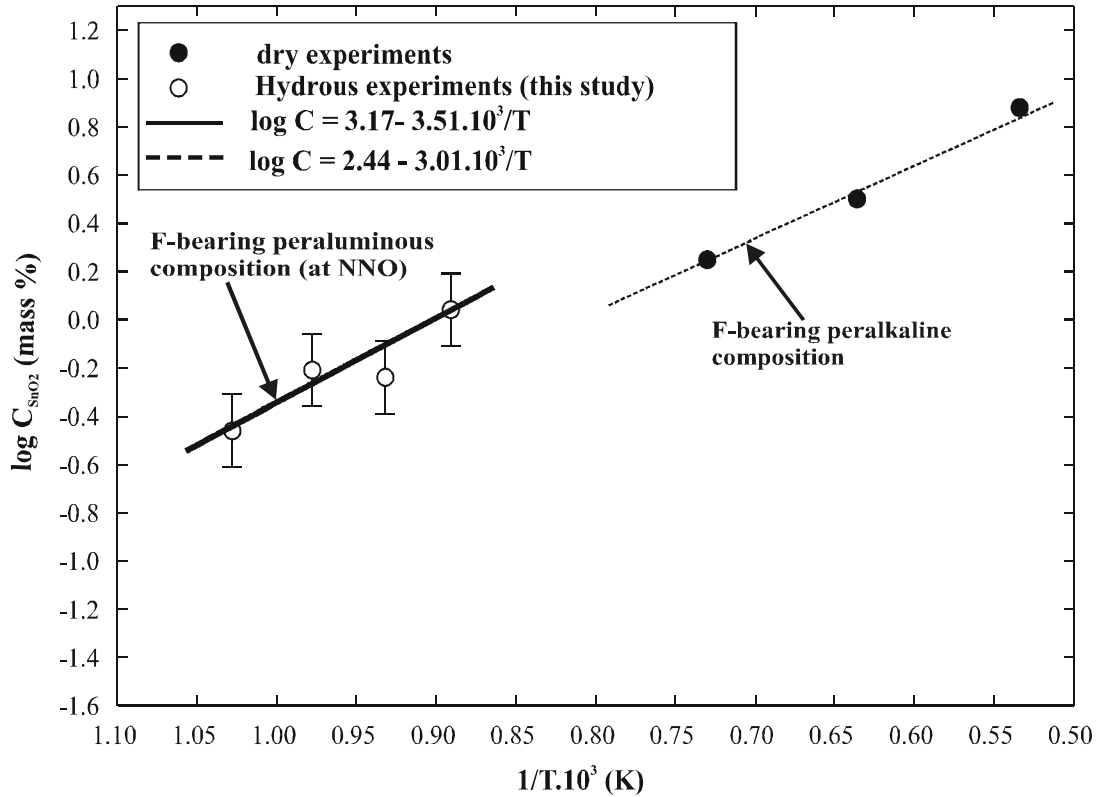
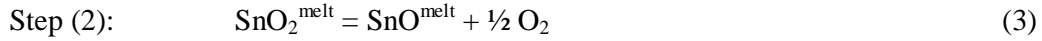


**Figure 1.6:** The logarithm of mass% cassiterite solubility ( $C_{\text{SnO}_2}$ ) versus  $1/T$  (K) for hydrous and dry granitic melts. Data for F-bearing peraluminous composition at 2 kbar are from this study. F-bearing peralkaline composition at 1 atm and oxidizing conditions are from Štemprok (1982), Štemprok and Voldan (1978) and Nekrasov (1984).

The effect of temperature is of the same order of magnitude as what has been observed in previous studies, especially in dry conditions. High pressure (hydrothermal) experiments are not available (except at 850 °C), because of experimental problems (see Linnen et al., 1995). However, the slope for the dry F-bearing peralkaline composition at 1100-1600 °C (Štemprok, 1990b) in Fig. 1.6 is identical within error to the slope of glass 1 with peraluminous composition. Thus, the temperature effect seems to be of the same order of magnitude for all geologically relevant melt compositions. The dissolution of SnO<sub>2</sub> in

the melt can be treated as a two-step reaction:



where *cas* refer to cassiterite and *melt* to dissolved species in the melt. At oxidizing conditions, the concentration of SnO is negligible and the total concentration of dissolved Sn does not vary with oxygen fugacity. In this case, the slope in plots of log C<sub>SnO<sub>2</sub></sub> versus 1/T corresponds to ΔH°/2.303 R, where ΔH° is the standard enthalpy of reaction (2) and R is the gas constant. At moderately reducing conditions, a slope of -0.5 is observed in plots of log C<sub>SnO<sub>2</sub></sub> versus log *f*O<sub>2</sub>. This can be explained by the increasing abundance of divalent Sn with decreasing oxygen fugacity (see Linnen et al., 1995). In the experiments from this study, the *f*O<sub>2</sub> was buffered for a given solid buffer, allowing *f*O<sub>2</sub> to change with temperature. Therefore, the slope in plots of log C<sub>SnO<sub>2</sub></sub> versus 1/T does not strictly represent the dissolution enthalpy.

### 1.3.3 Effect of fluorine on SnO<sub>2</sub> solubility

The comparison of data from glass 1 with the subaluminous composition of Linnen et al. (1995) may indicate that fluorine has a significant effect on SnO<sub>2</sub> solubility, as has been often assumed in natural granitic systems (e.g., Pichavant et al., 1987). The solubility of SnO<sub>2</sub> at NNO increases from 0.30 wt.% SnO<sub>2</sub> in a F-free granitic system (at 850 °C) to 1.10 wt.% (average value) SnO<sub>2</sub> in a F-bearing system (glass 1 at 840 ± 10 °C). However, increasing F content from 1.12 to 2.12 wt.% (glass 1 and 2) does not lead to a further increase in SnO<sub>2</sub> solubility. The measured SnO<sub>2</sub> concentration was even slightly lower in the more F-rich melt [0.45 wt.% SnO<sub>2</sub> at 750 °C in glass 2, 0.55 wt.% SnO<sub>2</sub> (average value) in glass 1]. The results obtained with the F-free glass 3, which has the same corundum content as glass 1 and 2, confirm that the effect of F is low or even negligible at an *f*O<sub>2</sub> of NNO. Data at 840 °C for glasses 1 and 3 are almost identical [1.10 wt.% SnO<sub>2</sub>

**Table 1.2: Experimental run conditions and run products (fluorine-bearing melts)**

Exp. Ref. No.	Starting glass		P (bar)	T (°C)	t (hours)	buffer used	solubility of SnO <sub>2</sub> (in log ppm)		
	*initial H <sub>2</sub> O (wt.%)	**fluorine content (wt.%)					avg.	max.	min.
GGC 3	6.20	1.12	2000	840	22	NNO	4.01	4.03	4.00
GGC 4	6.20	“	2000	840	22	NNO	4.02	4.03	4.00
GGC 5	6.20	“	2000	845	22	NNO	3.95	3.98	3.93
GGC 11	6.88	“	2010	840	145	NNO	3.93	3.93	3.93
GGC 18	6.26	“	2000	840	18	NNO	4.05	-	-
GGC 19	6.26	“	2000	840	18	NNO	4.08	-	-
GGC 30	5.28	“	2000	840	16	NNO	4.08	-	-
GGC 32	5.17	“	2000	843	16	NNO	4.07	-	-
GGC 36	5.14	“	2000	843	16	NNO	4.03	-	-
GGC 31	5.28	“	2000	788	5	NNO	3.74	-	-
GGC 34	5.28	“	2080	795	5	NNO	3.76	-	-
GGC 35	5.17	“	2000	790	5	NNO	3.77	-	-
GGC 12	6.26	“	2005	755	22	NNO	3.67	-	-
GGC 21	5.14	“	2015	750	20	NNO	3.79	-	-
GGC 22	5.14	“	2015	755	20	NNO	3.75	3.78	3.75
GGC 23	5.14	“	1990	750	18	NNO	3.86	-	-
GGC 24	5.14	“	1990	745	18	NNO	3.78	-	-
GGC 27	6.26	“	2000	760	20	NNO	3.74	-	-
GGC 28	5.14	“	2000	755	20	NNO	3.70	-	-
GGC 10	6.20	“	2000	708	24	NNO	3.51	3.51	3.51
GGC 13	6.26	“	2000	708	16	NNO	3.57	-	-
GGC 14	6.88	“	2000	710	16	NNO	3.52	-	-
GGC 16	6.88	“	2000	704	16	NNO	3.45	-	-
GGC 25	5.14	“	2000	705	48	NNO	3.54	-	-
GGC 29	5.17	“	2000	705	16	NNO	3.60	-	-
GGC 39	5.28	“	2030	836	16	NNO+2.3	3.13	3.18	3.09
GGC 40	5.28	“	2030	750	16	NNO+2.3	2.78	2.78	2.78
GGC 43	5.28	“	2030	746	16	NNO+2.3	2.80	2.82	2.78
GGC 44	5.28	“	2010	836	6	NNO+2.3	3.19	-	-
GGC 20 <sup>a</sup>	5.20	2.12	2015	750	20	NNO	3.65	3.68	3.64

**Abbreviations:** Initial H<sub>2</sub>O (\*) is the water content measured by KFT (Karl Fischer Titration). Fluorine content (\*\*) is the fluorine measured by electron microprobe. All run products were glasses. Sample GGC 11 was partially crystallized after the experiment (not included in average solubility data at 850 ± 10 °C).

<sup>a</sup> No prehydrated starting glass was used, water content was determined by KFT. The minimum and maximum values are obtained from different concentration profiles.

(average value) and 1.06 wt.% SnO<sub>2</sub>, respectively]. There is a small difference at 750 °C for glasses 1 and 3 (0.35 wt.% SnO<sub>2</sub> and 0.56 wt.% SnO<sub>2</sub>), but the variation is still within the ±20% error. Based on the effect of temperature on F-free and F-bearing glasses (Fig. 1.5), this study concludes that F does not significantly effect SnO<sub>2</sub> solubility. This study also concludes that, at reducing conditions, F has a minor influence on tin solubility and that the



difference between the data of Linnen et al. (1995) for subaluminous haplogranite and the data obtained in this study is related to another compositional factor. The difference in Q-Ab-Or proportions does not seem to affect the SnO<sub>2</sub> solubility significantly. Glass 3 does not have exactly the same composition as glasses 1 and 2, and Linnen et al. (1996) observed very similar SnO<sub>2</sub> solubilities in haplogranite, quartz-albite and quartz-feldspar melts at same P, T and *f*O<sub>2</sub>. The main difference is the normative corundum content as the melts used in this study are all peraluminous. Under oxidizing conditions, there may be a larger effect of F on Sn solubility. In run GGC 39 at 836 °C, 0.14 wt.% of SnO<sub>2</sub> dissolved in the F-bearing melt, whereas according to Linnen et al. (1996) less than 0.10 wt.% SnO<sub>2</sub> can be dissolved in subaluminous to peraluminous melts containing no F. This result is consistent with the observation of Keppler (1993) that dissolved F promotes the solubility of HFSE because, under oxidizing conditions, tin is present dominantly in the +4 valence state.

### 1.3.4 Effect of corundum content on SnO<sub>2</sub> solubility

Although this study does not systematically evaluate the effect of normative corundum (C), it is evident by comparing the data of Linnen et al. (1996) with this study that SnO<sub>2</sub> solubility increases with increasing corundum content. SnO<sub>2</sub> solubility at NNO increases progressively at 850 °C from 0.47 wt.% SnO<sub>2</sub> at C = 0.2 wt.% to 0.57 wt.% SnO<sub>2</sub> at C = 1.14 wt.% and to 0.85 wt.% SnO<sub>2</sub> at C = 2.3 wt.% (Fig. 1.7).

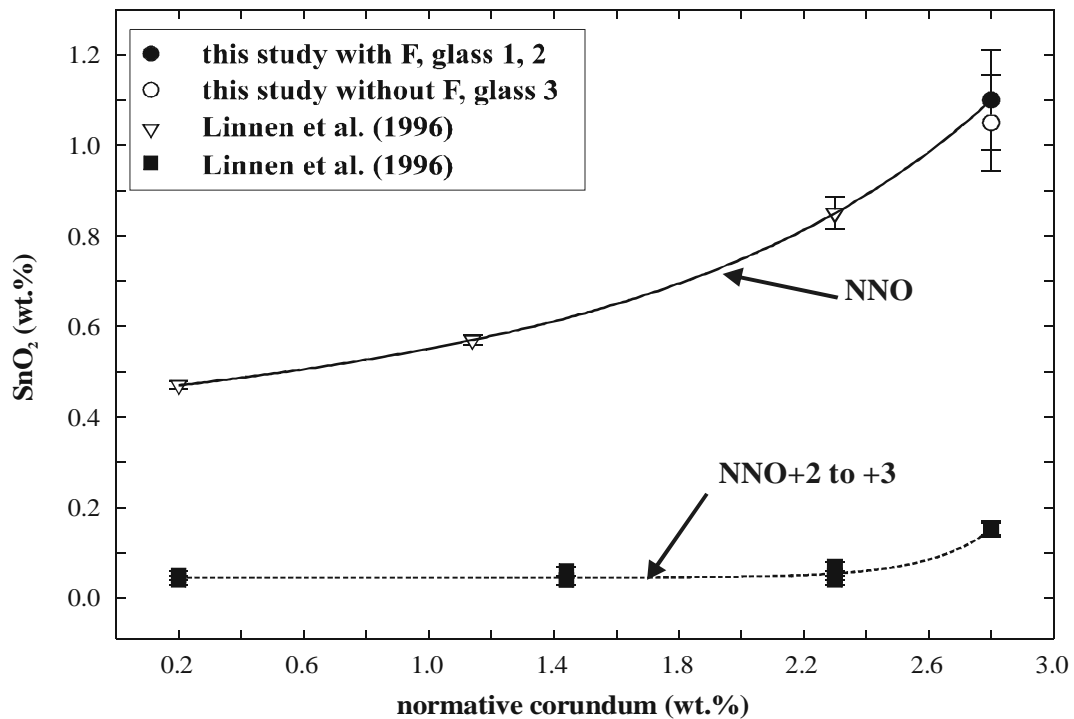


**Figure 1.7:** Effect of excess alumina (expressed as normative corundum) on SnO<sub>2</sub> solubility in silicate melt at 850 °C for two oxygen fugacity ranges (~Ni-NiO, and Ni-NiO +2 to +3). The data obtained in this study for F-bearing glasses are average values.

In this study, an average SnO<sub>2</sub> solubility of 1.05 wt.% SnO<sub>2</sub> at NNO for glasses 1, 2 and 3 has been found. This value is higher than the maximum value found by Linnen et al. (1996). At 850 °C, the results from this study can be fitted with those of Linnen et al. (1996) and they show that there is a slight non-linear increase in SnO<sub>2</sub> solubility with normative corundum of the melt (Fig. 1.8). However, considering a precision of ±10% relative, the points at NNO in Fig. 1.8 could also be fitted by a linear trend. This effect of

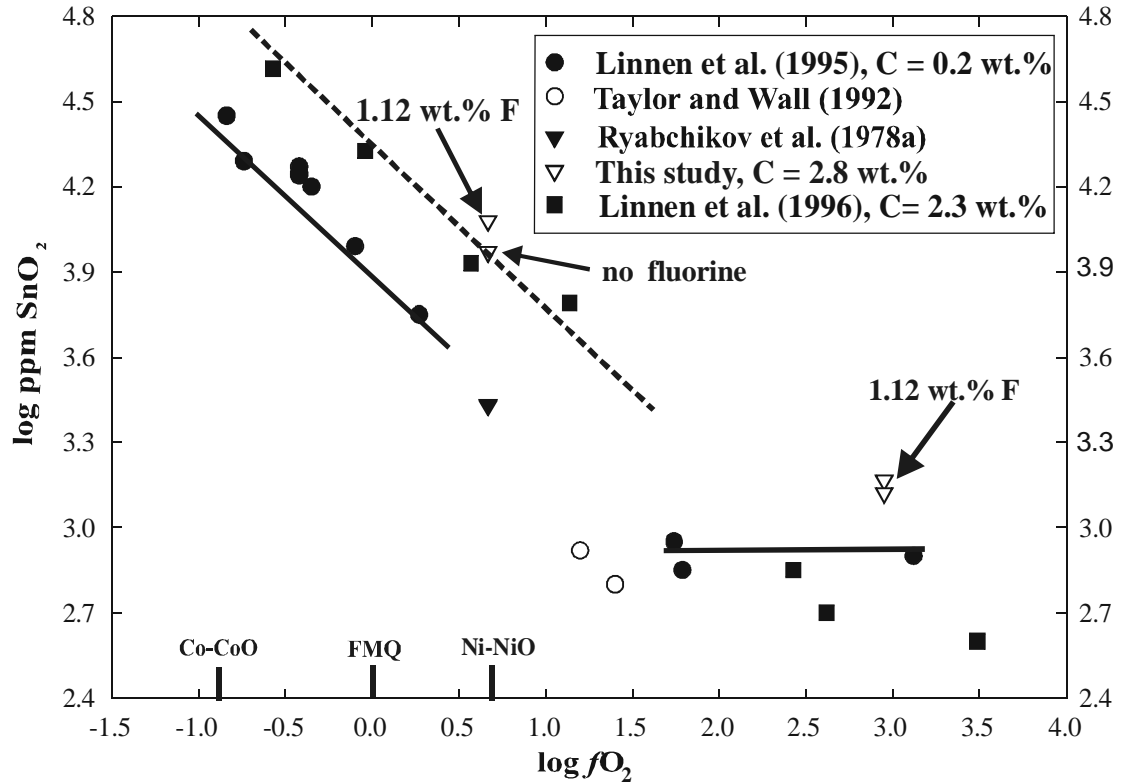


**Figure 1.8: Log solubility of Sn (ppm SnO<sub>2</sub>) versus log fO<sub>2</sub> in granitic melts at 2 kbar. All data are obtained at 850 °C, except for the study of Taylor and Wall (1992) at 800 °C. The solid lines connecting the data of Linnen et al. (1995) are for samples with 0.2 wt.% normative corundum (C). The dashed lines connect the data of Linnen et al. (1996) obtained from samples with 2.3 wt.% C.**

normative corundum may also be observed at more oxidizing (NNO+2.3) conditions. Because of the low concentrations and relatively high uncertainty, it is difficult to distinguish between a linear and non-linear increase in SnO<sub>2</sub> solubility as a function of corundum content. In any case, the effect of normative corundum on SnO<sub>2</sub> solubility is significantly lower at Ni-NiO+2.3 than at NNO.

### 1.3.5 Effect of chlorine on SnO<sub>2</sub> solubility

The effect of chlorine on the SnO<sub>2</sub> solubility in granitic melts was also determined (Fig. 1.5). The present study found a solubility of 0.59 wt.% SnO<sub>2</sub> at 760 °C and 1.24 wt.%

SnO<sub>2</sub> at 860 °C in a melt containing 0.20 wt.% Cl at NNO (glass 4). In a Cl-free melt at NNO (glass 3), these values were 0.35 wt.% SnO<sub>2</sub> at 750 ± 10 °C and 1.06 wt.% SnO<sub>2</sub> at 860 °C. Thus, the results from the present study indicate that SnO<sub>2</sub> solubility increases slightly with Cl-content of the melt. This contrasts with the data of Taylor and Wall (1992)

**Table 1.3: Experimental run conditions and run products (fluorine-free melts)**

Exp. Ref. No.	Starting glass		P	T	t	Buffer used	Solubility of SnO <sub>2</sub> (in log ppm)
	initial H <sub>2</sub> O	chlorine content					
GGC 51	5.59	0.20	2000	860	18	NNO	4.093
GGC 57	5.73	0.00	2000	855	18	NNO	4.020
GGC 59	5.61	0.00	2000	852	18	NNO	4.030
GGC 53	5.59	0.20	2030	760	18	NNO	3.770
GGC 56	6.12	0.37	2030	760	18	NNO	3.785
GGC 60	5.61	0.00	2030	754	18	NNO	3.550
GGC 58	5.73	0.00	2030	752	18	NNO	3.530

**Abbreviations:** P is the total pressure in bars with an error bar of ±10 bar; T is the temperature in °C with an error bar of ±5; t is the experimental run duration in hours; Cl content is the Cl (in wt.%) measured from starting glass by electron microprobe. All run products were glasses.

who performed experiments in both Cl-free and Cl-bearing systems, in the temperature range 750-800 °C and in a wide range of *f*O<sub>2</sub> from NNO to Co-CoO and found a decrease in solubility of SnO<sub>2</sub> when Cl was added to the system. At 750 °C, 2 kbar and ~NNO, Taylor and Wall (1992) found 0.085 wt.% Sn in a Cl-free melt and 0.068 wt.% Sn with 0.11 wt.% Cl in the melt. This corresponds to a 20% relative decrease with the addition of 0.11 wt.% Cl, whereas this study observed an increase of about 40% relative with addition of 0.20 wt.% at 750-760 °C. This study also show that further addition of Cl leads to enhanced SnO<sub>2</sub> solubility (0.61 wt.% SnO<sub>2</sub> at 760 °C in a melt containing 0.37 wt.% Cl; Table 1.3).

These discrepancies may be related to experimental problems encountered by Taylor and Wall (1992). Linnen et al. (1995) demonstrated that the experimental methods applied by Taylor and Wall (1992) were not appropriate to determine the SnO<sub>2</sub> solubility at reducing conditions. In the presence of a fluid phase, transport of Sn to the capsule wall occurs at a faster rate than the diffusivity of Sn in silicate melts. Therefore, equilibrium between SnO<sub>2</sub>, silicate melt and Sn-Au alloy was not attained in the study of Taylor and Wall (1992).

## 1.4 Discussion

Linnen et al. (1995, 1996) investigated the effects of  $fO_2$ , peralkalinity and excess aluminum on tin solubility in granitic melts at 850 °C and found that cassiterite solubility ranges from 2.8 wt.% SnO<sub>2</sub> at FMQ -0.84 to approximately 0.08 wt.% SnO<sub>2</sub> at FMQ +3.12 in a synthetic granitic melt composition with 0.4 wt.% C at 850 °C and 2 kbar. At  $fO_2$  higher than FMQ +1.5,  $fO_2$  was not observed to affect SnO<sub>2</sub> solubility, implying that SnO<sub>2</sub> dissolves into the melt largely as Sn<sup>4+</sup> (see Fig. 1.8). At more reduced conditions, log SnO<sub>2</sub> solubility decreases with increasing log  $fO_2$  at a slope of -0.5, implying that Sn dissolves in the melt as Sn<sup>2+</sup> (cf. Paparoni, 2000).

This study extends the data set of Linnen et al. (1995, 1996) to lower temperatures and also confirm the data of Štemprok (1990b). The present study shows that the temperature effect can be modeled by assuming a linear dependence of log C<sub>SnO<sub>2</sub></sub> versus 1/T. In subaluminous to peraluminous compositions, F has only a minor effect on SnO<sub>2</sub> solubility at an  $fO_2$  of NNO, but the normative corundum of the melt is a compositional parameter, which needs to be taken into account to model cassiterite solubility in evolved granitic melts. A possible explanation for the relatively low effect of F on the SnO<sub>2</sub> solubility at NNO is that Sn is dissolved mainly as Sn<sup>2+</sup>. Thus the effect of F on solubility of HFSE shown by Keppler (1993) is not expected if Sn is not dissolved as Sn<sup>4+</sup> (Sn<sup>4+</sup> is a HFSE whereas Sn<sup>2+</sup> is not). For a peraluminous melt composition, this study also found a significant effect of chlorine. The data set from this study, when combined with that of Linnen et al. (1995, 1996), allows the prediction of SnO<sub>2</sub> solubility in natural granitic melts, peraluminous melts in particular, as a function of  $fO_2$ , temperature and melt composition.

By extrapolating the data from this study close to the solidus temperatures of natural topaz and cassiterite-bearing granite (<680 °C), SnO<sub>2</sub> concentrations required to produce magmatic cassiterite are approximately 0.30 wt.% (at NNO). Even if solidus temperatures as low as 600 °C were assumed (cf. Pichavant et al., 1987), the results from this study show that a relatively high concentration of SnO<sub>2</sub> (~0.20 wt.%) can be dissolved

in such melts. In this study, the  $SnO_2$  concentrations obtained at 700 °C are of the same order of magnitude than those observed in natural systems (1400 ppm in the Beauvoir granite; Cuney et al., 1992). As emphasized by Linnen et al. (1995), changing  $fO_2$  may result in the crystallization of a significant amount of  $SnO_2$  in the granitic melts, even at low temperatures.

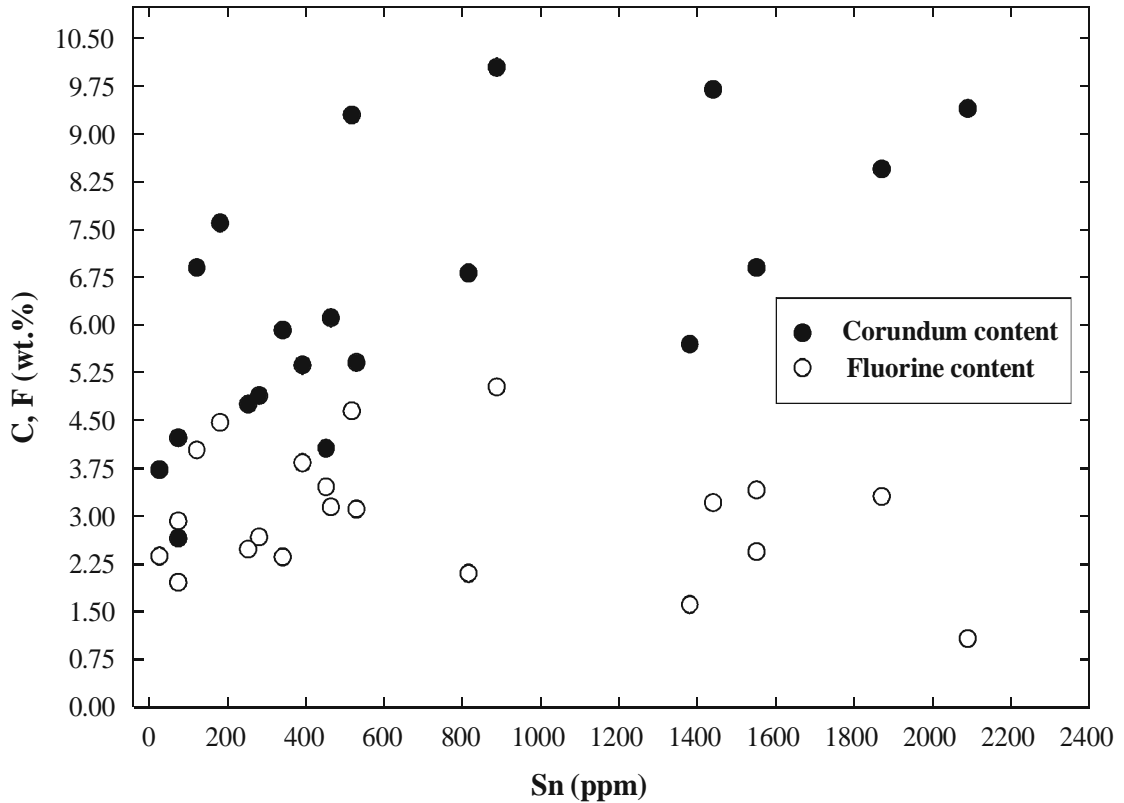


**Figure 1.9: Effect of fluorine (F) and normative corundum (C) on the solubility of Sn in natural melt inclusions in quartz from an evolved peraluminous pegmatite (data from Webster et al., 1997). All the data listed in Webster et al. (1997) have been plotted except one inclusion containing >3 wt.% CaO (other inclusions, in total 20, have <0.36 wt.% CaO). Note that there is no obvious correlation between F and Sn content, whereas normative corundum and Sn are positively correlated.**

One of the most surprising implications of this study is that corundum (excess alumina) content may be a compositional parameter controlling the  $SnO_2$  solubility. To test this hypothesis, this study compared glass inclusion compositions in quartz from a Sn-bearing, F- and P-rich evolved peraluminous pegmatite from Ehrenfriedersdorf, Central

Erzgebirge in southeastern Germany (Webster et al., 1997). All melt inclusions analyses by Webster et al. (1997), except one with a high CaO (3.02 wt.%), were used for this comparison. The normative corundum of all melt inclusions analyzed was calculated for the compositions given by Webster et al. (1997). Figure 1.9 shows the amount of F and normative corundum as a function of the Sn concentration in the glass inclusions. There is no evident correlation between F and Sn, but there is a positive correlation between normative corundum and Sn. This observation seems to confirm that the normative corundum (excess alumina) influences  $SnO_2$  solubility in natural magmatic systems.

Systematic variations between Sn and other elements cannot be observed from the data set of Webster et al. (1997). As emphasized by Webster et al. (1997), the P content of the inclusions is exceptionally high, yet there is no obvious correlation between P and Sn in the melt. Except for F, the volatile concentrations are low (average 1.2 wt.%  $H_2O$  and 0.1 wt.% Cl) in the melt inclusions, compared to melt inclusions from high-silica, high-Sn topaz rhyolites (Webster and Duffield, 1991, 1994; Webster et al., 1991; Lowenstern, 1995). No systematic correlation is observed between Sn and Cl or  $H_2O$ . The low  $H_2O$  and Cl contents suggest that the residual liquids entrapped in quartz were already highly degassed, suggesting in turn that Sn is not strongly partitioned to the fluid phase (cf. Taylor, 1988). Another explanation for variable content of  $SnO_2$  in the melt inclusions would be that melt inclusions with high  $SnO_2$  were trapped from melts at low  $fO_2$ . However, in the dataset of Webster et al. (1997), there is no compositional parameter that may reflect change in  $fO_2$ . One such parameter would be the Fe/(Fe+Mg) ratio, which is dependent of  $fO_2$ , but cannot be used as the MgO content of the melt inclusions reported by Webster et al. (1997) is close to zero.

Another dataset which may confirm the role of C in controlling Sn solubility in silicate melts is given by Charoy and Noronha (1996). These authors investigated a small volatile-rich, highly sodic and strongly peraluminous microgranite body in Argemela (Portugal) with extreme enrichments in F, P, Rb, Cs, Li, Sn and Be. Magmatic cassiterite was observed in the microgranite. Figure 1.10 shows the F and C as a function of the Sn concentration in the whole-rock compositions of the Argemela microgranite and associated



rocks. It is clear that there is a positive correlation between C and Sn concentration. In this example, there is also a positive, although less pronounced, correlation between F and Sn, as well as between F and other incompatible elements such as Li, Rb, Cs (Charoy and Noronha, 1996). Charoy and Noronha emphasized that the Argemela microgranite may represent mixing of two magmas (one of them enriched in F and incompatible elements) and thus the positive correlation of F and Sn, and C and Sn may be explained by the

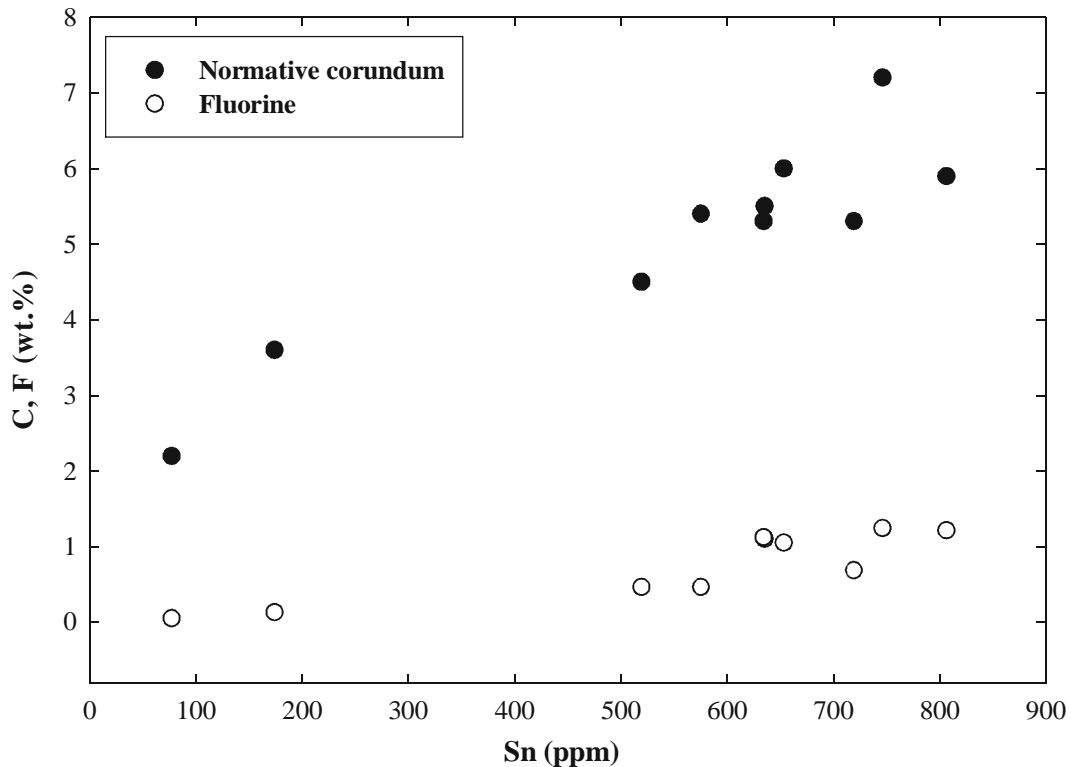


**Figure 1.10: Effect of fluorine (F) and normative corundum (C) on the Sn content in the Argemela microgranite from Portugal (data from Charoy and Noronha, 1996). Note that there is a positive correlation between Sn concentration and normative corundum of the melt.**

mixing hypothesis. In this case, however, high Sn and F concentrations are observed in the peraluminous end member. This is consistent with results from this study that imply a substantial role for Al in the solubility of Sn in evolved granitic melts, while the effect of F is relatively small.

## 2. Tin diffusivity and cassiterite solubility in granites and pegmatites; effect of T, $fO_2$ , halogens and melt composition

### Abstract

Experimental investigations of the behavior of tin in hydrous melts have been undertaken, in an attempt to evaluate the physical and chemical constraints on the mobilization as well as diffusion of tin in magmas and its transport as a function of temperature, oxygen fugacity, halogens (Cl, F) and other compositional parameters. In this study, experiments were performed on fluorine-bearing natural granitic melt (1.12 wt.% F) of peraluminous composition (normative corundum, C = 2.8 wt.%) and on F-free and F-bearing synthetic granitic melts (peralkaline to peraluminous) containing various amount of F-content (0 to 4.6 wt.% F in melt) at 600 to 850 °C, 2 kbar and at various log  $fO_2$  (Ni-NiO-2 to Ni-NiO+4), to examine the cassiterite ( $SnO_2$ ) solubility and diffusivity of tin in these melts as a function of T,  $fO_2$ , melt composition, Cl- and F-concentration in the melt. A  $SnO_2$  crystal was placed at the center of the capsule containing granitic melt (glass). The dissolution behavior of the  $SnO_2$  crystal was examined. All experiments were conducted in vertical or horizontal cold seal pressure vessels (*v*CSPVs or *h*CSPVs). The run duration of kinetic experiments varied from 5 to 72 hours, whereas few equilibrium experiments had duration of 528 hours (22 days). Bulk compositions and concentrations of  $SnO_2$ , Cl and F were measured by electron microprobe (EMP) and Inductively Coupled Plasma-Atomic Emission Spectroscopy (ICP-AES). In most of the experiments,  $fO_2$  was controlled using double capsule (hydrogen sensor) technique of Chou (1987a). Various diffusion (concentration) profiles were analyzed from glass-crystal ( $SnO_2$ ) interface towards glass boundary. The  $SnO_2$  concentration calculated at the  $SnO_2$ -glass interface is interpreted as  $SnO_2$  solubility.

Cassiterite solubility has been measured in granitic melts with different alumina saturation index (A.S.I.). In a peraluminous melt (A.S.I. = 1.24) at an  $fO_2$  of Ni-NiO (NNO), increases of cassiterite solubility (0.35 to 0.55 wt.%  $SnO_2$  at 750°C and 1.04 to 1.20 wt.%  $SnO_2$  at 850°C) are observed for increases of F melt from 0 to 1.12 wt.% F. At

~NNO-0.5, 800°C and 2 kbar, cassiterite solubility increases significantly (2.23 to 4.17 wt.% SnO<sub>2</sub> with an increase of F melt content from 2.4 to 4.6 wt.% F) in a subaluminous melt (A.S.I. = 1.0). At an  $fO_2$  of NNO, synthetic subaluminous melt composition (A.S.I. = 1.0) containing 2.4 wt.% F, shows an increase in Cassiterite solubility from 0.22 wt.% at 600 °C to 2.45 wt.% at 850 °C. Using the same subaluminous melt composition with 2.4 wt.% F, but at a log  $fO_2$  of NNO+3.5, Cassiterite solubility increases from 0.02 wt.% at 650 °C to 0.09 wt.% at 800 °C. Thus, cassiterite solubility at NNO-0.5 in the melt containing 2.4 wt.% F in melt, can be predicted as  $\log C_{SnO_2} = 6.09 - 6.26 \cdot 10^3/T$ , whereas at NNO+3.5, cassiterite solubility in the same melt can be predicted as  $\log C_{SnO_2} = 0.29 - 1.25 \cdot 10^3/T$ , where  $C_{SnO_2}$  and T are concentration of SnO<sub>2</sub> (wt.%) and temperature (K), respectively. Cassiterite solubility also increases from 1.05 wt.% to 1.25 wt.% SnO<sub>2</sub> with increasing Cl<sup>-</sup> content from 0 wt.% to 0.4 wt.% Cl<sup>-</sup> in granitic melt (A.S.I. = 1.24) at 850 °C. In a synthetic peralkaline melt (A.S.I. = 0.6) with 0 to 4.2 wt.% F in melt at 850 °C, 2 kbar and at an  $fO_2$  of NNO, Cassiterite solubility increases from 6.17 to 8.32 wt.% SnO<sub>2</sub>, respectively. At NNO, in the same peralkaline melt composition containing 3.7 wt.% F, cassiterite solubility increases from 3.17 wt.% SnO<sub>2</sub> to 8.32 wt.% SnO<sub>2</sub> over a temperature increase from 740 to 850 °C, respectively. Therefore, for F-free and F-bearing (3.7 wt.% F in melt) compositions, cassiterite solubility can be calculated as  $\log C_{SnO_2} = -3.51 + 4.41 \cdot 10^3/T$  and  $\log C_{SnO_2} = 5.16 - 4.76 \cdot 10^3/T$ , respectively, where,  $C_{SnO_2}$  is the log concentration of SnO<sub>2</sub> (wt.%) and T is temperature (K). At NNO, cassiterite solubility in a pegmatitic melt (which contains ~4 wt.% F, 2 wt.% B<sub>2</sub>O<sub>3</sub>, 1.5 wt.% P<sub>2</sub>O<sub>5</sub> and 1 wt.% Li<sub>2</sub>O) at 750 to 850 °C increases from 0.55 wt.% SnO<sub>2</sub> to 0.83 wt.% SnO<sub>2</sub>, respectively. Thus, cassiterite solubility at NNO+0.5 in such pegmatite can be expressed as  $\log C_{SnO_2} = 4.58 - 5.10 \cdot 10^3/T$ , where  $C_{SnO_2}$  is concentration of SnO<sub>2</sub> (wt.%) and T (K). At more oxidizing conditions (NNO+3.5), cassiterite solubility shows little dependence on temperature from 650 to 850 °C, and within error limits, the solubility is constant. Thus, at reducing conditions ( $\leq$  NNO buffer), tin is incorporated as Sn<sup>2+</sup> and cassiterite solubility in peraluminous melts increases from 0.47 to 1.20 wt.% SnO<sub>2</sub> with increasing normative corundum content from 0.1 to 2.8 wt.% C. At oxidizing conditions ( $\geq$  NNO+2.3), tin is mainly incorporated as Sn<sup>4+</sup> and the effect of normative corundum seems to be significantly lower than at reducing conditions.

The diffusivity of tin at a  $\log fO_2$  of NNO-0.5 to NNO-1.0 in a synthetic subaluminous melt (A.S.I. = 1.0) bearing 0 to 4.6 wt.% F at 800 °C and 2 kbar, increases from  $5.9 \cdot 10^{-14}$  to  $4.2 \cdot 10^{-12}$  m<sup>2</sup>/s, respectively. For the melt with 2.4 wt.% F at a  $\log fO_2$  of ~NNO-0.5, tin diffusivity can be well described by an Arrhenius relationship, as  $\log D = -8.28 - 4.21 \cdot 10^3/T$  where D and T are diffusivity coefficient (m<sup>2</sup>/s) and temperature (K), respectively. At more oxidized conditions, the diffusivity of tin becomes progressively slower. Using the same subaluminous melt composition, at NNO buffer, values for tin diffusivity, D, from 650 to 850 °C increases from  $7.8 \cdot 10^{-14}$  to  $1.5 \cdot 10^{-12}$  m<sup>2</sup>/s, respectively. At a  $\log fO_2$  of NNO+3.5, and temperature of 650 to 800 °C, D increases from  $8.1 \cdot 10^{-15}$  to  $1.5 \cdot 10^{-14}$  m<sup>2</sup>/s, respectively. In peralkaline melt at 750 °C, 2 kbar and NNO  $fO_2$  buffer, no significant variation in diffusivity of tin is observed over an increase in the F contents of these melts from 3.7 to 4.2 wt.% F, respectively. Tin diffusivity also increases by half a log unit with an increase of the Cl content in the melt from 0 to 0.4 wt.% Cl, and ~1 log unit for an increase of the F content in the melt from 0 to 1.12 wt.% F. At a  $\log fO_2$  of ~NNO in pegmatite melt from 650 to 850 °C, tin diffusivity, D, increases from  $6.7 \cdot 10^{-14}$  to  $8.2 \cdot 10^{-12}$  m<sup>2</sup>/s, respectively. Whereas at a  $\log fO_2$  of NNO+3.5 at 650 to 800 °C, D varies from  $4.5 \cdot 10^{-15}$  to  $5.5 \cdot 10^{-13}$  m<sup>2</sup>/s, respectively. Thus, at ~NNO in pegmatite, tin diffusivity can be described as  $\log D = -2.05 - 10.27 \cdot 10^3/T$ , whereas, at NNO+3.5, diffusivity in pegmatite melt can be described as  $\log D = 2.10 - 15.18 \cdot 10^3/T$ .

**Keywords:** Cassiterite; Diffusivity; Granite; Melt; Pegmatite; Peralkaline; Peraluminous; Subaluminous; Tin.

## 2.1. Introduction

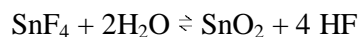
Like other minerals, metallic tin (Sn) occurs in crystal form, and it has been found in fine black or brown crystals. Due to the breaking of these crystals, a "tin cry" is heard when a bar is bent. It is surprising that tin was discovered and used so early in ancient civilizations. The metal was first found as water-worn pebbles or nuggets in streams, in placer deposits. Malay States, Bolivia, Indonesia, Belgian Congo, Nigeria contribute to the most of the world's supply of tin ore, whereas Cornwall (England) contributes most supply of tin. Regarding physical and chemical properties of tin, it resists distilled water, sea water, and soft tap water, but is attacked by strong acids, alkalis, and acid salts. Oxygen in solution accelerates the attack. When heated in air, tin forms cassiterite ( $SnO_2$ ). Since  $SnO_2$  (often called tinstone) has a non-metallic appearance, only its heavy weight suggests the presence of metal. Cassiterite is the most important ore mineral of tin, and the only ore mined in ancient times. It is found as a primary constituent of igneous rocks, especially pegmatites, and as a hydrothermal mineral in association with tungsten. Rare-metal ongonites are one of the sub-volcanic analogs of tin-bearing granites. These ongonites are an example of quenched or partially crystallized magmas from tin-bearing lithium-fluorine granites. Tin commonly accumulates in the residual tin-bearing magmas (Antipin et al., 1981). Antipin et al. (1981) also suggested that the distribution coefficient,  $K$ , of tin between mineral and melt is dependent on F-concentration of the melt, which indicates that F plays an important role in producing Sn-mineralization. Antipin et al. (1981) also found differences in values of mineral/melt coefficients of tin for potash feldspar and micas. Micas become successively enriched in tin as tin accumulates in magmas. This interpretation can lead to association of one of the mica mineral, Zinnwaldite, with tin minerals in nature.

Over the past 150 years, considerable effort has been devoted to genetic studies of geological features of primary tin deposits. Pioneering field work by Daubrée (1841) and De Beaumont (1847) led to realization that virtually all economic primary tin deposits are genetically associated with granitic intrusions. They also established the identity of common mineral assemblages associated with tin deposits in Europe. These observations were confirmed and extended by Vogt (1895), who recognized the association of  $SnO_2$

mineralization with vein formation. An early summary of tin deposits and theories of their origin were given by Singewald in 1912. At about the same time, Hess and Graton (1905) and Ferguson and Bateman (1912) made an inventory of the field relations and geological characteristics of tin deposits of the world known at that time. Schröcke (1954), Turneure (1960), Hosking (1969), Lugov (1965a,b), Bauman (1970), Kelly and Turneure (1970), Shcherba (1970), Groves et al. (1972), Bauman et al. (1974), Sillitoe et al. (1975), Patterson (1977), Nekrasov (1984), Heinrich (1990), Tischendorf and Forster (1990), Černý (1991a,b,c), Breiter et al. (1997), London (1997), Thomas and Klemm (1997), Audetat et al. (2000), Haapala and Thomas (2000), Thomas and Webster (2000), Muller et al. (2001), Kontak and Clark (2002), Benzaazoua et al. (2003), Lenharo et al. (2003), Mlynarczyk et al. (2003), Černý et al. (2004) and Webster et al. (2004), have carried out studies detailing the mineralogy and geology of natural tin and other rare-element deposits associated with granites and pegmatites. These have been accompanied by overviews of tin deposits, including those by Barsukov (1957), Schuiling (1967), Štemprok (1969), Hosking (1973, 1974), Štemprok and Voldán (1978), Taylor (1979a), Tyalor (1979b), Štemprok (1982), Wilson et al. (1983), and Štemprok (1990a,b). Jackson and Helgeson (1985) studied relative role of changing temperature,  $fO_2$ , pH, and solution composition on the hydrothermal solubility of cassiterite at temperatures  $\leq 350^\circ\text{C}$ , and recent study of Jiang et al. (2004) shows geochemical data on trace and rare-earth elements in cassiterite from Yunlong tin deposit, Yunnan (China). In addition to his field observations, Daubrée (1841) was the first to carry out geochemical investigation on the origin of tin deposits. He succeeded in crystallizing  $\text{SnO}_2$  by passing steam and volatilized stannic chloride through a heated porcelain tube. Based on the results of these experiments, he suggested that tin was transported as a chloride or fluoride complex in a vapor phase. The results were later confirmed by Sainte-Claire Deville (1861), Hesp and Rigby (1972), and Hosking (1972). The world's largest and most economically productive magmatic-hydrothermal Sn-W deposits of Europe, South America, and southeast Asia are derived from extremely evolved, peraluminous granites, granitic pegmatites, and aplites that are also variably mineralized with Li, Rb, Cs, Ta, Nb, Be, Mo, and Cu (e.g., Lehmann, 1990; London, 1992; London et al., 1993; Raimbault et al., 1995; Charoy and Noronha, 1996; Webster et al., 1997; Linnen, 1998a; Linnen, 1998b). The granites are considered to be the main source of volatiles, ore metals, and heat energy that is involved in ore formation (e.g., Lehmann,

1982; Lehmann, 1990; London, 1992; Raimbault et al., 1995; Webster et al., 1997; Webster and Rebbert, 2001; many others). Whole rock samples from these systems are also enriched in P and F, some samples contain abundances exceeding that reported for any subalkaline igneous rock (e.g., Schuiling, 1967; Kovalenko et al., 1968; Ryabchikov et al., 1978a,b; London, 1992; Raimbault et al., 1995; Webster et al., 1997) which implies that the granitic magmas were also enriched in P and F. Most of the tin ore that occurs as cassiterite in these systems is localized in structures generated by pneumatolytic mechanisms, the presence of disseminated SnO<sub>2</sub> in granites, pegmatites, and aplites has led many investigators to propose that SnO<sub>2</sub> may precipitate directly from granitic magmas (e.g., Schröcke, 1954; Thomas, 1989; Lehmann, 1990; Linnen et al., 1992; Thomas, 1994; Linnen, 1998a; Linnen, 1998b), but this interpretation needs to be reconsidered. So, it is fundamentally more important to improve our knowledge of late-stage, highly-evolved, mineralizing granitic liquids. Moreover, chemically-specialized granitic rocks experience multiple episodes of intrusion and hydrothermal alteration (e.g., Carten et al., 1988; Heinrich, 1990; Kontak, 1990; Holtz et al., 1993; Seltmann, 1994; Schwartz et al., 1995; Webster and Duffield, 1991), and consequently a whole-rock data also reflect the secondary influences of greisenization or other forms of hydrothermal alteration that are attendant on mineralization processes. A related problem is that it is very difficult to determine accurate bulk compositions of pegmatitic rocks and pre-emplacment compositions of liquids that crystallize as pegmatites because of their coarse and variable grain size. Silicate melt inclusions in natural rock-forming minerals are a valuable source for determining the conditions of formation of magmatic rocks and the concentration of trace elements, ore elements, and volatiles in natural aluminosilicate liquid(s).

Fluorine-bearing minerals such as fluorite, topaz, and some lithium micas are commonly associated with cassiterite in deposits of the so-called quartz cassiterite formation of magmatic origin. This observation led as early as about the middle of the past century (Daubrée, 1841) to the assumption that tin is transported from Earth's interior to the sites of deposition in the form of volatile tin fluoride. This reaction:



has been used since that time as a classical example of the pneumatolytic mechanism of mineral formation. Modern experimental modeling of this reaction was absent until 1972 when Hesp and Rigby volatilized tin from tin dioxide in a silica environment in a flow of ammonium halides. They applied an apparatus where sublimation occurred in the absence of water and concluded that the vapor phase transportation of tin in the form of tin fluoride could take place in the relatively narrow temperature range of 600-800 °C, and that the pneumatolytic transportation of tin by chloride appears more likely (Taylor, 1979a,b; Nekrasov et al., 1980; Taylor and Wall, 1992; Taylor and Wall, 1993; Kovalenko et al., 1996). The formation of tin tetrafluoride by the reaction of F with SnO<sub>2</sub> in a dry container was described by Haendler et al. (1954) and the reaction was found to be complete at 500-550 °C. However, tin tetrafluoride easily hydrolyses in the presence of water and thus Barsukov (1974) pointed out that Daubrée reaction can take place only in an anhydrous gas phase that can be hardly be postulated for the natural environment. The presence of abundant water eliminates the possibility of tin being transported as SnF<sub>4</sub> in the upper earth's crust. However, tin and fluorine might be associated in an under-crust environment if it is postulated that the mantle could be a possible source for the tin and accompanying tungsten and fluorine (Sillitoe, 1974).

Pegmatites are coarse-grained igneous rocks having a grain size of 3 cm or more and can host cassiterite. Most pegmatites have a granitic composition, i.e., are composed of quartz, feldspar and mica, and differ from granites by the fact that the crystals are larger in size. In addition to these basic minerals, there are also generally rare minerals. Pegmatites are known to contain aquamarine, tourmaline, beryl, topaz, cassiterite, fluorite, apatite, tin and tungsten and a host of other minerals. Minerals formed in pegmatites literally had the time to enjoy the benefits of a slow crystallization process from a rich chemical stew. One of the most common indicators of a potential pegmatite is the presence of an aplite dike. The pegmatite bodies occur as lenses within the aplite dike structures. Pegmatites are most famous for their large, high quality mineral specimens. Pegmatite begins as a concentrated residual rock, rich in water, chlorine, boron and other elements deep within the earth under tremendous pressure. As the surrounding rock begins to solidify, the minerals (quartz and feldspar) start to concentrate. Eventually the concentrated material cools off and if the cooling is slow enough, large crystals begin to form. Geologists have presumed that a



positive correlation exists between the size of a crystal and the time frame in which it grows; therefore, in comparison to much finer grain size of slowly cooled granite plutons, the crystals of pegmatitic dimensions should require geological eons to form (see London, 2004). The shape of pegmatite is influenced by type of rock that surrounds it. Pegmatites also exist in nature as spherical, bowed or curved, pipe-like, tear shaped or irregularly branched. Most often they are lens shaped or table like. But, recent efforts to model the cooling histories of some chemically evolved pegmatite dikes indicate that they cooled quickly. The calculated cooling rates [1. The large Harding pegmatite (20 meters thick), New Mexico, would have cooled completely to its solidus in approximately 3-5 months after emplacement (Chakoumakos and Lumpkin, 1990); 2. The gem-bearing Little Three dike (2 meters thick), Ramona, California, appears to have cooled to its solidus in about 25 days (Morgan and London, 1999); 3. The famous gem-producing Himalaya-San Diego pegmatites (about 30 cm thick), Mesa Grande, California, may have cooled to their solidi in just over one week (Webber et al., 1999)] are nothing short of revolutionary because most text books and dictionaries define pegmatites as the product of very slow cooling.

Pegmatites can be classified as either simple or complex. Simple pegmatites contain the common minerals of quartz, potassium feldspars (orthoclase) and mica (muscovite/biotite). On the other hand, Complex pegmatites result from the crystallization of the last gaseous portion of magma, which contains a higher concentration of rare-elements. Naturally, the complex pegmatites contain a greater variety of minerals, including rarer ones. But, the vast majority of pegmatites consist almost exclusively of quartz and feldspars and lack exotic minerals, miarolitic cavities, and hydrothermal alteration envelopes. Their compositions plot close to the haplogranite minimum at elevated  $H_2O$  content (Jahns and Tuttle, 1963; Norton, 1966). Rare-element pegmatites that are rich in quartz and feldspars or exotic minerals constitute  $< \sim 2\%$  of any particular pegmatite group (e.g., Černý, 1991c). Prior studies of granitic pegmatites have investigated some constituents in volatile-rich, silicate-bearing inclusions (Lemmler et al., 1962; London et al., 1982) and silicate melt inclusions (e.g., Reyf, 1973; Skryabin, 1976), the studies of Kovalenko et al. (1996) and Webster et al. (1997), represent the first attempts to constrain, comprehensively, the abundances of major, minor and trace elements in late-stage, pegmatite-forming liquid through the analysis of silicate melt inclusions (Lammler

et al., 1962; London et al., 1982; London, 1987; Černý, 1991b,c; Linnen et al., 1992; Linnen and William-Jones, 1993; London, 1996; Webster et al., 1997; Linnen, 1998b; Morgan and London, 1999; Thomas and Webster, 2000; Thomas et al., 2000; London, 2004).

Individual regions or districts within tinfields are often enriched with respect to certain components, and two main types can be recognized, boron-rich environments and fluorine-rich environments. These two environments can occur at the province scale (e.g. the boron-rich province of Southwestern Thailand or the fluorine-rich provinces of Nigeria and Erzgebirge) or as small components within provinces of mixed character, e.g., the SW England and Herberton (Australia) provinces. The enrichment in F and B can be expressed as a late magmatic stage in which fluorite, tourmaline, Li-mica, etc. crystallize, and/or at the postmagmatic stage characterized by the development of a similar suite of hydrothermal minerals (Pollard et al., 1987). Other components (e.g.,  $CO_2$ , Cl, and to a lesser extent  $CH_4$ ,  $N_2$ , etc.) in addition may be present in F- and B-rich environments, as well as in other, non B- and F-rich tin environments. The most predicted common styles of tin mineralization in boron-rich regions are the vein and stockwork deposits (e.g., Hosking, 1973; Jackson, 1979; Rivas, 1979; Taylor, 1979a,b).

In this study, the diffusion profile technique is used to determine cassiterite solubility and tin diffusivity as a function of the amounts of F and Cl in the melt, temperature,  $fO_2$  and A.S.I. melt composition in order to provide a better understanding of the behavior of tin in granitic melts. These results thus have direct implications to the understanding of the generation of tin granites. It is also known that the solubilities of a variety of other metals are  $fO_2$  dependent and that many of these metals also form alloys with Au, Pt, etc., the method employed here, potentially has further applications in experimental petrology. Lehmann (1990) proposed that the generation of tin granites is related to redox conditions and tin is in  $Sn^{2+}$  valence state in reduced silicate melts. Since many metals have at least two valences at geologically reasonable redox conditions the results of this work also have some implications for the behavior of metals in silicate melts in general. The problems of alloying were observed by some studies (e.g., Webster and Holloway, 1988; Taylor and Wall, 1992) where interaction of melt and excess water (or

fluid phase) causes modifications of melt composition. So, avoiding the problem of alloying was a major concern in the present study. This study eliminated the problems of Sn forming an alloy with noble metals used as containers, while maintaining a better control on redox conditions. A pure tantalum (Ta) foil (>99.9 % Ta) is placed inside a noble metal (Au) container, preventing contact between the cassiterite crystal and the surrounding walls of the Au container. The Ta foil is non-reactive so the tin diffusion as well as cassiterite solubility data in silicate melts should be more accurate. Cassiterite solubility in this study was determined in a hydrous, slightly H<sub>2</sub>O-undersaturated to H<sub>2</sub>O-saturated melt; thus, the problems of changes in melt composition and loss of Sn alloying were both avoided. The method of Harrison and Watson (1983) was adapted to measure diffusion profiles of SnO<sub>2</sub> away from cassiterite crystals at fixed oxygen fugacities, from which the information on the solubility, diffusivity, and structure of Sn in haplogranitic melts can be obtained.

## 2.2. Experimental and analytical methods

### 2.2.1. Starting materials

The starting glasses of peraluminous (A.S.I.  $\geq 1.2$ ), subaluminous (A.S.I. = 1.0), peralkaline (A.S.I. = 0.6) and pegmatite composition, were prepared by mixing carbonates and oxides as  $Na_2CO_3$ ,  $K_2CO_3$ ,  $Al_2O_3$  and  $SiO_2$ .  $AlF_3$  and  $K_2SiF_6$  were added to the carbonates and oxides mixture, as a source of fluoride to prepare all starting glass compositions from peraluminous (A.S.I.  $\geq 1.2$ ) to peralkaline (A.S.I. = 0.6). The ratio of both components was chosen so that the A.S.I. in the glasses remained unchanged. Four different starting compositions broadly with three different alumina saturation indices (A.S.I.) were synthesized: a peraluminous (A.S.I.  $\geq 1.2$ ), subaluminous (A.S.I. = 1.0), peralkaline (A.S.I.  $\leq 0.6$ ) and a subaluminous pegmatite composition.

Peraluminous starting glass compositions were synthesized by adding  $Na_3AlF_6$  and  $AlF_3$  to glass 1, so as to obtain 1.12 wt.% F and 2.12 wt.% F in the final product (to be used as a starting glass in experiments; see Appendix; Table A.1 for details). In glasses 1 and 2, F was introduced so that F replaced a stoichiometrically equivalent amount of O ( $2F = O$ ) while the molar Al/(Na + K) ratio was kept constant. The starting glass 3 (see Table A.1) was prepared with a mixture of oxides of Si, Al, Ca, Na, K and Fe, and is nearly same as glass 1, but F-free. The starting material was placed in an open platinum crucible and melted at 1600 °C / 1 atm for 2 to 3 hours in a furnace. After quenching the glass was crushed and melted again at 1600 °C / 1 atm for 1-2 hours to obtain a homogeneous glass. In order to produce  $H_2O$ -bearing starting glasses, dry glasses of peraluminous composition were hydrated for 4-6 days at 800-850 °C and 2 kbar. Three Cl-bearing starting glasses (glasses 4, 5 and 6; see Table A.1) were also synthesized at 850 °C and 2 kbar by adding diluted HCl- $H_2O$  fluid (slightly  $H_2O$ -undersaturated) to Cl- and F-free glass 3 (see Table A.1 for details). The glasses were synthesized in *h*CSPVs at 850 °C and 2 kbar for 6-7 days. The  $fO_2$  conditions were buffered by a Ni-NiO assemblage. For these experiments, deionised  $H_2O$  or dilute HCl (33.5 wt.%) was loaded in gold capsules (inner diameter 5.0 mm, outer diameter 5.4 mm, length 45 mm), together with the dry starting glasses (Glass 1

and 3). The samples were sealed in gold capsules by arc welding. Water contents in the hydrous starting materials were determined by Karl Fischer titration (KFT; cf. Behrens et al. 1996). The variation of the duplicate analyses was less than 0.03 wt.%. The water content of the most of hydrous glasses was kept to be close to slightly water-undersaturated or water-saturated varied between 5.1 and 6.2 wt.%, except for two starting glasses (oversaturated w.r.t.  $\text{H}_2\text{O}$ ) of peraluminous composition containing 1.12 wt.% F and no F (see Table 2.1 and Table 2.2 for details), in which water concentration is measured to be 6.88 and 7.26 wt.%  $\text{H}_2\text{O}$  in melt, respectively.

Subaluminous starting glass compositions were prepared by mixing carbonates and oxides of  $\text{Na}_2\text{CO}_3$ , and  $\text{Al}_2\text{O}_3$  and  $\text{SiO}_2$ , respectively (PP0%F, PP2%F, PP4%F, PP6%F and PP12%F; see Table A.3. for more details).  $\text{AlF}_3$  was added to the carbonates and oxides mixture as a source of fluoride to the starting glass. The mixtures were loaded into Pt crucibles, degassed at 800 °C, melted at 1200 °C for 20 minutes, and quenched by placing the Pt crucible in water. The freshly prepared starting glasses were grounded mechanically in an agate mortar, and finally melted at 1500 °C for 20 minutes, quenched by placing the Pt crucible in water, then again grounded in an agate mortar, whereas an another subaluminous glass composition, S2 (see Table A.3) was prepared using mixture of  $\text{Na}_2\text{CO}_3$ ,  $\text{Al}_2\text{O}_3$  and  $\text{SiO}_2$ . Unlike addition of  $\text{AlF}_3$  in peraluminous and another subaluminous starting glasses (see above),  $\text{K}_2\text{SiF}_6$  was added to carbonate and oxides mixture as a source of fluoride and potassium for glass S2. Thereafter, the prepared mixture was loaded into a Pt crucible, degassed at 850 °C, melted at 1600 °C for about 30 minutes, quenched by placing the Pt crucible in water. The freshly prepared starting glasses were grounded mechanically in an agate mortar, and finally melted at 1600 °C for 1 hour, quenched by placing the Pt crucible in water following grounded the starting glass in an agate mortar. The experiments were performed in vCSPVs at 2 kbar and in the temperature range of 700-850 °C for 5-43 hours, except for two experiments, which were conducted for 48 hours and 72 hours. The buffer assemblages composed of a cobalt rod (Ni-NiO-0.5 to 1.5) and hematite-magnetite powder (Ni-NiO+3 to +5) were used to obtain reducing and oxidizing conditions, respectively. For obtaining reducing conditions, water was used as a pressure medium, whereas Ar was used to obtain more oxidizing conditions during experiments. Same kind of procedure as for subaluminous starting compositions,

was adopted to obtain F-free and F-bearing peralkaline starting glass compositions (PB0%F, PB2%F, PB4%F, PB6%F and PB10%F; see Appendix; Table A.4 for more details).

The pegmatitic starting glass composition (P FDP; see Table A.5) is based on the intersection of the granite minimum curve, shifted by the addition of  $P_2O_5$  to the haplogranite system, with the Ab-Or tie-line (cf. London et al., 1993). This pegmatite starting composition, P FDP, contains ~1 wt.%  $Li_2O$ , 4.3 wt.% F, 1.7 wt.%  $P_2O_5$  and 2.25 wt.%  $B_2O_3$ . Freshly prepared dried pegmatitic (A.S.I.=1.0) starting glass was hydrated at high pressure and temperature to obtain water-bearing glass, which was later used as prehydrated starting material for further experiments. The water content of the hydrous glass was ~5 wt.% and the glass were slightly water-undersaturated. The experimental method adopted for pegmatitic starting glass compositions was identical as explained as explained above (see text). The experiments were performed in  $\nu$ CSPVs at 2 kbar and in the temperature range of 650-850 °C. The run duration of all experiments performed using pegmatite starting composition varied between 6-76 hours. The buffer assemblage was composed of a cobalt-rod and hematite-magnetite powder.

In order to produce  $H_2O$ -bearing starting glasses, all freshly prepared dried starting glasses (peraluminous, subaluminous, peralkaline and pegmatite) were hydrated for 4-6 days at 800-850 °C and 2 kbar, which were subsequently used as starting materials for further experiments. The  $fO_2$  conditions were buffered by a Ni-NiO assemblage. For doing so, deionised  $H_2O$  was loaded in gold capsules (inner diameter 5.0 mm, outer diameter 5.4 mm, length 45 mm), together with the dry starting glasses. The samples were sealed in gold capsules by arc welding. Water contents in the prehydrated starting materials were determined by Karl Fischer Titration (see Section 2.3.3.3 for more details on KFT). The variation of the duplicate analyses was less than 0.03 wt.%. The water content of the hydrous glasses varied between ~5.0-6.2 wt.%  $H_2O$  in melt except for two peraluminous starting glasses (see Table 2.1 and 2.7), which contains ~7.0 wt.%  $H_2O$  in melt. Thus, most of the starting compositions were either slightly water-undersaturated or close to water-saturated.

### 2.2.2. Experimental method

The experimental technique used was similar to that of Linnen et al. (1995), which was modified from Harrison and Watson (1983). Some modifications have also been done to avoid any loss of Sn to the noble metal containers (Au-capsules) used for the experiments in this study. For preparing a sample capsule, technique used by Bhalla et al. (2004), is modified and implemented to this study. For preparing thin sections in this study, five steps have been used to prepare a sample capsule: 1) Noble metal container (Au capsule) was welded at one end. 2) A tantalum (Ta) foil (thickness: 0.025 mm; purity: >99.9 % Ta) was chosen as a non-reactive medium to separate the sample from the capsule wall. For doing so, a circular piece of this foil was cut and placed at the bottom of the Au capsule. To isolate the  $SnO_2$  crystal completely from Au capsule walls, Ta foil was folded in rounded manner and placed along the inner walls of Au capsule, in such a way that  $SnO_2$  crystal does not come in contact with Au capsule walls. 3) Hydrous starting glass powder (silicate melt) is crushed and inserted in a ~15 mm long Au capsule. 4) A natural tabular  $SnO_2$  crystal (~1x1x2 mm) was polished, and placed in the center of the capsule. 5) The top end of the capsule was crimped and welded shut. All accessories except glass powder, used to make sample capsule is shown in Fig. 2.2. After the experiment, a concentration gradient of tin in a melt adjacent to a  $SnO_2$  crystal is measured. All the above steps helped to minimize the formation of Au-Sn alloy, which may result in serious experimental problems. The experiments were performed in a different  $\log fO_2$  ranges from NNO-2.0 to NNO+5.0 in  $hCSPVs$  and  $vCSPVs$  at 2 kbar and in the temperature range of 600-850 °C for 5-68 hours.

In addition to solubility and diffusion experiments, a few apparent equilibrium experiments have been performed for A.S.I. = 0.6 composition in the  $vCSPV$ . For these experiments, a mixture of roughly 50% cassiterite crystals and 50% water-saturated (prehydrated) glass were sealed in Au capsules (~10 mm length; 4.4 mm o.d.; 4.0 mm i.d.) and experiments were carried out at 800 °C, 2 kbar for 22 days (528 hours) in different  $\log fO_2$  ranges from NNO-1.0 to NNO+5.0. The equilibrium experiments conducted at a  $\log fO_2$  of NNO-1.0 failed; after quenching the Au capsule had numerous small holes from where  $SnO_2$  crystals had been in contact with the Au capsule walls. This resulted in tin

diffusion in Au from point sources, forming Sn-Au liquids, and when the diffusion was such that the liquid alloy reached the outer capsule wall the water pressure medium became in contact with melt, and by the end of the experiment the melt had been completely dissolved and the capsule was empty.

After quenching, the capsules were weighed to check for any weight loss. In order to find the exact orientation of cassiterite crystal in the silicate melt, capsules were opened before cutting the experimental sample with a saw-wheel (0.3 mm thickness) longitudinally or transversely. In most of the samples, the run product glass containing the cassiterite crystal was taken out of the capsule carefully (for details, see Fig. 2.4) and thereafter, SnO<sub>2</sub>-bearing glass was cut perpendicular to the base of the cassiterite crystal (see Fig. 2.5 for details). In rest of the experiments, after opening sample capsule, it is cut normal to the surface of SnO<sub>2</sub> crystal. Orientation was an important parameter to take into account in this study, as an orthogonal orientation of the section is necessary in order to accurately measure the diffusivity of tin in silicate melts. The experimental products were always glass + SnO<sub>2</sub>, except in runs GGC37 (see Table 2.1) and 52 (see Table 2.2 for details), which had quench crystals (feldspar) that formed near the SnO<sub>2</sub> crystal due to a slow cooling rate. Because the exact orientation of the SnO<sub>2</sub> crystal in the capsule was not known, the studied sections were not always strictly perpendicular to the SnO<sub>2</sub> crystal. This may have influenced the calculation of diffusivity of SnO<sub>2</sub>, but is not expected to have influenced the solubility of SnO<sub>2</sub>, which corresponds to the concentration of SnO<sub>2</sub> at the crystal-melt interface. But, a few experiments were repeated where the studied sections were prepared perpendicular to the SnO<sub>2</sub> crystal. It allowed this study to calculate diffusivity with a minimum error. In order to minimize the error on correct diffusivity of tin, systematic error is calculated (see Section 2.2.6 for calculation of systematic error in details). In some experiments [GGC 3, GGC 4, GGC 5 (see Table 2.1); 4, 6 (see Table 2.3); 4 DF3, 5 DF1 (see Table 2.1)] two sections were prepared, one longitudinally and one transversely relative to the axis of the capsule. This procedure allowed us to investigate concentration profiles of tin along three orthogonal directions.

### **2.2.3. Experimental Technique**



### **2.2.3.1. Equipment**

Experiments were performed in two laboratories (University of Hanover, Germany and University of Waterloo, Canada) using cold seal pressure vessels. The autoclaves in Waterloo are constructed of Udimet 720<sup>®</sup>, a Ni-rich alloy that contains Cr, Co, Ti, and Mo as well as several other elements at trace levels. The autoclaves used in Waterloo are vertically operated-cold seal pressure vessels ( $\nu$ CSPVs) equipped with a rapid quench. The upper part of the autoclave is placed inside a furnace and is separated from an extension tube by a coupling and a double cone. Water circulates inside the coupling, outside of the double cone, and the experiment is quenched by dropping capsules into this cold zone (see Fig. 2.1). This is accomplished by having the capsule held at the end of the autoclave during the experiment by a support rod. The support rod remains in place because a small stainless steel sleeve is fixed to the support rod by setscrews. The sleeve + rod assembly is held in place by a donut-shaped magnet, outside the extension tube, fixed in place by an O-ring with a setscrew. In order to quench an experiment, the setscrew is loosened, both the O-ring and magnet fall, and the capsule also falls into the cold zone such that quench is near instantaneous. Temperature was measured using an external Ni-CrNi thermocouple that was calibrated both against the melting temperature of pure NaCl as well as an internal multi-point thermocouple. The internal multi-point thermocouple had 4 measurement points, over a distance of 4 cm, and the thermocouple point at the tip was also calibrated against the melting temperature of pure NaCl. The internal thermocouples established that the temperature variation in these autoclaves at 700-800 °C and 2 kbars ( $\text{H}_2\text{O}$  pressure medium) was typically less than 5 °C over the top 3 cm where capsule are placed. The external thermocouple has an error of approximately  $\pm 1$  °C, so the total error in measuring the temperature of the experiments is  $\pm 5$  °C at 800 °C and 2 kbars. Pressure was measured by transducers and results were checked against a pressure gauge. The transducers and gauge are factory calibrated and have an accuracy of better than  $\pm 0.1$  kbars. Several experiments were conducted using Ar as the pressure medium, because of the use of Ar instead of water should produce more oxidized conditions (Matthews et al., 2003). In such cases the pressure is attained with a pressure pump run on current. Although the Ar pressure was slightly lower or higher than the  $\text{H}_2\text{O}$  pressure, it is not believed in the study that a small pressure difference has any significant effect on the redox conditions of the experiment [see Chou (1987a) for pressure effect on  $f_{\text{O}_2}$ ].

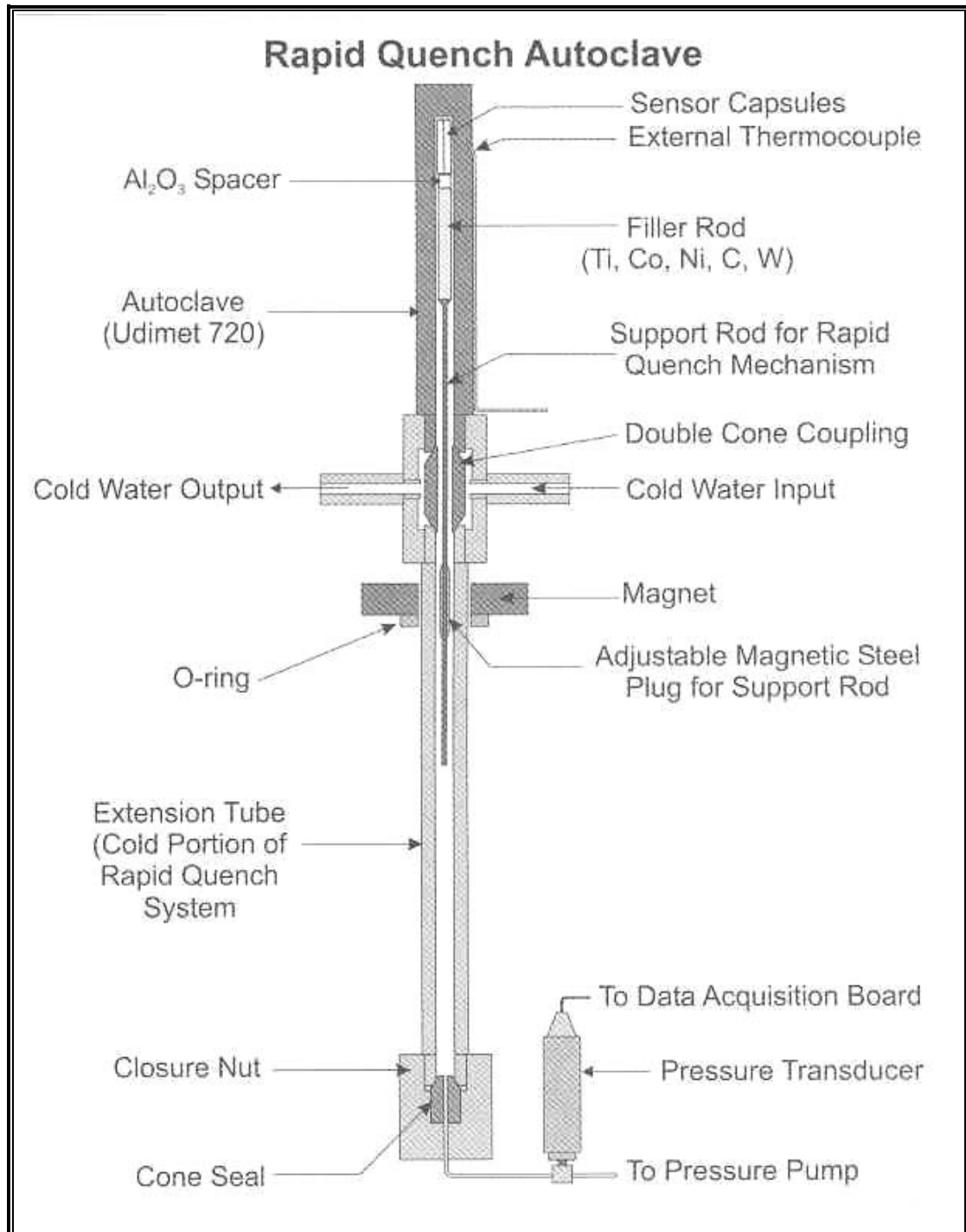
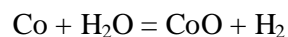


**Figure 2.1:** Systematic diagram of the rapid-quench, cold seal autoclave. The autoclaves were constructed of UDIMET 720 alloy, which has an approximate composition of 56.0% Ni, 16.0% Cr, 14.7 % Co, 5.0 %Ti, 3.0 % Mo, 2.5 % Al and 1.25 % W. (See [www.specialmetals.com/products/data\\_720.htm](http://www.specialmetals.com/products/data_720.htm)). This figure is redrawn from Matthews et al. (2003).

### 2.2.3.2. Experimental configuration

The experimental configuration for working at reduced conditions is shown in Figure 2.1. During experiment, the autoclave is inserted into a vertical furnace. Two hydrogen sensor capsules are placed at the top end within the autoclave. The capsules were made from 2 mm o.d., 1.8 mm i.d., 20 mm length Pt tubing after the method of Chou (1987a). In the “A” sensor, approximately 20  $\mu\text{L}$  of distilled water was loaded into a capsule together with a mixture of ~20 mg Ag and 20 mg AgCl, and the capsule was welded shut. The “B” sensor consists of the same solid mixture together with 20  $\mu\text{L}$  of 3 or 5 m HCl. The sensors were placed inside a container constructed of 5 mm o.d. Pt tube with a flat-bottom cap to prevent the sensors from catching on the sides of the autoclave during quenching. An  $\text{Al}_2\text{O}_3$  spacer, a filler rod, and the support rod for the rapid-quench mechanism are placed below the Pt container with the sensors. The spacer greatly reduces contamination of the Pt container by diffusion of metals (e.g., Co, Ti) from the filler rod during an experiment. Filler rods were constructed of materials that will change the intrinsic  $f_{\text{O}_2}$  of the autoclave. The filler rods were all 5 cm in length and 3-5 mm in diameter and Pt caps were placed over the ends of the rod to prevent any contact between the rod and the inside walls of the autoclave. Finally, the support rod for the quench mechanism is adjusted beneath the filler rod. The filler-rod technique is well suited to produce reduced conditions, by generating  $\text{H}_2$  through oxidation of a metal and dissociation of water, e.g.:



For producing oxidized (low  $f_{\text{H}_2}$ ) conditions, Ar is used as pressure medium. In such case,  $f_{\text{H}_2\text{O}}$  is much lower and thus the reactions are opposite to the ones that produced reduced conditions.  $\text{H}_2$  is consumed to produce  $\text{H}_2\text{O}$  and metal oxide is reduced to metal. Some of experiments were also performed in Hannover in the autoclaves which are horizontally operated-cold seal pressure vessels (*hCSPVs*). The *hCSPVs* used for the experiments were made of a Ni-rich alloy. The temperature was controlled by type K-thermocouple placed outside of the vessel close to the hot-spot zone. The vessels were

calibrated periodically and the temperature was known within  $\pm 10$  °C. The experiments were quenched by removing the vessel from the furnace and blowing compressed air around the vessel – the temperature inside the vessel dropped to  $\sim 200$  °C after 5 minutes (cf. Berndt et al., 2001). Pressure was measured with a strain-gauge manometer (accuracy  $\pm 0.03$  kbar), using two pressure media that allowed different  $fO_2$  ranges. In one case, water was used as pressure medium and the buffer was close to that of the Ni-NiO assemblage. In these experiments, the Ni-NiO powder was placed around the sample capsules. Because of the Ni-rich composition of the vessel, this buffer had a long lifetime and the buffer assemblage comprised Ni-NiO after the experiment (the intrinsic  $fO_2$  of the vessel was close to that of the Ni-NiO buffer). In other experiments, vessels were pressurized with argon and the oxygen fugacity was significantly higher. At 800-840 °C and 2 kbar, the oxygen fugacity measured by sensor capsules (Taylor et al., 1992) was Ni-NiO + 2.3 log units (Berndt et al., 2001). Hereafter, the runs buffered by the  $\leq$  Ni-NiO assemblage will be referred to as “NNO experiments” or runs under reducing conditions, and the experiments using hematite-magnetite assemblage and where argon is used as the pressure medium, will be referred to as “ $\geq$  NNO+2.0 experiments” or runs under oxidizing conditions.

## **2.2.4. Analytical techniques**

### ***2.2.4.1. Electron microprobe***

The compositions of the glasses were determined with a Cameca SX-100 electron microprobe with analytical conditions of 15 kV and 6 nA. Counting time for Na and K was 2 seconds for all starting glasses and run products, and 5 seconds for other elements. The beam was defocused to at least 10  $\mu\text{m}$  for starting glasses and run products. To measure Cl in the two starting glasses, 2-4 profiles of more than 40 analyses were performed. The length of each profile varied between 900-1200  $\mu\text{m}$ . Peak count time for each analysis of Cl in the melt was 30 seconds for the starting glasses as well as for the run products. The Cl content was homogeneous in the run product glasses (samples containing  $\text{SnO}_2$ ) as it was confirmed by traverses across the final run products. The precision of the Cl analyses in starting glasses is approximately 5% relative. The fluorine content of the starting glasses

was also analyzed by electron microprobe (see Lukkari and Holtz, 2000). Two analyses were typically done for checking the bulk composition of starting glasses. The precision of the analyses of the glass standard, and hence, the experimental glasses, is approximately 5% relative for Na<sub>2</sub>O and K<sub>2</sub>O, 5% for Al<sub>2</sub>O<sub>3</sub>, and 2% SiO<sub>2</sub>.

All the tin contents in the glasses were determined with a focused electron beam (2  $\mu$ m in diameter) and the peak counting time for determining SnO<sub>2</sub> was 120 seconds. Concentration profiles were determined at a 90° angle to the SnO<sub>2</sub>-glass interface. In few cases, first SnO<sub>2</sub> measurement point was on SnO<sub>2</sub> surface, which leads to an anomalous high concentration of SnO<sub>2</sub> in the melt. This problem has been solved by checking for same samples by selecting a measurement point at a distance of >20  $\mu$ m. To avoid fluorescence from the SnO<sub>2</sub> crystal in run products, each analysis has been done at a distance of >20  $\mu$ m from the SnO<sub>2</sub>-crystal boundary (cf. Linnen et al., 1995, 1996). Two to four profiles with 30-50 analytical points each were determined per sample. In most of the samples, the length of the profiles varied between 1000  $\mu$ m to 1200  $\mu$ m.

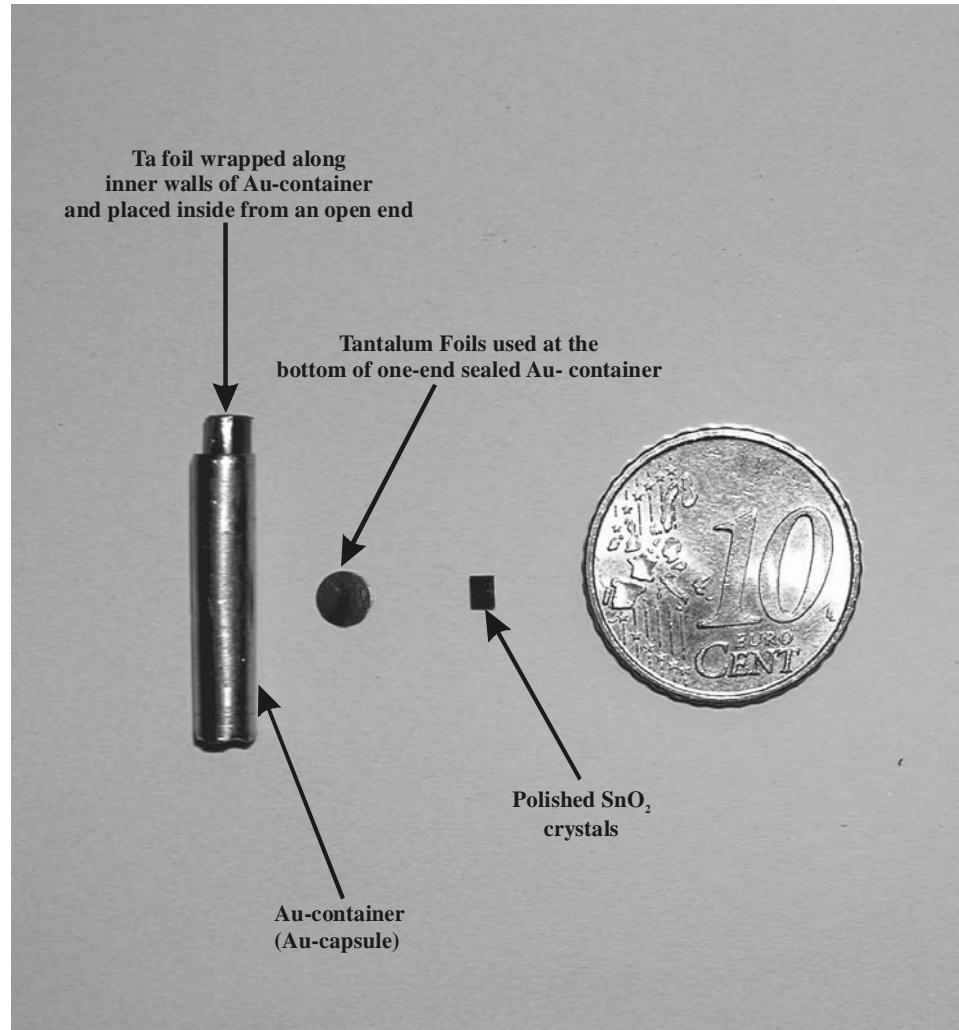
#### ***2.2.4.2. Inductively Coupled Plasma-Atomic Emission Spectroscopy***

The analyses were done by Actlabs in Lancaster, Ontario (Canada). Glasses were powdered with steel. Major elements were analyzed by inductively coupled plasma-Atomic Emission Spectroscopy (ICP-AES) after first fusing with lithium metaborate/tetraborate. Fluorine was measured by ion-sensitive electrode, boron by prompt gamma neutron activation analysis (PGNAA), and lithium by total digestion (without the lithium metaborate flux) followed by bulk analyses by ICP-AES.

#### ***2.2.4.3. Karl Fischer titration***

Water concentrations in the synthesized prehydrated glasses were determined by Karl-Fischer titration (KFT). KFT is based on the quantitative reaction of water with iodide:  $I_2 + SO_2 + H_2O = 2HI + SO_3$ . The amount of iodide necessary for this reaction is

**Figure 2.2:** The photograph is showing the set-up used for making sample capsule.



generated electrolytically (coulometric titration):  $2I^- = I_2 + 2e^-$ . Samples of 10-30 mg were loaded into the sample chamber and flushed by dried argon. Then water was extracted by heating the samples from room temperature to 1100-1300°C (typical duration of extraction: 7-10 min). Because hydrous glasses sometimes dehydrate explosively, leading to a sputtering of the glass out of the heating zone, the samples were wrapped in platinum foil. The extracted gas is transported by argon stream through an oxidation furnace, where  $H_2$  is oxidized to  $H_2O$ , into the titration cell (for more details see Behrens et al., 1996). Uncertainties in measured water contents were calculated on the basis of  $\pm 0.02 \mu g s^{-1}$  uncertainty in titration rate (Behrens et al., 1996).

#### 2.2.4.4. Preparation of samples and orientation of $SnO_2$ crystals in melt

**Figure 2.3:** The photograph is showing size of the samples used for the experiments in this study. This photograph shows two sealed sample capsules along with three different sample capsules cutting along a section perpendicular to one plane of  $SnO_2$  crystal after in the melt. This photograph also clearly shows the position of  $SnO_2$  crystal after the sample is cut along a chosen plane (exactly perpendicular to a plane of  $SnO_2$  crystal). The cassiterite ( $SnO_2$ ) crystal (black colored, embedded in the silicate melt) is pointed by an arrow.

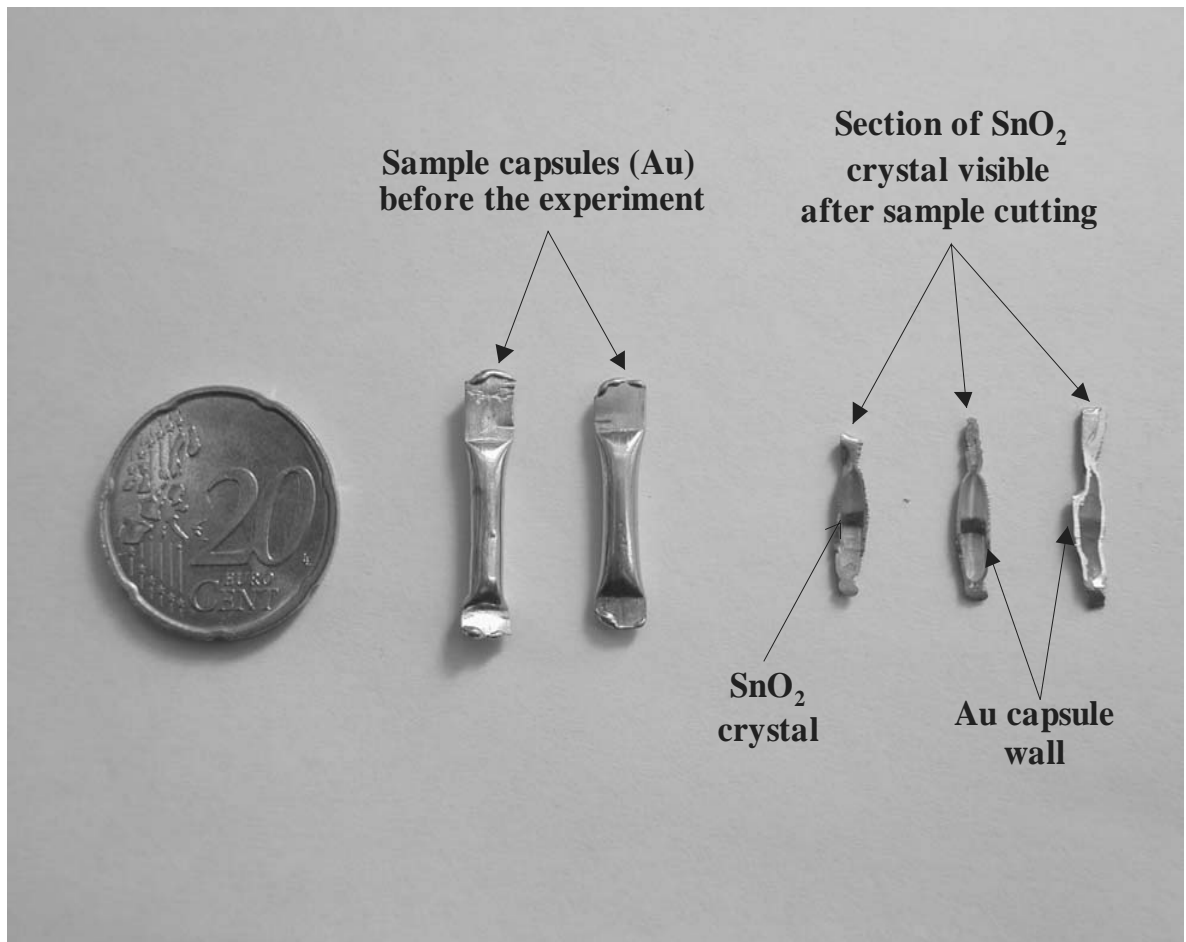




**Figure 2.4:** The photograph is showing average size of the run products. Two samples numbered (A) and (B) in the photograph (shown on right side), represent to the run products 4 DF3 and 5 DF1, respectively. Position of polished rectangular  $SnO_2$  crystal (black colored and embedded in silicate melt) marked by open oval circles, which can be clearly observed. In some cases, the samples were cut together with the surrounding metal capsule, whereas in most of cases, the silicate (glass) was removed carefully from the capsule walls. Latter case was a better technique to get a specific control on the orientation of  $SnO_2$  crystal and to cut the sample normal to crystal plane (shown in adjoining figure: Fig. 2.4). On the other hand, former case is adopted only, when capsules were crumpled badly after the experiment and thus, could not be extracted without any destruction to the silicate melt (glass). If this study assumes the former case, and cut the sample without opening the sample capsule, then cutting along the cylindrical axis, can led to a worse case.

$SnO_2$  crystal can be seen in the silicate melt after the experiment



**Figure 2.5:** The photograph is showing possible plane adopted for cutting the run product to get minimum discrepancy in calculating Sn diffusivity in melt. The  $SnO_2$  crystal as shown in the silicate melt (Run product 5 DF1; for more details see Table 2.1) after the experiment was always cut perpendicular to the respective position of the crystal into the silicate melt. The cutting plane was always considered to be perpendicular to at least two planes of the crystal.

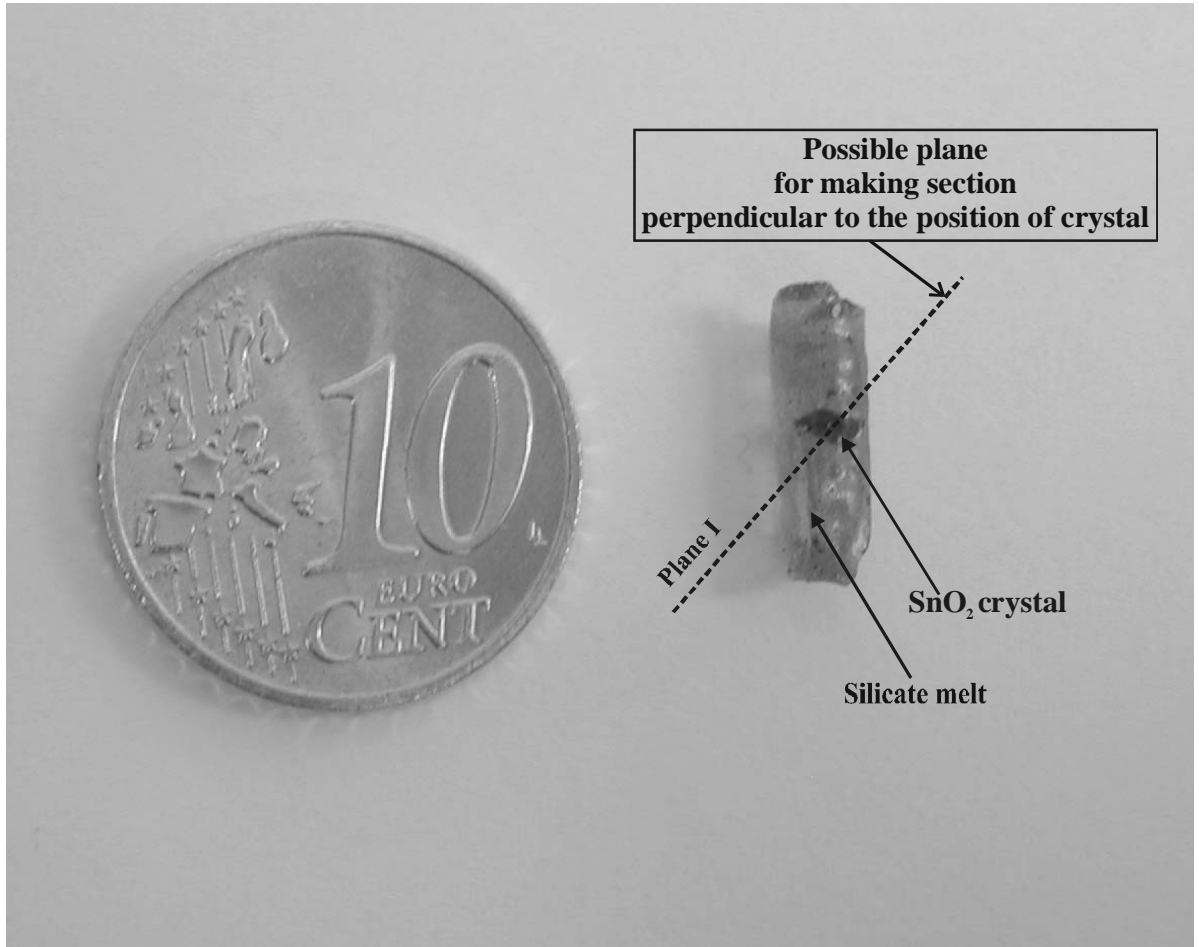


**Figure 2.6:** The photograph is showing two different run products with their halves after cutting them perpendicular to the possible plane adopted while taking into account the final position of  $SnO_2$  crystal in the melt. The figure shows two halves of a run product in which  $SnO_2$  crystal can be clearly seen while cut in two halves. The cutting plane was always considered to be perpendicular to at least two planes of the crystal.

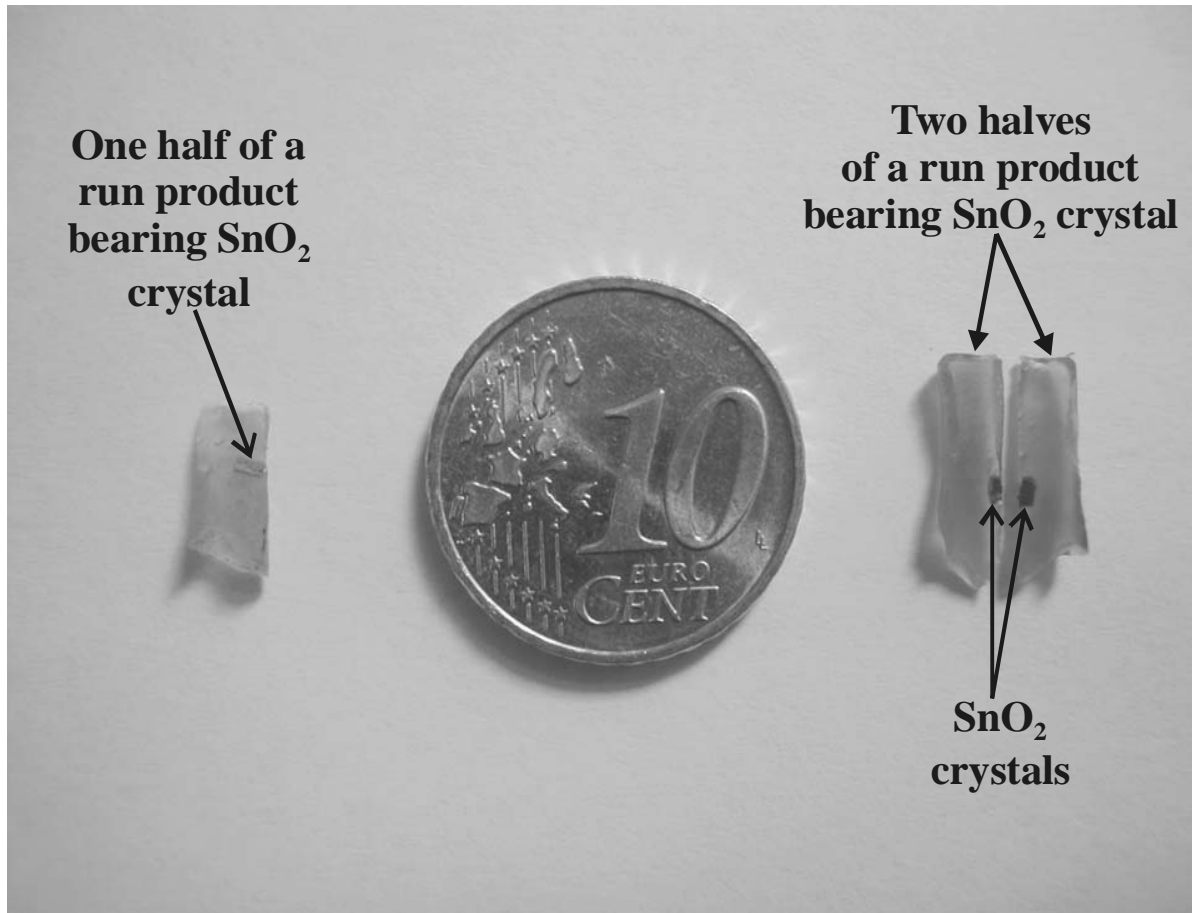


**Figure 2.7:** On the right side, is the backscattered electron image of two polished planes of a  $\text{SnO}_2$  crystal embedded in silicate melt (glass). The showed  $\text{SnO}_2$  crystal refers to the run product number DFW1 (See Appendix; see Table A.2 for details). In this electron image, the linear sets of points were chosen away from the boundary of  $\text{SnO}_2$  crystal towards the boundary of silicate melt. Those linear sets of points were meant to get the diffusion behavior of  $\text{SnO}_2$  crystal. Position and rotation of  $\text{SnO}_2$  crystal can easily be seen in this image. Note that  $\text{SnO}_2$ -glass interface is the  $\text{SnO}_2$  solubility. Scale bar equals  $2540 \mu\text{m}$  as total width of the showed run product bearing  $\text{SnO}_2$  crystal in it.

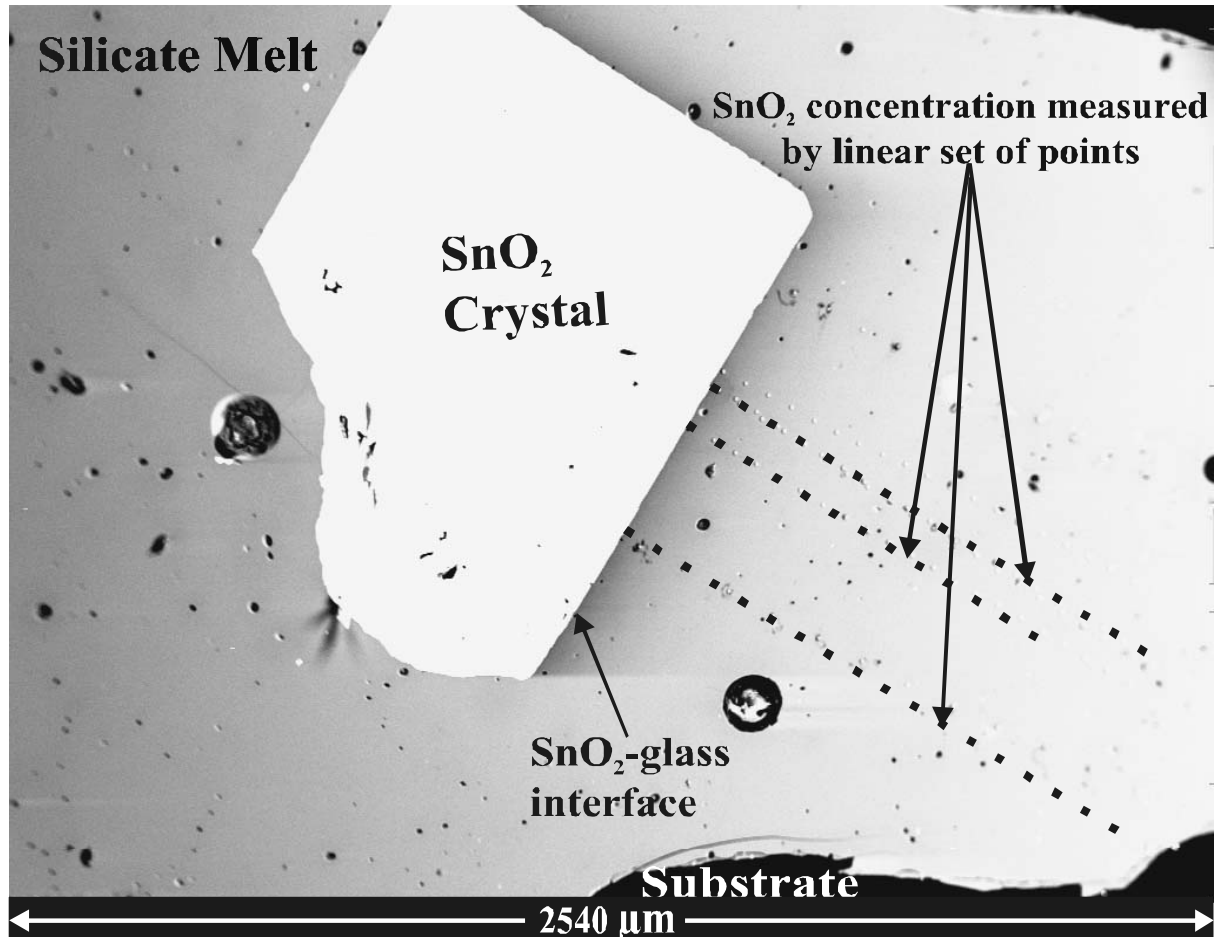


**Figure 2.8:** On the right side, is the backscattered electron image of two polished planes of a  $SnO_2$  crystal embedded in silicate melt (glass). The showed  $SnO_2$  crystal refers to the run product number 79 (for more details, see Table 2.5). In the adjoining electron microprobe image, two linear sets of points were chosen away from the boundary of  $SnO_2$  crystal towards the boundary of silicate melt. Those linear sets of points were meant to get the diffusion behavior of  $SnO_2$  crystal. Position and rotation of  $SnO_2$  crystal can easily be seen in this image. Note that  $SnO_2$ -glass interface is the  $SnO_2$  solubility. Scale bar equals 2545  $\mu m$  as total width of the showed run product bearing  $SnO_2$  crystal in it.

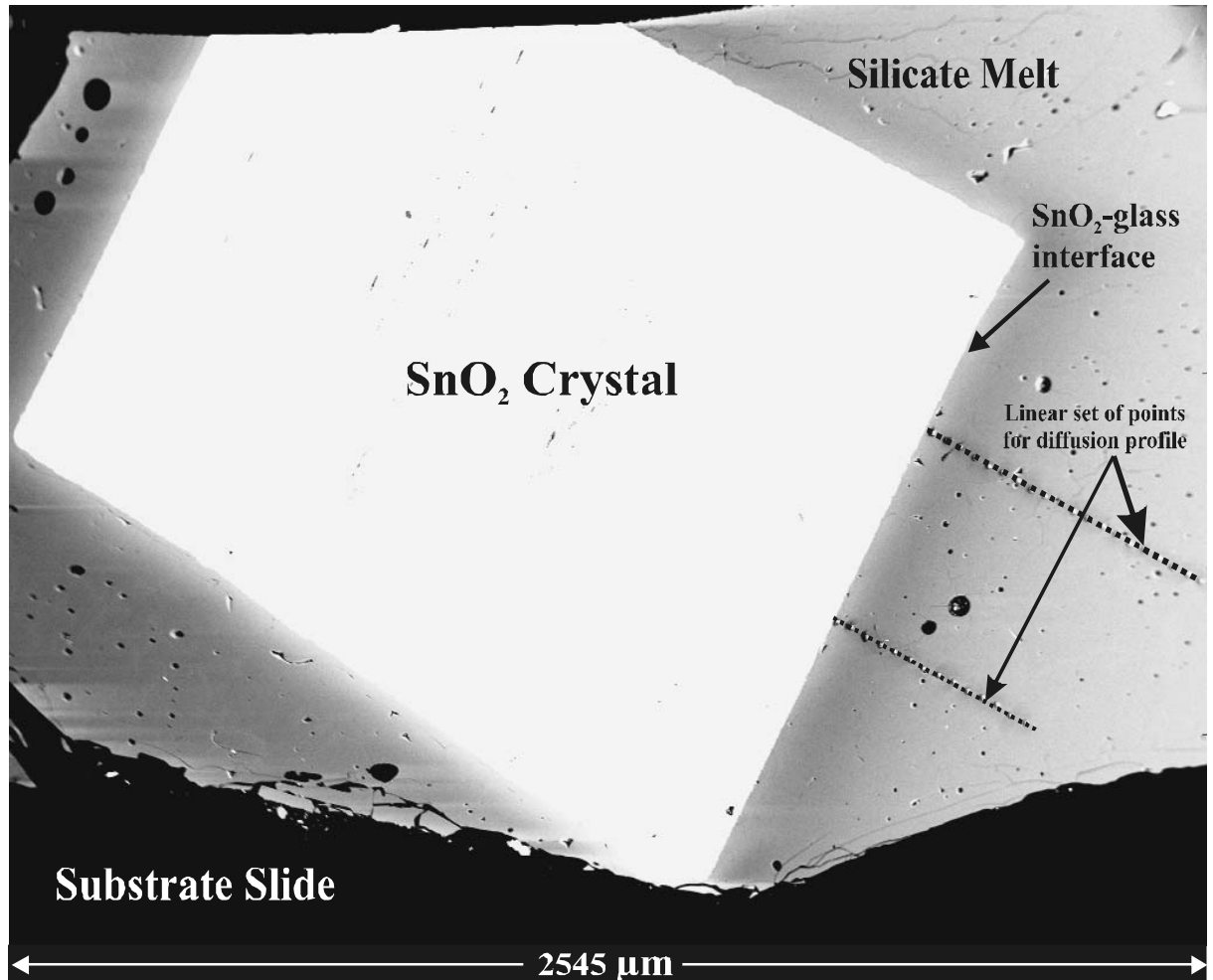


**Figure 2.9:** Backscattered electron microprobe images (placed on the right side) of four different run products termed as A, B, C and D. Those four images *viz.*, A, B, C and D, refer to run products 83 (see Table 2.3), DFW3, DFW2 and DFF2 (see Table A.2), respectively.  $SnO_2$  crystal in each run product is clearly visible in the silicate melt (glass). Linear sets of points have been fixed to get concentration profiles of  $SnO_2$  from the crystal surface towards the boundary of the run product. Width of each backscattered electron image equals to a scale bar of  $2540 \mu m$ .

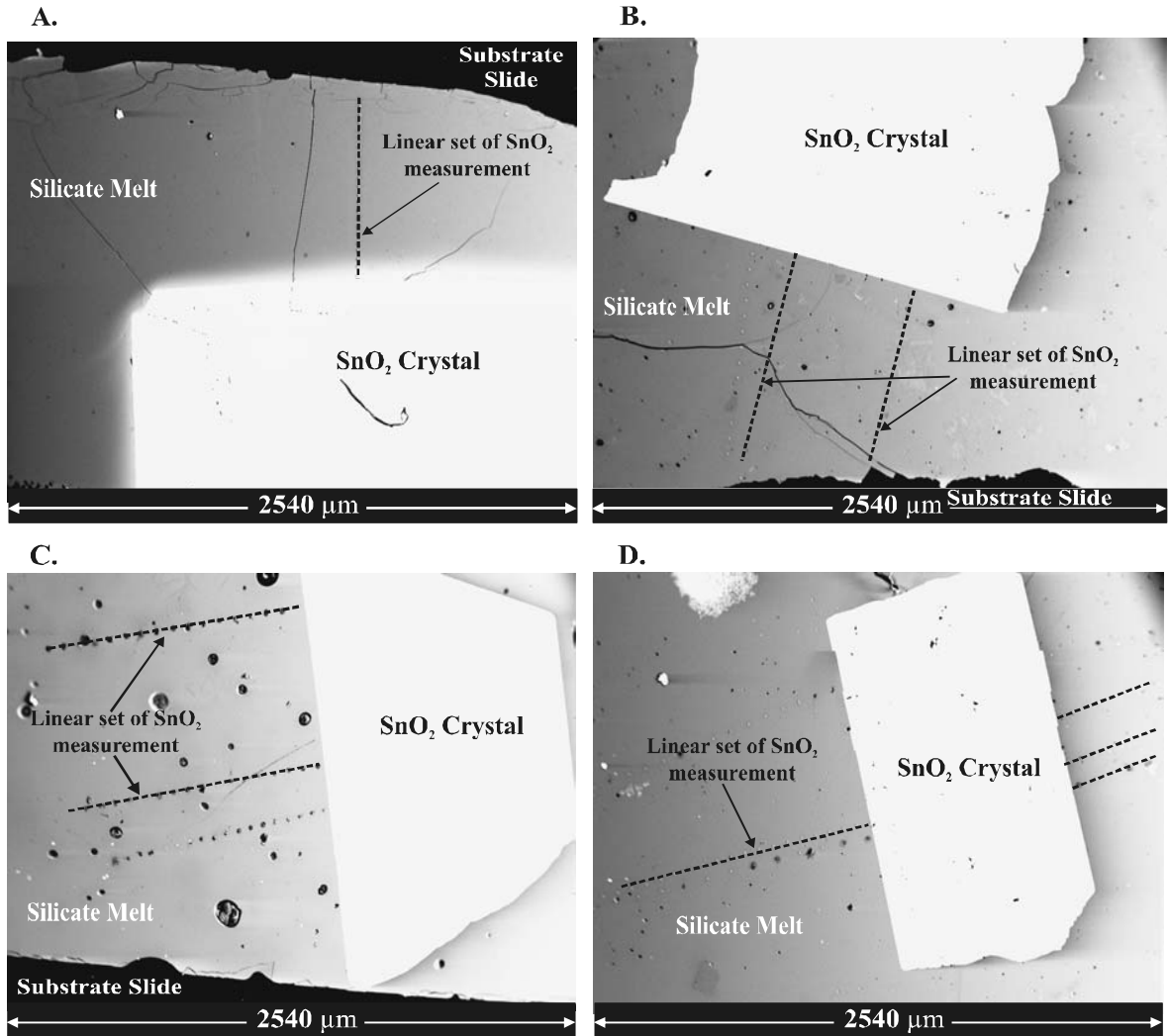
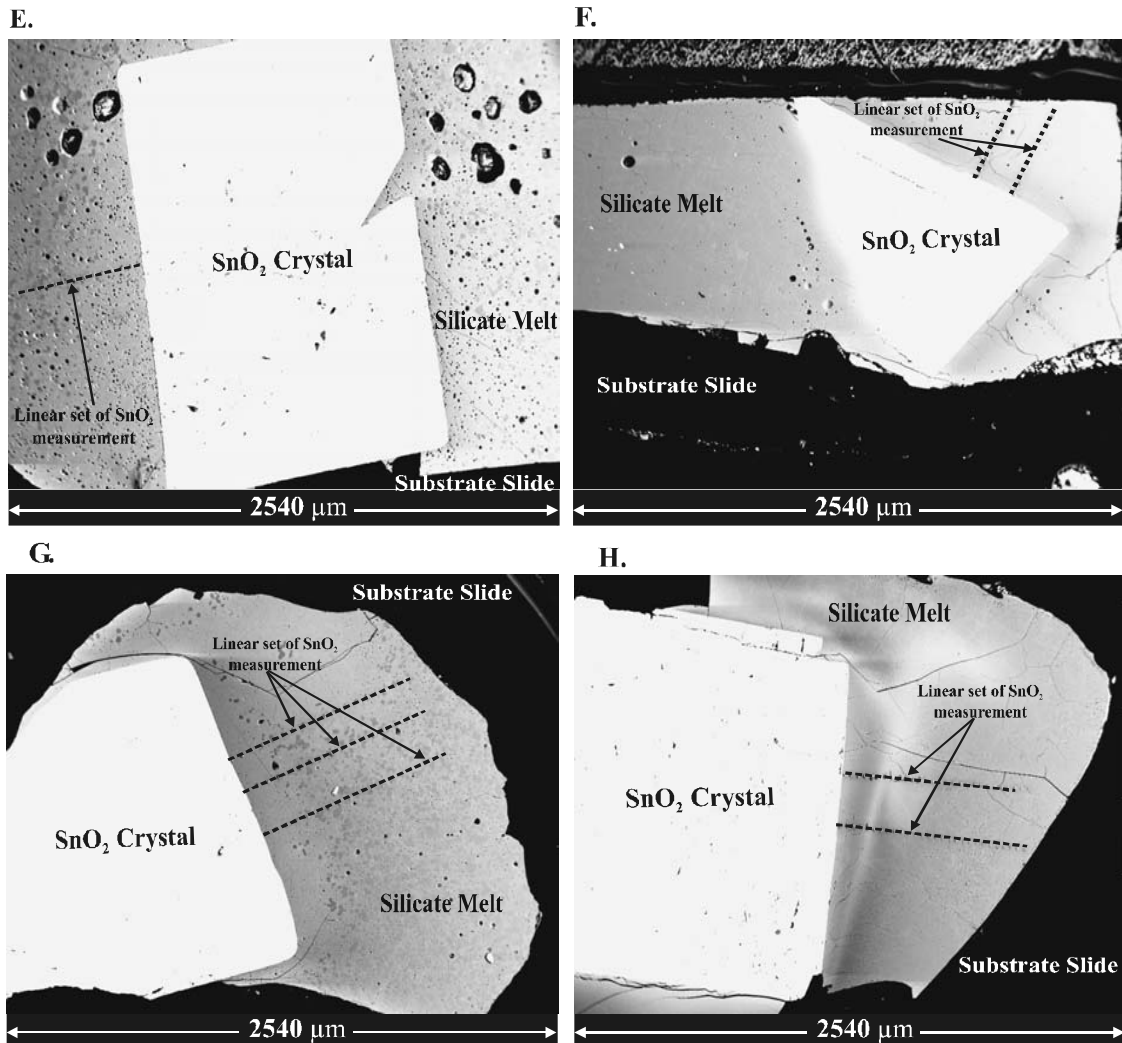


**Figure 2.10:** Backscattered electron microprobe images (placed on the right side) of four different run products termed as E, F, G and H. Those four images viz., E, F, G and H, refer to run products numbers 88, 85, 87 and 80 (Table 2.5), respectively.  $SnO_2$  crystal in each run product is clearly visible in the silicate melt (glass). Linear sets of points have been fixed to get concentration profiles of  $SnO_2$  from the crystal surface towards the boundary of the run product. Width of each backscattered electron image equals to a scale bar of 2540  $\mu m$ .



## 2.2.5. Determination of cassiterite solubility and diffusivity of tin

### 2.2.5.1. General equations for transport of tin in melts

In the present study, solubility of  $\text{SnO}_2$  is examined as a function of composition of starting material with varying concentrations of fluorine in the melts, followed by the effect of  $fO_2$  on solubility of  $\text{SnO}_2$ . Effect of temperature has been examined on the solubility of  $\text{SnO}_2$  in different starting compositions were also examined. A typical concentration profile obtained from the experiment GGC36 (see Table 2.1 for more details) at 843 °C, 16 hours and NNO is shown in Fig. 2.11(b). This profile fits well with the solution of Fick's second law,

$$C_{Sn} = C_{Sn,O} \cdot \left\{ 1 - \text{erf} \frac{x}{\sqrt{4Dt}} \right\} \quad (1)$$

assuming infinite one dimensional diffusion, a concentration independent diffusivity  $D$  of Sn and a constant concentration  $C_o$  of SnO at the surface of the crystal.  $x$  is the distance to the surface and  $t$  is the run duration. The solubility of  $\text{SnO}_2$  in the melt can be calculated by extrapolating the error function to the  $\text{SnO}_2$ -glass interface. Not all concentration profiles could be fitted accurately by an error function, however. In these cases the run duration may have been too long and concentration of  $\text{SnO}_2$  along the profile never reached a value close to zero, or the profile may have been longer than the half-size of the crystal so that the source cannot be considered as an infinite plane. Furthermore, the  $\text{SnO}_2$  crystal may have descended in the melt during the experiment and the experimental section has been cut perpendicular to the  $\text{SnO}_2$  surface, except for few experiments where experimental section may not have been cut perpendicular to the surface. In the latter case, the error in the final diffusivity of tin is large.

Cassiterite can dissolve in the melt by two reactions:





or



Where *cas* refers to the cassiterite solid and *melt* to a dissolved species in the melt represented as an oxide (the actual species is unknown). Combining equations (2) and (3), a new equation (4) can be as underwritten:



From equation (4), it can be understood that both species coexist in the melt, and their ratio depends upon  $fO_2$ . A new reaction (5) for metallic tin can be defined as:



If activity coefficients are constant at fixed melt composition, T and P, the valence of tin in the melt can be estimated. The solubility of cassiterite dissolving as  $Sn^{4+}$  (reaction 2) is independent of  $fO_2$  whereas if  $SnO_2$  dissolves by reaction 3 the log solubility as a function of  $\log fO_2$  will define a line with a slope of -0.5. In this case, the slope in plots of

$$\log C_{SnO_2} \text{ vs. } 1/T \text{ correspond to } \Delta H^\circ/2.303 R \quad (6)$$

where  $\Delta H^\circ$  is the standard enthalpy of reaction (3) and R is the gas constant. At moderately reducing conditions, a slope of -0.5 is observed in plots of  $\log C_{SnO_2}$  vs.  $\log fO_2$  due to the increasing abundance of divalent Sn with decreasing oxygen fugacity (see Linnen et al., 1995). In the experiments performed in this study, the  $fO_2$  was buffered but for a given solid buffer,  $fO_2$  changes with temperature. Therefore, the slope in plots of  $\log C_{SnO_2}$  vs.  $1/T$  does not strictly represent the dissolution enthalpy.

### 2.2.5.2. An evaluation of $SnO_2$ solubility and tin diffusivity

SnO<sub>2</sub> solubility is the value obtained at cassiterite-melt interface. In Fig. 2.11 (a) and 2.11 (b), two parameters *viz.*,  $a$ , and  $b$  are shown, where,  $a$ , is the SnO<sub>2</sub>-melt (glass) interface and parameter  $b$ , is used to calculate diffusivity of tin from equation (1) from Section 2.2.5. Equation 1 can be written as under:

$$D = \frac{1}{4(b)^2 t} \quad (7)$$

where,  $b$  is measured in mm<sup>-1</sup> and  $t$  in seconds. Therefore, from equation 7, diffusivity of tin,  $D$ , can be calculated. In Fig. 2.11 (a), a typical diffusion profile is shown from experiment GGC36 (see Table 2.1), where solubility of SnO<sub>2</sub> is measured to be 1.07 wt.% SnO<sub>2</sub> in the melt. Whereas, in Fig. 2.11 (b), another typical diffusion profile from an experiment 50 shows a SnO<sub>2</sub> solubility of 0.93 wt.% SnO<sub>2</sub> in the melt. In the latter case, SnO<sub>2</sub> solubility is obtained by extrapolating the concentration profile empirically (by hand), thus final SnO<sub>2</sub> solubility measured in this way is 0.85 wt.% SnO<sub>2</sub> in the melt. Whereas, in the latter case, parameter  $a$ , is value of SnO<sub>2</sub> solubility at SnO<sub>2</sub>-melt interface, which is obtained by fitting an error function. Thus, in most of experiments, where concentration profile fits well with an error function, in those cases the value of parameter  $a$ , is considered as the final SnO<sub>2</sub> solubility. Figure 2.11 (c-f) represents typical diffusion profiles from four different experiments.

Chemical diffusivities are widely reported to obey an exponential dependence on reciprocal temperature over considerable ranges in temperature, a type of relation referred to as Arrhenian (e.g., Glasstone et al., 1941):

$$D = D_o \cdot \exp\left(\frac{-E_a}{RT}\right) \quad (8)$$

Where,  $E_a$  is activation energy (J/mol),  $R$  is the ideal gas constant (J mol<sup>-1</sup> K<sup>-1</sup>),  $T$  is absolute temperature (K) and  $D_o$  is a temperature dependent constant (or preexponential

factor). The Arrhenian relation can be derived from absolute rate theory by the fact that ions move from one location in the melt to another in discrete diffusive jumps. Each jump requires an ion vibrating within a stable potential energy well in melt structure to acquire sufficient kinetic energy to rise over a potential energy barrier, to move to an adjacent stable site in the structure (e.g., Glasstone et al., 1941). In classical rate theory, the exponential factor  $D_o$  can be related to the frequency of the vibration, which allows diffusive steps to occur and has therefore often been called the frequency factor. The frequency factor (preexponential factor) is very weak function of temperature, and is for most purposes a constant. In this study, activation energy ( $E_a$ ) and  $D_o$  as constant for diffusion of tin in silicate melts, a linear regression has been plotted between  $\log D$  versus  $1/T \cdot 10^3$  from the analyzed data points. In Fig. 2.15, data are plotted for diffusion of tin in peraluminous melts. To calculate diffusion of tin, Arrhenius equation is

$$\ln D = \ln(D_o) + \left( \frac{-E_a}{RT} \right) \quad (9)$$

From equation 9, a new equation can be written as:

$$\ln D = \ln D_o - \frac{E_a}{R} \cdot \frac{1}{T} \quad (10)$$

As equation 10 is similar to the equation,  $y = b + mx$  (11)

where,  $\ln(D) = y$ , and  $\frac{1}{T} = x$ , the slope is  $m = \frac{-E_a}{R}$  and  $b = \ln(D_o)$ .

$E_a$  can be calculated from following equation as,

$$E_a = -m \cdot R \cdot 1000 \cdot \ln(10) \quad \text{where, } \log x \cdot \ln 10 = \ln x \quad (12)$$

By plotting the value of  $b$  and  $m$  (which are obtained from the linear regression slope of the tin diffusion in different melt compositions at various  $fO_2$  conditions) in equation 10,  $\ln D$

can be easily calculated. Activation energy,  $E_a$ , can be calculated directly from equation 12.

### 2.2.5.3. Attainment of equilibrium

This study also consider that all equilibrium experiments (total: 4) represent minimum estimates of saturation values. Equilibrium experiments under oxidized conditions may be successful since the solubility of tin in Au is  $fO_2$  dependent and for alloy compositions of <0.2 wt.% Sn, diffusion of tin in the alloy is slower than in the silicate liquid. Therefore, few equilibrium experiments were conducted at relatively oxidized conditions (NNO-1.0 to NNO+5.0) in an attempt to confirm the solubilities determined by diffusion. As mentioned above (see text), experiments conducted at NNO-1.0 buffer were failed, whereas for the other experiments at a log  $fO_2$  of NNO+5.0, there were no leaks due to Sn-Au alloying problems. The  $SnO_2$  profile adjacent to a  $SnO_2$  crystal was typically flat, which then progressively decreased with further distance from the crystal. The equilibrium solubility is taken to be the value of the flat profile adjacent to the crystal. The diffusion profile method is valid for determining solubilities at trace element levels (e.g., Harrison and Watson, 1983). Cassiterite solubility in this study ranges from trace element abundance, ~300 ppm  $SnO_2$ , to a major constituent of the silicate liquid, up to ~8 wt.% (Table 2.5).

It is known that hydrogen diffusivity in the melt is fast, but hydrogen solubility is probably small compared to  $H_2O$  solubility. In the present study,  $fH_2$  is controlled due to presence of water in the melts used for this study.



Thus, it may not be a problem to reach the required  $fO_2$  in the experiments in this study.

In any case, even if the concentration profiles had different shapes, the maximum  $SnO_2$  concentration in the glass at the interface, corresponding to the equilibrium solubility

value, should still be discernible. This is illustrated in Fig. 2.11., in which two different Sn diffusion profiles from two separate experiments (50 and GGC36) are shown. The diffusion profile of experiment 50 (see Figure 2.11 (a-b); Section 2.2.5.2) is extrapolated empirically (by hand) as shown in Fig. 2.11 (a). Whereas in most of experiments, SnO<sub>2</sub> solubility could be fitted successfully by an error function in experiment GGC 36 (see Section 2.2.5.2) as shown in Fig. 2.11 (b). The values of parameters,  $a$  and  $b$ , were obtained after plotting to the solution of Fick's second law,  $C = C_0 (1 - \text{erf } x/(4Dt)^{1/2})$ , where, concentration at the SnO<sub>2</sub>-melt interface is represented as  $a$  (see Section 2.2.5.2 for more details). After fitting an error function, tin diffusivities obtained in the silicate melts, after measuring diffusion profiles for experiments 50 and GGC36, were calculated to be  $5.10 \cdot 10^{-13} \text{ m}^2/\text{s}$  and  $1.4 \cdot 10^{-12} \text{ m}^2/\text{s}$ , respectively (in run products 50 and GGC36, tin diffusivity values were calculated from four different diffusion profiles using increments of about 20-40  $\mu\text{m}$ , where maximum and minimum value of tin diffusivity is calculated and mentioned in Table 2.1). Same procedure has been adopted for calculating tin diffusivity in most of the experiments.

### 2.2.6. Calculation of systematic error

If proper care is not taken, there is always a possibility of getting a deviation (not perpendicular to the crystal surface) of concentration profile of the metal (or gas), which is chosen in the direction of its diffusion away from the boundary of SnO<sub>2</sub> crystal towards silicate melt. Thus a systematic error has to be measured to get a reliable and correct data on diffusivity. Instead of choosing the direction of diffusion normal to the SnO<sub>2</sub> crystal towards melt, if the direction of diffusion of tin is chosen at an angle of 10° ( $\alpha = 10^\circ$ ), then the calculated systematic error will be ~3% for diffusion coefficient of tin,  $D_{Sn}$  in silicate melts. Systematic error can be calculated using following equation:

$$x^2 = 2Dt \tag{14}$$

In ideal cases, while using electron microprobe, is  $x = b$ . If there is a deviation of 10°, then  $x = c$ , therefore  $b$  can be written as under:

$$b = \cos \alpha \cdot c \Rightarrow c = \frac{b}{\cos \alpha} \quad (15)$$

To measure potential deviation from  $D$ , an equation can be written as:

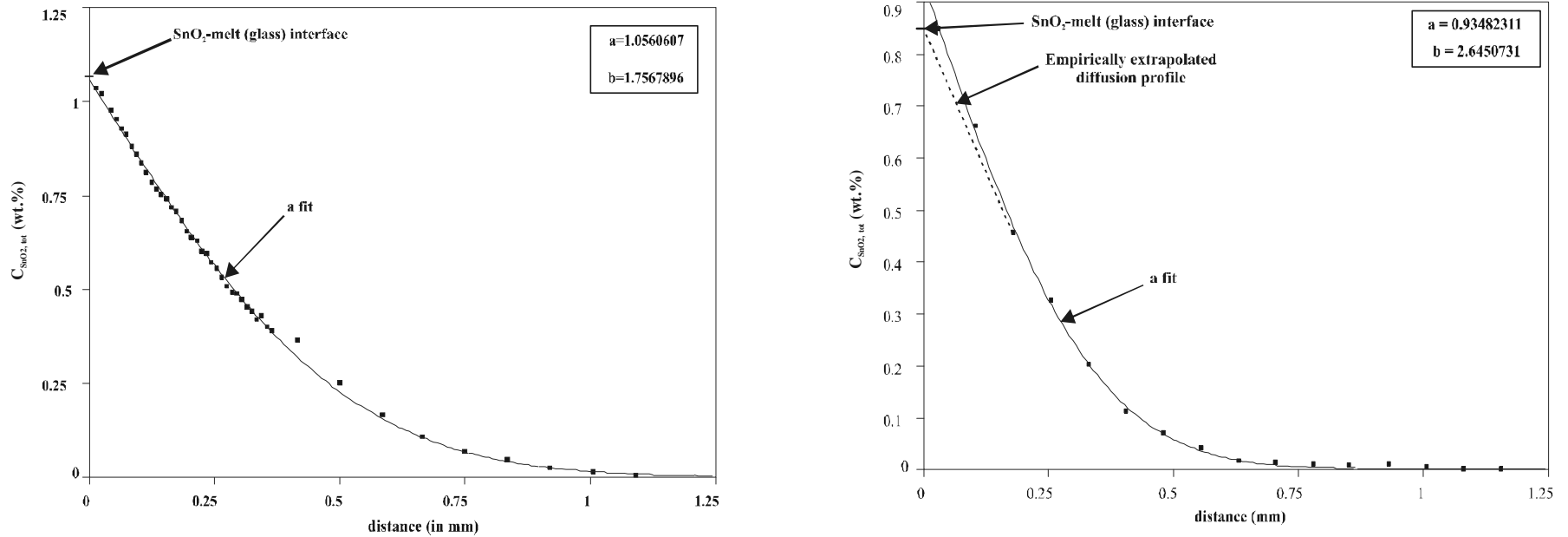
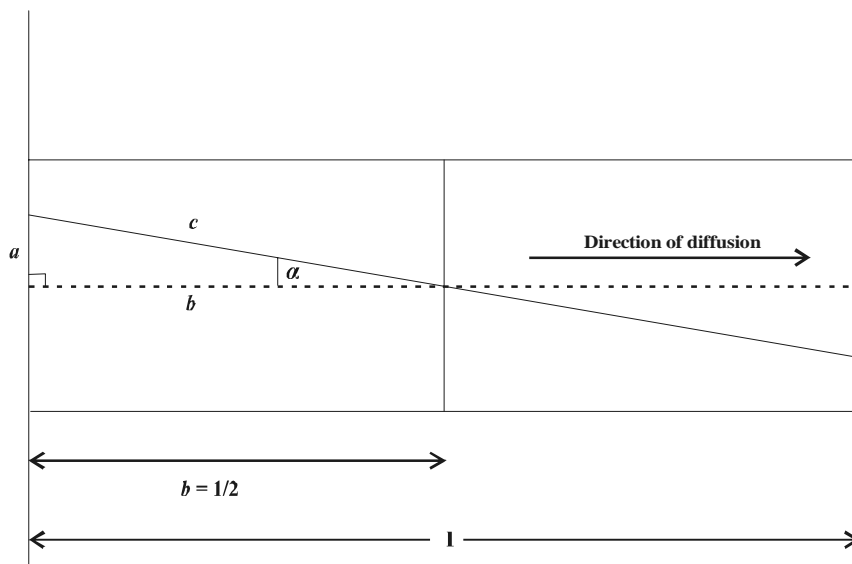


Figure 2.11 (a-b): a) Typical diffusion profile of tin fitted with an error function in experiment GGC36 (see Table 2.1). The concentration at SnO<sub>2</sub>-melt (glass) interface is the SnO<sub>2</sub> solubility. (b) A typical diffusion profile of tin fitted with an error function in experiment 50 (see Table 2.1). The concentration at the interface was extrapolated empirically (by hand) from the data points close to SnO<sub>2</sub>-melt (glass) interface. a and b, are the two parameters used for calculating the tin diffusivity.

$$D = \frac{x^2}{2t} \quad (16)$$

If diffusion is time independent, then an equation can be modified as:

$D \sim x^2$ , where  $x = c$  and  $b = 1$ , then  $D$  can be written as:



**Figure 2.11 (c): Schematic diagram represents a thin section of the run product prepared for an electron microprobe. The dotted line represents direction of diffusion of tin with a length,  $l$ , and  $c$  shows the measured concentration profile of the tin at an angle of  $\alpha = 10^\circ$ .**

$$D \sim \left( \frac{b}{\cos \alpha} \right)^2 \sim \frac{1}{(\cos \alpha)^2} \quad (17)$$

$$D \sim \frac{1}{\cos^2 \alpha} \quad (18)$$



The standard deviation of  $D$  can be calculated as  $(1 - \cos^2 \alpha) \cdot 100$ , which gives an error of 3% in the diffusion coefficient of metal (or gas) when a deviation of  $10^\circ$  is noted during analytical measurements on electron microprobe. Figure 2.11 (c) shows a sketch for calculation of systematic error for tin diffusion in silicate melts in the present study.

## 2.3. Results

### 2.3.1. Fluorine-bearing peraluminous ( $A.S.I. \geq 1.2$ ) melts

#### 2.3.1.1. Interdiffusion of major elements

Dissolution of  $SnO_2$  in the melt is a complex multi-component diffusion process

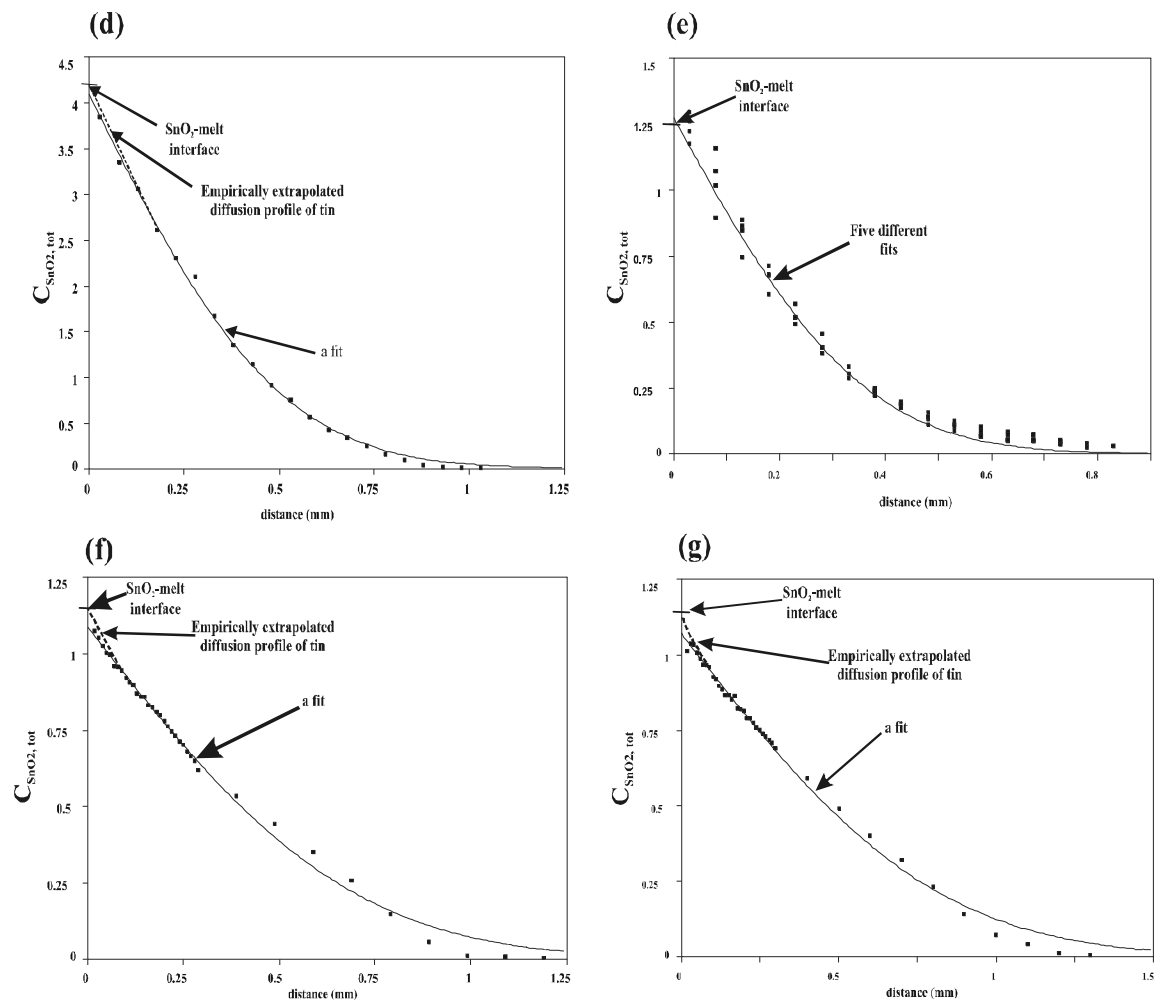


Figure 2.11(d-g): Typical diffusion profiles of tin for some of the experiments done in the present study. In clockwise direction, from d, e, f, and g, represent experiments 6 (see Table 2.4), GGC51 (see Table 2.7), GGC32 (see Table 2.1) and GGC18 (see Table 2.1), respectively. In all sub-figures,  $C_{SnO_2, tot}$  is in wt.%. Diffusion profiles were fitted with an error function and in experiment 6, GGC32 and GGC18, diffusion profiles were empirically (by hand) extrapolated.

and the concentration of other melt components may change relative to each other along the Sn diffusion profiles. Such compositional variations in the melt were observed by Linnen et al. (1995, 1996) especially at reducing conditions when the solubility of  $SnO_2$  is high. In this case, alkalis were found to be depleted near the surface of the crystal. Solubility of  $SnO_2$  varies with the alkali/Al ratio of the melt (Taylor and Wall, 1992; Linnen et al., 1995, 1996; Ellison et al., 1998) and, hence, the measured concentration of  $SnO_2$  at the surface is not representative of the initial melt but for a more peraluminous composition. In this study at a  $\log fO_2$  of NNO-0.1, the  $SnO_2$  concentration in the melt was at most 2.1 wt.%  $SnO_2$  at experimental conditions of 800 °C and 2 kbar (see experiment 54 in Table 2.2). No couple diffusion was observed in experiment 54 (with maximum cassiterite concentration at cassiterite-glass interface) using peraluminous melt composition in the present study. Major-element concentrations along the profiles were also analyzed on selected samples with the highest  $SnO_2$  concentrations. Typical results of major-element concentration profiles are shown in the study of Bhalla et al. (2004). They found no significant variation in alkalis and Al. As, this study using peraluminous melt is an extension of study of Bhalla et al. (2004), thus taking it in consideration, coupled diffusion would not be considered a problem in this study.

**Table 2.1: SnO<sub>2</sub> solubility and diffusion experiments in F-bearing melt with A.S.I. = 1.24**

Exp. Ref. No.	P (bar)	T (°C)	Run duration (hours)	Initial H <sub>2</sub> O in glass <sup>1</sup>	F-content in melt (wt.%) <sup>2</sup>	Buffer Used <sup>3</sup> ( $fO_2$ measured) <sup>4</sup>	log $fO_2$ $\Delta$ FMQ <sup>5</sup>	Number of profiles measured <sup>6</sup>	Solubility log ppm SnO <sub>2</sub> <sup>7</sup>			Diffusivity D (m <sup>2</sup> /s) <sup>8</sup>		
									ave.	max.	min.	ave.	max.	min.
GGC20°	2015	750	20	5.20	2.12	Ni-NiO	0.57	3	3.65	3.68	3.64	1.8E-12	3.1E-12	1.0E-12
DFF1	2000	855	22	5.85	1.12	Ni-NiO	0.57	3	4.06	4.06	4.05	2.8E-12	4.3E-12	1.7E-12
4 DF1	2010	845	6	5.70	1.12	Ni-NiO	0.57	4	4.04	4.05	4.03	1.9E-12	2.9E-12	1.1E-12
GGC32 <sup>†</sup>	2000	843	16	5.17	1.12	Ni-NiO	0.57	2	4.07	-	4.06	2.1E-12	2.5E-12	-
GGC36	2000	843	16	5.14	1.12	Ni-NiO	0.57	4	4.03	4.04	4.02	1.4E-12	2.6E-12	-
GGC37 <sup>n</sup>	2000	843	16	6.26	1.12	Ni-NiO	0.57	3	4.02	4.04	4.01	9.2E-13	1.1E-12	7.9E-13
GGC3	2000	840	22	6.20	1.12	Ni-NiO	0.57	4	4.01	4.03	4.00	2.0E-12	3.3E-12	1.1E-12
GGC4	2000	840	22	6.20	1.12	Ni-NiO	0.57	4	4.02	4.03	4.00	2.2E-12	3.4E-12	1.5E-12
GGC18	2000	840	18	6.26	1.12	Ni-NiO	0.57	3	4.05	4.06	4.04	3.1E-12	4.2E-12	2.6E-12
GGC19	2000	840	18	6.26	1.12	Ni-NiO	0.57	3	4.08	4.08	4.07	1.1E-12	2.1E-12	8.2E-13
GGC30	2000	840	16	5.28	1.12	Ni-NiO	0.57	3	4.08	-	-	2.7E-12	3.4E-12	2.2E-12
GGC39	2030	836	16	5.28	1.12	Ar gas	2.87	2	3.13	3.18	3.09	1.2E-13	1.9E-12	-
GGC44°	2010	836	6	5.28	1.12	Ar gas	2.87	1	3.19	-	-	-	-	-
43	2000	810	24	-	1.12	Co-rod (-14.61)	-0.26	3	3.95	3.97	3.94	4.3E-12	5.2E-12	3.3E-12
40°	1950	800	20	-	1.12	Ti-rod (-15.74)	-1.39	3	4.26	4.28	4.24	8.9E-13	1.2E-12	-
GGC34	2080	795	5	5.28	1.12	Ni-NiO	0.57	2	3.76	-	-	9.2E-13	1.1E-12	8.3E-13
GGC35	2000	790	5	5.17	1.12	Ni-NiO	0.57	3	3.77	3.79	3.75	2.8E-12	3.6E-12	2.1E-12
GGC31	2000	788	5	5.28	1.12	Ni-NiO	0.57	2	3.74	3.75	3.72	1.1E-12	1.9E-12	8.4E-13
DFF2	2020	760	26	5.85	1.12	Ni-NiO	0.57	4	3.74	3.75	3.73	8.4E-13	6.9E-13	1.1E-12
GGC27	2000	760	20	6.26	1.12	Ni-NiO	0.57	2	3.74	-	-	9.5E-13	1.3E-12	-
GGC28 <sup>†</sup>	2000	755	20	5.14	1.12	Ni-NiO	0.57	2	3.70	3.72	3.69	1.7E-12	-	-
4 DF3	2030	755	5.5	5.70	1.12	Ni-NiO	0.57	4	3.73	3.78	3.68	6.7E-13	9.5E-13	5.3E-13
GGC12	2005	755	22	6.26	1.12	Ni-NiO	0.57	3	3.67	3.70	3.65	9.9E-13	1.5E-13	-

**Table 2.1 (continued):**

Exp. Ref. No.	P (bar)	T (°C)	Run duration (hours)	Initial H <sub>2</sub> O in glass <sup>1</sup>	F-content in melt (wt.%) <sup>2</sup>	Buffer Used <sup>3</sup> ( $f_{O_2}$ measured) <sup>4</sup>	log $f_{O_2}$ $\Delta$ FMQ <sup>5</sup>	Number of profiles measured <sup>6</sup>	Solubility log ppm SnO <sub>2</sub> <sup>7</sup>			Diffusivity D (m <sup>2</sup> /s) <sup>8</sup>		
									ave.	max.	min.	ave.	max.	min.
GGC22	2015	755	20	5.14	1.12	Ni-NiO	0.57	3	3.75	3.78	3.75	8.4E-13	1.5E-12	7.1E-13
GGC21	2015	750	20	5.14	1.12	Ni-NiO	0.57	3	3.79	3.81	3.78	6.2E-13	4.9E-13	-
GGC23 <sup>†</sup>	1990	750	18	5.14	1.12	Ni-NiO	0.57	2	3.86	-	-	2.1E-12	-	-
GGC40	2030	750	16	5.28	1.12	Ar gas	2.87	3	2.78	2.78	2.78	4.6E-14	6.2E-14	3.7E-14
GGC41	2030	750	16	5.34	1.12	Ni-NiO	0.57	1	3.79	-	-	1.8E-13	-	-
GGC43	2010	746	16	5.28	1.12	Ar gas	2.87	3	2.80	2.82	2.78	9.3E-14	1.4E-13	8.2E-14
4 DF2	1990	745	5.5	5.70	1.12	Ni-NiO	0.57	4	3.67	3.87	3.47	5.5E-13	7.4E-13	3.9E-13
GGC24 <sup>°</sup>	1990	745	18	5.14	1.12	Ni-NiO	0.57	1	3.78	-	-	1.7E-12	-	-
GGC14	2000	710	16	6.88	1.12	Ni-NiO	0.57	3	3.52	-	-	1.0E-12	1.8E-12	7.6E-13
GGC10	2000	708	24	6.20	1.12	Ni-NiO	0.57	3	3.51	3.51	3.51	1.2E-12	2.1E-12	-
GGC13 <sup>°</sup>	2000	708	16	6.26	1.12	Ni-NiO	0.57	1	3.57	-	-	1.1E-12	-	-
44	2150	705	22	6.05	1.12	Co-rod (-13.05)	1.30	3	3.65	3.68	3.62	5.2E-13	6.7E-13	4.1E-13
GGC25 <sup>†</sup>	2000	705	48	5.14	1.12	Ni-NiO	0.57	2	3.45	-	3.44	3.3E-13	4.8E-13	-
GGC29	2000	705	16	5.17	1.12	Ni-NiO	0.57	3	3.60	3.63	3.58	2.8E-13	3.7E-13	1.9E-13
GGC16 <sup>°</sup>	2000	704	16	6.88	1.12	Ni-NiO	0.57	2	3.45	-	-	-	-	-
DF3	2060	685	20	5.85	1.12	Ni-NiO	0.57	4	3.45	3.50	3.39	6.6E-13	8.4E-13	5.1E-13
GGC57	2000	860	18	5.73	0.00	Ni-NiO	0.57	4	4.04	4.05	4.03	0.9E-12	1.2E-12	7.0E-13
GGC59	2000	850	18	5.61	0.00	Ni-NiO	0.57	3	4.03	-	4.01	0.8E-12	1.0E-12	5.6E-13
DFW1	2000	847	22	5.72	0.00	Ni-NiO	0.57	3	4.06	4.03	4.04	1.7E-12	2.7E-12	1.2E-12
50	1950	800	20	6.13	0.00	Co-rod (-13.95)	0.40	3	3.93	3.96	3.90	5.0E-13	6.8E-13	3.7E-13
47 <sup>†</sup>	1960	800	24	6.13	0.00	Co-rod (-14.82)	-0.47	2	3.90	3.92	3.88	7.5E-13	9.8E-13	-
5 DF1	2000	755	6	6.13	0.00	Ni-NiO	0.57	4	3.74	3.78	3.70	4.8E-13	6.5E-13	2.9E-13
GGC60	2030	754	18	5.61	0.00	Ni-NiO	0.57	3	3.55	-	3.52	3.4E-13	5.5E-13	2.1E-13

**Table 2.1 (continued):**

Exp. Ref. No.	P (bar)	T (°C)	Run duration (hours)	Initial H <sub>2</sub> O in glass <sup>1</sup>	F-content in melt (wt.%) <sup>2</sup>	Buffer Used <sup>3</sup> ( $fO_2$ measured) <sup>4</sup>	log $fO_2$ $\Delta$ FMQ <sup>5</sup>	Number of profiles measured <sup>6</sup>	Solubility log ppm SnO <sub>2</sub> <sup>7</sup>			Diffusivity D (m <sup>2</sup> /s) <sup>8</sup>		
									ave.	max.	min.	ave.	max.	min.
GGC58	2030	752	18	5.73	0.00	Ni-NiO	0.57	2	3.53	3.55	-	6.2E-13	8.3E-13	-
DFW2	2000	745	26	5.72	0.00	Ni-NiO	0.57	4	3.66	3.67	3.64	7.5E-13	1.2E-12	6.2E-13
49	1900	700	20	6.13	0.00	Co-rod (-13.47)	0.88	2	3.72	3.74	3.71	2.8E-13	4.3E-13	2.5E-13
DFW3	2000	680	20	5.85	0.00	Ni-NiO	0.57	3	3.29	3.31	3.28	2.8E-13	4.3E-13	-
DFW4	2060	680	20	5.71	0.00	Ni-NiO	0.57	3	3.25	3.27	3.23	3.2E-13	5.2E-13	2.1E-13

**Abbreviations:** P, pressure (in bars); T, temperature (in degree Celsius); F, Fluorine;  $fO_2$ , oxygen fugacity; FMQ, Fayalite-Magnetite-Quartz buffer.

<sup>1</sup> Amount of water (in weight percent) measured in prehydrated glass using Karl Fischer technique (KFT). The calculated error varies from  $\pm 0.10$  to  $\pm 0.15$  wt.%.  
<sup>2</sup> Fluorine content of the melt (in weight percent). Different melt compositions were prepared using different fluorine concentrations.  
<sup>3</sup> Buffer was used in the form of rod (e.g. "Co" stands for Cobalt) or in the powdered form (e.g. "HM" and "NNO" stand for Hematite-Magnetite and Nickel-Nickel Oxide, respectively).  
<sup>4</sup> Oxygen fugacity measured using double capsule technique from Chou, 1987a (see text for details).  
<sup>5</sup> Log  $fO_2$  calculated with respect to FMQ buffer (Linnen et al., 1995, 1996; Berndt et al., 2001; Matthews et al., 2003).  
<sup>6</sup> Number of profiles measured in the run product by electron microprobe.  
<sup>7</sup> SnO<sub>2</sub> concentration measured in parts per million (ppm), as ave. (average), max. (maximum) and min. (minimum).  
<sup>8</sup> D is the diffusion coefficient measured in m<sup>2</sup>/s. For those run products where D is measured only from one single SnO<sub>2</sub> diffusion fit, data is plotted within an error bars between ~10-15%.  
<sup>n</sup> Run product was crystallized, which may lead to a big error to the final diffusivity.  
<sup>o</sup> Bad run product (run product was partially crystallized. Thus concentration profiles were selected in crystal-free areas of the glass). Thus, it may contain error in SnO<sub>2</sub> solubility and diffusion data.  
<sup>†</sup> Systematic error may be >5% (see Section 2.2.6 for more details).

### 2.3.1.2. Effect of T and $fO_2$ on cassiterite solubility in peraluminous melts

There are only few data sets available to estimate temperature effect on solubility of cassiterite in silicate melts. There is a lack of experimental data on solubility of  $SnO_2$  in silicate melts conducted at T and P, except data of Linnen et al., 1995, 1996 (at 850 °C and 2 kbar). Few studies (e.g., Taylor and Wall, 1992; Webster and Holloway, 1988) encountered experimental problems i.e., interaction between melt and excess water (or fluid phase) causes change in composition of the melt and diffusion of tin in the noble metal capsule. The experimental results on the solubility of cassiterite in the melt with

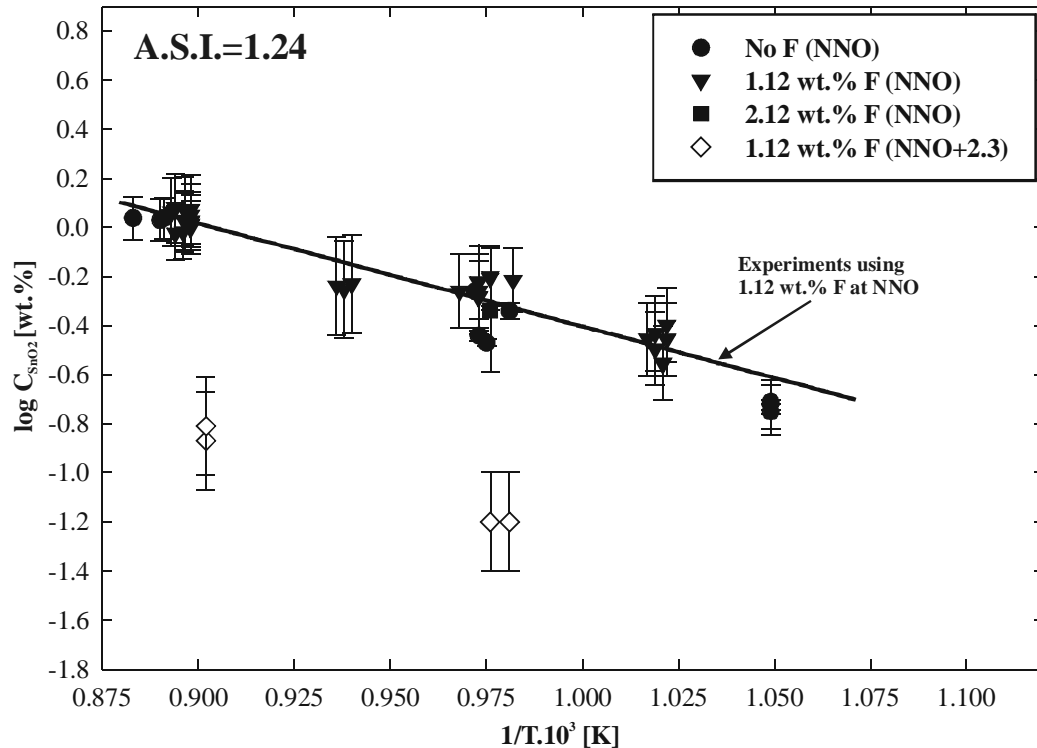


**Figure 2.12:** The Graph is plotted between  $1/T \cdot 10^3$  (K) and  $\log C_{SnO_2}$  (wt.%), for a natural F-bearing composition (all experiments are performed with glass 1, except one experiment GGC 20 with glass 2). At NNO,  $SnO_2$  solubility can be calculated as  $C_{SnO_2} = 3.79 - 4.20 \cdot 10^3/T$  and whereas at NNO+2.3,  $SnO_2$  solubility can be calculated as  $C_{SnO_2} = 3.40 - 4.70 \cdot 10^3/T$  (not shown in the figure).

composition of glass 1 containing 1.12 wt.% F in the melt (see Section 3.1; see Appendix for composition of glass 1 in Table A.1) are shown in Table 2.1 and Fig. 2.12. The solubility of cassiterite at NNO increases from  $0.18 \pm 0.01$  wt.%  $SnO_2$  at  $680 \text{ °C} \pm 10 \text{ °C}$  to

$1.20 \pm 0.05$  wt.%  $SnO_2$  at  $840 \text{ }^\circ\text{C} \pm 10 \text{ }^\circ\text{C}$  (corresponding to DFW4 and GGC 19), respectively. The solubility of cassiterite is significantly lower at NNO+2.3, in agreement with Linnen et al. (1995), and varies from  $0.06 \pm 0.01$  wt.% ( $630 \pm 100$  ppm)  $SnO_2$  at  $750 \text{ }^\circ\text{C} \pm 10 \text{ }^\circ\text{C}$  to  $0.15 \pm 0.02$  wt.% ( $1550 \pm 200$  ppm)  $SnO_2$  at  $840 \text{ }^\circ\text{C} \pm 10 \text{ }^\circ\text{C}$ . There is also a significant effect of  $fO_2$  on solubility of cassiterite in silicate melts at  $800 \text{ }^\circ\text{C} \pm 10 \text{ }^\circ\text{C}$ . A  $\log fO_2$  versus  $\log$  ppm  $SnO_2$  diagram (at  $800 \pm 10 \text{ }^\circ\text{C}$ ; Fig. 2.13), shows that cassiterite solubility increases from 0.59 wt.%  $SnO_2$  at NNO to 1.82 wt.%  $SnO_2$  at NNO-1.4.

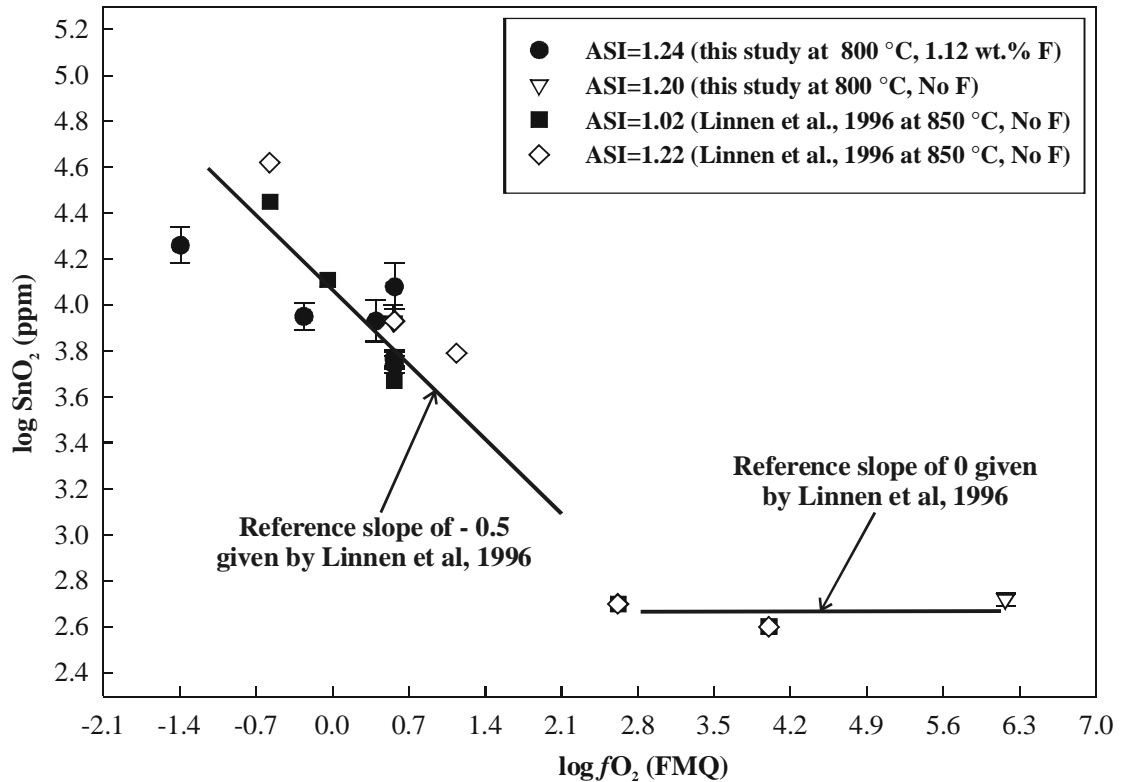


**Figure 2.13: Comparison of data from this study with the study of Linnen et al. (1996) at 800-850 °C and 2 kbar.**

Thus, it can be concluded that  $fO_2$  plays a very important role in controlling cassiterite solubility in natural as well as synthetic granitic melts. Results of the present study are in good agreement with study of Linnen et al. (1996). The effect of temperature can also be estimated from experiments with glass 3 (F-free starting glass composition; see Appendix; Table A.1). The same trend (not shown in Fig. 2.12) for glass 3 is observed as obtained for glass 1.



### 2.3.1.3. Effect of fluorine on the solubility of cassiterite in peraluminous melts

A comparison of the data obtained from glass 1 (with 1.12 wt.% F) with the peraluminous composition from Linnen et al. (1995) indicate that fluorine may have a significant effect on  $\text{SnO}_2$  solubility, as it has been often assumed for natural granitic systems (e.g., Pichavant et al., 1987; Pollard et al., 1987). The solubility of  $\text{SnO}_2$  in granitic melts at 700-850 °C, 2 kbar and at NNO, increases from ~0.20 wt.%  $\text{SnO}_2$  (run DFW3, see Table 2.1) in a F-free melt to 1.11 wt.%  $\text{SnO}_2$  (average value from all runs using glass 1 at  $840 \pm 10$  °C and 2 kbar; see Table 2.1) in a F-bearing (1.12 wt.% F) melt.

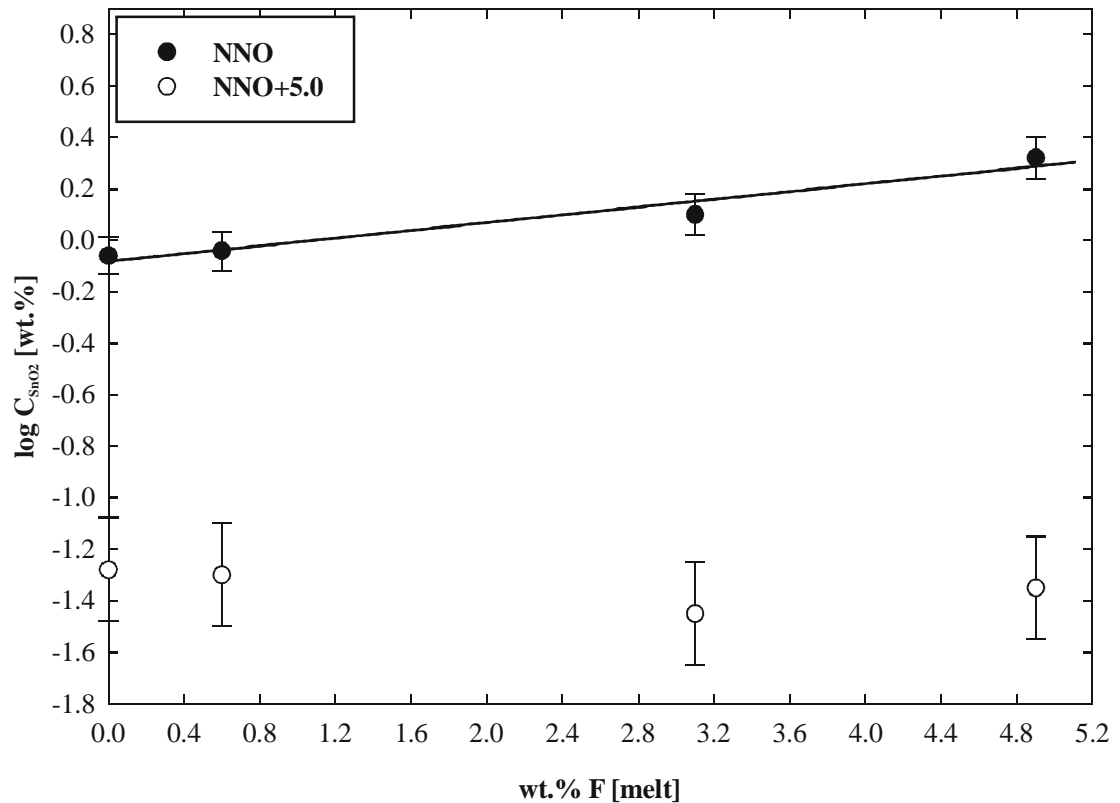


**Figure 2.14: The effect of fluorine on  $\text{SnO}_2$  solubility in peraluminous melts (A.S.I. = 1.20) at 800 °C and 2 kbar.**

It can be seen from Fig. 2.12 that an increasing F-content from 1.12 (average value from all runs using glass 1 at  $840 \pm 10$  °C) to 2.12 wt.% F (run GGC20 using glass 2; for composition of glass 2, see Table A.1) does not lead to a further increase in  $\text{SnO}_2$

solubility. Data at  $850 \text{ }^\circ\text{C} \pm 10 \text{ }^\circ\text{C}$  for glasses 1 and 3 show a small increase [ $1.15 \pm 0.05$  wt.%  $\text{SnO}_2$  (run DFF1) and  $1.07 \pm 0.04$  wt.%  $\text{SnO}_2$  (run GGC59), respectively] in cassiterite solubility with an increase in F-content from 0 wt.% F to 1.12 wt.% F in the melt. There is also a small increase in the average cassiterite solubilities reported at  $750 \text{ }^\circ\text{C}$  for glasses 1 and 3 ( $0.56 \pm 0.1$  wt.%  $\text{SnO}_2$  and  $0.43 \pm 0.08$  wt.%  $\text{SnO}_2$ ), but the variation is still within the  $\pm 20\%$  error (see Bhalla et al., 2004). Whereas, experiments (see Experiment 40; Table 2.1) performed at more reducing conditions of  $\log fO_2$  of NNO-1.4, the effect of F on cassiterite solubility is significantly higher than that observed at NNO.

Based on the effect of fluorine in F-free to F-bearing ( $\sim 1$  wt.% F in melt) peraluminous melts (see Fig. 2.12), it is concluded that at least at a  $\log fO_2$  of NNO, there is small effect of fluorine on cassiterite solubility when F-content in the melt varies between 0 to  $\sim 1$  wt.% F, but in the same melts at more reducing conditions ( $< \log fO_2$  of NNO), fluorine has a considerably higher effect on cassiterite solubility.

In run GGC 39 at  $836 \text{ }^\circ\text{C}$  (see Table 2.1), 0.14 wt.% of  $\text{SnO}_2$  dissolved in the F-bearing melt, whereas according to Linnen et al. (1996), less than 0.10 wt.%  $\text{SnO}_2$  can be dissolved in subaluminous to peraluminous melts containing no F. This result is consistent with the observation of Keppler (1993) that dissolved F promotes the solubility of HFSE (High Field Strength Elements), because, under oxidizing conditions, tin is present dominantly in the +4 valence state. In the study of Bhalla et al. (2004) using peraluminous melt with 2.12 wt.% F in melt, it might be feasible that there may be a discrepancy in the relevant data (using glass 2 containing 2.12 wt.% F in melt; Table A.1) due to the use of non-prehydrated starting glass material for experiment GGC20 (see Table 2.1). Thus, it is not possible to show any effect of F-content ( $> 2$  wt.% F in melt) on cassiterite solubility in peraluminous melts (A.S.I. = 1.24). Thus, run GGC20 may lead to many possible problems (e.g., uneven distribution of  $\text{H}_2\text{O}$  in melt) in the solubility as well as diffusivity data as water may or may not be evenly distributed in the melt. In run GGC20, uneven distribution of  $\text{H}_2\text{O}$  in the melt was confirmed from bulk composition total measured by electron microprobe. Run GGC20 showed a standard deviation,  $1\sigma$ , of  $\pm 4.0$  wt.% in the total of bulk composition. However, for all the experiments performed in the present study, prehydrated glasses were used to ensure an even distribution of  $\text{H}_2\text{O}$  in melt. Thus, it is

difficult or even not exactly possible to assume a complete effect of F on cassiterite solubility using this single experiment with 2.12 wt.% F).

In order to know the effect of varying F-contents (from 0-5 wt.% F in the melt) on cassiterite solubility in peraluminous melt (A.S.I. = 1.20), a series of additional experiments were performed using this composition. The results are plotted in Fig. 2.14, where it is well shown that solubility of cassiterite increases with an increase in F-content of the melt from 0.6 to 4.9 wt.% F in melt. At  $800\text{ }^\circ\text{C} \pm 5\text{ }^\circ\text{C}$ , 2 kbar and NNO, it is found that cassiterite solubility increases from  $0.91 \pm 0.12$  to  $2.09 \pm 0.24$  wt.%  $\text{SnO}_2$  for F melt contents of 0.6 to 4.9 wt.% F, respectively. Whereas, at  $800\text{ }^\circ\text{C} \pm 5\text{ }^\circ\text{C}$ , 2 kbar and NNO+5.0, with an increase of F-content from 0.6 to 4.9 wt.% F in the melt, there is a small increase in cassiterite solubility from  $0.05 \pm 0.03$  to  $0.08 \pm 0.04$  wt.%  $\text{SnO}_2$ , respectively. Thus, although low, the solubility of cassiterite is doubled within error at such oxidizing conditions, where tin is transported in the melt as  $\text{Sn}^{4+}$  ( $\text{Sn}^{4+}$  is a HFSE whereas  $\text{Sn}^{2+}$  is not) agrees well with study of Keppler (1993) who suggested this effect of F on solubility of HFSE.

The results at reducing conditions ( $\sim$ NNO) concludes that solubility of cassiterite shows a significant increase when F-content in the silicate melt is  $>2$  wt.% F. Whereas, at  $800\text{ }^\circ\text{C}$ , 2 kbar and at highly oxidizing conditions (NNO+5.0), small concentration of tin are reported in melt and there is also a strong effect of F on the solubility of cassiterite. Cassiterite solubility in F-free peraluminous melt (A.S.I. = 1.20) of same composition at NNO is  $0.87 \pm 0.07$  wt.%  $\text{SnO}_2$ , whereas, at highly oxidizing  $fO_2$  of NNO+5.0, cassiterite solubility is found to be  $0.05 \pm 0.03$  wt.%  $\text{SnO}_2$ . This study conclude that at least at reducing conditions, F has a major influence on tin solubility and thus fluorine plays a very important role in controlling cassiterite solubility in reduced peraluminous melts. At  $800\text{ }^\circ\text{C}$ , 2 kbar and at a varying  $\log fO_2$  from NNO to NNO+5.0, cassiterite solubility data using F-free melts in the present study agrees well with cassiterite solubility data obtained by the study of Linnen et al. (1995, 1996). Linnen et al. (1996) observed very similar cassiterite solubilities in haplogranite, quartz-albite and quartz-feldspar melts at same P, T and  $fO_2$ .

**Table 2.2: SnO<sub>2</sub> solubility and diffusion experiments in F-bearing melt with A.S.I. = 1.20**

Exp. Ref. No.	P (bar)	T (°C)	Run duration (hours)	Initial H <sub>2</sub> O in glass <sup>1</sup>	F-content in melt (wt.%) <sup>2</sup>	Buffer Used <sup>3</sup> ( $fO_2$ measured) <sup>4</sup>	log $fO_2$ $\Delta$ FMQ <sup>5</sup>	Number of profiles measured <sup>6</sup>	Solubility log ppm SnO <sub>2</sub> <sup>7</sup>			Diffusivity D (m <sup>2</sup> /s) <sup>8</sup>		
									ave.	max.	min.	ave.	max.	min.
54	2010	800	6	5.30	4.9	Co-rod (-13.92)	0.43	3	4.32	4.37	4.27	9.8E-13	1.6E-12	7.5E-13
58°	2060	800	68	5.30	4.9	HM (-9.52)	4.83	2	2.91	-	2.63	6.5E-14	-	4.3E-14
53 <sup>†</sup>	2020	805	6	6.16	3.1	Co-rod (-13.92)	0.43	2	4.10	4.13	4.07	6.5E-13	8.7E-13	-
57	2060	805	68	6.16	3.1	HM (-9.52)	4.83	1	2.55	-	-	3.5E-14	-	-
52 <sup>n</sup>	2030	810	6	6.22	0.6	Co-rod (-13.79)	0.56	1	3.96	-	-	2.9E-13	-	-
56	2050	810	68	6.22	0.6	HM (-8.18)	6.17	3	2.70	2.80	2.70	1.5E-14	2.8E-14	9.5E-15
55	1960	805	43	7.26	0.0	HM (-8.18)	6.17	3	2.72	2.78	2.64	1.2E-14	2.7E-14	8.8E-15
51	1900	800	6	7.26	0.0	Co-rod (-13.79)	0.56	2	3.94	3.97	-	-	-	-

**Abbreviations:** P, pressure (in bars); T, temperature (in degree Celsius); F, Fluorine;  $fO_2$ , oxygen fugacity; FMQ, Fayalite-Magnetite-Quartz buffer.

<sup>1</sup> Amount of water (in weight percent) measured in prehydrated glass using Karl Fischer technique (KFT). Calculated error is  $\pm 0.1$  wt.%.  
<sup>2</sup> Fluorine content of the melt (in weight percent). Different melt compositions were prepared using different fluorine concentrations.  
<sup>3</sup> Buffer was used in the form of rod (e.g. “Co” stands for Cobalt) or in the powdered form (e.g. “HM” stands for Hematite-Magnetite).  
<sup>4</sup> Oxygen fugacity measured using double capsule technique from Chou, 1987a (see text for details).  
<sup>5</sup> Log  $fO_2$  calculated with respect to FMQ buffer (Linnen et al., 1995, 1996; Berndt et al., 2001; Matthews et al., 2003).  
<sup>6</sup> Number of profiles measured in the run product by electron microprobe.  
<sup>7</sup> SnO<sub>2</sub> concentration measured in parts per million (ppm), as ave. (average), max. (maximum) and min. (minimum).  
<sup>8</sup> D is the diffusion coefficient measured in m<sup>2</sup>/s. D is the diffusion coefficient measured in m<sup>2</sup>/s. For most of the run products, data for tin diffusivity are plotted with ~10% error bars (calculated as average error after measuring different profiles in each sample).  
<sup>n</sup> Run product was crystallized, which may lead to a big error to the final diffusivity.  
<sup>o</sup> Bad run product (run product was partially crystallized. Thus concentration profiles were selected in crystal-free areas of the glass). Thus, it may contain error in SnO<sub>2</sub> solubility and diffusion data.  
<sup>†</sup> Systematic error may be >5% (see Section 2.2.6 for more details).

### 2.3.1.4. Effect of F on tin diffusivity in peraluminous melt compositions

The effect of fluorine on tin diffusivity has not previously been investigated. However, many studies suggested that fluorine is an important parameter controlling tin transport in natural and synthetic granitic melts (e.g., Pichavant et al., 1987; Pollard et al., 1987). Thus, it is important to understand the transport (diffusion) of tin in natural as well as synthetic granitic melts under both reducing and oxidizing conditions. The results obtained on Sn diffusion in F-free and F-bearing peraluminous granitic melts (see Table 2.1 for more details) indicate that F plays a very important role in transporting Sn in reduced granitic systems. In the present study at 850 °C, 2 kbar and at NNO, tin diffusivity

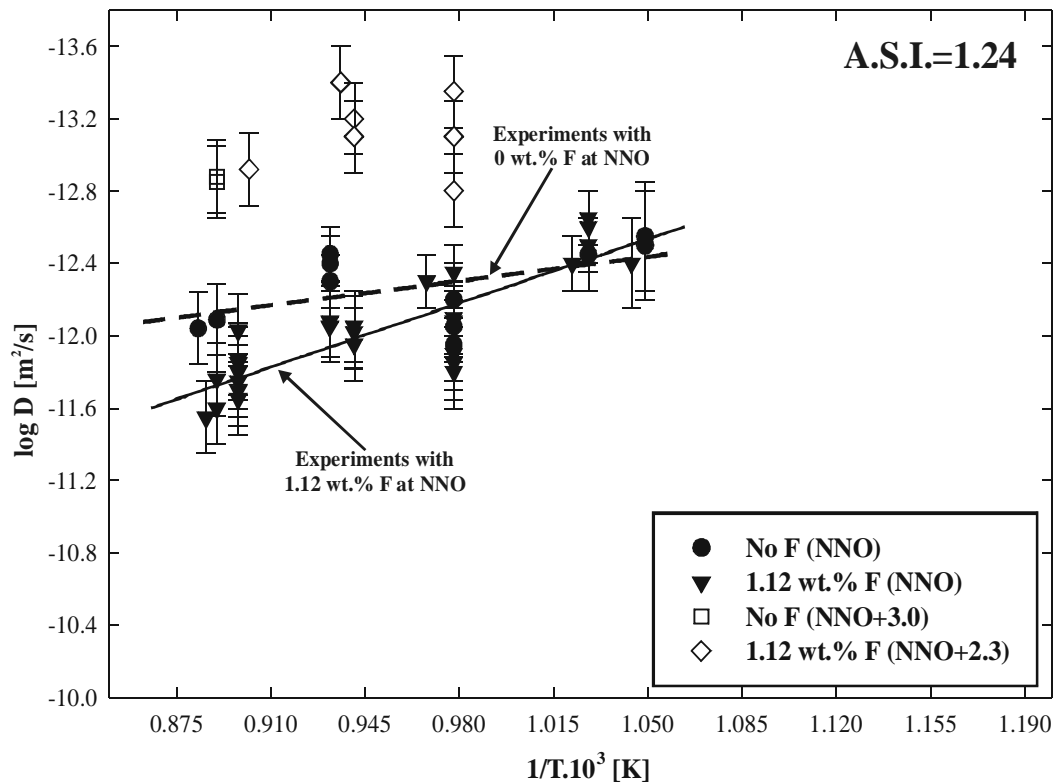


**Figure 2.15:** Arrhenius plot between diffusivity,  $D$  [ $m^2/s$ ] and temperature,  $T$  [K] in granitic melt (A.S.I. content = 1.24).  $SnO_2$  diffusivity can be calculated as  $\log D = -7.23 - 5.06 \cdot 10^3/T$ . Linear regression gives  $E_a = 96 \pm 4.5$  kJ/mol for the diffusivity of tin in peraluminous melt containing 1.12 wt.% F.

in F-free to F-bearing (1.12 wt.% F) peraluminous melt increases from  $0.8 \cdot 10^{-12}$  to  $2.8 \cdot 10^{-12}$   $m^2/s$ , respectively (see Fig. 2.15). However, at temperature ranges from 680-850 °C and at

NNO, diffusivity of tin can be calculated as  $\log D = -7.23 - 5.06.10^3/T$ , where D and T are measured in ( $m^2/s$ ) and (K), respectively (see Fig. 2.15), whereas, at same experimental temperatures but at more oxidizing conditions (NNO+2.3), diffusivity of tin can be calculated as  $\log D = -10.13 - 3.13.10^3/T$  (not shown in Fig. 2.15).

At  $750 \pm 10$  °C, 2 kbar and at NNO, diffusivity of tin increases from  $6.2.10^{-13} m^2/s$  in a melt containing 0 wt.% F to  $1.8.10^{-12} m^2/s$  in a melt containing 2.12 wt.% F (data for tin diffusivity in the melt containing 2.12 wt.% F, is not plotted in Fig. 2.15; see Table 2.1 for details). Thus, there is a significant increase of about  $\frac{1}{2}$  a log unit, for an increase of F-content of the melt from 0 to ~2 wt.% F. The diffusivity of tin also varies from oxidizing to reducing conditions. At 750 °C, 2 kbar using peraluminous melt containing 1.12 wt.% F, Sn diffusivity increases from  $4.6.10^{-14} m^2/s$  at NNO+2.3 to  $2.1.10^{-12} m^2/s$  at NNO buffer. Results on the Sn diffusivity in F-free and F-bearing peraluminous melts (A.S.I. = 1.24) are shown in Fig. 2.15. Therefore, at NNO buffer, activation energy ( $E_a$ ), calculated from a linear regression of tin diffusion in peraluminous melts is  $96 \pm 4.5$  kJ/mol, whereas at an  $fO_2$  of NNO+2.3, calculated  $E_a$  from a linear regression of tin diffusion in peraluminous melts is  $60 \pm 3$  kJ/mol.

### 2.3.2. Chlorine-bearing peraluminous compositions

In preliminary experiments, Bhalla et al. (2004) reported a significant effect of chlorine on the solubility of cassiterite in granitic melts. Very little is known about the effects of Cl on the cassiterite solubility in silicate melts (Taylor and Wall, 1992; Taylor and Wall, 1993; Webster et al., 2004). Other studies (e.g., Keppler and Wyllie, 1989; Keppler and Wyllie, 1991) explain the partitioning behaviour of HFSE (High Field Strength Elements) between granitic melts and fluid phases.

#### 2.3.2.1. Effect of Cl on cassiterite solubility and tin diffusivity

The results obtained from Cl-bearing starting glasses 4 (with 0.20 wt.% Cl in melt;

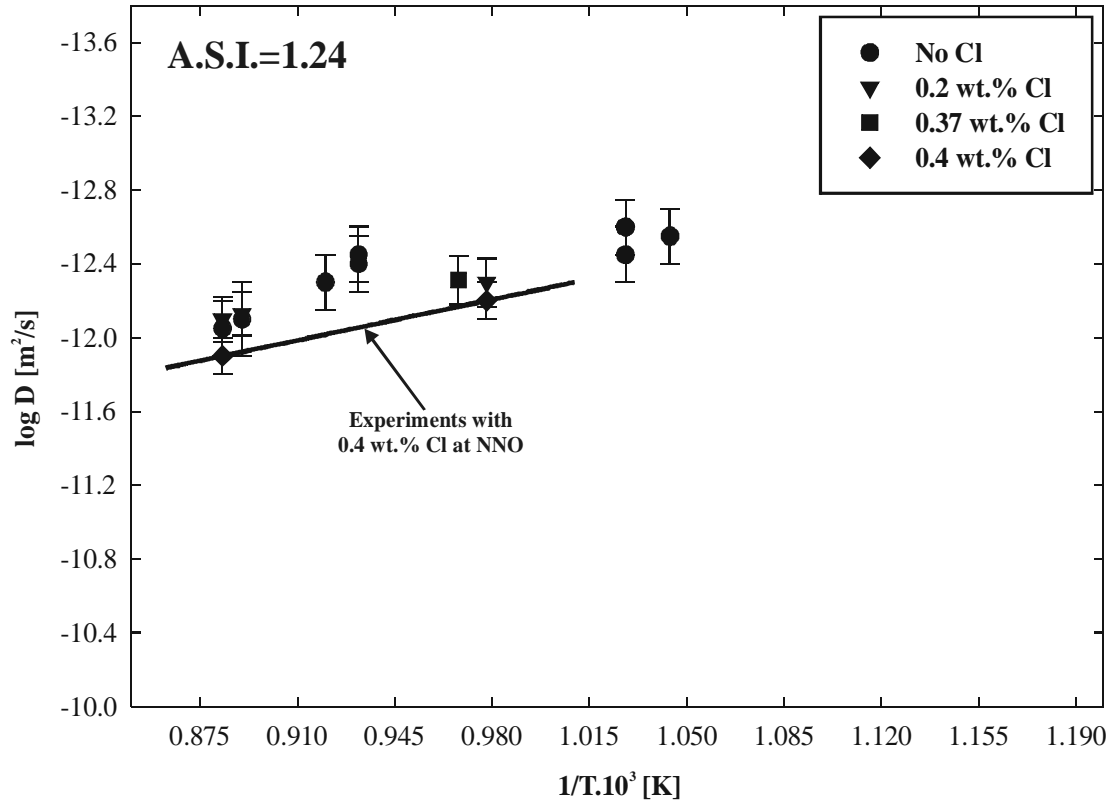


**Figure 2.16.:** Arrhenius plot between diffusivity,  $D$  [ $\text{m}^2/\text{s}$ ] versus  $1/T \cdot 10^3$  [K] in peraluminous melt (A.S.I. = 1.24) with various Cl-concentrations in melt at NNO buffer. Diffusivity of tin can be calculated as  $\log D = -9.11 - 3.15 \cdot 10^3/T$ . Linear regression gives  $E_a = 60 \pm 3$  kJ/mol for tin diffusion in peraluminous melts containing 0.4 wt.% Cl.

Table A.1), 5 (with 0.37 wt.% Cl<sup>-</sup> in melt; Table A.1), and 6 (with 0.40 wt.% Cl<sup>-</sup> in melt; Table A.1) indicate that chlorine does play an important role in concentrating cassiterite in the peraluminous melt (A.S.I. = 1.24) at NNO. From Cl<sup>-</sup> and F-free runs (see Table 2.1 and Table 2.3), it can be seen that there is a small but clear effect of Cl<sup>-</sup> on cassiterite solubility. The results from this study show that the solubility of cassiterite increases from  $1.07 \pm 0.04$  wt.% SnO<sub>2</sub> (GGC59; see Table 2.1) to 1.23 wt.% SnO<sub>2</sub> (run GGC51; see Table 2.3) when Cl<sup>-</sup> content in the melt increases from 0 to 0.2 wt.% Cl<sup>-</sup>. However, no further increase in cassiterite solubility has been found when Cl<sup>-</sup> content in the melt increases from 0.20 to 0.40 wt.% Cl<sup>-</sup>. Therefore, it can be concluded that in reducing environments, chlorine has a tendency to transport cassiterite by building tin-chloride complexes in silicate melts and thus, presence of chlorine into the melt may enhance the cassiterite solubility.

The results also show that there is very small effect of Cl<sup>-</sup> on diffusion of tin in peraluminous melts. It has also been expected in the studies (e.g., Taylor, 1979a; Taylor and Wall, 1992) that chlorine may affect transportation and mobilization of tin species in silicate melts. In this study at  $850 \pm 10$  °C, 2 kbar and at NNO using Cl-free and Cl-bearing (0.4 wt.% Cl in melt) synthetic granitic melts, diffusivity of SnO<sub>2</sub> increases from  $0.8 \cdot 10^{-12}$  to  $1.3 \cdot 10^{-12}$  m<sup>2</sup>/s, respectively. In a peraluminous melt containing 0.4 wt.% Cl, at an  $fO_2$  of NNO, Sn diffusivity increases from  $6.5 \cdot 10^{-13}$  m<sup>2</sup>/s to  $1.3 \cdot 10^{-12}$  m<sup>2</sup>/s, with an increase in temperature from 750 to  $850 \pm 10$  °C. It can be concluded that there is a very small or negligible effect of Cl<sup>-</sup> on the diffusivity of tin in silicate melts. Results on the Sn diffusivity in Cl-free and Cl-bearing peraluminous melts (A.S.I. = 1.24) are shown in Fig. 2.16 and Table 2.3.



**Table 2.3: SnO<sub>2</sub> solubility and diffusion experiments in Cl-bearing melt with A.S.I = 1.24**

Exp. Ref. No.	P (bar)	T (°C)	Run duration (hours)	Initial H <sub>2</sub> O in glass <sup>1</sup>	Cl-content in melt (wt.%) <sup>2</sup>	Buffer Used <sup>3</sup>	log $f_{O_2}$ $\Delta$ FMQ <sup>4</sup>	Number of profiles measured <sup>5</sup>	Solubility log ppm SnO <sub>2</sub> <sup>6</sup>			Diffusivity D (m <sup>2</sup> /s) <sup>7</sup>		
									ave.	max.	min.	ave.	max.	min.
DFC1	2000	860	20	5.65	0.4	Ni-NiO	0.57	4	4.08	4.10	4.06	1.3E-12	1.8E-12	1.0E-12
DFC3	2000	750	21	5.65	0.4	Ni-NiO	0.57	3	3.71	3.74	3.68	6.5E-13	8.1E-13	5.2E-13
GGC55	2020	860	18	6.12	0.37	Ni-NiO	0.57	3	4.08	4.10	4.07	6.7E-13	9.4E-13	4.6E-13
GGC56 <sup>o</sup>	2030	760	18	6.12	0.37	Ni-NiO	0.57	2	3.78	3.81	-	5.0E-13	6.7E-13	-
GGC51	2000	860	18	5.59	0.2	Ni-NiO	0.57	5	4.09	4.11	4.09	8.0E-13	1.1E-12	5.8E-13
GGC53	2030	760	18	5.59	0.2	Ni-NiO	0.57	3	3.77	3.80	3.75	5.2E-13	6.5E-13	3.9E-13

**Abbreviations:** P, pressure (in bars); T, temperature (in degree Celsius); Cl, chlorine;  $f_{O_2}$ , oxygen fugacity; FMQ, Fayalite-Magnetite-Quartz buffer.

<sup>1</sup> Amount of water (in weight percent) measured in prehydrated glass using Karl Fischer technique (KFT). The error is calculated to be  $\pm 0.10$  wt. %.

<sup>2</sup> Chlorine content of the melt (in weight percent). Different melt compositions were prepared using different chlorine concentrations.

<sup>3</sup> Buffer was used in a powdered form, where “NNO” stands for Nickel-Nickel Oxide.

<sup>4</sup> Log  $f_{O_2}$  calculated with respect to FMQ buffer (Linnen et al., 1995, 1996; Berndt et al., 2001; Matthews et al., 2003).

<sup>5</sup> Number of profiles measured in the run product by electron microprobe.

<sup>6</sup> SnO<sub>2</sub> concentration measured in parts per million (ppm), as ave. (average), max. (maximum) and min. (minimum).

<sup>7</sup> D is the diffusion coefficient measured in m<sup>2</sup>/s. For most of the run products in Table 2.3, data for tin diffusivity are plotted within ~10% error bars (calculated as average error after measuring different profiles in each sample).

<sup>o</sup> Bad run product. Thus, it may contain error in SnO<sub>2</sub> solubility and diffusion data.

### 2.3.3. Behavior of $SnO_2$ in subaluminous (A.S.I. = 1.0) melts

#### 2.3.3.1. Interdiffusion of major elements

Linnen et al. (1996) showed that couple diffusion of tin with the major elements of the melt is discernible from electron microprobe

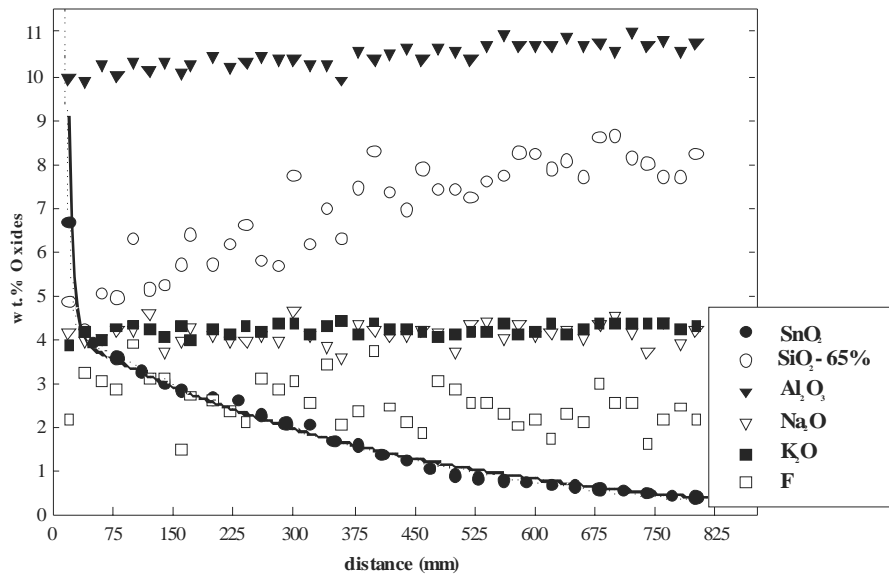


Figure 2.17: Couple diffusion in experiment 6 (Table 2.4).

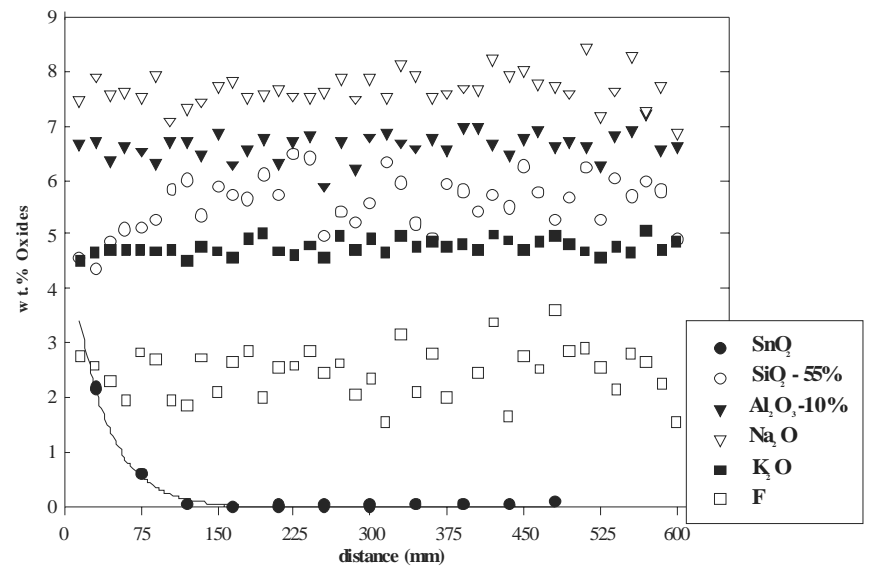


Figure 2.18: Interdiffusion of major elements in experiment 4 (see Table 2.4).

analyses when the cassiterite saturation value is greater than approximately 1 wt.%  $SnO_2$  and increases in importance with higher tin concentrations. As explained in Section 2.3.1.1, major-element concentrations along the profiles were analyzed on selected samples with the highest  $SnO_2$  concentrations. As shown in Fig. 2.17 and Fig. 2.18, there is no case of couple diffusion is observed by any diffusion of sodium towards the  $SnO_2$  crystal (see Linnen et al., 1996). It is observed from the concentration profiles of major elements w.r.t. the profile of  $SnO_2$ , as no variation in concentration of  $Na_2O$  is observed along the concentration profile of  $SnO_2$  obtained in the runs 4 and 6 (for experimental conditions of the runs; see Table 2.4). However, there is also no significant variation in alkalis and Al in experiment 4, as shown in Fig. 2.18. Thus, in the present study, coupled diffusion would not be considered a problem using subaluminous melt composition.

### ***2.3.3.2. Effect of fluorine as a $f(T)$ on $SnO_2$ solubility in subaluminous melts***

Fig. 2.19 shows results on effect of fluorine as a function of temperature on a series of experiments done in the present study. At a fixed F-content of the melt, this study shows an increase in solubility of cassiterite with an increase in temperature. The solubility of cassiterite in a subaluminous melt with 2.4 wt.% F at 2 kbar and at an  $fO_2$  of NNO, increases from 0.22 wt.%  $SnO_2$  at 600 °C to 2.45 wt.%  $SnO_2$  at 850 °C. This shows that there is a significant effect of T on  $SnO_2$  solubility and thus T plays an important role in controlling solubility of cassiterite in silicate melts. At more oxidizing conditions (NNO+3.5), cassiterite solubility does not change significantly with temperature, over the range from 650 to 800 °C and at a pressure of 2 kbar. Nearly the same trend (slope) is observed for the experiments with a melt containing 4.6 wt.% F (Starting glass: PP12%F; see Appendix; Table A.3), as a granitic melt containing 2.4 wt.% (Starting glass: PP4%F, see Table A.3). Using melt containing 4.6 wt.% F at  $800 \pm 10$  °C, 2 kbar and NNO-1.0,  $SnO_2$  solubility is measured to be 4.17 wt.%  $SnO_2$ . Whereas, from 750 to 850 °C in the latter melt at NNO,  $SnO_2$  solubility increases from 1.32 to 3.31 wt.%  $SnO_2$ , respectively.  $SnO_2$  solubility is 0.2 wt.%  $SnO_2$  when measured at  $800 \pm 10$  °C, 2 kbar and at NNO+3.5.

At a temperature of  $850 \pm 10$  °C, 2 kbar and at NNO, with an increase in F-content in the melt from 2.4 wt.% F to 4.6 wt.% F, the cassiterite solubility increases from 2.45 to 3.31 wt.% SnO<sub>2</sub>, respectively. Linnen et al. (1996) used a starting glass composition of A.S.I. =1.02 without F, and at 850 °C, 2 kbar and NNO, they reported a SnO<sub>2</sub> solubility of 0.47 wt.% SnO<sub>2</sub> in melt. When compared with study of Linnen et al. (1996) at same P, T and  $f_{O_2}$ , this study found a SnO<sub>2</sub> solubility of  $3.31 \pm 0.20$  wt.% SnO<sub>2</sub> when 4.6 wt.% F is present in the melt of A.S.I. =1.0. But at more reducing condition of NNO-1.0, Linnen et al. (1996) found a SnO<sub>2</sub> solubility of 2.78 wt.% SnO<sub>2</sub> in melt at 850 °C. Whereas at 800 °C

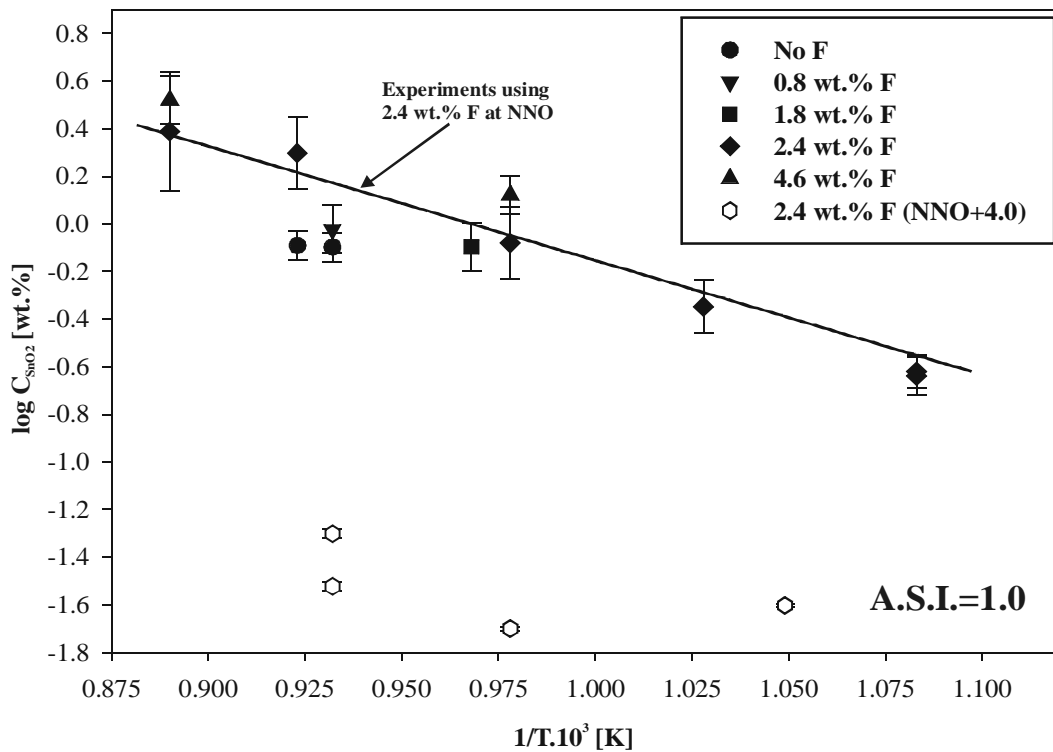


**Figure 2.19:** The graph plotted between  $C_{SnO_2}$  [wt.-%] and T (K), shows an effect of T on SnO<sub>2</sub> solubility at various  $f_{O_2}$  range from NNO to NNO+3.5. The starting glass used for all the experiments plotted in this figure, has an A.S.I. = 1.0.

and 2 kbar, this study found a SnO<sub>2</sub> solubility of  $4.17 \pm 0.25$  wt.% SnO<sub>2</sub> in melt. Thus, the data showed by the present study indicates a significant increase in SnO<sub>2</sub> solubility for experiments performed using different range of temperatures in reducing as well as in

oxidizing conditions. Results from this study show that reduced melts may dissolve much more  $SnO_2$  when compared with the solubility of  $SnO_2$  in oxidized silicate melts.

### ***2.3.3.3. Effect of $fO_2$ on $SnO_2$ solubility in subaluminous melts***

In the present study, effect of  $fO_2$  on the cassiterite solubility is measured in a series of experiments using a melt composition (A.S.I. = 1.0), shown in Table 2.4. There is a significant decrease in cassiterite solubility at oxidizing conditions compared to reducing conditions. At 800 °C and 2 kbar, cassiterite solubility decreases from 4.17 wt.%  $SnO_2$  to 0.20 wt.%  $SnO_2$  with decrease in  $\log fO_2$  from NNO-1.0 to NNO+5.0, respectively. Thus, the solubility of cassiterite is far greater in reduced (at a  $\log fO_2$  of NNO-1.0) melts when compared with oxidized (at a  $\log fO_2$  of NNO+5.0) melts.

### ***2.3.3.4. Effect of fluorine on tin diffusivity in subaluminous melt compositions***

In a synthetic subaluminous (A.S.I. = 1.0) melt at  $800 \pm 10$  °C, 2 kbar and at a  $\log fO_2$  of NNO-0.5 to NNO-1.0, Sn diffusivity increases from  $5.9 \cdot 10^{-14}$  m<sup>2</sup>/s for a F-free melt to  $4.2 \cdot 10^{-12}$  m<sup>2</sup>/s for F-bearing (4.6 wt.% F in melt) melt. Tin diffusivity in subaluminous melt with 2.4 wt.% F can fit to an equation  $\log D = -8.28 - 4.21 \cdot 10^3/T$ , where D and T are diffusivity coefficient (m<sup>2</sup>/s) and temperature (K), respectively. In a melt containing 2.4 wt.% F, tin diffusivity measured at NNO buffer varies from  $7.8 \cdot 10^{-14}$  m<sup>2</sup>/s at 650 °C to  $1.5 \cdot 10^{-12}$  m<sup>2</sup>/s at 850 °C. At NNO+3.5, an increase in temperature from 650 to 800 °C, results in an increase of D from  $8.1 \cdot 10^{-15}$  m<sup>2</sup>/s to  $1.5 \cdot 10^{-14}$  m<sup>2</sup>/s, respectively. A linear regression at NNO buffer for tin diffusivity in subaluminous melts gives an  $E_a = 80 \pm 4$  kJ/mol.

**Table 2.4: SnO<sub>2</sub> solubility and diffusion experiments in F-bearing melt with A.S.I = 1.0**

Exp. Ref. No.	P (bar)	T (°C)	Run duration (hours)	Initial H <sub>2</sub> O in glass <sup>1</sup>	F-content in melt (wt.%) <sup>2</sup>	Buffer Used <sup>3</sup> ( $f_{O_2}$ measured) <sup>4</sup>	log $f_{O_2}$ $\Delta$ FMQ <sup>5</sup>	Number of profiles measured <sup>6</sup>	Solubility log ppm SnO <sub>2</sub> <sup>7</sup>			Diffusivity D (m <sup>2</sup> /s) <sup>8</sup>		
									ave.	max.	min.	ave.	max.	min.
12FDP1	2000	850	5.5	6.08	4.6	Ni-NiO	0.57	3	4.52	4.53	4.51	2.1E-11	3.5E-11	1.3E-11
6	1950	810	6	6.08	4.6	Co-rod (-14.86)	-0.5	5	4.62	4.61	4.63	4.2E-12	5.7E-12	3.5E-12
12	2215	798	42	6.08	4.6	HM (-8.65)	5.70	3	3.30	3.31	2.29	5.2E-15	7.1E-15	3.9E-15
12FDP2	2000	750	5.5	6.08	4.6	Ni-NiO	0.57	4	4.12	4.14	4.10	3.8E-12	5.4E-12	1.9E-12
6 FDP1	2000	850	5.5	6.79	2.4	Ni-NiO	0.57	5	4.39	4.40	4.38	1.5E-12	2.1E-12	1.1E-12
4	2010	810	6	6.79	2.4	Co-rod (-13.97)	0.38	5	4.30	4.34	4.27	2.8E-12	3.7E-12	2.1E-12
10	1880	802	45	6.79	2.4	HM (-9.85)	4.50	3	2.99	3.00	2.98	1.5E-14	2.8E-14	1.2E-14
13 <sup>†</sup>	1950	755	46	6.79	2.4	Co-rod (-13.70)	0.65	3	3.92	3.92	3.91	8.3E-13	-	-
16	1940	753	45	6.79	2.4	HM (-9.90)	4.45	3	2.58	2.60	2.56	1.3E-14	2.1E-14	1.1E-14
6 FDP2	2000	750	5.5	6.79	2.4	Ni-NiO	0.57	5	3.79	3.81	3.77	7.9E-13	9.8E-13	6.1E-13
14	2000	705	48	6.79	2.4	Co-rod (-12.98)	1.37	2	3.65	3.66	-	-	-	-
17	1880	697	42	6.79	2.4	HM (-10.4)	3.95	3	2.55	2.60	2.50	0.8E-14	1.1E-14	8.8E-15
18	1870	655	42	6.79	2.4	HM (-10.1)	4.25	3	2.35	2.36	2.35	8.1E-15	9.8E-15	6.4E-15
15	1850	655	72	6.79	2.4	Co-rod (-13.62)	0.73	3	3.38	3.40	3.36	7.8E-14	1.2E-13	5.6E-14
42	2000	605	24	5.50	2.4	Co-rod (-14.51)	-0.16	4	3.35	3.40	3.31	1.2E-13	1.6E-13	9.1E-14
5°	2030	810	6	5.50	2.3	Co-rod (-13.98)	0.37	3	4.29	4.30	4.28	9.8E-13	1.5E-12	7.4E-13
11°	2250	795	42	5.50	2.3	HM (-9.70)	4.65	3	3.00	3.12	2.88	2.2E-14	3.6E-14	1.4E-14
48° <sup>†</sup>	1900	700	20	5.50	2.3	Co-rod (-13.47)	0.88	3	4.06	4.10	4.02	-	-	-
45°	1500	655	22	5.50	2.3	Co-rod (-13.47)	0.88	3	3.10	3.14	3.06	8.4E-14	1.2E-13	6.2E-14
4 FDP1	2010	845	6	5.82	1.9	Ni-NiO	0.57	4	3.96	3.98	3.94	1.7E-12	2.3E-12	1.2E-12
3*	2030	810	6	5.82	1.9	Co-rod (-14.21)	-0.14	1	4.08	-	-	-	-	-
9	1940	800	43	5.82	1.9	HM (-9.60)	4.75	3	2.55	2.58	2.52	3.6E-14	4.7E-14	2.5E-14

**Table 2.4 (continued):**

Exp. Ref. No.	P (bar)	T (°C)	Run duration (hours)	Initial H <sub>2</sub> O in glass <sup>1</sup>	F-content in melt (wt.%) <sup>2</sup>	Buffer Used <sup>3</sup> ( $fO_2$ measured) <sup>4</sup>	log $fO_2$ $\Delta$ FMQ (bar) <sup>5</sup>	Number of profiles measured <sup>6</sup>	Solubility log ppm SnO <sub>2</sub> <sup>7</sup>			Diffusivity D (m <sup>2</sup> /s) <sup>8</sup>		
									ave.	max.	min.	ave.	max.	min.
4 FDP2	2000	750	6	5.82	1.9	Ni-NiO	0.57	4	3.89	3.90	3.88	5.5E-13	7.1E-13	3.8E-13
2 FDP2	2030	855	5.5	5.68	0.8	Ni-NiO	0.57	4	4.04	4.06	4.02	2.4E-12	3.2E-12	1.8E-12
2	2020	810	6	5.68	0.8	Co-rod (-13.78)	0.57	3	3.93	3.94	3.92	7.7E-13	9.9E-13	5.8E-13
8	1940	800	43	5.68	0.8	HM (-9.44)	4.91	3	2.45	2.49	2.41	2.3E-14	3.8E-14	1.4E-14
2 FDP1	2000	750	5.5	5.68	0.8	Ni-NiO	0.57	4	3.79	3.81	3.77	6.8E-13	8.9E-13	5.5E-13
1	1900	805	10	5.10	0.0	Co rod (-14.09)	0.26	4	3.91	3.92	3.90	5.9E-14	7.3E-14	4.1E-14
7	1930	800	43	5.10	0.0	HM (-9.55)	4.88	4	2.55	2.57	2.53	4.2E-14	5.6E-14	2.7E-14

**Abbreviations:** P, pressure (in bars); T, temperature (in degree Celsius); F, Fluorine;  $fO_2$ , oxygen fugacity; FMQ, Fayalite-Magnetite-Quartz buffer.

<sup>1</sup> Amount of water (in weight percent) measured in prehydrated glass using Karl Fischer technique (KFT). Calculated error is  $\pm 0.1$  wt.%.  
<sup>2</sup> Fluorine content of the melt (in weight percent). Different melt compositions were prepared using different fluorine concentrations.  
<sup>3</sup> Buffer was used in the form of rod (e.g. "Co" stands for Cobalt) or in the powdered form (e.g. "HM" and "NNO" stand for Hematite-Magnetite and Nickel-Nickel Oxide, respectively).  
<sup>4</sup> Oxygen fugacity measured using double capsule technique from Chou, 1987a (see text for details).  
<sup>5</sup> Log  $fO_2$  calculated with respect to FMQ buffer (Linnen et al., 1995, 1996; Berndt et al., 2001; Matthews et al., 2003).  
<sup>6</sup> Number of profiles measured in the run product by electron microprobe.  
<sup>7</sup> SnO<sub>2</sub> concentration measured in parts per million (ppm), as ave. (average), max. (maximum) and min. (minimum).  
<sup>8</sup> D is the diffusion coefficient measured in m<sup>2</sup>/s. D is the diffusion coefficient measured in m<sup>2</sup>/s. For most of the run products in Table 2.3, data for tin diffusivity are plotted within ~10% error bars (calculated as average error after measuring different profiles in each sample).  
\* Run product was partially destroyed and could lead to any discrepancy in solubility data. SnO<sub>2</sub> diffusivity is not calculated in such case.  
<sup>o</sup> Bad run product (run product was partially crystallized. Thus concentration profiles were selected in crystal-free areas of the glass). Thus, it may contain error in SnO<sub>2</sub> solubility and diffusion data.  
<sup>†</sup> Systematic error may be >5% (see Section 2.2.6 for more details).

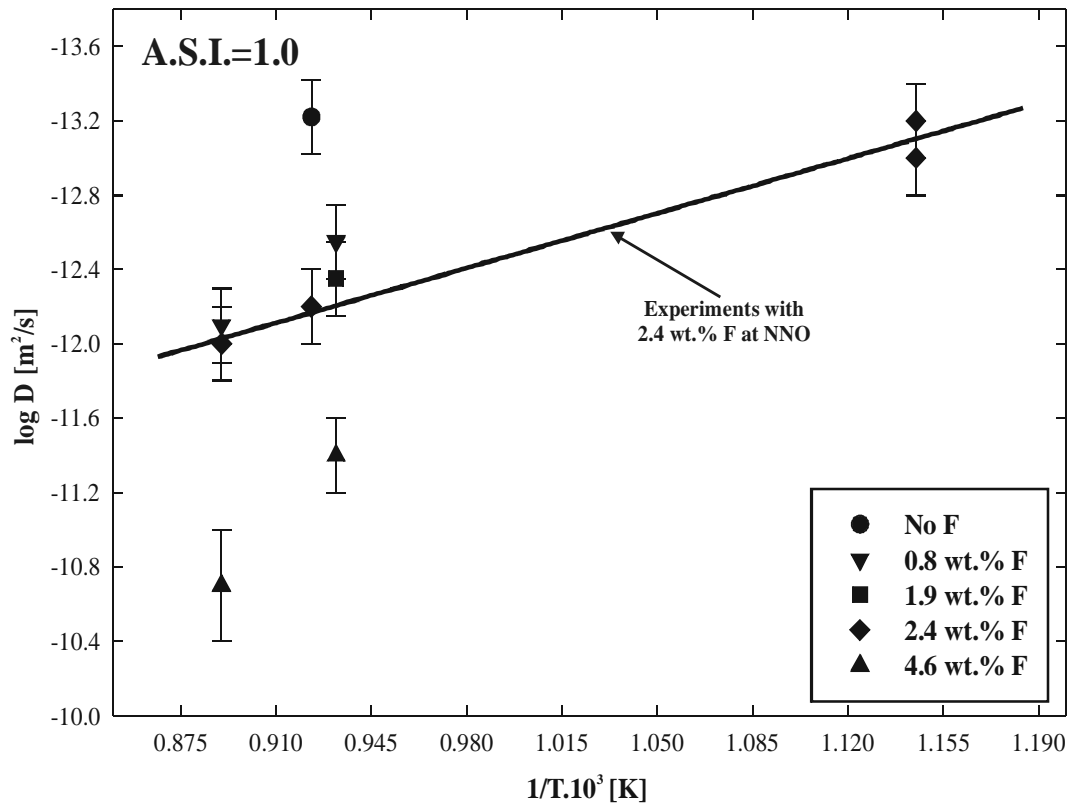


**Figure 2.20: At NNO-0.5 to NNO-1, graph shows an Arrhenius relation between  $D$  and  $T$  in subaluminous melt. Diffusivity of tin can be calculated as  $\log D = -8.28 - 4.21 \cdot 10^3/T$ . Linear regression for tin diffusivity in subaluminous melts containing 2.4 wt.% F gives an  $E_a = 80 \pm 4$  kJ/mol.**

Linnen et al. (1996) reported the tin diffusivity in melts with different A.S.I. at constant  $T$  and  $P$  but at different  $fO_2$ , therefore, the Sn diffusivity data obtained by this study using melt composition with A.S.I.=1.0 can be compared with F-free melt composition (A.S.I. = 1.02) from study of Linnen et al. (1996). In a F-free melt (A.S.I. = 1.0) at 850 °C, 2 kbar and NNO buffer, Linnen et al. (1996) found a Sn diffusivity of  $1.6 \cdot 10^{-12}$  m<sup>2</sup>/s, whereas at same  $P$ ,  $T$  and  $fO_2$  but using F-bearing (4.6 wt.% F in melt) melt composition, this study found a tin diffusivity of  $2.1 \cdot 10^{-11}$  m<sup>2</sup>/s. Thus, at 850 °C, 2 kbar and at a  $\log fO_2$  of  $\sim$ NNO, an increase of one order of magnitude has been observed for Sn diffusivity in subaluminous melts (A.S.I. = 1.0) when F-content of the melt increases from 0 to 4.6 wt.% F. Results on tin diffusivity in silicate melts with different F-contents are shown in Fig. 2.20 and Table 2.4.



### **2.3.4. F-bearing peralkaline (A.S.I. $\leq$ 0.6) melts**

#### ***2.3.4.1. Interdiffusion of major elements***

Linnen et al. (1996) showed the problem of couple diffusion of tin with the major elements of the melt in the peralkaline melt (A.S.I. = 0.64) used in their study. Major-element concentrations along the profiles were analyzed on selected samples (using peralkaline melt composition) with the highest SnO<sub>2</sub> concentrations. In this study, the run products showed a small variation of sodium concentration towards the SnO<sub>2</sub> crystal. However, no significant variation in alkali (K), Si and Al has been observed in all run products using peralkaline melt composition.

#### ***2.3.4.2. Effect of T and $fO_2$ on cassiterite solubility in peralkaline melts***

Run products obtained using F-bearing peralkaline melt compositions (where concentration of F in the melt has been varied) show an increase in cassiterite solubility with an increase of temperature at 2 kbar. All experiments were performed at a log  $fO_2$  of NNO. Therefore, at a log  $fO_2$  of NNO from 650 to 750 °C in a peralkaline melt containing 4.2 wt.% F, SnO<sub>2</sub> solubility increases from 1.73 to 3.24 wt.% SnO<sub>2</sub>, respectively. Whereas, in a peralkaline melt containing 3.7 wt.% F at NNO, cassiterite solubility increases from 3.17 wt.% SnO<sub>2</sub> to 8.32 wt.% SnO<sub>2</sub> with an increase in temperature from 740 to 850 °C, respectively. In a F-free peralkaline melt at 2 kbar and at a log  $fO_2$  of NNO, cassiterite solubility increases from 2.40 to 6.17 wt.% SnO<sub>2</sub> with an increase in temperature from 750 to 860 °C, respectively. Thus, it is concluded that temperature does play an important role in transporting tin in silicate melts.

#### ***2.3.4.3. Effect of F on cassiterite solubility in peralkaline melts***

There are no studies that have examined the effect of fluorine on solubility of cassiterite in peralkaline melts. Results from the present study (see Table 2.5), show that SnO<sub>2</sub> solubility

in a peralkaline melt containing 0 to 4.2 wt.% F in melt, varies from  $6.17 \pm 1.10$  wt.% to  $8.32 \pm 1.10$  wt.%  $\text{SnO}_2$ , respectively.  $\text{SnO}_2$  solubilities obtained at 850 °C and 2 kbar in a F-free peralkaline melt, are in a good agreement with the study of Linnen et al. (1996). Cassiterite solubility data is plotted in Fig. 3.9, where regression line trends are calculated for two different compositions. For F-free and F-bearing (3.7 wt.% F in melt) compositions, cassiterite solubility can be fitted by the equation  $\log C_{\text{SnO}_2} = -3.51 + 4.41 \cdot 10^3/T$  and  $\log C_{\text{SnO}_2} = 5.16 - 4.76 \cdot 10^3/T$ , respectively, where,  $C_{\text{SnO}_2}$  is the log concentration of  $\text{SnO}_2$  (wt.%) and T is temperature (K). It can be seen in Fig. 3.9 that cassiterite solubility increases from 2.40 to 3.23 wt%  $\text{SnO}_2$  with an increase in F-content of

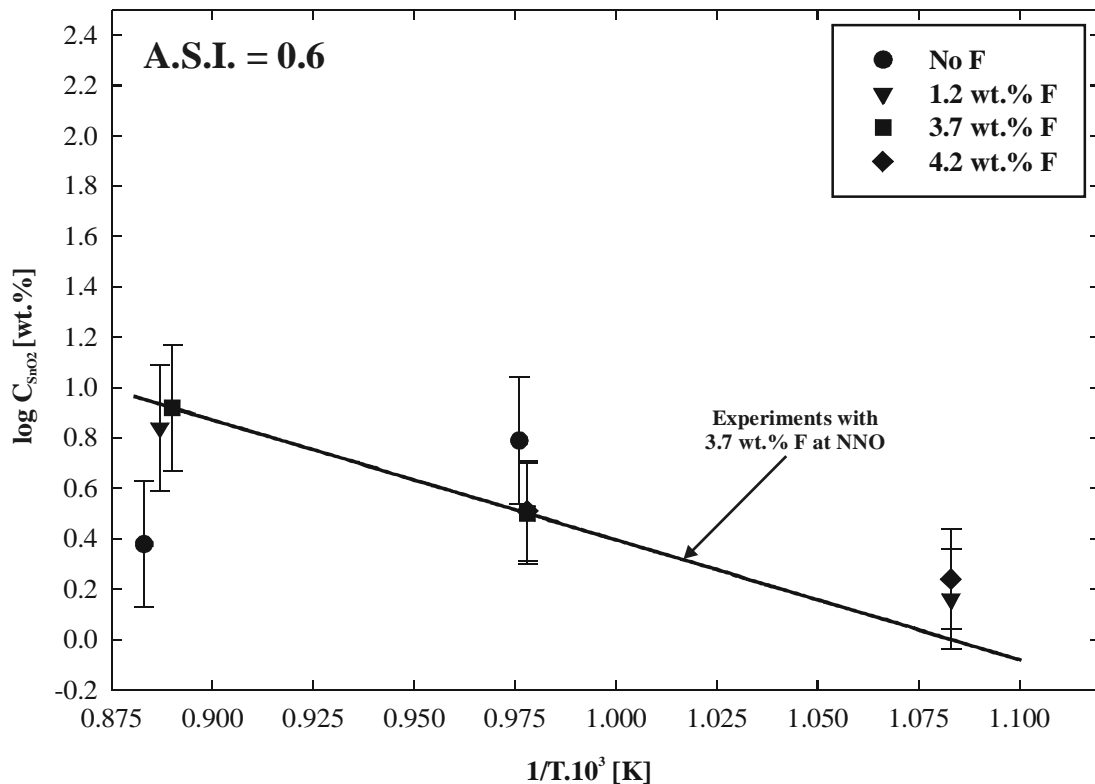


**Figure 2.21: Graph between  $\log C_{\text{SnO}_2}$  (ppm) versus T (K) for peralkaline melt (A.S.I. = 0.6). Regression line (solid line) is plotted for experiments using F-bearing composition with 3.7 wt.% F.**

the melt from 0 to 4.2 wt.% F. Thus, it can be concluded that fluorine does influence solubility of  $\text{SnO}_2$  in peralkaline melts.

**Table 2.5: SnO<sub>2</sub> solubility and diffusion experiments in F-bearing melt with A.S.I. = 0.6**

Exp. Ref. No.	P (bar)	T (°C)	Run duration (hours)	Initial H <sub>2</sub> O in glass <sup>1</sup>	F-content in melt (wt.%) <sup>2</sup>	Buffer Used <sup>3</sup>	log $f_{O_2}$ $\Delta$ FMQ <sup>4</sup>	Number of profiles measured <sup>5</sup>	Solubility log ppm SnO <sub>2</sub> <sup>6</sup>			Diffusivity D (m <sup>2</sup> /s) <sup>7</sup>		
									ave.	max.	min.	ave.	max.	min.
78	1960	745	6.5	6.50	4.2	Ni-NiO	0.57	4	4.51	4.43	4.06	1.0E-12	1.6E-12	0.8E-12
79	2030	650	6.5	6.50	4.2	Ni-NiO	0.57	2	4.24	-	-	5.4E-14	7.1E-14	-
80	2030	850	6.5	6.20	3.7	Ni-NiO	0.57	2	4.92	-	-	3.8E-12	4.5E-12	-
81°	1980	740	6.5	6.20	3.7	Ni-NiO	0.57	2	4.50	4.48	-	1.3E-12	-	-
83	2035	855	6.5	6.20	1.2	Ni-NiO	0.57	1	4.84	-	-	1.2E-12	-	-
85†	2010	650	6.5	6.20	1.2	Ni-NiO	0.57	2	4.16	-	4.18	0.5E-14	-	-
88°	2030	860	6.5	6.50	0.0	Ni-NiO	0.57	1	4.79	-	-	3.6E-12	-	-
87	1980	750	6.5	6.50	0.0	Ni-NiO	0.57	3	4.38	4.41	4.36	8.3E-12	9.0E-12	7.8E-12

**Abbreviations:** P, pressure (in bars); T, temperature (in degree Celsius); F, Fluorine;  $f_{O_2}$ , oxygen fugacity; FMQ, Fayalite-Magnetite-Quartz buffer.

<sup>1</sup> Amount of water (in weight percent) measured in prehydrated glass using Karl Fischer technique (KFT). The calculated error is  $\pm 0.2$  wt. %.

<sup>2</sup> Chlorine content of the melt (in weight percent). Different melt compositions were prepared using different chlorine concentrations.

<sup>3</sup> Buffer was used in a powdered form, where “NNO” stands for Nickel-Nickel Oxide.

<sup>4</sup> Log  $f_{O_2}$  calculated with respect to FMQ buffer (Linnen et al., 1995, 1996; Berndt et al., 2001; Matthews et al., 2003).

<sup>5</sup> Number of profiles measured in the run product by electron microprobe.

<sup>6</sup> SnO<sub>2</sub> concentration measured in parts per million (ppm), as ave. (average), max. (maximum) and min. (minimum).

<sup>7</sup> D is the diffusion coefficient measured in m<sup>2</sup>/s. For those run products where D is measured only from one single SnO<sub>2</sub> diffusion fit, data is plotted with 10% error bars. In this Table, D (max.) and D (min.) values are plotted for most of the experiments.

° Bad run product (run product was partially crystallized. Thus concentration profiles were selected in crystal-free areas of the glass). Thus, it may contain error in SnO<sub>2</sub> solubility and diffusion data.

† Systematic error may be >5% (see Section 2.2.6 for more details).

#### ***2.3.4.4. Effect of F on diffusivity of tin in peralkaline melt compositions***

Tin diffusivity data obtained in the present study (Table 2.5) using peralkaline melts is also compared with study of Linnen et al. (1996) who also used peralkaline melt with a different A.S.I. content. Results obtained in this study show that F does not seem to change diffusivity of tin in peralkaline melt compositions. At  $750 \pm 10$  °C, 2 kbar and NNO buffer, this study found that diffusivity of tin varies from  $1.3 \cdot 10^{-12}$  m<sup>2</sup>/s to  $1.10^{-12}$  m<sup>2</sup>/s for an increase in the melt F-content of 3.7 to 4.2 wt.% F, respectively. Therefore, there is no apparent effect of F on the diffusion of tin.

#### ***2.3.4.5. Apparent equilibrium experiments***

A comparison of the cassiterite solubility results of this study with those of Linnen et al. (1996) show that the two studies are close. To cross-check the cassiterite solubility in peralkaline melts (A.S.I. = 0.6), apparent equilibrium experiments were performed. At 850 °C, 2 kbar and  $\sim$ NNO+3.0, Linnen et al. (1996) found SnO<sub>2</sub> solubility of  $\sim$  5.8 wt.% SnO<sub>2</sub> after performing apparent equilibrium experiments. Whereas, at 800 °C, 2 kbar and an  $fO_2$  of NNO+5.0, this study found SnO<sub>2</sub> solubility ranging from  $\sim$ 4.5 to 7.1 wt.% SnO<sub>2</sub> (see Table 2.6 for more details). The cassiterite solubility values of this study are lower than those of Linnen et al. (1996). This may be due to the lower experimental temperature and higher oxidizing conditions adopted in the present study. Results on apparent equilibrium experiments are illustrated in Fig. 2.21.

**Table 2.6: Apparent equilibrium experiments using F-bearing melt with A.S.I. = 0.6**

Exp. Ref. No.	P (bar)	T (°C)	Run duration (hours)	Initial H <sub>2</sub> O in glass <sup>1</sup>	F-content in melt (wt.%) <sup>2</sup>	Buffer Used <sup>3</sup> ( $fO_2$ measured) <sup>4</sup>	log $fO_2$ $\Delta$ FMQ (bar) <sup>5</sup>	Number of profiles measured <sup>6</sup>	Solubility log ppm SnO <sub>2</sub> <sup>7</sup>		
									ave.	max.	min.
73	2010	800	528	6.50	0.0	HM (-9.70)	4.65	2	4.85	4.87	4.82
74	2010	800	528	6.50	0.0	HM (-9.70)	4.65	2	4.66	4.68	4.65
75°	2010	800	528	6.50	0.0	HM (-9.34)	5.01	2	4.70	4.71	4.68
76	2010	800	528	6.50	0.0	HM (-9.34)	5.01	2	4.78	4.80	4.77

**Abbreviations:** P, pressure (in bars); T, temperature (in degree Celsius); F, Fluorine;  $fO_2$ , oxygen fugacity; FMQ, Fayalite-Magnetite-Quartz buffer.

<sup>1</sup> Amount of water (in weight percent) measured in prehydrated glass using Karl Fischer technique (KFT). The calculated error is  $\pm 0.2$  wt. %.

<sup>2</sup> Fluorine content of the melt (in weight percent). Different melt compositions were prepared using different fluorine concentrations.

<sup>3</sup> Buffer was used in powdered form (e.g. "HM" stands for Hematite-Magnetite).

<sup>4</sup> Oxygen fugacity measured using double capsule technique from Chou, 1987a (see text for details).

<sup>5</sup> Log  $fO_2$  calculated (in bars) with respect to FMQ buffer (Linnen et al., 1995, 1996; Berndt et al., 2001; Matthews et al., 2003).

<sup>6</sup> Number of profiles measured in the run product by electron microprobe.

<sup>7</sup> SnO<sub>2</sub> concentration measured in parts per million (ppm), as ave. (average), max. (maximum) and min. (minimum).

<sup>°</sup> Bad run product (run product was partially crystallized). Thus concentration profiles were selected in crystal-free areas of the glass). Thus, it may contain error in SnO<sub>2</sub> solubility and diffusion data.

### 2.3.5. Behavior of $SnO_2$ in Pegmatite melt composition

#### 2.3.5.1. Interdiffusion of major elements

At 800-850 °C, 2 kbar and at a  $\log fO_2$  ranges from NNO to NNO-1.0, no diffusion coupling has been observed in experiments using pegmatitic melt composition. All major element, e.g., alkalis (Na, K), Al and Si show small variation. In Fig. 2.22, both  $Na_2O$  and

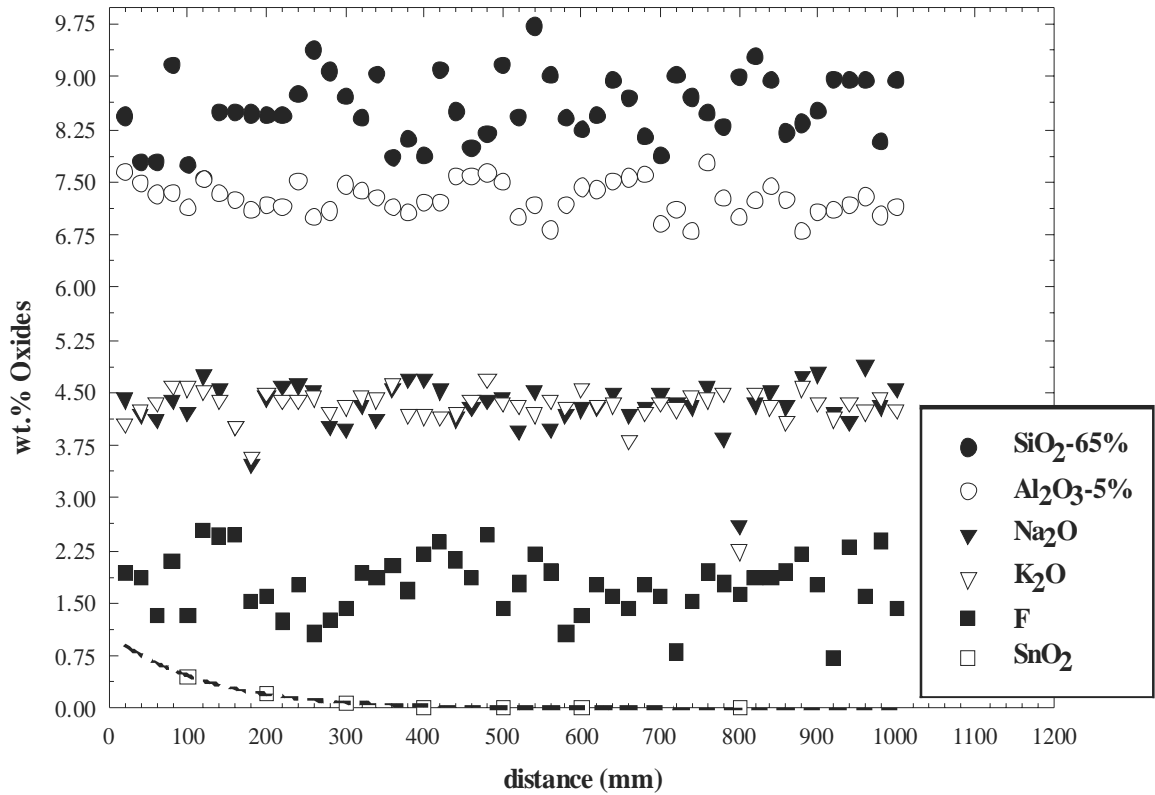
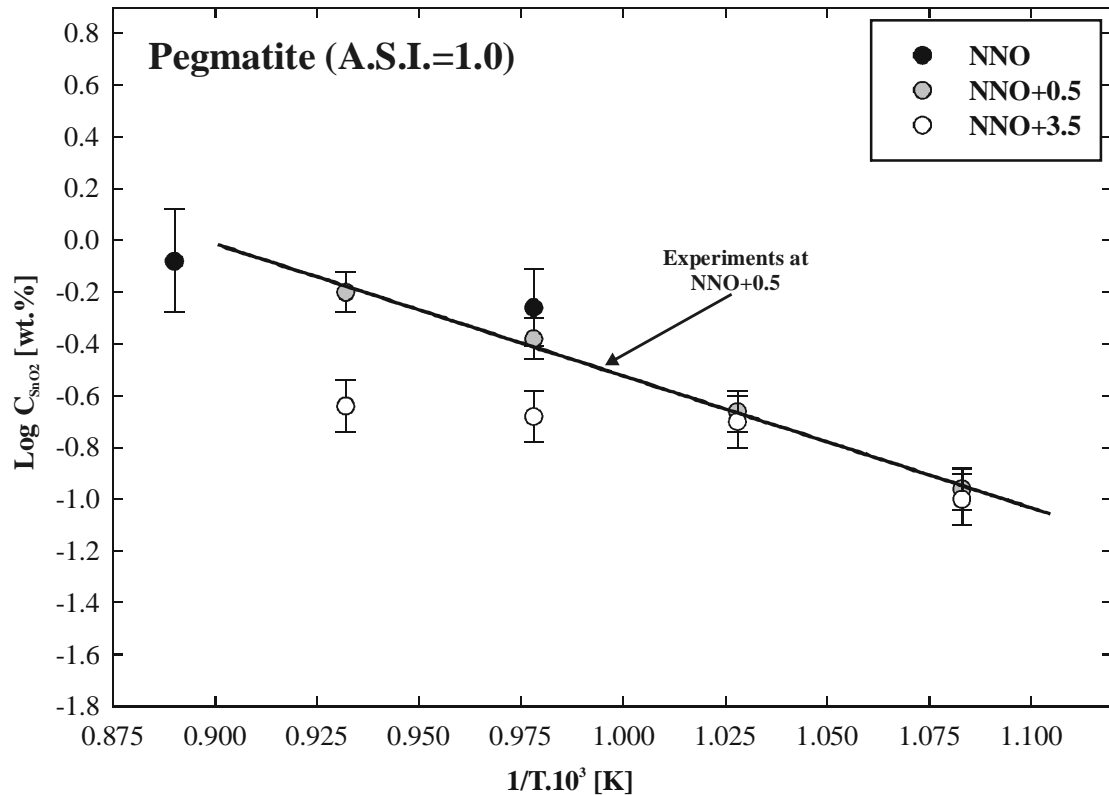


Figure 2.22: Interdiffusion of major elements in experiment 19.

$K_2O$  show  $\sim 4.25 \pm 0.25$  wt.%, whereas  $SiO_2$ -65% shows a bigger variation of about  $\pm 0.5$  wt.%. All other elements are homogeneous within error.

### 2.3.5.2. Effect of T and $fO_2$ on cassiterite solubility in pegmatitic melt

Experiments have been done using pegmatitic melt, at different temperatures and also at different buffer conditions. The  $fO_2$  varies from reducing (NNO) conditions to more oxidizing (NNO+3.5) conditions. By plotting the data, it can be concluded that temperature has a very significant effect on cassiterite solubility in pegmatitic melt. At a log  $fO_2$  of NNO,  $SnO_2$  solubility in a pegmatitic melt (contains ~ 4 wt.% F, 2 wt.%  $B_2O_3$ , 1.5 wt.%



**Figure 2.23:** Graph between  $1/T \cdot 10^3$  (K) versus  $\log C_{SnO_2}$  (wt.%), shows effect of temperature in various  $fO_2$  in a pegmatitic melt. A linear fit has been shown for the runs at an  $fO_2$  (reducing: NNO+0.5).

$P_2O_5$  and 1 wt.%  $Li_2O$ ; see Appendix; Table A.5 for more details) at 750 to 850 °C increases from 0.55 wt.%  $SnO_2$  to 0.83 wt.%  $SnO_2$ , respectively. Whereas, at a log  $fO_2$  of NNO+0.5,  $SnO_2$  solubility in pegmatitic melt from 650 to 800 °C, varies from 0.13 wt.%  $SnO_2$  to 0.63 wt.%  $SnO_2$ , respectively. At a log  $fO_2$  of NNO+0.5, cassiterite solubility in the pegmatitic melt can be fitted to the equation:  $\log C_{SnO_2} = 4.58 - 5.10 \cdot 10^3/T$ , where

$C_{SnO_2}$  and T are concentration of  $SnO_2$  (wt.%) and temperature (K), respectively, whereas, run at a  $\log fO_2$  of NNO has nearly the same slope as observed for run a  $\log fO_2$  of NNO+0.5. However, runs at a  $\log fO_2$  of NNO+3.5 can be fitted to the equation:  $\log C_{SnO_2} = 1.47 - 2.21 \cdot 10^3/T$ . Cassiterite solubility data in the pegmatitic melt composition is well illustrated in Fig. 2.23.

Oxygen fugacity also plays an important role in controlling cassiterite solubility in the pegmatitic melt composition. At a  $\log fO_2$  of NNO+0.5, cassiterite solubility decreases from 0.63 wt.%  $SnO_2$  at 850 °C to 0.11 wt.%  $SnO_2$  at 650 °C, whereas at NNO, solubility of  $SnO_2$  decreases from 0.83 wt.%  $SnO_2$  at 850 °C to 0.55 wt.%  $SnO_2$  at 750 °C. But a very small effect of temperature on  $SnO_2$  solubility is observed for the experiments that were performed at more oxidizing conditions. At more oxidizing conditions (NNO+3.5),  $SnO_2$  solubility increases from 0.10 wt.%  $SnO_2$  at 650 °C to 0.23 wt.%  $SnO_2$  at 850 °C. This indicates that  $SnO_2$  solubility does show a small increase with an increase in temperature from 650 to 850 °C, whereas  $fO_2$  plays also a very important role in controlling solubility of  $SnO_2$  in pegmatite.

### 2.3.5.3. Diffusivity of tin in pegmatitic melt composition

At a  $\log fO_2$  of ~NNO in pegmatite melt (A.S.I. = 1.0), the diffusivity of tin increases from  $6.7 \cdot 10^{-14}$  m<sup>2</sup>/s at 650 °C to  $8.2 \cdot 10^{-12}$  m<sup>2</sup>/s at 850 °C, whereas, at a  $\log fO_2$  of NNO+3.5, D varies from  $4.5 \cdot 10^{-15}$  m<sup>2</sup>/s at 650 °C to  $5.5 \cdot 10^{-13}$  m<sup>2</sup>/s at 800 °C. In Fig. 2.24, it can be also seen that in this melt (A.S.I. = 1.0) at ~NNO between 650-850 °C, tin diffusivity can be fitted to the equation:  $\log D = -2.05 - 10.27 \cdot 10^3/T$ . Thus, activation energy ( $E_a$ ) for  $SnO_2$  diffusivity in experiments done at a  $\log fO_2$  of NNO is calculated to be  $196 \pm 20$  kJ/mol (see Table 2.8 for details). Similarly, at an  $\log fO_2$  of NNO+3.5 and temperature between 650-800 °C, diffusivity in the pegmatite melt can be fitted to the equation:  $\log D = 2.10 - 15.18 \cdot 10^3/T$  (not shown in Fig. 2.24).  $E_a$  calculated for  $SnO_2$  diffusivity in experiments with Pegmatite at NNO+3.5, is  $290 \pm 30$  kJ/mol. Arrhenius



**Table 2.7: SnO<sub>2</sub> solubility and diffusion experiments in pegmatitic melt with A.S.I. 1.0**

Exp. Ref. No.	P (bar)	T (°C)	Run duration (hours)	Initial H <sub>2</sub> O in glass <sup>1</sup>	F-content in melt (wt.%) <sup>2</sup>	Buffer Used <sup>3</sup> ( $fO_2$ measured) <sup>4</sup>	log $fO_2$ $\Delta$ FMQ <sup>5</sup>	Number of profiles measured <sup>6</sup>	Solubility log ppm SnO <sub>2</sub> <sup>7</sup>			Diffusivity D (m <sup>2</sup> /s) <sup>8</sup>		
									ave.	max.	min.	ave.	max.	min.
PFDP1	1990	850	6	4.91	2.0	Ni-NiO	0.57	3	3.92	3.94	3.90	8.2E-12	9.8E-12	6.5E-12
19	2010	800	6	4.91	2.0	Co-rod (-14.02)	0.33	3	3.80	3.82	3.78	1.7E-12	2.6E-12	9.7E-13
20	1950	755	46	4.91	2.0	Co-rod (-13.70)	0.65	4	3.63	3.65	3.61	8.5E-13	1.5E-12	6.6E-13
PFDP2°	2030	750	6	4.91	2.0	Ni-NiO	0.57	2	3.74	-	-	7.4E-13	-	-
21	2010	705	48	4.91	2.0	Co-rod (-13.60)	0.75	4	3.36	3.40	3.32	4.5E-13	6.5E-13	2.8E-13
22	2010	655	72	4.91	2.0	Co-rod (-13.62)	0.73	3	3.10	3.10	3.00	6.7E-14	9.6E-14	4.8E-14
23°	1880	802	45	4.91	2.0	HM (-10.25)	4.10	1	3.37	-	-	5.5E-13	-	-
24	1940	753	45	4.91	2.0	HM (-10.41)	3.94	3	3.32	3.35	3.29	4.8E-13	7.1E-13	1.9E-13
25	1880	695	42	4.91	2.0	HM (-10.93)	3.42	3	3.40	3.43	3.37	2.0E-14	3.8E-14	1.3E-14
26°	1870	650	42	4.91	2.0	HM (-9.87)	4.48	1	3.05	-	-	4.5E-15	-	-

**Abbreviations:** P, pressure (in bars); T, temperature (in degree Celsius); F, Fluorine;  $fO_2$ , oxygen fugacity; FMQ, Fayalite-Magnetite-Quartz buffer.

<sup>1</sup> Amount of water (in weight percent) measured in prehydrated glass using Karl Fischer technique (KFT). The calculated error is  $\pm 0.1$  wt. %.

<sup>2</sup> Fluorine content of the melt (in weight percent). Different melt compositions were prepared using different fluorine concentrations.

<sup>3</sup> Buffer was used in the form of rod (e.g. “Co” stands for Cobalt) or in the powdered form (e.g. “HM” and “NNO” stand for Hematite-Magnetite and Nickel-Nickel Oxide, respectively).

<sup>4</sup> Oxygen fugacity measured using double capsule technique from Chou, 1987a (see text for details).

<sup>5</sup> Log  $fO_2$  calculated with respect to FMQ buffer (Linnen et al., 1995, 1996; Berndt et al., 2001; Matthews et al., 2003).

<sup>6</sup> Number of profiles measured in the run product by electron microprobe.

<sup>7</sup> SnO<sub>2</sub> concentration measured in parts per million (ppm), as ave. (average), max. (maximum) and min. (minimum).

<sup>8</sup> D is the diffusion coefficient measured in m<sup>2</sup>/s. For those run products where D is measured only from one single SnO<sub>2</sub> diffusion fit, data is plotted with 10% error bars. In this Table, D (max.) and D (min.) values are plotted for most of the experiments.

<sup>°</sup> Bad run product. Thus, it may contain error in SnO<sub>2</sub> solubility and diffusion data.

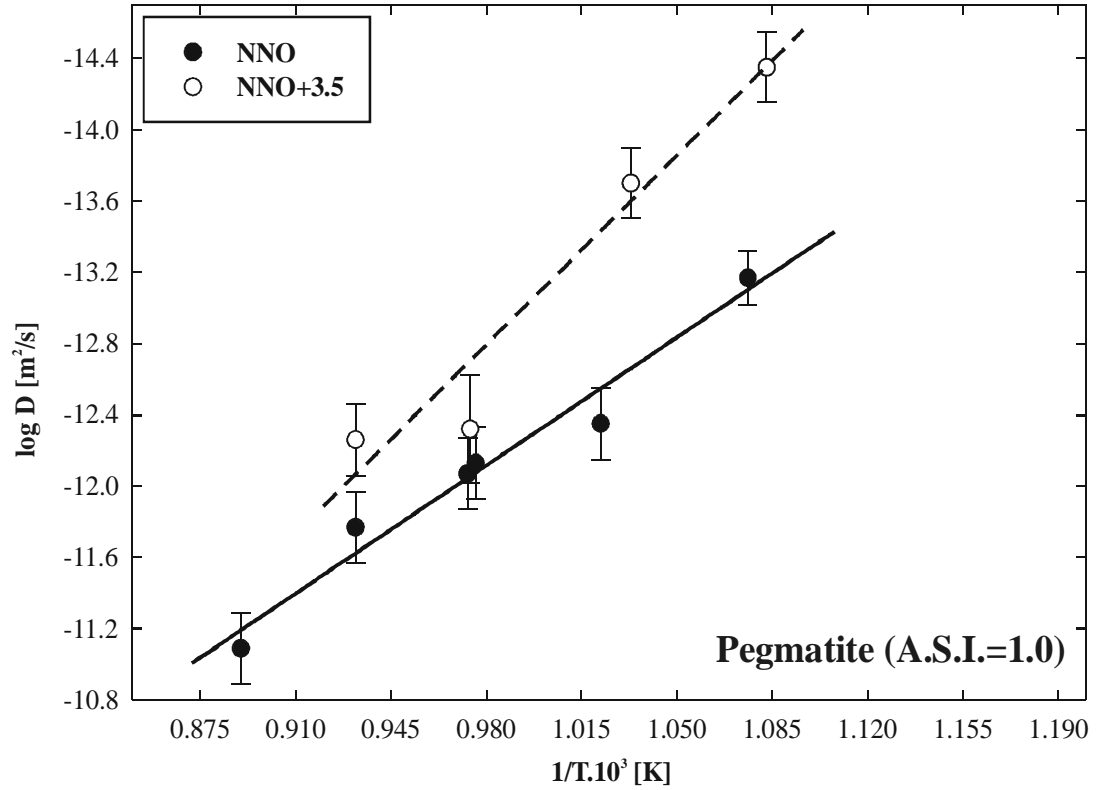


**Figure 2.24: Diffusivity in tin in pegmatite melt (A.S.I. = 1.0) at various  $fO_2$ . At NNO, a linear regression gives an  $E_a = 196 \pm 20$  kJ/mol, whereas, diffusivity of tin can be calculated as  $\log D = -2.05 - 10.27 \cdot 10^3/T$ .**

parameters for tin diffusion are listed in Table 2.8.

## 2.4. Discussion

### 2.4.1. This study versus natural systems

#### 2.4.1.1. *Effect of T, $fO_2$ and fluorine on the transport of cassiterite in silicate melts*

Charoy and Noronha (1996) studied a  $SnO_2$ -saturated ( $SnO_2$ -enriched) Argemela microgranite body in central Portugal, which displays many of mineralogical and chemical features characteristic of peraluminous, Li, P-rich, rare element pegmatites. This microgranite body contains cassiterite, beryl and columbite as main accessory minerals. It also shows extreme enrichment in incompatible elements such as F, P, Rb, Cs, Li, Sn and Be, and extreme depletion in Sr, Ba, Zr and REE. It is also highly sodic and peraluminous. However, Antipin et al. (1981) also concluded that the rare-metal ongonites are subvolcanic analogs of the tin-bearing granites and that at the end of crystallization of the ongonite magma, the tin extensively transferred to the fluid. Antipin et al. (1981) also mentioned that the empirical signs of potential tin content in acid magmas (elevated tin contents in the rocks, accumulation in the late phases, high contents in biotite, and abundant fluorine in the rocks, etc.), are consequences of low values of combined distribution coefficient, K and dependence on the contents of tin and fluorine. Webster et al. (1997) report up to 1200 ppm Sn in P- and F-rich melt inclusions from Erzgebirge, indicating that some highly evolved granites contain high tin concentrations, in support of a magmatic origin of some tin deposits. Another study of Jiang et al. (2004) show geochemical data on trace and rare-earth elements in cassiterite from Yunlong tin deposit, Yunnan (China), and propose two different models for the origin of this deposit. One model suggests that this deposit is a granite-related magmatic – hydrothermal deposit, possibly as distal deposit related to regionally occurring granitic bodies or deep unexposed granite intrusions in the mine area. Whereas, the other model suggests that the deposit has no direct genetic connection to granites; rather it is of magmatic – hydrothermal origin and was formed during a strong deformation and metamorphic event of Caledonian age. Jiang et al. (2004) suggested that cassiterite was likely precipitated from migmatitic – hydrothermal fluids. All these studies indicate a possible magmatic origin for cassiterite in silicate melts.

There are number of studies (e.g., London et al., 1982; Pichavant, 1987; Pollard et al., 1987; Linnen et al., 1992; London, 1992; Raimbault et al., 1995; Webster et al., 1997; Linnen, 1998a, 1998b; many others) which analyzed fluid-/melt-inclusions and their significance in pegmatites. It is believed that pegmatite-forming liquids achieved extreme levels of chemical differentiation (Webster et al., 1997). These liquids contain generally high abundances of Sn, F, P, Li, Rb, Cs, Nb, Ta and Be (Webster et al., 1997). However, two studies (e.g., Charoy and Noronha, 1996; Webster et al., 1997) on natural melt inclusions reported data on strong tin enrichments in F-rich residual liquids. Webster et al. (1997) sampled quartz phenocrysts from a pegmatite that occur in a Variscan granite genetically associated with cassiterite- and wolframite-mineralized greisen veins at the Ehrenfriedersdorf Sn-W deposit, Central Erzgebirge, SE Germany. Their study observed aluminosilicate liquid that contains 1000-2000 ppm tin. These levels of tin enrichment were up to 2 orders of magnitude greater than that ever reported for nonmineralized, metaluminous and peraluminous igneous materials and are consistent with some experimentally-derived tin solubilities in cassiterite-saturated granitic liquids at geologically relevant pressures and temperatures. By extrapolating the data from the present study close to the solidus temperatures of natural topaz and cassiterite-bearing granite (<680 °C), SnO<sub>2</sub> concentrations required to produce magmatic cassiterite are approximately 0.30 wt.% (at NNO). Even if solidus temperatures as low as 600 °C were assumed (cf. Pichavant et al., 1987), this study shows that a relatively high concentration of SnO<sub>2</sub> (~0.20 wt.%) can be dissolved in such melts. In the present study, the SnO<sub>2</sub> concentrations obtained at 700 °C are of the same order of magnitude than those observed in natural systems (1400 ppm in the Beauvoir granite; Cuney et al., 1992). As emphasized by Linnen et al. (1995), changing  $fO_2$  may result in the crystallization of a significant amount of SnO<sub>2</sub> in the granitic melts, even at low temperatures.

This study extends the data set of Linnen et al. (1995, 1996) to lower temperatures (down to ~600 °C) and also confirm the data of Štemprok (1990b). In this study, it has been shown that the temperature effect on SnO<sub>2</sub> solubility can be modeled by assuming a linear dependence of  $\log C_{SnO_2}$  versus  $1/T$ . It has also been shown that effect of temperature on diffusivity of tin can be modeled by assuming a linear dependence of  $\log D$

versus  $1/T$ . Linnen et al. (1996) reported the tin diffusivity in melts with different alumina saturation indices, constant T and P but at different  $fO_2$ . Tin diffusivity data obtained from the present study using melt composition (A.S.I. = 1.0) are compared with F-free melt composition (A.S.I. = 1.02) from study of Linnen et al. (1996). In a F-free melt (A.S.I. = 1.0) at 850 °C, 2 kbar and NNO buffer, Linnen et al. (1996) found a tin diffusivity of  $1.6 \cdot 10^{-12}$  m<sup>2</sup>/s, whereas at same P, T and  $fO_2$  but using F-bearing (4.6 wt.% F in melt) melt composition, this study found a tin diffusivity of  $2.1 \cdot 10^{-11}$  m<sup>2</sup>/s. Thus, an increase of one order of magnitude has been observed for diffusivity of tin in silicate melt (A.S.I. = 1.0) at 850 °C, 2 kbar and at an  $fO_2$  close to NNO.

Linnen et al. (1995, 1996) investigated the effects of  $fO_2$ , peralkalinity and excess aluminum on tin solubility in granitic melts at 850 °C and found that cassiterite solubility ranges from 2.8 wt.% SnO<sub>2</sub> at FMQ -0.84 to approximately 0.08 wt.% SnO<sub>2</sub> at FMQ+3.12 in a synthetic granitic melt composition with 0.4 wt.% C at 850 °C and 2 kbar. At  $fO_2$  higher than FMQ+1.5,  $fO_2$  was not observed to affect SnO<sub>2</sub> solubility, implying that SnO<sub>2</sub> dissolves into the melt largely as Sn<sup>4+</sup>. At more reduced conditions, log SnO<sub>2</sub> solubility decreases with increasing log  $fO_2$  at a slope of -0.5, implying that Sn dissolves in the melt as Sn<sup>2+</sup> (cf. Paparoni, 2000).

In subaluminous to peraluminous melt compositions, F has a minor effect on SnO<sub>2</sub> solubility at an  $fO_2$  of NNO, when F-content in the melt is <2.0 wt.% F. To compare the validity of the data from this study, results from the present study are compared with Charoy and Noronha (1996). It can be well interpreted from study of Charoy and Noronha (1996) that there is a small effect of F on SnO<sub>2</sub> solubility when F-content is <1.3 wt.% F in melt. Charoy and Noronha (1996) reported a small increase in SnO<sub>2</sub> content from  $575 \pm 30$  to  $746 \pm 30$  ppm SnO<sub>2</sub> in melts containing 0.47 to 1.25 wt.% F in melt, respectively. However, the present study shows that there is a significant effect of F-content (> 2 wt.% F in the melt) on the solubility of cassiterite in silicate melts, as this study using peraluminous-peralkaline melts, found an increase in cassiterite solubility when F-content of melt increases from 2.0 to 4.5 wt.% F in melt.

Systematic variations between Sn and other elements cannot be observed from the data set of Webster et al. (1997). As emphasized by Webster et al. (1997), the P content of the glass inclusions is exceptionally high, yet there is no obvious correlation between P and Sn in the melt. Except for F, the volatile concentrations are low (average 1.2 wt.% H<sub>2</sub>O and 0.1 wt.% Cl) in the melt inclusions, compared to melt inclusions from high-silica, high-Sn topaz rhyolites (Webster et al., 1991; Webster and Duffield, 1991; Lowenstern, 1994; Webster and Duffield, 1994; Lowenstern, 1995). No systematic correlation is observed between Sn and Cl or H<sub>2</sub>O. The low H<sub>2</sub>O and Cl contents suggest that the residual liquids entrapped in quartz were already highly degassed, suggesting in turn that Sn is not strongly partitioned to the fluid phase (cf. Taylor, 1988). Another explanation for variable content of SnO<sub>2</sub> in the melt inclusions would be that melt inclusions with high SnO<sub>2</sub> were trapped from melts at low  $fO_2$ . However, in the dataset of Webster et al. (1997), there is no compositional parameter that may reflect change in  $fO_2$ . One such parameter would be the Fe/(Fe+Mg) ratio, which is dependent of  $fO_2$ , but cannot be used as the MgO content of the melt inclusions reported by Webster et al. (1997) is close to zero.

#### **2.4.2. Effect of F on cassiterite solubility in subaluminous and peraluminous melts**

One of the motivations of this study was to investigate the behavior of a melt composition with a known A.S.I. (Alumina Saturation Index) with variable fluorine contents. Thus, effect of compositional factor (A.S.I.) on SnO<sub>2</sub> solubility as a function of fluorine is measured. The only study which explains the effect of A.S.I. on SnO<sub>2</sub> solubility is the study of Linnen et al. (1996). To know the effect of fluorine on solubility of cassiterite in silicate melts, results from this study are compared with Linnen et al. (1996). Though Linnen et al. (1996) performed experiments at 850 °C, but the results from the present study obtained at 800 °C have been compared with the study of Linnen et al. (1996) assuming that temperature would not be a critical parameter. At 850 °C, 2 kbar and at a log  $fO_2$  of NNO, our results using F-bearing (4.6 wt.% F in melt; A.S.I. = 1.0) melt show a cassiterite solubility of  $3.31 \pm 0.10$  wt.% SnO<sub>2</sub> when compared with F-free melt. Though Linnen et al. (1996) performed experiments at 850 °C the results obtained at 800 °C from the present study have been compared with the study of Linnen et al. (1996).

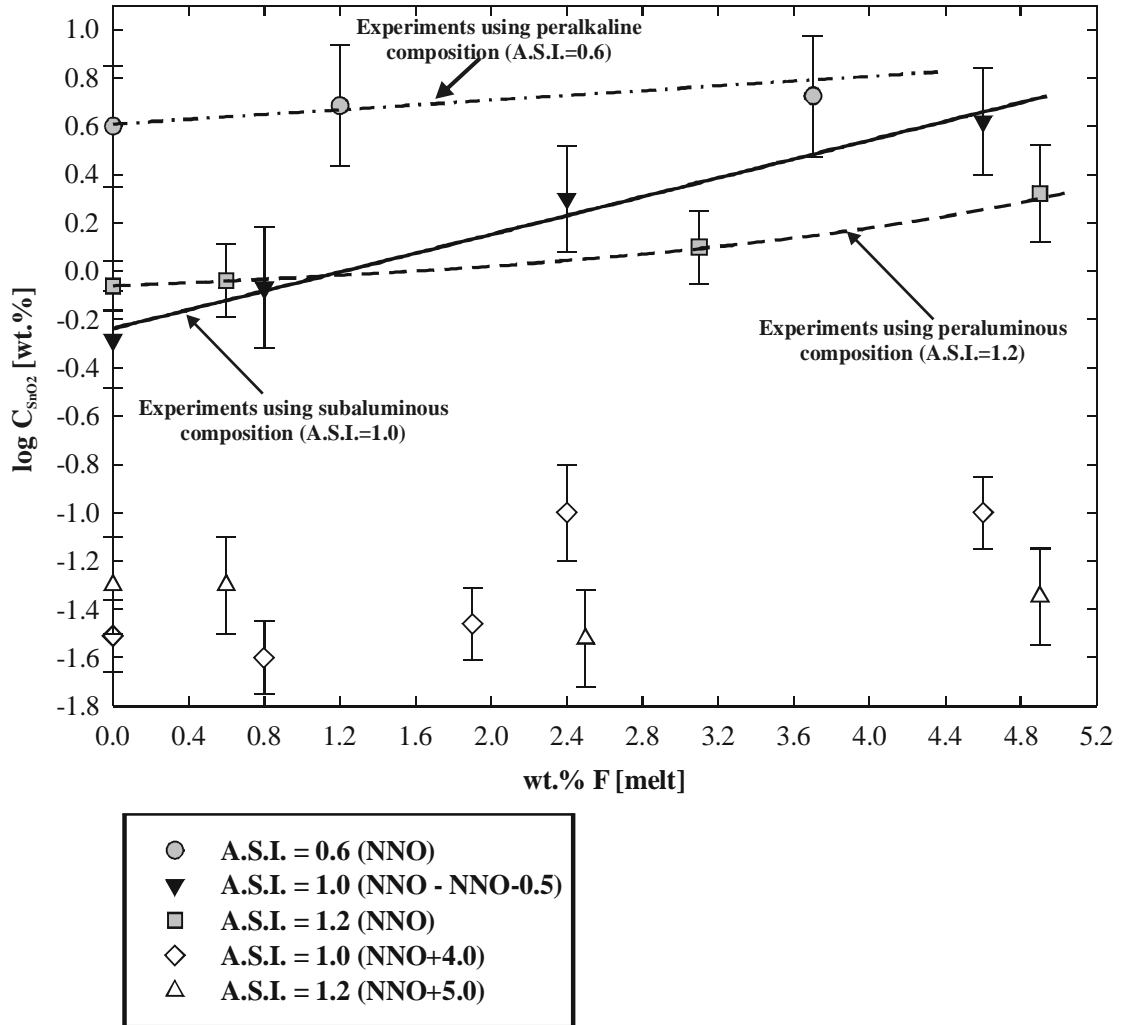


**Figure 2.25: Effect of compositional factor (A.S.I. content) at 800 °C as a function of F on  $\text{SnO}_2$  solubility in silicate melts.**

In Fig. 2.25, it can be clearly seen that in F-free melts, cassiterite solubility increases with an increase in A.S.I. of the melt. However, a strong effect of F has been found in a subaluminous melt composition (A.S.I. = 1.0) when compared with an effect of F in peraluminous melt composition (A.S.I. = 1.20). At 800 °C, 2 kbar,  $\log fO_2$  (NNO to NNO-0.5) and F-content (~4.5 wt.% F in melt), a significant decrease in  $\text{SnO}_2$  solubility from  $\sim 4.2 \pm 0.25$  to  $\sim 2.0 \pm 0.20$  wt.%  $\text{SnO}_2$  is observed with an increase in the A.S.I. of melt from 1.0 to 1.20, respectively. Whereas, using two different melts with different alumina saturation indices, but with same F-content (~2.5 wt.% F in melt), cassiterite solubility

tends to decrease from ~2.0 to ~1.0 wt.%  $SnO_2$  in melt with an increase in A.S.I. of melt from 1.0 to 1.20. This can be well explained by the fact that the tendency of fluorine to make compounds with Al and Sn is obvious and therefore, at a constant F-content (e.g., 2.4 wt.% F in melt) of two different melts with different A.S.I. contents, we found that peraluminous melt dissolve lower amounts of cassiterite when compared to the subaluminous melt.

Therefore, few possible explanations can be given for such behaviour (transport) of tin in F-bearing silicate melts. In the case of peraluminous melts, cassiterite solubility shows a small increase with an increase in F-content of the melt when compared with F-bearing subaluminous melts which show a strong increase in cassiterite solubility with an increase in F-content (>1 wt.% F in melt). This explanation can be supported by the fact that F lowers solidus and liquidus temperatures, enhances cation diffusivities, and decreases melt viscosities (Wyllie and Tuttle 1961; Manning 1981; Dingwell 1985). In silicate melts, F tends to make complexes with alkalis and Al (Manning et al. 1980, 1984; Mysen and Virgo 1985). Therefore, from this interpretation, it can be assumed that an increase in F-content in subaluminous melt, would possibly lead to an increase of the diffusivity of Al-cations in the melt. On the other hand, a strong positive correlation between F and “fluorophile” rare-metal contents in fractionated granites, pegmatites, and rhyolites has led to a widely held hypothesis that metal-fluoride complexing in the aqueous vapor may be important in rare-metal transport and formation of hydrothermal ores (Bailey 1977; Kovalenko et al. 1977; Burt et al. 1982; Černý et al. 1985 and many others). The available experimental data do not corroborate this hypothesis (Candela and Holland 1986; Manning and Henderson 1984; Tingle and Fenn 1984), but they do not refute the possibility of complexing between F and high-charge-density cations (e.g., Mn, Sn, Ta, Zr) in melt.

There are many studies (e.g., Wyllie and Tuttle, 1961; Manning, 1981; Dingwell, 1985) suggesting that F enhances the cation diffusivities and decreases melt viscosities. On the other hand, at more oxidizing conditions, the effect of A.S.I. on cassiterite solubility as a function of fluorine, is very small or negligible. Fig. 2.25 shows the effect of compositional factor (A.S.I.) and F on cassiterite solubility in silicate melts. In the present study a minimum for cassiterite solubility is observed in F-free subaluminous melt



composition (A.S.I.=1.0). Whereas, in F-bearing melts (>1 wt.% F in melt), there is a increase in cassiterite solubility with a decrease in A.S.I. content of the melt. In Fig. 2.25, at same T, P, and at a  $\log fO_2$  of NNO, the results from our study using melt with A.S.I. = 0.6, show that cassiterite concentrations in the melt are much higher when compared to the melt with higher A.S.I. = 1.0. In F-free silicate melts, a small effect of A.S.I. has been observed in peraluminous and subaluminous melts. Whereas, the effect of A.S.I. is much higher when F content of the melt is >2 wt.% F. Therefore, the effect of fluorine on the solubility of cassiterite in the melts with higher A.S.I. is lower than that of fluorine in melts with lower A.S.I. This also supports the findings of Bhalla et al. (2004) who show that excess alumina (corundum) plays an important role in controlling solubility of cassiterite in silicate. In conclusion, both the F-content of a melt and the A.S.I. play a very important role in dissolving cassiterite in the silicate melts. In peralkaline melts, F may tend to form complexes with Si of the melt, and in such way, F may depolymerize the melt structure. Such mechanism of incorporation of F in the melt would lead to a much stronger decrease in viscosity when compared to peraluminous melts in which complexes between Al and F, as  $AlF_6^{3-}$  and  $AlF_5^{2-}$ , are formed (Giordano et al., 2004).

**Table 2.8: Arrhenius parameters for tin diffusion and SnO<sub>2</sub> solubility in silicate melts with A.S.I. (0.6-1.24); effect of T,  $f_{O_2}$ , F and Cl-content**

A.S.I. of melt	T- range (°C) <sup>1</sup>	$f_{O_2}$ used (buffer) <sup>2</sup>	F-content in melt (wt.%) <sup>3</sup>	Cl-content in melt (wt.%) <sup>4</sup>	Arrhenius Parameters			
					SnO <sub>2</sub> Solubility		Activation energy, E <sub>a</sub> (kJ/mol) <sup>6</sup>	Tin diffusion measured as log D (m <sup>2</sup> /s) as a f(T) <sup>7</sup>
					log C <sub>SnO<sub>2</sub></sub> (wt.%) <sup>5</sup>			
1.24	680-850	NNO	1.12	-	3.79 – 4.20.10 <sup>3</sup> /T	96 ± 4.5	-7.23 – 5.06.10 <sup>3</sup> /T	
1.24	680-800	NNO+2.3	1.12	-	3.40 – 4.70.10 <sup>3</sup> /T	60 ± 3	-10.13 – 3.13.10 <sup>3</sup> /T	
1.24	680-800	NNO+2.3	0.0	-	3.40 – 4.70.10 <sup>3</sup> /T	38 ± 2	-10.37 – 1.97.10 <sup>3</sup> /T	
1.24	750-850	NNO	-	0.4	-	60 ± 3	-9.11 – 3.15.10 <sup>3</sup> /T	
1.0	600-850	NNO	4.6	-	4.55 – 4.53.10 <sup>3</sup> /T	-	-	
1.0	600-850	~NNO-1.0	2.4	-	-	80 ± 3	-8.28 – 4.21.10 <sup>3</sup> /T	
1.0	600-850	NNO-0.5	2.4	-	6.09 – 6.26.10 <sup>3</sup> /T	-	-	
1.0	600-850	NNO	2.4	-	4.64 – 4.80.10 <sup>3</sup> /T	-	-	
1.0	600-850	NNO+3.5	2.4	-	-0.29 – 1.25.10 <sup>3</sup> /T	-	-	
0.6	750-750	NNO	3.7	-	5.16 – 4.76.10 <sup>3</sup> /T	-	-	
0.6	750-750	NNO	1.2	-	3.91 – 3.46.10 <sup>3</sup> /T	-	-	
0.6	750-750	NNO	0.0	-	-3.51 + 4.41.10 <sup>3</sup> /T	-	-	
1.0 (Pegmatite)	750-850	NNO	2.0	-	-	-	-	
1.0 (Pegmatite)	650-850	NNO	2.0	-	-	196 ± 20	-2.05 – 10.27.10 <sup>3</sup> /T	
1.0 (Pegmatite)	650-800	NNO+0.5	2.0	-	4.58 – 5.10.10 <sup>3</sup> /T	-	-	
1.0 (Pegmatite)	650-800	NNO+3.5	2.0	-	1.47 – 2.21.10 <sup>3</sup> /T	290 ± 30	2.10 – 15.18.10 <sup>3</sup> /T	

**Abbreviations:** A.S.I., is Alumina Saturation Index of the starting glass (melt).

**Table 2.8 (continued):**

---

<sup>1</sup>Temperature range (°C), in which experiments have been performed.

<sup>2</sup>Oxygen fugacity,  $fO_2$ , is measured (see text for details). “NNO” stands for Nickel-Nickel Oxide.

<sup>3</sup>Fluorine-content of the melt (in weight percent).

<sup>4</sup>Chloride-content of the melt (in weight percent).

<sup>5</sup>Log  $C_{SnO_2}$  measured in weight percent (wt.%).

<sup>6</sup>Activation energy ( $E_a$ ), is calculated in kilo-Joule per mole (kJ/mol). The error is calculated to be 5-10%.

<sup>7</sup>Logarithm of D is calculated as a function of T, where D is the diffusion coefficient measured in ( $m^2/s$ ) and T is the temperature in (K).

### 2.4.3. Comparison with other studies using synthetic melts

Linnen et al. (1996) explained that  $SnO_2$  solubility depends strongly on alkali mole fraction. At oxidizing conditions, they found that  $SnO_2$  solubility increased nearly by two orders of magnitude, from 500-39000 ppm  $SnO_2$ , for A.S.I. 1.02 to A.S.I. 0.64 compositions. They also found a break in slope of the log  $SnO_2$  solubility vs. log  $fO_2$ , at  $\sim FMQ+2.0$ , evident in the subaluminous and peraluminous compositions but which becomes progressively less pronounced with increasing alkali content and this break cannot be distinguished for A.S.I. 0.64 composition. Linnen et al. (1996) explained this fact as a negative dependence of log  $fO_2$  on log solubility of  $SnO_2$  for A.S.I. 0.64, which in turn explained that some of the  $SnO_2$  is dissolved as  $Sn^{2+}$ , but the strong contrasts with the reduced subaluminous and peraluminous melts which dominantly contain  $Sn^{2+}$ , but the shallow slopes again are influenced by changes in composition at  $SnO_2$ -melt interface. Finally, Linnen et al. (1996) explained that for a fixed  $fO_2$  value the  $Sn^{4+}/Sn^{2+}$  ratio increases with increasing alkali content in peralkaline liquids. Ellison et al. (1998) described that  $Sn^{4+}$  shares with other large +4 cations a very low solubility in peraluminous alkali aluminosilicate liquids. The solubility of  $SnO_2$  in peraluminous  $K_2O-Al_2O_3-SiO_2$  liquids at 1350 °C to 1550 °C is comparable to solubilities of  $ZrO_2$ ,  $HfO_2$ , and  $LaPO_4$  at 1400 °C in alkali aluminosilicate liquids with similar  $M^+/Al^{3+}$  ratios and silica concentrations.  $TiO_2$  is similar to  $SnO_2$  in that it saturates as an oxide (rutile) in silica-rich alkali aluminosilicate liquids (Dickinson et al., 1985; Ellison and Hess, 1986).  $TiO_2$  saturation concentrations in alkali aluminosilicate liquids are more than 10 times greater than the saturation concentration of  $SnO_2$  in comparable liquids. The question arises: Is the solubility of  $TiO_2$  in peraluminous melts “unusually” high, or is the solubility of  $SnO_2$  in peraluminous melts “unusually” low?

Comparing the data from the present study with previous studies (e.g., Štemprok and Voldán, 1978; Štemprok, 1982;) in Fig. 2.26, it can be seen that the slope of the linear regression between the data from 650 to 800 °C at NNO-0.5 is  $-6.26$  and from 650 to 800 °C at NNO+3.5 is  $-3.97$ . However, there are only two points for the regression at oxidizing conditions. Thus the slopes between the previous studies with dry experiments and hydrothermal experiments (at NNO +3.5) from this study are almost similar. But the slope

obtained from this study with hydrothermal experiments at NNO -0.5, shows a different trend when compared with the dry experiments from the previous studies. This change in slope can be related to an addition of fluorine to the melt or change in  $fO_2$  of the melt or it can be due to various compositional factors used in the present experimental study.

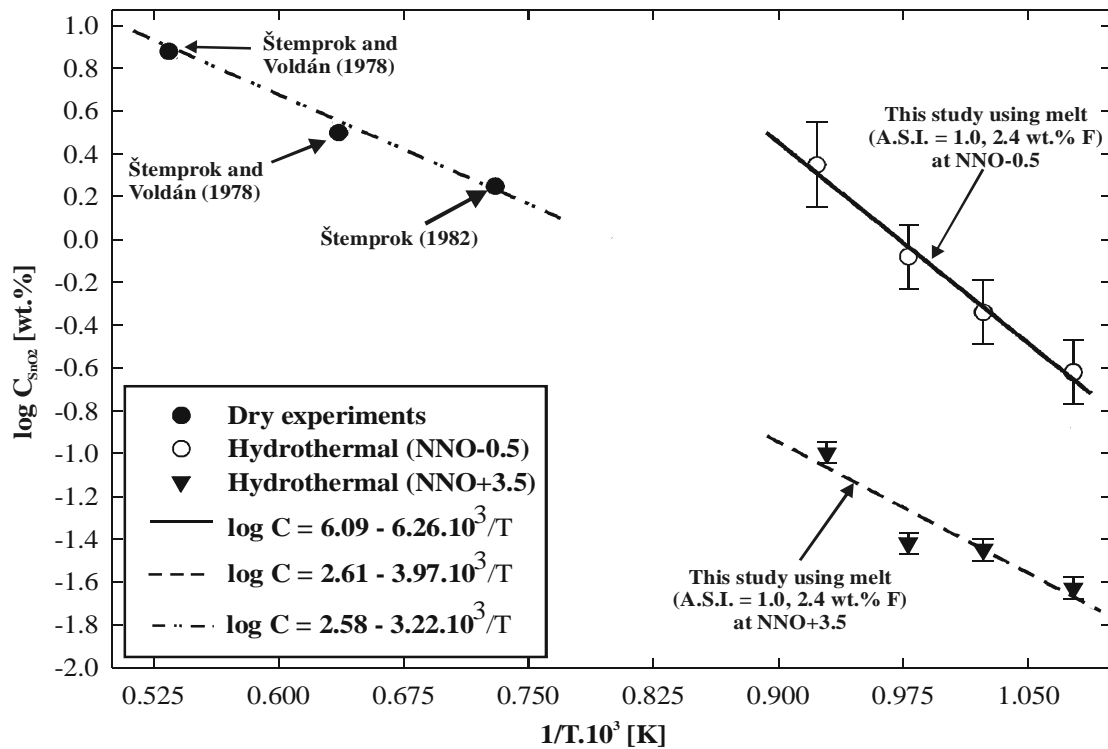


**Figure 2.26: Solubility of  $SnO_2$  in granitic melts: Comparison of the results of hydrothermal and dry experiments on  $SnO_2$  solubility in granitic melts in  $\log C_{SnO_2}$  vs.  $1/T$  plot.**

The effect of temperature is almost of the same order of magnitude as what has been observed in previous studies especially in dry conditions. There are relatively few solubility studies that can be compared directly to estimate the temperature effect. An excellent comparison of the present study can be done with the study of Linnen et al. (1996). Previous data from experiments conducted at high pressure (hydrothermal experiments) are not available (except at 850 °C) because of experimental problems in former studies (see Linnen et al., 1995). However the slope for the F-bearing peralkaline composition (1100 °C-1600 °C) at dry conditions (Štemprok, 1990b) in the Fig. 2.26 is almost identical within error to the slope of a peraluminous glass composition (PP4%F; see

Table A.3 for more details). Thus, the temperature effect seems to be of almost the same order of magnitude for all geologically relevant melt compositions.

Using F-bearing (2.4 wt.% F in melt) subaluminous composition (A.S.I. = 1.0), this study found that there is an increase of cassiterite solubility of approximately 1.0 log unit  $\text{SnO}_2$  at reducing conditions (at a  $\log fO_2$  of NNO) when compared with the F-free

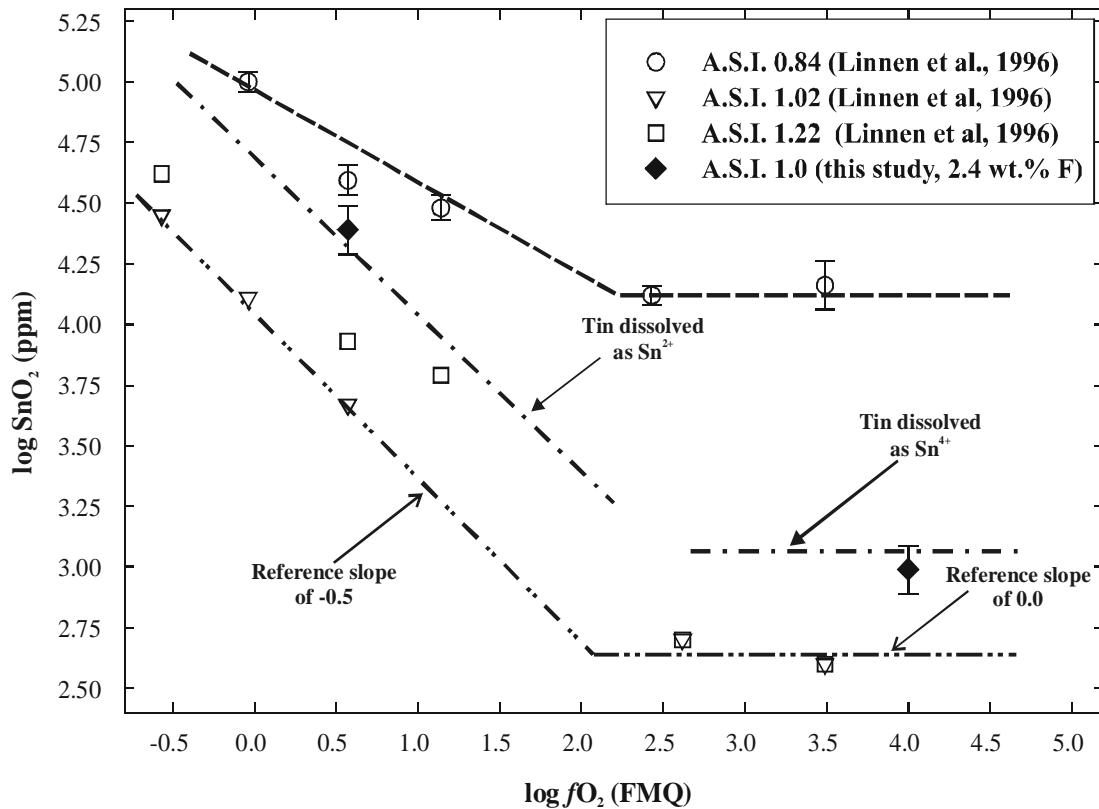


**Figure 2.27: Comparison of this study with study of Linnen et al. (1995, 1996) at 850 °C and 2 kbar in silicate melts.**

subaluminous composition (A.S.I. = 1.02) used in the study of Linnen et al. (1996). Whereas, at more oxidizing conditions (NNO+3.5 to 4.0), this study reported an increase in  $\text{SnO}_2$  solubility of the order of about 0.5 log unit  $\text{SnO}_2$ , which is far lesser than that reported at reducing conditions. This difference in the reported cassiterite solubilities can be related to mineral-melt partition behavior of  $\text{SnO}_2$  as  $\text{Sn}^{2+}$  and as  $\text{Sn}^{4+}$ . As reported and explained by earlier studies (e.g., Linnen et al., 1995; Linnen et al., 1996; Lehmann, 1990)

that at more oxidizing conditions ( $>NNO+2.0$ ), Sn is mainly transported (dissolved) as  $Sn^{4+}$  in the melt. Fig 2.27 shows the data from study of Linnen et al. (1996), who reported a reference slope of -0.5, thus mentioned that tin is mainly transported as  $Sn^{2+}$  in reduced silicate melts, whereas, a reference slope of 0.0 is found which indicates the transportation of tin as  $Sn^{4+}$  in oxidized silicate melts. The results from this study when compared with the study of Linnen et al. (1996) are illustrated in Fig. 2.27.

In Fig. 2.28, the present study using melt with ~0.4 wt.% Cl, is compared to the

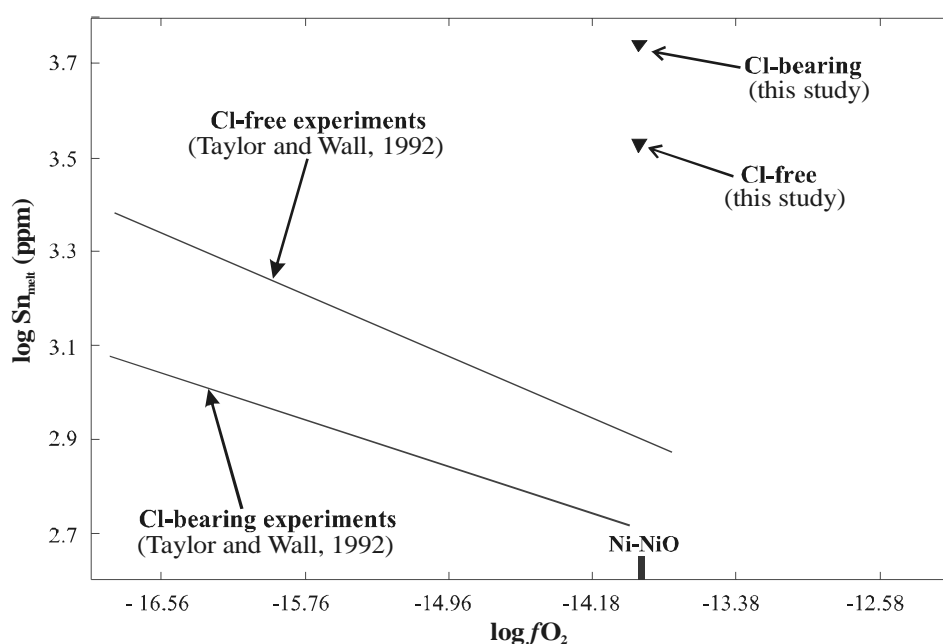


**Figure 2.28: Comparison of Cl-free and Cl-bearing data from the present study with study of Taylor and Wall (1992). Trends in solid lines represent Cl-free and Cl-bearing data points from Taylor and Wall (1992).**

study of Taylor and Wall (1992). Taylor and Wall (1992) explained that with an introduction of chloride to the melt,  $SnO_2$  solubility decreases in melt. But, exactly an opposite effect has been found when compared with results from Taylor and Wall (1992). One possible explanation for finding such negative correlation between the results from this study and study of Taylor and Wall (1992) may be due to the equilibrium experiments performed by Taylor and Wall (1992) that suffered severe tin loss to the walls of the capsule (Au-container). This tin loss would have been enhanced by the formation of Cl compounds.

## 2.5. Implications

In terms of pegmatite and granite petrogenesis, it is evident that a late stage oxidation of a highly evolved peraluminous granitic melt (e.g., Cuney et al., 1992; Linnen and William-Jones, 1994) will cause cassiterite to crystallize. Results from the present study when combined with the study of Linnen et al. (1996) show that in oxidized granites (Li, F, P, B etc. free), cassiterite saturation value could be as low as ~400 ppm  $SnO_2$  at 850 °C. Webster et al. (1997) report up to 1200 ppm Sn in P- and F-rich melt inclusions from Erzgebirge indicating some highly evolved granites do contain high tin concentrations, in support of a magmatic origin for some tin deposits. Cassiterite may also crystallize as a magmatic mineral in weakly peralkaline granites or pegmatites. Another important implication is that the fractionation of tin in reduced peraluminous granites may be quite different from that in peralkaline granites at any redox state.

Granite related tin deposits are considered to have had a redox state between those of the FMQ and Ni-NiO buffers (Dubessy et al., 1987); thus the  $fO_2$  range in this study is directly applicable to natural studies. Oxygen fugacity is also interpreted to have increased during late magmatic to early hydrothermal stages, which is reported by studies (e.g., Cuney et al., 1992; Linnen et al., 1992; Linnen and William-Jones, 1993) on Nong Sua aplite-pegmatite systems. Linnen and William-Jones (1993) also showed solidus temperature of about 650 °C for Nong Sua pegmatite-aplite system. Whereas, solidus temperature at Beauvoir was experimentally determined to have been <600 °C (Pichavant et al., 1987), this study shows that a relatively high concentration of  $SnO_2$  (~0.20 wt.%) can be dissolved in such melts. Cassiterite solubility in silicate melts is almost certainly temperature dependent (Štemprok, 1990a,b), which is experimentally confirmed in the present study at a temperature range from 600-850°C, 2 kbar and at varying log  $fO_2$  of NNO-2.0 to NNO+5.0. It is clear from the previous experimental work that a late stage increase of  $fO_2$  is an effective mechanism for cassiterite crystallization from a highly evolved granitic melt.

Except data from Linnen et al. (1995, 1996), there is very little data on the effect of redox conditions on the solubility or speciation of multivalent elements in granitic melts,



and even few data on the combined effects of melt composition and redox state. Though, there are few studies who reported a possible effect of halogens on cassiterite in natural systems, but no experimental data (except the study of Bhalla et al., 2004) is available on the effect of volatiles (e.g., halogens namely Cl and F) on solubility of cassiterite in granites as well as in pegmatites, as halogens do play an important role in transporting such elements in the melt. There are few studies who reported an effect of Cl and F on  $SnO_2$  solubility in peraluminous to peralkaline compositions and at various  $fO_2$  (reducing to oxidizing) conditions or at different redox states. One more implications as reported by Linnen et al. (1996) is that at reduced conditions ( $< NNO+1.5$ ), the speciation of tin appears to change from  $>95\%$   $Sn^{2+}$  in peraluminous melts to  $\sim 40-80\%$   $Sn^{4+}$  in peralkaline melts. Thus slower diffusion has been observed in peraluminous melt as compared to diffusion rates of tin in peralkaline melts, which can be explained by a decrease in coordination number of tin from peraluminous to peralkaline melt compositions.

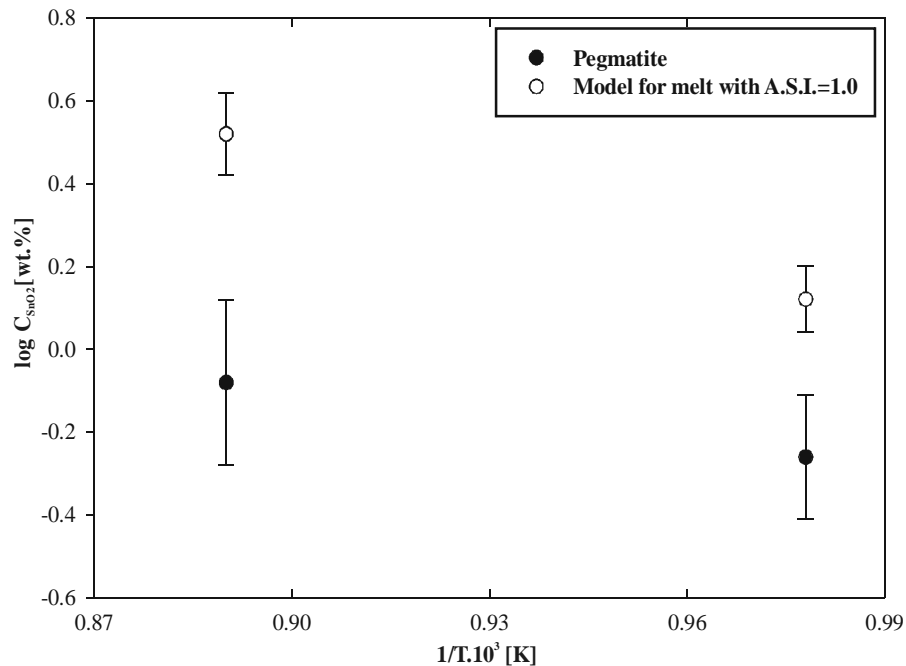


**Figure 2.29:** The graph shows comparison of  $SnO_2$  solubilities between subaluminous and pegmatite melt compositions. Both these melts have an A.S.I.=1.0 and contain 4 wt.% F in the melt.

In Fig. 2.29, the data obtained from this study using pegmatite melt composition (A.S.I. = 1.0;  $\sim 4$  wt.% F in melt) have been compared with subaluminous composition (A.S.I. = 1.0;  $\sim 4$  wt.% F in melt). It can be observed that there is significant decrease in

cassiterite solubility in pegmatite melt. This decrease in solubility of cassiterite can be explained by the presence of rare elements (i.e., B, Li and P) which may collectively influence the cassiterite solubility in pegmatite melt.

A possible explanation for the relatively low effect of F on the  $SnO_2$  solubility at NNO is that Sn is dissolved mainly as  $Sn^{2+}$ . Thus the effect of F on solubility of HFSE shown by Keppler (1993) is not expected if Sn is not dissolved as  $Sn^{4+}$  ( $Sn^{4+}$  is a HFSE whereas  $Sn^{2+}$  is not). For a peraluminous melt composition, a significant effect of Cl has also been found by the present study. This data set from this study when combined with data set of Linnen et al. (1995, 1996), allows the prediction of cassiterite solubility in natural granitic melts, as a function of  $fO_2$ , temperature and melt composition.

## 6. Appendix

**Table A.1: Analyses of starting materials (A.S.I. = 1.24)**

Starting Materials	* Glass 1	* Glass 2	Glass 3	Glass 4	Glass 5	Glass 6
SiO <sub>2</sub> (wt.%)	73.87	72.57	75.79	75.06	77.10	75.80
Al <sub>2</sub> O <sub>3</sub>	15.46	15.88	14.66	15.06	13.95	14.50
Σ FeO	0.99	0.95	0.99	1.06	0.38	0.90
CaO	0.80	0.79	0.73	0.80	0.69	0.60
Na <sub>2</sub> O	4.03	4.33	3.65	3.64	3.56	3.90
K <sub>2</sub> O	4.30	4.24	4.18	4.18	3.95	3.90
SnO <sub>2</sub>	0.02	0.02	0.00	0.00	0.00	0.00
F	1.12	2.12	0.00	0.00	0.00	0.00
F=O	0.47	0.88	0.00	0.00	0.00	0.00
Cl	0.00	0.00	0.00	0.20	0.37	0.40
Total	100.17	100.06	100.00	100.00	100.00	100.00
Quartz	35.20	32.30	37.90	37.20	41.00	38.00
Orthoclase	27.70	27.50	25.90	26.10	24.20	24.20
Albite	37.10	40.20	36.20	36.70	34.80	37.80
Corundum	2.8	2.8	2.8	3.1	2.6	2.8
A/CNK	1.21	1.21	1.24	1.26	1.23	1.24
NK/A	0.73	0.74	0.72	0.70	0.73	0.73

\*Data from Lukkari et al. (in prep.). Glass compositions 3, 4, 5 and 6 are normalized to 100%.

**Table A.2: Analyses of starting materials (A.S.I. = 1.20)**

Starting Materials	P0%F		P2%F		P4%F		P6%F		P12%F		P2%F (reground)
	EMP	ICP	EMP	ICP	EMP	ICP	EMP	ICP	EMP	ICP	EMP
SiO <sub>2</sub> (wt.%)	75.5	77.87	79.6	78.08	76.7	77.73	75.7	78.28	79.0	77.80	80.1
TiO <sub>2</sub>	-	0.020	-	0.016	-	0.019	-	0.016	-	0.016	-
Al <sub>2</sub> O <sub>3</sub>	14.8	13.25	13.9	13.06	13.8	13.22	13.9	13.33	12.0	12.51	14.5
Σ FeO	0.0	0.07	0.0	0.06	0.0	0.08	0.0	0.06	0.0	0.07	0.0
MnO	-	0.001	-	0.001	-	0.001	-	0.001	-	0.001	-
MgO	-	0.04	-	0.04	-	0.05	-	0.04	-	0.04	-
CaO	0.0	0.05	0.0	0.05	0.0	0.05	0.0	0.05	0.0	0.05	0.0
Na <sub>2</sub> O	4.4	4.14	4.1	4.09	4.0	4.07	4.0	4.09	4.0	4.18	4.0
K <sub>2</sub> O	4.0	3.60	3.8	3.56	3.8	3.58	3.8	3.53	3.8	3.57	3.8
P <sub>2</sub> O <sub>5</sub>	-	0.05	-	0.05	-	0.05	-	0.05	-	0.05	-
SnO <sub>2</sub>	0.0	0.0	0.0	0.0	0.0	0.0	0.0	0.0	0.0	0.0	0.0
F	0.1	0.01	0.6	0.68	2.9	2.89	3.1	3.24	4.9	5.99	0.6
F=O	-0.1	-0.01	-0.5	-0.57	-2.4	-2.43	-2.6	-2.73	-4.1	-5.05	-0.5
Total	98.7	98.86	101.5	98.90	98.8	99.06	97.9	99.74	99.6	99.0	102.5
Quartz	36.20	41.50	41.90	42.20	40.90	42.00	40.30	42.50	42.20	41.40	42.90
Orthoclase	24.80	22.10	22.80	21.90	23.60	22.10	23.80	21.60	23.10	21.90	22.80
Albite	39.00	36.40	35.30	35.90	35.50	35.90	35.90	35.90	34.70	36.70	34.90
Corundum	3.23	2.54	3.04	2.51	3.11	2.68	3.21	2.78	1.31	1.80	3.81
A/CNK	1.28	1.24	1.28	1.22	1.29	1.24	1.30	1.26	1.12	1.15	1.15
NK/A	0.78	0.81	0.78	0.81	0.77	0.80	0.77	0.79	0.89	0.86	0.74

**Abbreviations:** EMP and ICP stand for Electron Microprobe and Inductively Coupled Plasma-Atomic Emission Spectroscopy, respectively.

**Table A.3: Analyses of starting materials (A.S.I. = 1.0)**

Starting Materials	PP0%F		PP2%F		PP4%F		PP6%F		PP12%F		PP2%F (reground) S2	
	EMP	ICP	EMP	ICP	EMP	ICP	EMP	ICP	EMP	ICP	EMP	EMP
SiO <sub>2</sub> (wt.%)	76.9	76.65	78.9	77.61	78.3	77.65	77.6	73.8	79.4	78.83	81.8	76.2
TiO <sub>2</sub>	-	0.026	-	0.02	-	0.017	-	0.017	-	0.019	-	-
Al <sub>2</sub> O <sub>3</sub>	13.6	13.0	13.5	12.53	13.4	12.7	13.1	12.4	11.4	11.35	13.4	12.01
Σ FeO	0.0	0.06	0.0	0.06	0.0	0.08	0.0	0.06	0.0	0.06	0.0	0.0
MnO	-	0.001	-	0.001	-	0.001	-	0.001	-	0.001	-	-
MgO	-	0.03	-	0.04	-	0.05	-	0.04	-	0.04	-	-
CaO	0.0	0.06	0.0	0.05	0.0	0.06	0.0	0.05	0.0	0.05	0.0	0.0
Na <sub>2</sub> O	4.6	4.73	4.6	4.66	4.6	4.61	4.5	4.5	4.2	4.53	4.3	4.59
K <sub>2</sub> O	5.3	5.01	4.3	4.03	4.3	4.00	4.3	3.6	4.1	3.87	4.2	4.9
P <sub>2</sub> O <sub>5</sub>	-	0.02	-	0.05	-	0.03	-	0.04	-	0.05	-	-
SnO <sub>2</sub>	0.0	0.0	0.0	0.0	0.0	0.0	0.0	0.0	0.0	0.0	0.0	0.0
F	0.1	0.02	1.2	0.8	2.4	1.9	3.7	2.4	4.6	6.05	0.7	2.3
F=O	-1.0	-0.01	-1.0	-0.68	-2.0	-1.6	-3.1	-3.12	-3.9	-5.10	-0.6	0.0
Total	99.5	99.4	101.5	98.95	101.0	99.26	100.1	93.58	99.8	99.53	103.8	100.0
Quartz	29.80	30.70	35.69	35.70	35.30	36.10	35.50	36.30	39.60	39.20	39.90	34.40
Orthoclase	31.30	29.90	25.40	24.20	25.60	24.10	25.80	22.80	24.50	23.30	24.40	29.90
Albite	38.90	39.40	38.90	40.10	39.10	39.80	38.70	40.90	35.90	37.50	35.70	35.70
Corundum	0.30	-	1.28	0.53	1.18	0.79	1.04	1.10	0.05	0.03	1.78	-
A/CNK	1.02	0.98	1.10	1.03	1.10	1.07	1.09	1.10	1.01	0.97	1.15	0.93
NK/A	0.98	1.02	0.91	0.96	0.91	0.94	0.92	0.91	1.0	1.03	0.87	1.07

**Abbreviation:** EMP and ICP stand for Electron Microprobe and Inductively Coupled Plasma-Atomic Emission Spectroscopy, respectively.

**Table A.4: Analyses of starting materials (A.S.I. = 0.6)**

Starting Materials	PB0%F		PB2%F		PB4%F		PB6%F		PB10%F		PB0%F (reground)
	EMP	ICP	EMP	ICP	EMP	ICP	EMP	ICP	EMP	ICP	EMP
SiO <sub>2</sub> (wt.%)	79.8	78.43	79.7	78.55	79.6	78.23	80.2	78.84	80.9	78.88	81.1
TiO <sub>2</sub>	-	0.023	-	0.022	-	0.019	-	0.017	-	0.017	-
Al <sub>2</sub> O <sub>3</sub>	10.3	9.36	10.1	9.27	9.9	9.44	9.9	9.46	8.4	9.48	10.2
Σ FeO	0.0	0.10	0.0	0.09	0.0	0.08	0.0	0.07	0.0	0.07	-
MnO	-	0.001	-	0.001	-	0.001	-	0.001	-	0.001	-
MgO	-	0.07	-	0.05	-	0.05	-	0.05	-	0.04	-
CaO	0.0	0.10	0.0	0.06	0.0	0.06	0.0	0.06	0.0	0.06	0.0
Na <sub>2</sub> O	5.8	5.71	5.6	5.65	5.1	5.68	5.2	5.56	4.7	5.36	5.6
K <sub>2</sub> O	5.5	5.01	5.3	4.99	5.1	4.87	5.1	4.69	4.7	4.65	5.3
P <sub>2</sub> O <sub>5</sub>	-	0.05	-	0.05	-	0.05	-	0.05	-	0.05	-
SnO <sub>2</sub>	0.0	0.0	0.0	0.0	0.0	0.0	0.0	0.0	0.0	0.0	0.0
F	0.1	0.03	1.2	1.26	2.2	2.96	3.7	3.85	4.2	6.27	0.0
F=O	-0.1	-0.03	-1.0	-1.06	-1.8	-2.96	-3.1	-3.25	-3.5	-5.28	0.0
Total	101.4	98.51	101.9	98.66	100.1	98.22	101.0	99.15	99.4	99.36	102.2
Quartz	42.40	45.80	43.30	46.30	44.50	45.40	44.80	45.90	52.10	45.90	43.80
Orthoclase	34.10	32.20	33.10	32.10	31.80	31.30	31.60	29.80	29.70	24.60	23.80
Albite	23.50	22.00	23.60	21.60	23.70	23.30	23.60	24.30	18.20	29.50	32.40
Corundum	-	-	-	-	-	-	-	-	-	-	-
A/CNK	0.66	0.62	0.68	0.63	0.71	0.64	0.70	0.66	0.64	0.68	0.68
NK/A	1.50	1.58	1.48	1.59	1.41	1.55	1.42	1.50	1.53	1.46	1.47

**Abbreviation:** EMP and ICP stand for Electron Microprobe and Inductively Coupled Plasma-Atomic Emission Spectroscopy, respectively.

**Table A.5: Analyses of pegmatitic melt (A.S.I. = 1.0)**

Starting Materials	P FDP ICP
SiO <sub>2</sub> (wt.%)	67.68
TiO <sub>2</sub>	0.016
Al <sub>2</sub> O <sub>3</sub>	17.03
Σ FeO	0.06
MnO	0.001
MgO	0.04
CaO	0.05
Na <sub>2</sub> O	7.78
K <sub>2</sub> O	4.11
B <sub>2</sub> O <sub>3</sub>	2.25
Li <sub>2</sub> O	1.04
P <sub>2</sub> O <sub>5</sub>	1.68
SnO <sub>2</sub>	0.0
F	4.38
F=O	-3.68
Total	102.43
Quartz	7.60
Orthoclase	25.20
Albite	67.20
Corundum	-
A/CNK	0.99

Abbreviation: ICP stands for Inductively Coupled Plasma-Atomic Emission Spectroscopy.

### **3. Solubility of chlorine and effect of chloride on platinum solubility in haplobasaltic melts**

#### **Abstract**

Experiments were performed in the temperature and pressure range of 1200-1250 °C and 1-2 kbar using a synthetic haplobasaltic composition (Ab<sub>25</sub>-An<sub>55</sub>-Di<sub>20</sub>) to determine the partitioning of chloride between fluid and melt, and the effect of Cl<sup>-</sup> on platinum solubility in silicate melts. Starting materials were diluted hydrochloric (HCl) solutions (5 wt.% Cl<sup>-</sup> – 25 wt.% Cl<sup>-</sup>) and dry glass sealed in platinum capsules. All experiments were conducted in internally heated pressure vessels equipped with a rapid quench set-up. The experimental products were always bubble-free glasses (except one experiment with vesicles).

The chloride content in the glasses varies between 0.4 to 2.9 wt.% Cl<sup>-</sup>, depending upon the amount of fluid and also on fluid concentration. The calculated distribution coefficient,  $D_{Cl} = \text{wt.\% Cl}^- \text{ in fluid} / \text{wt.\% Cl}^- \text{ in melt}$ , varies from 2.0 to 8.4.  $D_{Cl}$  increases slightly with increasing chloride content of the charge. The solubility of H<sub>2</sub>O increases with increasing amount of chloride in the system in the pressure range of 1-2 kbar and at 1200 °C. The experimental results show that H<sub>2</sub>O solubility is higher when Cl<sup>-</sup> is present in the melt ( $4.9 \pm 0.15$  and  $6.1 \pm 0.20$  wt.% H<sub>2</sub>O in melts containing 0 wt.% Cl<sup>-</sup> and 3.2 wt.% Cl<sup>-</sup>, respectively). This suggests that the solubility of H<sub>2</sub>O in basaltic melts does not vary inversely with Cl<sup>-</sup> content in melts containing up to 2 wt.% Cl<sup>-</sup>, in contrast to the recent solubility model of Webster et al. (1999).

Determination of platinum in the quenched glasses was made by isotope-dilution-multi-collector inductively coupled mass spectroscopy (ID-MC-ICPMS). At a constant  $\log fO_2 = -4$ , platinum concentration in the melt increases from  $105 \pm 8$  to  $920 \pm 65$  ppb Pt, when Cl<sup>-</sup> concentration in melt increases from 0.4 to 3.2 wt.% Cl<sup>-</sup>, respectively. Combined with data in a Cl-free system from the study of Blaine et al. (2004), an effect of Cl<sup>-</sup> on Pt solubility in nearly H<sub>2</sub>O-saturated melts (~5–6 wt.% H<sub>2</sub>O) can be predicted with following



equation:  $C_{Pt} = 57.30 + 260.24 \cdot Cl$ , where  $C_{Pt}$  and  $Cl$  are concentration of platinum (ppb) and amount of chloride content (wt.%) in the melt.

Previous results on the effect of H<sub>2</sub>O on Pt solubility from Ertel et al. (1998) need to be reconsidered. In these experiments, problems due to the formation of Pt-micronuggets lead to strong overestimations of Pt solubilities.

**Keywords:** Chloride; Distribution coefficient; Fluid; Partitioning; Platinum; Pt-micronuggets

### 3.1. Introduction

Noble metals possess some unique geochemical characteristics. They are very refractory, having high melting points and strong affinity for iron (siderophile) and for sulfur (chalcophile). The occurrences of precious metals in trace levels, uncertainties in world prices and economic importance are the natural causes for the interest in their exploration as well as in their analyses. They are present in silicate rocks at very low levels. The precious metals often form discrete phases, such as alloys and therefore, unlike the rare-earth elements, they do not appear to partition themselves extensively between silicate phases. PGE are composed of platinum (Pt), palladium (Pd), rhodium (Rh), ruthenium (Ru), iridium (Ir) and osmium (Os), with gold (Au) generally added to PGE, because its behaviour can be likened to some elements forming the group PGE.

Being a most important member of PGE, Pt is present in the Earth crust as millionth part of one percent. Because of its behavior of inertness to many mineral acids, and on the contrary, its ability to form compounds rapidly, if attacked by the halogens (Cl, F), the properties of Pt are of keen interest to scientists since several decades and led to a significant research in this field. A few laboratory studies have demonstrated the feasibility of the transport of PGE and Au in late-magmatic systems (Hill, 1984; Fleet and Wu, 1993; Ballhaus et al., 1994). Field and geochemical observations as well as experimental studies pointed out the important role of fluids in concentrating PGE in mafic and ultramafic igneous complexes (e.g., Razin, 1968; McCallum et al., 1976; Campbell et al., 1983; Ballhaus and Stumpfl, 1986; Boudreau et al., 1986; Boudreau and McCallum, 1986; Johan et al., 1989; Mathez et al., 1989; Nyman et al., 1990; Mogessie et al., 1991; Stumpfl and Weiblen, 1991; Boudreau and McCallum, 1992; Farrow and Watkinson, 1992; Jaireth, 1992; Ohnenstetter, 1992; Boudreau, 1993; Chen et al., 1993; Marcantonio et al., 1994; Stone et al., 1994; Borisov and Palme, 1997; Bezmen et al., 1998; Amossé et al., 2000; Willmore et al., 2000; Ballhaus et al., 2001; Augé et al., 2002; Barnes and Maier, 2002; Cawthorn et al., 2002; Maier and Barnes, 2003; Boorman et al., 2004).

One crucial element for transporting PGE or ore forming elements in magmatic volatile phases (fluids) is chlorine (Eugster, 1985; Boudreau et al., 1986; Eugster, 1986; Mountain and Wood, 1988; Sassani and Shock, 1990; Hsu et al., 1991; Boudreau and

McCallum, 1992; Fleet and Wu, 1993; Ballhaus et al., 1994; Gammons, 1996; Sassani and Shock, 1998). Cl is ranked as one of the most important volatile after H<sub>2</sub>O and CO<sub>2</sub> in magmatic systems (Metrich and Rutherford, 1992). Though Cl-bearing vapors are not fundamental to explosive volcanic eruptions, they do carry enhanced metal contents specifically because of dissolved chlorine (Symonds et al., 1990; Symonds et al., 1992). Thus, it is potentially important in magma evolution, element differentiation and partitioning of elements between vapor phases and melt (Burnham, 1979; Candela and Holland, 1984; Keppler and Wyllie, 1989; Raia et al., 1997; Raia et al., 2000). It is generally considered that magmas are a common source of ore metal-laden fluids and hydrous chloride melts (Burnham, 1967; Anderson, 1974; Bai and Koster Van Groos, 1994; Hedenquist and Lowenstern, 1994; Candela and Piccoli, 1995; Webster et al., 2003a,b). There are many examples, which report extreme magmatic enrichments in chlorine. These examples include, silicate melt inclusions in Mt. Somma-Vesuvius, Italy, which contain more than 1 wt.% Cl (Vagelli et al., 1993; Belkin et al., 1998; Fulignati et al., 2000; Webster et al., 2003b), and melt inclusions from basaltic lavas of the Austral Islands contain as much as 2.5 wt.% Cl (Lassiter and Hauri, 2001). Cl-bearing fluids play an important role in melting processes that generate calc-alkaline and alkaline magmas (Harris and Anderson, 1984; Sisson and Layne, 1993; Jambon et al., 1995). Cl plays an essential role in various hydrothermal and geothermal mechanisms (Johnston, 1980; Lessiter and Hauri, 2001) such as hot water springs and aerosols, known as Chloro-Fluoro-Carbons, CFCs. Cl is also a key component of aqueous fluids in subduction zones (Barr, 1990; Scambelluri et al., 1997; Bureau, 1999; Svensen et al., 1999; Scambelluri and Phillipot, 2001; Touret, 2001; Jarrard, 2003; many others).

To summarize, the behavior of Cl compounds in magmatic and hydrothermal solution systems under high pressure is believed to be closely related to the formation of PGE deposits. Thus, fundamental data needed to understand the enrichment processes of PGE in magmatic and hydrothermal systems are: 1) the distribution of chlorine between melt and fluid phases; 2) the solubility of PGE in these Cl-bearing phases. There are many studies on the partitioning of Cl and H<sub>2</sub>O between melt and fluid (e.g., Shinohara et al., 1989; Kravchuk and Keppler, 1994; Shinohara, 1994; Webster, 1997; Webster and De Vivo, 2002) and a general model has been proposed by Webster et al. (1999). However,

this model is empirical and can not be extrapolated to any silicate melt composition. Few experimental studies have been performed to understand the effect of Cl on the solubility of PGE in high temperature fluids and silicate melts. Most available data have been obtained at 1 atm (Capobianco and Drake, 1990; Capobianco and Drake, 1994; Ertel et al., 1998; Ertel et al., 1999). However, H<sub>2</sub>O and Cl are incorporated in silicate melts only at high pressure and the effect of Cl on Pt solubility in H<sub>2</sub>O-bearing silicate melts has only been investigated in one recent study (Blaine et al., 2004).

This experimental work is planned to get information on the effect of Cl on Pt solubility in a haplobasaltic melt. This composition has also been used to determine the distribution of Cl<sup>-</sup> between aqueous fluids and melt. A series of experiment were performed at 1200-1250 °C and in the pressure range 1-2 kbar. The results are helpful to understand stability and mobilization of natural Pt alloys in magmatic and high temperature hydrothermal processes occurring in the upper crust.

## 3.2. Experimental and analytical methods

### 3.2.1. Experimental Method

#### 3.2.1.1. Starting Material

The experiments were mainly performed using a synthetic haplobasaltic melt composition in the system Albite-Anorthite-Diopside ( $\text{Ab}_{25}\text{An}_{55}\text{Di}_{20}$ ) prepared from pure silicate powdered oxides and decarbonated  $\text{Na}_2\text{CO}_3$  and  $\text{CaCO}_3$ . All silicate powders were mixed properly to avoid problems regarding inhomogeneity of the final starting glass used for further experiments. Those dried silicate-starting oxides and carbonate powders were placed in a Pt crucible and melted at 1600 °C/1 atm for 2-3 hours to get glass. To attain a better homogeneity of the starting glass, the starting material was grounded after the first fusion and melted again. This melting was repeated at 1600 °C and 1 atm after putting the Pt crucible in the furnace for 1-2 hours. This final glass (HBM 1, see Table 3.1) was mechanically separated from the Pt crucible and checked for its composition by electron microprobe. The glass was crushed using agate mortar and pestle.

**Table 3.1: Chemical composition of the dry starting glasses (wt.%).**

	HBM 1	HBM 2
SiO <sub>2</sub>	52.07	51.20
Al <sub>2</sub> O <sub>3</sub>	25.04	26.10
CaO	16.22	16.20
Na <sub>2</sub> O	2.95	2.90
MgO	3.72	3.60
Total	100.00	100.00

HBM 1 and HBM 2 starting glasses were prepared in a platinum crucible and an Al<sub>2</sub>O<sub>3</sub> crucible, respectively. Average composition of 80 and 60 analyses have been done for glasses HBM 1 and HBM 2, respectively. Both starting glass compositions were normalized to 100 %.

The same procedure was adopted for preparing a second glass (HBM 2, see Table 3.1) having the same composition as of HBM 1. However, the starting materials used for the preparation of starting glass HBM 2 were melted in an Al<sub>2</sub>O<sub>3</sub> crucible at 1500 °C/1 atm

instead of a Pt crucible. Al<sub>2</sub>O<sub>3</sub> crucible was used in order to avoid problems regarding unwanted contamination of Pt<sup>o</sup> into the starting glass while melting the starting material at high temperature.

### **3.2.2. Experimental Procedure**

The experiments were performed in Pt capsules (length: 2.75 cm; inner diameter: 3.0 mm; outer diameter: 3.4 mm) which served at the same time as the source of Pt. The Pt capsules were first sealed at one end. The fluid was always loaded first at the base of the capsule. The glass was added in a second step. Chlorine-bearing fluids were prepared by diluting concentrated HCl (33.5 wt.%) using distilled H<sub>2</sub>O to make different chloride concentrations, varying from 5 wt.% Cl<sup>-</sup> to 25 wt.% Cl<sup>-</sup>. Different amounts of fluids (ratio starting glass/fluid) were used. After sealing, the capsules were checked for weight loss after heating at 110 °C for 4-6 hours.

Most of the experiments were conducted in internally heated pressure vessels equipped with rapid quench technique (r-IHPVs) and a few experiments were performed in internally heated pressure vessels with normal quench device (n-IHPVs). Temperature was regulated with two S-type thermocouples. Two additional S-type thermocouples were used to check for possible thermal gradients along the capsule. Temperature variation of most of the experiments was  $\pm 5$  °C. Most of the experiments were conducted using rapid quench device to avoid any quench products. All experiments were conducted in the temperature range 1200-1250 °C and in the pressure range 1-2 kbar. Maximum pressure variation in the vessel was  $\pm 15$  bar. The run duration of the experiments varied from 24-96 hours, but most of the experiments were performed for 25 hours. Blaine et al., 2004 performed experiments following the same procedure and showed that equilibrium distribution between fluid and melt was attained after this duration. All the run products were glasses (except one glass sample with bubbles). The free fluid of the charge after the experiment was collected to determine the chloride content in the aqueous vapor phase.

### **3.2.3. Analytical Methods**

#### ***3.2.3.1. Determination of chloride content***

### 3.2.3.1.1. Titration method

The fluid was collected for most of the experiments. The chloride concentration of this phase was analyzed following the procedure detailed below: (1) Cleaning of closed Pt capsule with deionized H<sub>2</sub>O and subsequent drying. (2) The Pt capsule was punctured with a steel needle to collect most of the free fluid/aqueous phase from the capsule. (3) The free fluid/aqueous phase was collected with the help of a 10 µl micropipette. (4) The capsule was cut transversely from one of its edge and the remaining fluid/aqueous phase was collected. (5) Lastly, the Pt capsule and the sample (glass) were placed in a specific amount of distilled H<sub>2</sub>O. The above five steps were performed in order to collect whole Cl<sup>-</sup> content of the charge. All the materials (collected in step 3, 4 and 5) were transferred to a teflon beaker placed in an ultrasonic bath for 10-15 minutes and kept for at least 24 hours in the teflon beaker. The chloride content of the solution was measured in a Mettler tolcado DL 25 titrator. The titer used to collect the chloride from the diluted solution was 0.002 N AgNO<sub>3</sub>. The activity of the system (Mettler tolcado DL 25 titrator) was determined after analyzing the chloride standard solution containing 1000 mg Cl<sup>-</sup>/l. An error of ± 2 % relative was calculated for the precision of the system.

### 3.2.3.1.2. Electron Microprobe

Glasses were analyzed with a CAMECA SX-100 electron microprobe using the wavelength-dispersive techniques at optimal conditions of 15 kV and 5 nA beam current for Si, Al, Ca, Na, Mg and Cl. All the analyses were conducted with a defocused electron beam (20 µm diameter) and peak count time for matrix was selected between 2 to 10 seconds and peak count time for analysis of chloride in the melt was fixed to 30 seconds for every run product. For checking the homogeneity of chloride in the melt, most of the glass (run product) blocks were cut longitudinally and also transversely, and were analyzed by electron microprobe. Top and bottom part (indicated as upper and lower part, see Table 3.2 and Table 3.3 for details) from most of the samples were analyzed separately. About 50 to 85 analyses were performed per glass sample.

### 3.2.3.2. Determination of H<sub>2</sub>O solubility

#### 3.2.3.2.1. Karl Fischer Titration (KFT)

The H<sub>2</sub>O content of the quenched glasses was determined by Karl Fischer titration. Karl Fischer titration is an analytical procedure by which H<sub>2</sub>O reacts quantitatively in presence of specific reagents, with coulometrically generated iodine (coulometer used for this study: Mitsubishi<sup>®</sup> CA 05). This procedure is successfully applied to determine relatively high H<sub>2</sub>O content in silicate materials (up to 5 wt %, cf. Turek et al., 1976) as well as low H<sub>2</sub>O contents (down to 0.1 wt.% H<sub>2</sub>O, cf. Westrich, 1987). Only small amounts of glass are necessary to get reliable data (typically 10 – 20 mg of substances containing ~ 6 wt.% H<sub>2</sub>O). The glass was roughly crushed and the H<sub>2</sub>O content was determined directly after crushing. This is necessary to avoid errors due to absorption of H<sub>2</sub>O for glasses with low H<sub>2</sub>O contents or due to desorption for glasses with high H<sub>2</sub>O contents. The analytical error given for KFT measurements for all experiments in Table 3.3, is typically ± 0.05 to ± 0.10 wt.% and this error depends upon the mass of the sample (in mg), titration rate ( in µg/s), duration of the measurement (in seconds). For one glass (Experiment 4, see Table 3.3), measurements obtained by using both a single piece and a freshly crushed powder yielded nearly identical H<sub>2</sub>O contents (with a precision of ± 5 %). To check the homogeneity of H<sub>2</sub>O, two different parts (e.g. lower and upper part) from one sample were analyzed separately for experiment 4. The H<sub>2</sub>O measured in the lower and upper part of the sample, were 4.81 ± 0.1 wt.% and 5.05 ± 0.1 wt.%, respectively.

#### 3.2.3.2.2. IR-spectroscopy

IR spectroscopy was used to check the homogeneity of distribution of H<sub>2</sub>O in the glasses. Doubly polished glass wafers with thickness of 0.4 mm were prepared. The thickness of the sections was measured using a digital micrometer (Mitutoyo) with an uncertainty of 2 µm. The spectra were recorded using an IR microscope (A590) attached to a Bruker IFS88 FTIR spectrometer. Measurement conditions were: a halogen light source, A CaF<sub>2</sub>-beamsplitter and a narrow band MCT detector. The analyzed spots were on



average 30-50  $\mu\text{m}$ . 50-100 scans were accumulated for each spectrum with a spectral resolution of 4  $\text{cm}^{-1}$ . Total concentration of water,  $C_{\text{H}_2\text{O}}$ , in the run products is calculated following Lambert-Beer's law using molar absorption coefficient,  $\epsilon$ , of  $0.56 \pm 0.01 \text{ l mol}^{-1} \text{ cm}^{-1}$  for OH group (4500  $\text{cm}^{-1}$  band) and  $0.56 \pm 0.01 \text{ l mol}^{-1} \text{ cm}^{-1}$  for H<sub>2</sub>O group (5200  $\text{cm}^{-1}$  band) given by Ohlhorst et al. (2001). Density of haplobasaltic glasses is calculated using the equation,  $\rho = -20.8c_{\text{water}} + 2819$ , derived from data of Yamashita et al. (1997), where  $\rho$  is the density of glass and  $c_{\text{water}}$  is the concentration of water. The error in sample thickness is  $\pm 2 \mu\text{m}$ .

#### 3.2.3.2.3. *Electron Microprobe*

Water concentration in some glasses was determined by electron microprobe (difference method). An estimate of precision of  $\pm 10 \%$  relative was calculated for the data obtained from microprobe, by comparing with the data from KFT. For example, in the experiment number 12, the H<sub>2</sub>O solubility measured by KFT and electron microprobe are  $6.10 \pm 0.05 \text{ wt.}\%$  and  $6.40 \pm 0.50 \text{ wt.}\%$ . It is emphasized that the error on H<sub>2</sub>O concentrations estimated by the difference method is much higher than that from KFT and IR measurements.

#### 3.2.3.3. *Determination of platinum in haplobasalts*

In all run products, platinum was analyzed by isotope-dilution and using multi-collector inductively coupled mass spectroscopy (ID-MC-ICPMS). Contamination of the samples with capsule material was a large concern in this study and care was taken to minimize the problem. Due to small absolute amounts of platinum dissolved in the glasses, any contamination by the capsule material would result to very high apparent concentrations. Therefore to minimize (avoid) such problem of sample contamination from Pt capsule, glasses were removed from the capsule and thoroughly cleaned in different stages.

#### *3.2.3.3.1. Cleaning of glass samples*

Firstly, after removing the glass samples from the Pt capsule, they were broken into pieces of approximately 100 mg. One 100 mg piece was chosen for analysis by isotope dilution and placed in a Teflon Savillex bomb together with 2 ml of dilute (1:20) hydrofluoric acid (HF). HF was used to etch the surface of the sample to get rid of any Pt metal that could be stuck to the surface of the glass sample. The Savillex bomb was placed in an ultrasonic bath for 10 minutes. The samples and containers were rinsed thoroughly with Nanopure water. Water was added into the containers and it was again placed in an ultrasonic bath for approximately 5 minutes. The water was then discarded and the sample was dried overnight.

After cleaning, the samples were crushed to a fine powder using an agate mortar and pestle. The samples were then weighed and placed in a clean Savillex bomb and spiked with a platinum isotope standard solution. The samples and spike were then digested using 0.5 ml concentrated HF + 0.5 ml concentrated HCl + 0.5 ml concentrated HNO<sub>3</sub>. All acids used were suitable for trace analysis: HCl and HNO<sub>3</sub> were distilled and HF was doubly distilled: The containers were sealed and placed on a hot plate at 80 degrees for 24 hours. After one hour, the samples were removed from the hot plate to be placed in an ultrasonic bath for five minutes before being returned to the hot plate. After 24 hours of digestion the containers were uncovered, put back on the hot plate and the acids were allowed to evaporate. After the samples were thoroughly dried, 0.5 ml of concentrated HNO<sub>3</sub> was added to the sample and allowed to evaporate on the hot plate. A further 0.2 ml concentrated HNO<sub>3</sub> was added and again allowed to evaporate. The final stage of the digestion process was the addition of 2 ml of 0.8 N HNO<sub>3</sub> saturated with Br<sub>2</sub>, the savillex bombs were sealed tightly and placed again on the hot plate overnight. This final step ensured that the platinum present was in highest valence state, required for column separation.

#### *3.2.3.3.2. Column technique and analysis*

Bior-Rad AG IX 8 resin (200-400 mesh) was prepared the day before column separation with the addition of 0.8N HNO<sub>3</sub> saturated with Br<sub>2</sub>. Resin was added to the column and two 1 ml aliquots of 0.8N HNO<sub>3</sub> saturated with Br<sub>2</sub> and allowed to pass through the column. The samples were then loaded onto the column and again two 1 ml aliquots of 0.8N HNO<sub>3</sub> saturated with Br<sub>2</sub> were added. The resin was cleaned by adding 5 ml 10N HNO<sub>3</sub> to the column. After the resin was cleaned, 10 ml of 14N HNO<sub>3</sub> was added to the column, eluting the Pt, and the sample was collected. Samples were evaporated and then stored until analysis.

Analysis was done using one of two multicollector ICP-MSs, a Micromass Isoprobe at the University of Münster, or a NU Instruments ICP-MS at the MPI für Chemistry in Mainz. All wet chemistry was also performed at the MPI in Mainz.

### **3.3. Results and discussion**

All experimental products consisted of bubble-free glasses except one (3E; see Table 3.3) and a fluid phase. In previous studies (e.g., Carroll and Webster, 1994; Lowenstern, 1994; Kravchuk and Keppler, 1994; Shinohara et al., 1989; Shinohara, 1994; Webster, 1997 and Webster et al., 1999) most experimental products were vesicular glasses, which might create problems to determine chloride contents in the run products. To overcome this problem, proper steps (rapid quench) were adopted while performing the experiments. Thus, the experimental products can be used to better quantify the partitioning behavior of chloride between haplobasaltic melt and fluid.

#### **3.3.1. Compositional Variation of glasses after experiment**

The major element composition of glasses was examined before and after performing the experiments. Table 3.2 shows that the major element composition before and after the experiment is nearly identical. Thus, changes of melt compositions due to incongruent dissolution of silicate in the hydrous fluid phase can be neglected.

**Table 3.2: Microprobe analysis of starting material of different glasses (in weight percent) before and after performing the experiment.**

	Composition before experiment for HBM 1	Composition after the experiment							
		1B (U)	1B (L)	1C (U)	1C(L)	7 (U)	7 (L)	9 (U)	9 (L)
SiO <sub>2</sub> (wt.%)	52.07	52.53	52.83	52.57	52.85	52.31	51.51	52.52	51.72
Al <sub>2</sub> O <sub>3</sub>	25.04	24.83	24.81	24.85	24.69	24.98	24.96	24.68	24.79
CaO	16.22	16.23	16.02	16.19	16.11	16.28	16.95	16.42	16.99
MgO	3.72	3.67	3.62	3.64	3.62	3.58	3.70	3.60	3.67
Na <sub>2</sub> O	2.95	2.74	2.72	2.75	2.73	2.85	2.88	2.78	2.83
Total	100.00	100.00	100.00	100.00	100.00	100.00	100.00	100.00	100.00

All the experiments are done at T = 1200 °C and P = 2000 bar. All compositions are being normalized to 100%.

Abbreviations: 1B, 1C, 7 and 9 are different experiments (see Table 3.3). U, upper part of the run product; L, lower part of run product.

### 3.3.2. Effect of Cl<sup>-</sup> on H<sub>2</sub>O solubility in Haplobasaltic melt

The experiments with pure H<sub>2</sub>O fluid show that the H<sub>2</sub>O solubility in haplobasaltic melt is  $4.9 \pm 0.15$  wt.% at 2 kbar and  $3.30 \pm 0.05$  wt.% at 1 kbar. A small but significant increase in solubility of H<sub>2</sub>O in haplobasaltic melt is observed when chloride is added to the system. H<sub>2</sub>O solubility increases with an increasing chloride content of the charge (and also with increasing chloride content of the melt). At 2 kbar, H<sub>2</sub>O solubility is  $4.9 \pm 0.15$  wt.% H<sub>2</sub>O (see Berndt et al., 2002) and  $6.1 \pm 0.15$  wt.% H<sub>2</sub>O in melts containing 0 and 2.9

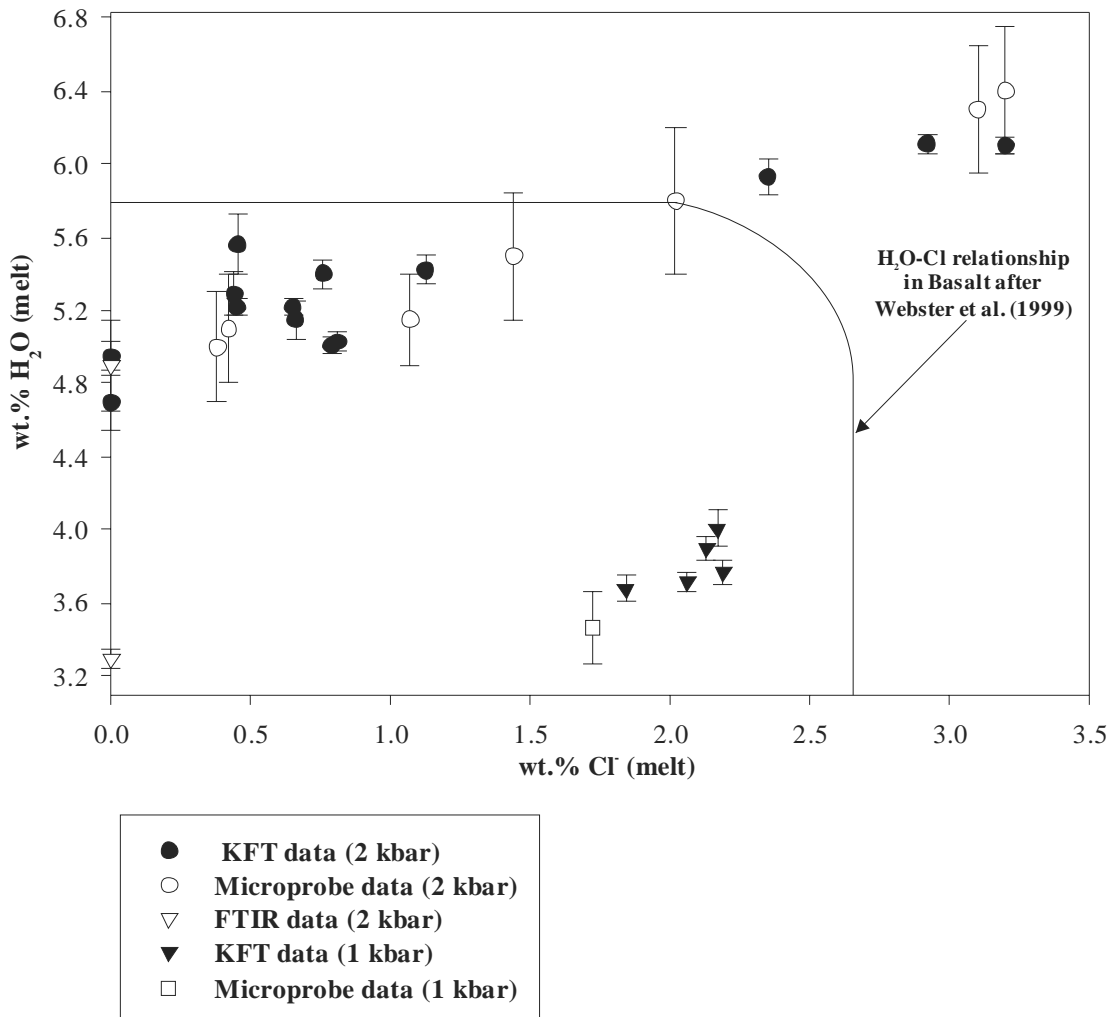


**Figure 3.1: H<sub>2</sub>O versus Cl concentration in haplobasaltic melt at 1200-1250 °C. Comparison of the present study with the model given by Webster et al. (1999). The solid line represents trend line given by the model of Webster et al. (1999) for basaltic system at 1080-1170 °C and at 2 kbar**

wt.% Cl<sup>-</sup>, respectively. At 1 kbar, H<sub>2</sub>O solubility increases from  $3.30 \pm 0.05$  to  $3.98 \pm 0.07$  wt.% when Cl<sup>-</sup> concentration in the melt increases from 0 wt.% Cl<sup>-</sup> to 2.17 wt.% Cl<sup>-</sup>. The results are compared with model of Webster et al. (1999) for basalts in Figure 3.2. The model of Webster et al. (1999) predicts that the H<sub>2</sub>O solubility should remain constant with increasing chlorine content up to ~2 wt.% Cl<sup>-</sup> in the melt. The data from this study clearly show an increasing H<sub>2</sub>O solubility in the range 0 to 2 wt.% Cl<sup>-</sup> in the melt. Although the model of Webster et al. (1999) remains valid in a general way (strongly non-ideal mixing of H<sub>2</sub>O and Cl<sup>-</sup>), it is shown that solubility of H<sub>2</sub>O in basaltic melts is not constant with chloride content in basaltic melts containing up to 2 wt.% Cl<sup>-</sup>. The experimental observations from this study suggest that the presence of Cl-bearing species in the melt enhances H<sub>2</sub>O incorporation.

**Table 3.3: Solubility of platinum measured in haplobasaltic melts.**

Exp. Ref. No.	P (bar)	T (°C)	Run duration (hours)	Starting material (glass) <sup>1</sup>	Cl <sup>-</sup> in melt (wt.%) <sup>2</sup> [1σ] <sup>3</sup>	Cl <sup>-</sup> in free aqueous or vapor phase (wt.%) <sup>4</sup> [D <sub>Cl</sub> ] <sup>5</sup>	H <sub>2</sub> O in melt (wt.%) <sup>6</sup>	H <sub>2</sub> O in melt (wt.%) <sup>7</sup>	H <sub>2</sub> O in melt (wt.%) <sup>8</sup>	Concentration and amount of fluid (wt.%) <sup>9</sup> [wt.%) <sup>10</sup>	Pt conc. [ppb] <sup>11</sup>
S1°	1	1600	4	HBM 1	-	-	dry	-	-	-	1153
1A	2000	1200	25	HBM 1	0.61 (L) [0.01] 1.01 (U) [0.06]	3.22 [≈ 4.00]	6.20	5.03 ± 0.07	-	5.7 [16]	15540
1B*	2000	1200	25	HBM 1	0.74 (L) [0.01] 0.84 (U) [0.05]	3.38 [≈ 4.40]	6.10	5.01 ± 0.07	-	5.7 [13]	5179
1C*	2000	1200	25	HBM 1	0.41 (L) [0.01] 0.55 (U) [0.01]	1.00 [≈ 2.00]	6.08	5.56 ± 0.16	-	5.7 [10]	18625
1D	2000	1200	25	HBM 1	0.43 (L) [0.02] 0.92 (U) [0.03]	2.10 [≈ 3.00]	6.53	5.79 ± 0.06	-	5.7 [20]	11061
2A**	2000	1200	93	HBM 1	0.46 [0.02]	-	4.60	-	-	5.7 [10]	
2B**	2000	1200	93	HBM 1	0.76 [0.02]	-	-	5.40 ± 0.08	-	5.7 [14]	
4 <sup>+</sup>	2000	1200	25	HBM 1	0.00 (L) 0.00 (U)	0.00 0.00	-	4.85 ± 0.1 5.05 ± 0.1	4.90	[10] [10]	2657
6 <sup>+</sup>	2000	1200	25	HBM 1	0.00	0.00	-	4.70 ± 0.15	-	[10]	3327
7	2000	1200	25	HBM 1	0.25 (L) [0.06] 0.65 (U) [0.06]	-	5.51 5.60	5.22 ± 0.05	-	5.7 [15]	1970 2018
9	2000	1200	25	HBM 1	0.40 (L) [0.01] 0.82 (U) [0.01]	-	6.14	5.15 ± 0.09	-	5.7 [10]	2043
10	2000	1200	25	HBM 1	0.44 [0.02]	-	5.38	5.29 ± 0.12	-	5.7 [10]	3267
3C*	1000	1200	24	HBM 1	2.06 [0.10]	10.5-11.0 [≈ 5.22]	3.95	3.72 ± 0.05	-	25 [10]	
3D*	1000	1200	24	HBM 1	2.13 [0.12]	12.0-12.5 [≈ 5.75]	4.03	3.90 ± 0.07	-	25 [10]	
3E*	2000	1200	71	HBM 1	2.92 [0.05]	22.0-23.0 [≈ 7.71]	6.20	6.11 ± 0.05	-	25 [25]	8094
4A*	1000	1200	24	HBM 1	2.17 [0.10]	13.0-14.0 [≈ 6.30]	3.92	3.98 ± 0.07	-	20 [15]	
4B*	1000	1200	24	HBM 1	1.84 [0.12]	5.0-6.3 [≈ 3.50]	3.73	3.68 ± 0.07	-	20 [5]	
4C*	1000	1200	24	HBM 1	1.72 [0.1]	5.0-6.5 [≈ 3.00]	3.47	-	-	20 [5]	
5A*	2000	1200	43	HBM 1	2.35 [0.15]	19.0-20.0 [≈ 8.40]	6.48	5.93 ± 0.05	-	25 [15]	2442



**Table 3.3 (continued):**

Exp. Ref. No.	P (bar)	T (°C)	Run duration (hours)	Starting material (glass) <sup>1</sup>	Cl <sup>-</sup> in melt (wt.%) <sup>2</sup> [1σ] <sup>3</sup>	Cl <sup>-</sup> in free aqueous or vapor phase (wt.%) <sup>4</sup> [D <sub>Cl</sub> ] <sup>5</sup>	H <sub>2</sub> O in melt (wt.%) <sup>6</sup>	H <sub>2</sub> O in melt (wt.%) <sup>7</sup>	H <sub>2</sub> O in melt (wt.%) <sup>8</sup>	Concentration and amount of fluid (wt.%) <sup>9</sup> [wt.%) <sup>10</sup>	Pt conc. [ppb] <sup>11</sup>
5C	2000	1200	61	HBM 1	0.94 (L) [0.05] 1.32 (U) [0.05]	4.40-4.80 [≈ 4.00]	5.98	5.42 ± 0.08	5.60	25 [14]	
5D*	1000	1250	22	HBM 1	2.19 (L) [0.05]	16.5-18.0 [≈ 7.90]	4.07	3.77 ± 0.07		25 [14]	
5E*	1000	1250	24	HBM 1	0.00	0.00	3.70	3.30 ± 0.05		25 [14]	
S2°	1	1500	3-4	HBM 2	-	-	dry	-		-	198
8	2030	1200	38	HBM 2	0.42 [0.06]	-	5.1	-		5.7 [11]	105
9	2030	1200	62	HBM 2	0.38 [0.06]	-	5.0	-		5.7 [10]	150
10 <sup>n</sup>	2030	1200	22	HBM 2	2.02 [0.27]	-	5.8	-		20 [12]	25263
12	2030	1200	38	HBM 2	3.20 [0.07]	-	6.4	6.10 ± 0.05		25 [17]	920
13 <sup>n</sup>	2030	1200	23	HBM 2	3.10 [0.17]	-	6.7	-	6.15	25 [16]	19165
14 <sup>n</sup>	2020	1200	18	HBM 2	-	-	4.8	-	4.05	-	9407
15	2030	1200	68	HBM 2	-	-	3.9	-	2.77	-	1153
16 <sup>n</sup>	2030	1200	18	HBM 2	-	-	4.7	-	3.30	-	6717
17	2030	1200	68	HBM 2	1.44 [0.22]	-	5.5	-		-	402

**Abbreviations:** P, Pressure; T, Temperature; L, Lower part of run product analyzed; U, Upper part of the run product analyzed. Experiment reference number marked with the sign of asterisk (\*) belongs to the fairly homogenized samples with chloride concentration in those run products. Experiment reference number marked by double asterisks (\*\*) depicts very well homogenized sample with chloride concentration, but a small amount of starting material (≈ 50 mg) is used in that experiment. Experiment reference number marked by cross sign (+) indicates the sample capsules which contain fluid as distilled H<sub>2</sub>O instead of Cl<sup>-</sup>. Sample numbers, S1° and S2° represent the glass composition used for measuring initial Pt concentration in each of the two starting glass compositions, HBM 1 and HBM 2, respectively.

<sup>1</sup> Starting glass compositions used in this study are HBM 1 and HBM 2 (see Table 3.1).

<sup>2</sup> Chloride concentration examined in melt after being analyzed by the electron microprobe.

<sup>3</sup> 1σ is the standard deviation calculated (in wt.%) for the mentioned Cl<sup>-</sup> content of the starting glass used.

<sup>4</sup> Chloride concentration collected and examined in free aqueous phase after the experiment.

**Table 3.3 (continued):**

---

<sup>5</sup> Distribution coefficient ( $D_{Cl}$ ) is mentioned in brackets, and is calculated as “Chloride concentration in free fluid ( $Cl^-_{fluid}$ )/Chloride concentration in melt ( $Cl^-_{melt}$ )”. Chloride concentration is analyzed by Mettler Toledo DL 25 titrator for all the experiments.

<sup>6</sup> Solubility of H<sub>2</sub>O in the melt calculated by difference method by electron microprobe. Assumed error for all experiment measured only by electron microprobe, varies from ± 0.30 to ± 0.40 wt. %.

<sup>7</sup> Solubility of H<sub>2</sub>O in the melt is measured by KFT (Karl Fischer titration).

<sup>8</sup> Solubility of H<sub>2</sub>O in the melt is measured by NIR (Near Infra-Red) spectroscopy. The error in all the final solubility values of H<sub>2</sub>O is calculated to be ± 0.25 wt. %.

<sup>9</sup> Different concentrations of fluids {as dilute HCl (5 wt. % Cl<sup>-</sup> - 25 wt. % Cl<sup>-</sup>) and H<sub>2</sub>O} were used

<sup>10</sup> Determines the amount of fluid in weight percent (marked by closed brackets) as it was put into the capsule before the experiment.

<sup>11</sup> The Pt concentration in all of experiments has an error of about ± 7% relative to the measured concentration of platinum in the melt.

<sup>n</sup> Run product might contain problem regarding formation of Pt-micronuggets (Borisov and Palme, 1997; Blaine et al., 2004), resulting in very high values of Pt concentration in the melt.

---

### 3.3.3. Distribution coefficient of chloride ( $D_{Cl}$ )

The chloride content in the free fluid was determined to be 1 to 22 wt.%, depending upon the amount of chloride content in the fluid and the amount of fluid added in the charge. At 1200-1250 °C and 2 kbar, in the system containing Cl<sup>-</sup> (from 5 wt.% to 25 wt.% Cl added to charge),  $D_{Cl}$  varies from 2.0 to 8.4 (for details, see Table 3.3). Figure 3.2 shows that  $D_{Cl}$  increases almost linearly with an increase in Cl<sup>-</sup> content of the free fluid.

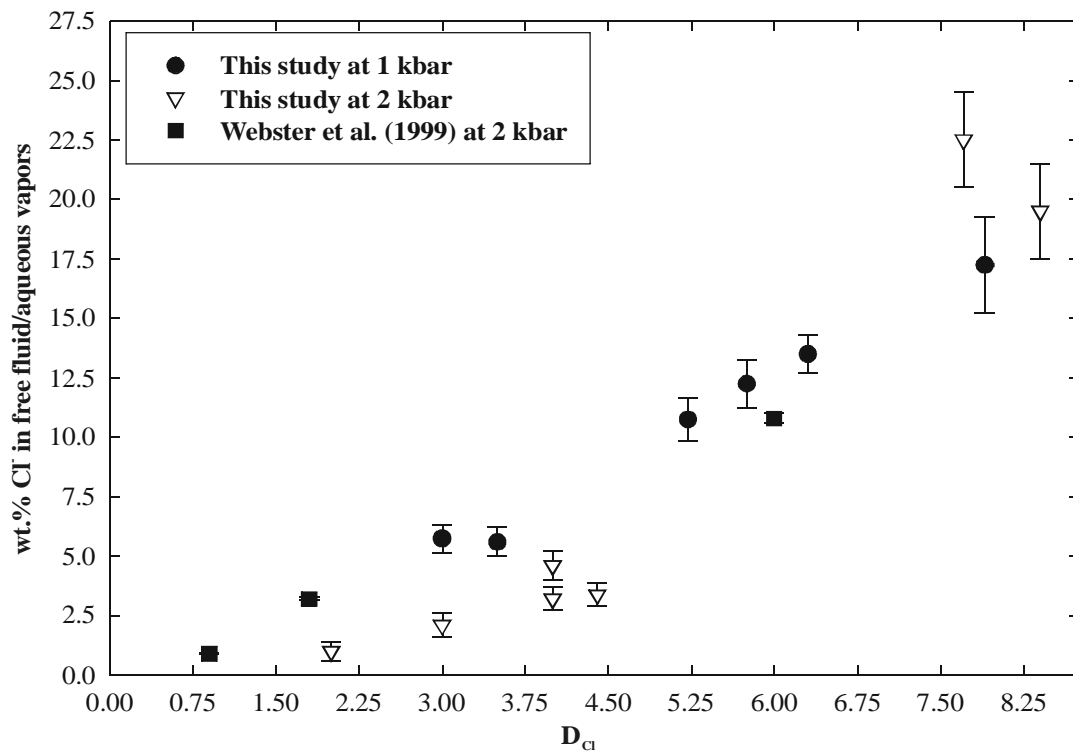


**Figure 3.2:** Graph showing  $D_{Cl}$  versus Cl<sup>-</sup> content in free fluid/aqueous phase in basaltic melt at 1200 °C and 1-2 kbar. Comparison with study of Webster et al. (1999) shows a good agreement with the results from this study.

These results are in well agreement with the experimental study of Webster et al. (1999) at 1080-1170 °C and 2 kbar, who observed that  $D_{Cl}$  increases from 0.9 to 6.0 when Cl<sup>-</sup> content in aqueous liquid increases from 0.9 to 10.8 wt.% Cl<sup>-</sup>. Figure 3.3 shows the effect

of chlorine content of the melt on distribution coefficient of the charge. The results suggest that for a given Cl<sup>-</sup> content of the melt,  $D_{Cl}$  is dependent on pressure.

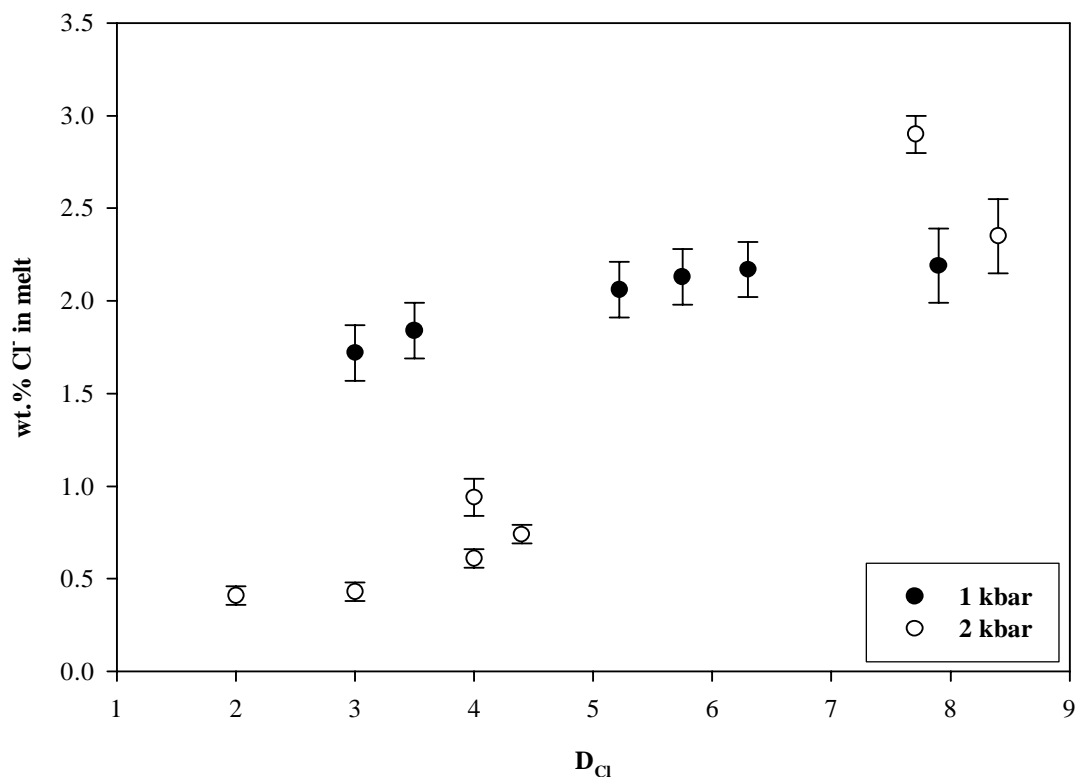


Figure 3.3: Graph shows  $D_{Cl}$  versus wt.% Cl<sup>-</sup> in melt at pressure ranges from 1-2 kbar and temperature 1200 - 1250 °C.

### 3.3.4. Platinum concentrations in glasses

#### 3.3.4.1. Pt concentrations in glasses synthesized in Pt crucible: The Pt-micronugget problem

Platinum concentrations obtained from the starting glass HBM 1 (see Table 3.3 for more details) and plotted in Fig. 3.4 as a function of H<sub>2</sub>O content of the glasses. Water contents in Fig. 3.4 are determined by difference method and have to be considered as indicative. As mentioned above, the starting glass HBM 1 used in this study has high platinum concentrations (dry starting composition contains ~1150 ppb of platinum),

because it was synthesized in Pt crucible at high  $fO_2$  (atmospheric conditions). Following the results of Borisov and Palme (1997) and Ertel et al. (1998) at 1 atm, Pt solubility at this conditions, is >6000 ppb. The Pt concentrations in the H<sub>2</sub>O-bearing glasses are also extremely high. However, the concentrations are much higher than those expected from

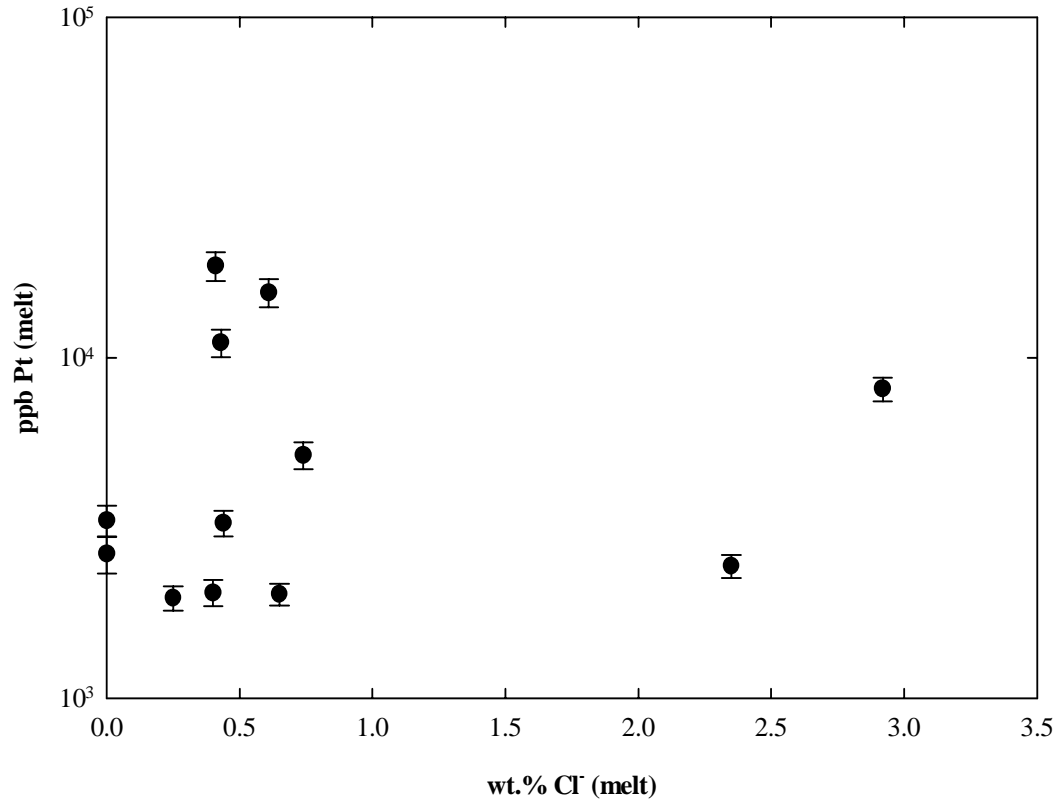


**Figure 3.4: Graph between ppb Pt (melt) and concentration of Cl<sup>-</sup> (wt.%) for glass HBM 1 used in this study.**

Borisov and Palme (1997) and Ertel et al. (1999) at 1 atm the corresponding  $fO_2$ . At log  $fO_2$  of  $10^{-4}$  (experimental conditions), the Pt concentrations vary extremely from 1970 to 18625 ppb (see Table 3.3). Figure 3.4 shows that there is no systematic variation with changing Cl<sup>-</sup> content of the glass. Considering the precision of analytical method ( $\pm 7\%$ ), these variations can only be explained by experimental problems.

These experimental problems arise from the high starting Pt concentration in glass HBM 1. It is inferred that Pt-micronuggets formed during high pressure experiments. These Pt-micronuggets have a higher density than that of the melt and should segregate at

the bottom of the capsule. However, they were probably too small to be completely removed from the melt. Thus, the Pt concentrations which were determined do not represent Pt solubility. The same observation was made by Blaine et al. (2004) for a glass synthesized in a Pt crucible.

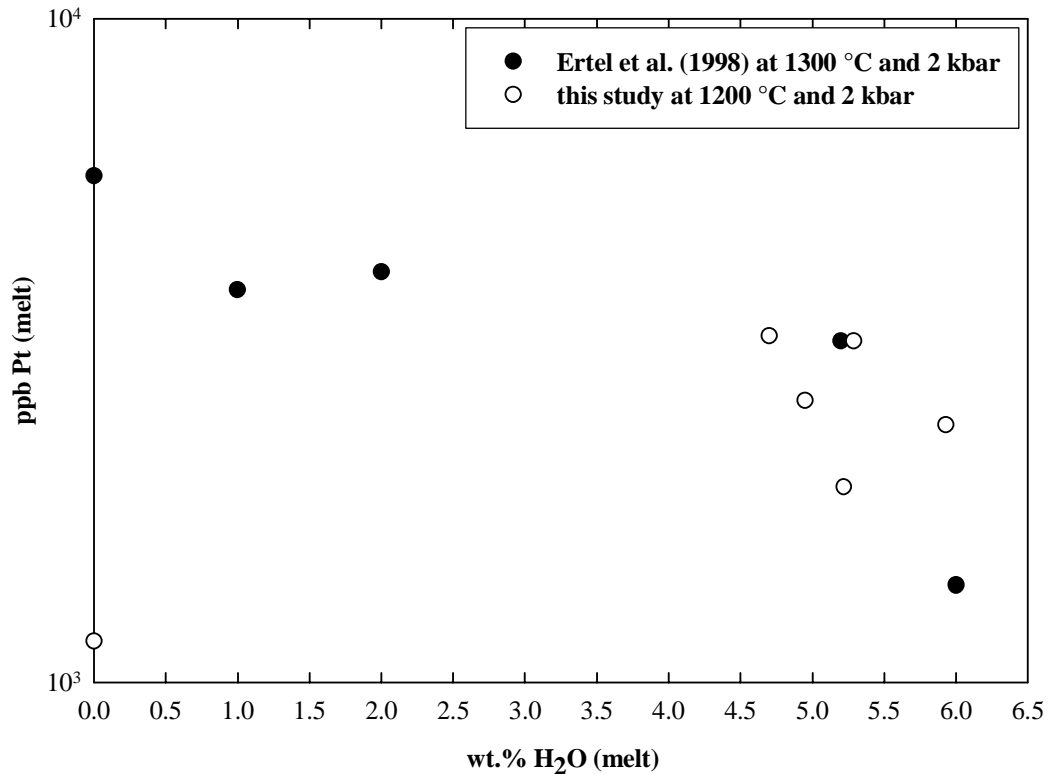


**Figure 3.5: Comparison of this study with study of Ertel et al. (1998) at a  $\log f_{\text{O}_2} = -4$ .**

It is interesting to note that Ertel et al. (1998) also determined extremely high Pt concentrations in a haplobasaltic An-Di glass synthesized in a Pt crucible. Ertel et al. (1998) investigated the effect of H<sub>2</sub>O on Pt solubility at 2 kbar and fitted the data for given melt H<sub>2</sub>O contents. The values obtained by Ertel et al. (1998) for given H<sub>2</sub>O contents at 1300 °C and 2 kbar, are reported in Fig. 3.5. Ertel et al. (1998) suggested that Pt solubility is lower in H<sub>2</sub>O-bearing basaltic melt, when compared with the anhydrous melts. In a dry melt, Ertel et al. (1998) reported 8 ppm of Pt concentration, whereas in a H<sub>2</sub>O-saturated melt Ertel et al. (1998) found a Pt concentration of about 1 ppm. For water contents

between 4.5 and 6.0% H<sub>2</sub>O, the results from this study agree roughly with the data of Ertel et al. (1998). Figure 3.5 shows the comparison between data obtained by this study and study of Ertel et al. (1998). At 1200 °C and 2 kbar, in run products 4 and 6 (see Table 3.3 for details), which contain 4.85 wt.% H<sub>2</sub>O and 4.70 wt.% H<sub>2</sub>O, the concentrations of platinum in the melt are 2657 ppb and 3327 ppb, respectively. However, the Pt concentrations determined by Ertel et al. (1998) can not be Pt solubilities (see above).

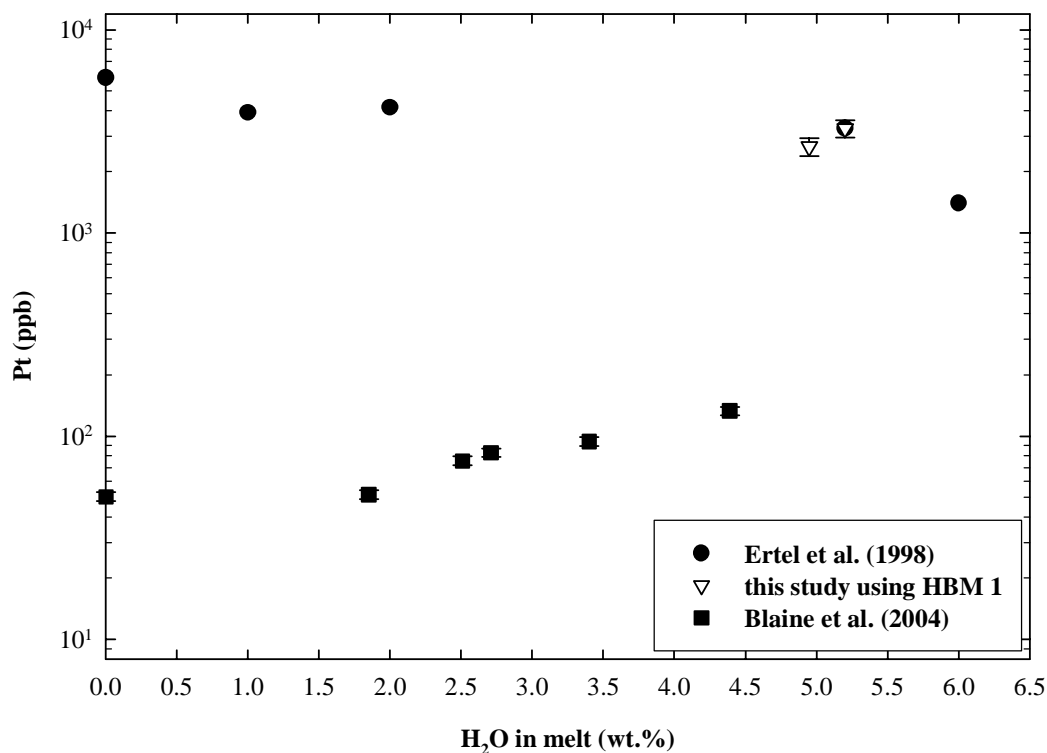


**Figure 3.6: Graph showing H<sub>2</sub>O in melt (wt.%) versus Pt concentration (ppb) in haplobasaltic melts at 1200-1300 °C, 2 kbar and log  $f_{O_2} = -4$ . One data point from the study of Blaine et al. (2004) is the dry starting glass synthesized at 1 bar.**

The variations of Pt concentrations are probably resulting from different amounts of Pt nuggets in the glasses. The trend observed by Ertel et al. (1998) is most probably due to a difference in viscosities of melts. Dry melts have higher viscosities than H<sub>2</sub>O-bearing melts. Thus, the segregation between Pt-micronuggets and silicate melt is favored in hydrous melts. In conclusion, the Pt concentrations analyzed in Glass HBM 1 given in

Table 3.3 do not represent Pt solubilities because the Pt concentrations in starting glass were higher than the expected Pt solubilities.

Another argument showing that Pt concentrations determined by Ertel et al. (1998) and with composition HBM 1 do not represent Pt solubilities is given by recent study of Blaine et al. (2004) showing an increase of Pt concentrations with increasing H<sub>2</sub>O contents (see Fig. 3.6). Blaine et al. (2004) were able to reverse their experiments and the observed trend is consistent with an incorporation mechanism of Pt as Pt<sup>2+</sup>. The increase in Pt concentrations with increasing H<sub>2</sub>O contents is explained by increasing  $fO_2$ .

### 3.3.4.2. Effect of chloride on Pt solubility

Considering the experimental problems which occurred with glass HBM 1, another series of experiments have been conducted with starting glass HBM 2, synthesized in a corundum crucible to avoid platinum contamination in the glass. The results are given in Table 3.3 and plotted in Fig. 3.5 as a function of chloride content of the melt. The glasses contain  $5.1 \pm 0.35$  wt.% (measured by electron microprobe; see Table 3.3) to  $6.1 \pm 0.05$  wt.% (measured by KFT; see Table 3.3) H<sub>2</sub>O in melt. Pt concentrations in run products using HBM 2 tend to increase from 140 ppb to 920 ppb, when Cl<sup>-</sup> concentration in the melt increases from 0.5 wt.% Cl<sup>-</sup> to 3.23 wt.% Cl<sup>-</sup>. At 1250 °C and 2 kbar, the concentration of platinum in a Cl-free haplobasaltic melt, containing 4.4 wt.% H<sub>2</sub>O, has been determined by Blaine et al. (2004) and is  $133 \pm 9.31$  ppb Pt. This Pt concentration obtained by Blaine et al. (2004) at the same  $fO_2$  than that prevailing in runs from this study is plotted in Fig. 3.6. Blaine et al. (2004) found that H<sub>2</sub>O does not have any effect on Pt solubility, but that solubility of platinum varies linearly with  $fO_2$ . Blaine et al. (2004) explains oxidation reaction of Pt, which promotes its dissolution in the melt is as under written:



The starting glass used by Blaine et al. (2004) is a dry diopside-anorthite eutectic composition (An<sub>42</sub>-Di<sub>58</sub>). The composition of the dry glass used in this study is Ab<sub>25</sub>-An<sub>55</sub>-



Di<sub>20</sub>. Thus, small differences in composition will probably not influence significantly the Pt solubility. By considering a precision of about  $\pm 7$  relative, the points for Pt solubility in HBM 2 (see open circles in Fig. 3.7) possibly show a linear trend. Because of very low concentration of Pt (in ppb) and relatively a high uncertainty, it is rather difficult to access the linear or non-linear increase of solubility of platinum as a function of Cl<sup>-</sup> concentration in the melt. However, the evolution of Pt concentrations with Cl<sup>-</sup> content is consistent with recent data of Blaine et al. (personal communication, 2004).

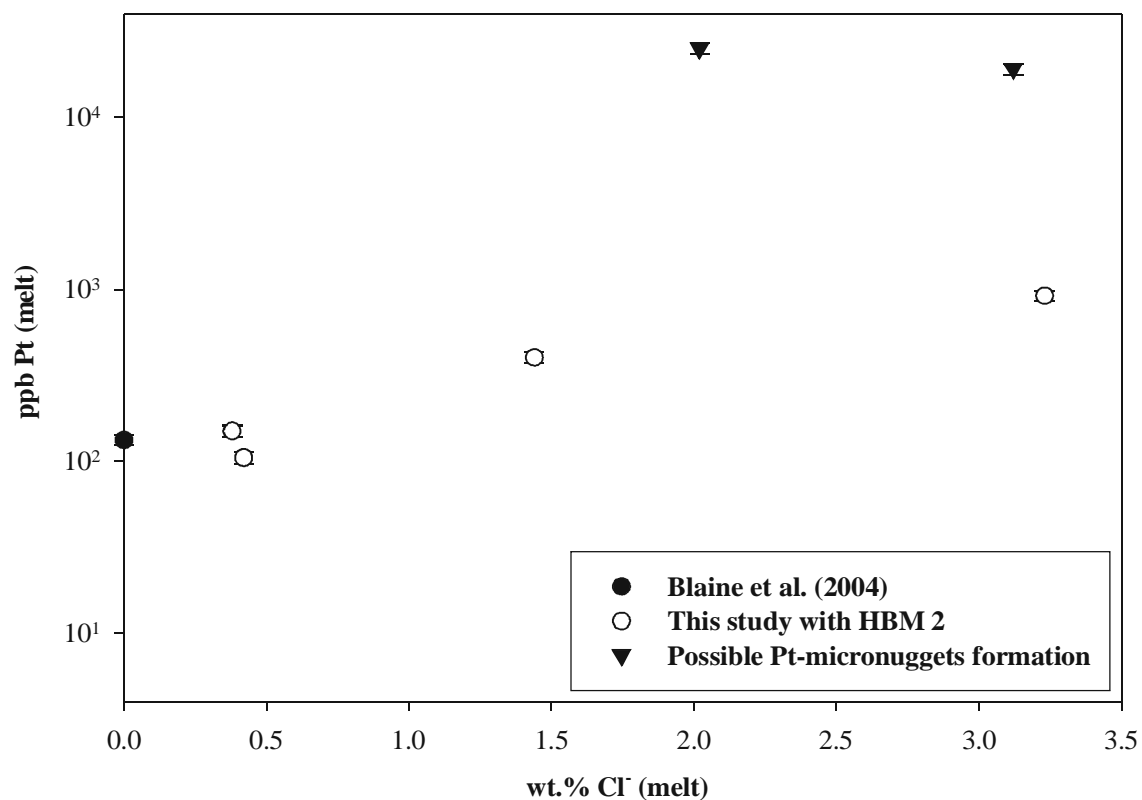


**Figure 3.7: Graph showing effect of Cl<sup>-</sup> on Pt solubility in nearly water-saturated experiments.**

Considering the possible formation of Pt-micronuggets in silicate melts (e.g., Borisov and Palme, 1997), there is also a possible formation of Pt-micronuggets in some of the HBM 2 glasses from the present study. Those run products showed unexpected high concentrations of Pt (solid triangles in Fig. 3.7, e.g.,  $19165 \pm 1350$  ppb and  $25263 \pm 1700$  ppb Pt in a melt containing 2.0 wt.% Cl<sup>-</sup> and 3.1 wt.% Cl<sup>-</sup>; see Table 3.3).

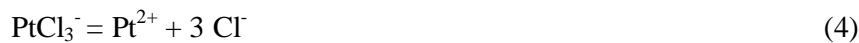
This study shows a positive dependence of solubility of platinum with an increase in chloride content of the melt (see Figure 3.7). If it is assumed that Pt solubility depends linearly on chloride concentration in melt, then at a fixed  $fO_2$ , the addition of 1 wt.% Cl<sup>-</sup> in the melt leads to a concentration of 317 ppb platinum in melt. Such an increase can only be explained by Pt and Cl<sup>-</sup> complexes. Assuming that Pt is dissolved as Pt<sup>2+</sup> in hydrous melts at the investigated  $fO_2$  conditions (Blaine et al., 2004), possible reactions for the formation of Pt-Cl<sup>-</sup> complexes are:



*or*



*or*



*or*

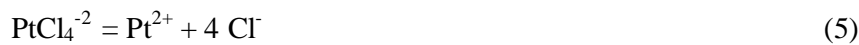
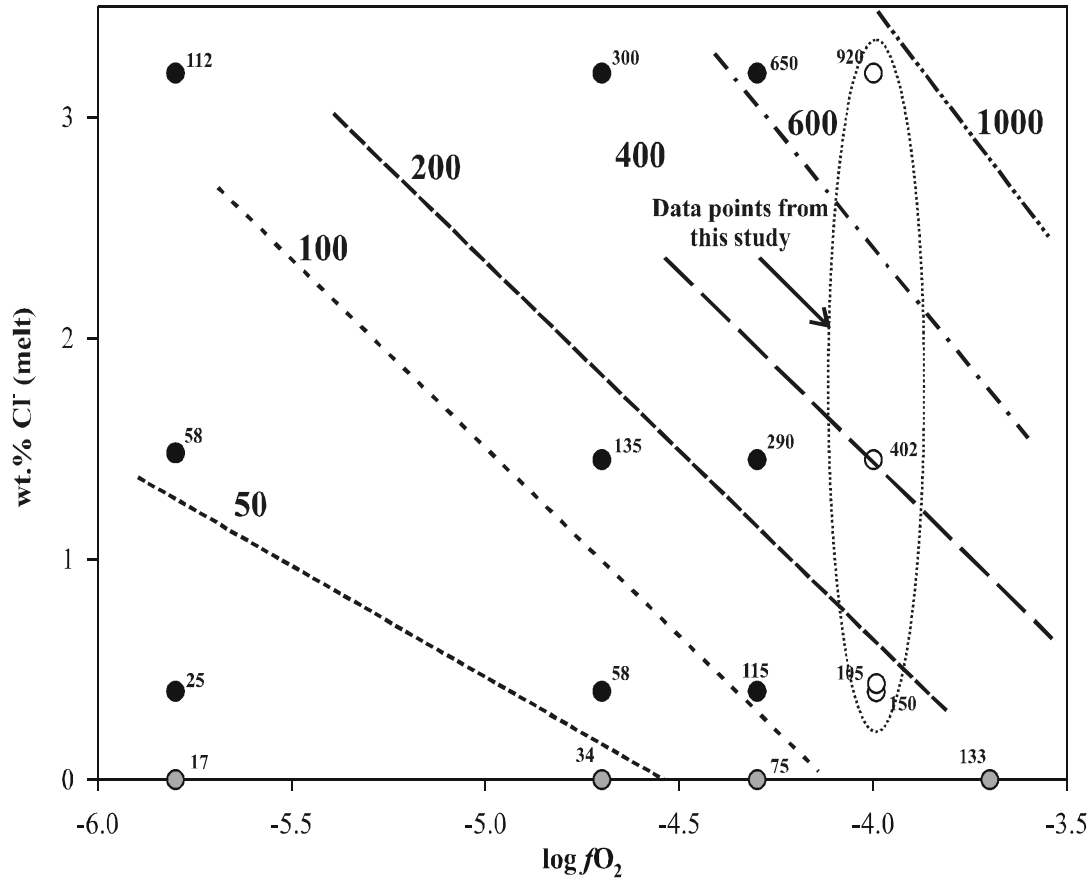


Figure 3.8 shows a modeled effect of chloride and  $fO_2$  on the concentration of Pt in haplobasaltic melt. From the study of Blaine et al. (2004), it can be seen that the predicted platinum solubility in a basaltic magma is less than 1 ppb, if Pt trend is extrapolated to more reduced conditions, such as those estimated for Bushveld Complex at an  $fO_2$  of NNO-2.0 (Ballhaus and Sylvester, 2000). Considering that  $fO_2$  is close to NNO and at 1200 °C (the liquidus temperature for the early Merensky Reef), Pt solubility in basaltic melts from Bushveld complex can be predicted as 20-30 ppb Pt. Thus, when calculated for silicate melt in parental magma, it can be well suggested in this study that platinum is still



**Figure 3.8:** Schematic plot between Cl in melt (wt.%) and log  $fO_2$  in haplobasaltic melts. Isolines are linear fits for different platinum concentrations calculated in ppb. Platinum concentration in the melt can be calculated for a given  $fO_2$  as well as for given Cl content in the melt. Open circles (plotted at a log  $fO_2 = -4.0$ ) are taken from this study, whereas, the grey solid circles (plotted for experiments with 0 wt.% Cl in melt) are taken from the study of Blaine et al. (2004), which show a slope of  $C_{Pt} = 49.11 - 4.44 (H_2O) + 5.40 (H_2O)^2$  with R-squared = 0.974. Black solid circles are extrapolated by slope of the equation given in this study,  $C_{Pt} = 57.30 + 260.24 \cdot Cl$ . In both equations,  $C_{Pt}$  is concentration of platinum (ppb), and concentration of both chloride and  $H_2O$  is in (wt.%).

oversaturated by two orders of magnitude. Blaine et al. (2004) also suggested that Pt as well as other PGEs, could have been contained in a phase separate from either the sulphide or silicate phase possibly a PGE alloy or a coexisting fluid phase.

## 4. References

- Amossé, J., Dable, P., Allibert, M., 2000.** Thermodynamical behaviour of Pt, Ir, Rh and Ru vs  $fO_2$  and  $fS_2$  in a basaltic melt. Implications for the differentiation and precipitation of these elements. *Mineralogy and Petrology* 68, 29-62.
- Anderson, A.T., 1974.** Chlorine, sulfur, and water in magmas and oceans. *Geological Society of America Bulletin* 85, 1485-1492.
- Antipin, V.S., Kovalenko, V.I., Kuznetsova, A.I., Persikova, L.A., 1981.** Distribution of tin and tungsten in ore-bearing acid igneous rocks. *Geochemistry International* 18, 92-106.
- Audetat, A., Gunter, D., Heinrich, C. A., 2000.** Magmatic-hydrothermal evolution in a fractionating granite: A microchemical study of the Sn-W-F-mineralized Mole Granite (Australia). *Geochimica et Cosmochimica Acta* 64, 3373-3393.
- Augé, T., Salpeteur, I., Bailly, L., Mukherjee, M.M., Patra, R.N., 2002.** Magmatic and Hydrothermal Platinum-Group Minerals and basemetal sulphides in the Baula Complex, India. *Canadian Mineralogist* 40, 277-309.
- Bai, T.B., Koster Van Groos, A.F., 1994.** Diffusion of chlorine in granitic melts. *Geochimica et Cosmochimica Acta* 58, 113-123.
- Ballhaus, C., Stumpfl, E.F., 1986.** Sulfide and platinum mineralization in the Merensky Reef: evidence from hydrous silicates and fluid inclusions. *Contributions to Mineralogy and Petrology* 94, 193-204.
- Ballhaus, C., Ryan, C.G., Mernagh, T.P., Green, D.H., 1994.** The partitioning of Fe, Ni, Cu, Pt, and Au between sulfide, metal, and fluid phases: A pilot study. *Geochimica et Cosmochimica Acta* 58, 811-826.
- Ballhaus, C., Sylvester, P., 2000.** Noble metal enrichment processes in the Merensky Reef, Bushveld Complex. *Journal of Petrology* 41, 545-561.
- Ballhaus, C., Tredoux, M., Späth, A., 2001.** Phase relations in the Fe-Ni-Cu – PGE – S system at magmatic temperature and application to massive sulphide ores of the Sadbury Igneous Complex. *Journal of Petrology* 42, 1911-1926.
- Barnes, S.-J., Maier, W.D., 2002.** Platinum-group elements and microstructures of normal Merensky Reef from Impala platinum mines, Bushveld Complex. *Journal of Petrology* 43, 103-128.

- Barr, H., 1990.** Preliminary fluid inclusion studies in a high grade blueschist terrane, Syros, Greece. *Mineralogical Magazine* 54, 159-168.
- Barsukov, V.L., 1957.** The geochemistry of tin. *Geochimistry* 1957, 41-52.
- Barsukov, V.L., 1974.** Principal features of the geochemistry of tin. *Izd. Nauka, Moskva* (in Russian).
- Barsukov, V.L., Durasova, N.A., 1966.** Metal content and metallogenic specialization of intrusive rocks in the regions of sulphide-cassiterite deposits (Miao-Chang and Sikhote Alin.). *Geochemistry International* 3, 97-107.
- Bauman, L., 1970.** Tin deposits of the Erzgebirge. *Trans. Inst. Mining and Metallurgy, Section B (Applied Earth Science)* 79, 68-75.
- Bauman, L., Štemprok, M., Tischendorf, G., Zoubek, V., 1974.** Metallogeny of tin and tungsten in the Krusne Hory-Erzgebirge excursion guide. *Metallization Associated with Acid Magmatism* Symposium Karlovyvary. Geological Survey, Prague, p. 66.
- Behrens, H., Romano, C., Nowak, M., Holtz, F., Dingwell, D.B., 1996.** Near-infrared spectroscopic determination of water species in glasses of the system  $\text{MAISi}_3\text{O}_8$  (M = Li, Na, K): an interlaboratory study. *Chemical Geology* 128, 41-64.
- Belkin, H.E., De Vivo, B., Török, K., Webster, J.D., 1998.** Pre-eruptive volatile content, melt inclusion chemistry, and microthermometry of interplinian Vesuvius lavas (pre-1631 A.D.). *Journal of Volcanology and Geothermal Research* 82, 79-95.
- Benzaazoua, M., Marion, P., Pinto, A., Migeon, H., Wagner, F.E., 2003.** Tin and indium mineralogy within selected samples from the Neves Corvo ore deposit (Portugal): a multidisciplinary study. *Minerals Engineering* 16, 1291-1302.
- Berndt, J., Holtz, F., Koepke, J., 2001.** Experimental constraints on storage conditions in the chemically zoned phonolitic magma chamber of the Laacher See volcano. *Contributions to Mineralogy and Petrology* 140, 469-486.
- Berndt, J., Liebske, C., Holtz, F., Freise, M., Nowak, M., Ziegenbein, D., Hukruck, W., Koepke, J., 2002.** A combined rapid-quench and  $\text{H}_2$ -membrane setup for internally heated pressure vessels: Description and application for water solubility in basaltic melts. *American Mineralogist* 87, 1717-1726.
- Bezmen, N.I., Naldrett, A.J., Asif, M., 1998.** Solubilities of Pt and Pd in the hydrous silicate melt. *Exp. In Geosciences*, 7, 17-18.

- Bhalla, P., Holtz, F., Linnen, R.L., Behrens, H., 2005.** Solubility of cassiterite in evolved granitic melts: effect of T,  $fO_2$  and additional volatiles. *Lithos* 80, 387-400.
- Blaine, F.A., Linnen, R.L., Holtz, F., Brüggmann, G.E., 2004.** Platinum solubility in haplobasaltic melt at 1250°C and 0.2 GPa: The effect of water content and oxygen fugacity. *Geochimica et Cosmochimica Acta* (*in press*).
- Boorman, S., Boudreau, A., Kruger, F.J., 2004.** The Lower Zone–Critical Zone transition of the Bushveld Complex: a quantitative textural study. *Journal of Petrology* 45, 1209-1235.
- Borisov, A., Palme, H., 1997.** Experimental determination of the solubility of platinum in silicate melts. *Geochimica et Cosmochimica Acta* 61, 4349-4357.
- Boudreau, A.E., 1993.** Chlorine as an exploration guide for platinum-group elements in layered intrusions. *Journal of Geochemical Exploration* 48, 21-37.
- Boudreau, A.E., Mathez, E.A., McCallum, I.S., 1986.** Halogen geochemistry of the Stillwater and Bushveld Complexes: Evidence for transport of the platinum-group elements by Cl-rich fluids. *Journal of Petrology* 27, 967-986.
- Boudreau, A.E., McCallum, I.S., 1986.** Investigations of Stillwater Complex: III. The Picket Pin Pt/Pd deposit. *Economic Geology* 81, 1953-1975.
- Boudreau, A.E., McCallum, I.S., 1992.** Concentration of platinum-group elements by magmatic fluids in layered intrusions. *Economic Geology* 87, 1830-1848.
- Bureau, H., 1999.** Salty supracrustal fluids in subduction zones: geochemical consequences. *Terra Nostra* 99/7, 15-16.
- Burnham, C.W., 1967.** Hydrothermal fluids at the magmatic stage. In H.L. Barnes (Ed.), *Geochemistry of Hydrothermal Ore deposits*. pp. 34-76, Wiley, New York.
- Burnham, C.W., 1979.** Magmas and hydrothermal fluids. In H.L. Barnes (Ed.), *Geochemistry of Hydrothermal Ore Deposits*. pp. 71-136, Wiley, New York.
- Breiter, K., Frýda, J., Seltmann, R., Thomas, R., 1997.** Mineralogical evidence for two magmatic stages in the evolution of an extremely fractionated P-rich rare-metal granite: the Podlesí stock, Krušné Hory, Czech Republic. *Journal of Petrology* 38, 1723-1739.
- Campbell, I.H., Naldrett, A.J., Barnes, S.J., 1983.** A model for the origin of the platinum-rich sulfide horizons in the Bushveld and Stillwater complexes. *Journal of Petrology* 24, 133-165.

- Candela, P.A., Holland, H.D., 1984.** The partitioning of copper and molybdenum between silica melts and aqueous fluid. *Geochimica et Cosmochimica Acta* 48, 373-380.
- Candela, P.A., Piccoli, P.M., 1995.** Model ore-metal partitioning from melts into vapor and vapor/brine mixtures. In J.F.H. Thompson (Ed.), *Magma, Fluids, and ore deposits*. Mineralogical Association of Canada Short Course Series 23, pp. 101-127, Victoria, British Columbia.
- Capobianco, C.J., Drake, M.J., 1990.** Partitioning of ruthenium, rhodium, and palladium between spinel and silicate melt and implications for platinum group element fractionation trends. *Geochimica et Cosmochimica Acta* 54, 869-874.
- Capobianco, C.J., Drake, M.J., 1994.** Partitioning and solubility of PGE in oxides and silicates. *Mineralogical Magazine* 58A, 144-145.
- Carroll, M.R., Webster, J.D., 1994.** Solubilities of sulfur, noble gases, nitrogen, chlorine, and fluorine in magmas. In M.R. Carroll and J.R. Holloway (Eds.), *Volatiles in Magmas*. Reviews in Mineralogy 30, Mineralogical Society of America, pp. 231-279, Washington, D.C.
- Carten, R.B., Geraghty, E.P., Walker, B.M., Shannon, J.R., 1988.** Cyclic development of igneous features and their relationship to high-temperature hydrothermal features in the Henderson Porphyry molybdenum deposit, Colorado. *Economic Geology* 83, 266-296.
- Cawthorn, R.G., Lee, C.A., Schouwstra, R.P., Mellowship, P., 2002.** Relationship between PGE and PGM in the Bushveld Complex. *Canadian Mineralogist* 40, 311-328.
- Černý, P., 1991a.** Fertile granites of Precambrian rare-element pegmatite fields: is geochemistry controlled by tectonic setting or source lithologies? *Precambrian Research* 51, 429-468.
- Černý, P., 1991b.** Rare-element granite pegmatites. Part I: anatomy and internal evolution of pegmatite deposits. *Geoscience Canada* 18, 49-67.
- Černý, P., 1991c.** Rare-element granite pegmatites. Part II: regional to global environments and petrogenesis. *Geoscience Canada* 18, 68-81.
- Černý, P., Chapman, R., Ferreira, K., Smeds, S.-A., 2004.** Geochemistry of oxide minerals of Nb, Ta, Sn, and Sb in the Varusträsk granitic pegmatite, Sweden: The case of an “anomalous” columbite-tantalite trend. *American Mineralogist* 89, 505-518.
- Chakoumakos, B.C., Lumpkin, G.R., 1990.** Pressure-temperature constraints on the crystallization of the Harding pegmatite, Taos County, New Mexico. *Canadian*

Mineralogist 28, 287-298.

**Charoy, B., Noronha, F., 1996.** Multistage growth of a rare-element, volatile-rich microgranite at Argemela (Portugal). *Journal of Petrology* 37, 73-94.

**Chen, Y., Fleet, M.E., Pan, Y., 1993.** Platinum-group minerals and gold in arsenic-rich ore at the Thompson mine, Thompson Nickel Belt, Manitoba, Canada. *Mineralogy and Petrology* 47, 127-146.

**Chou, I-Ming, 1987a.** Oxygen buffer and hydrogen sensor techniques at elevated pressures and temperatures. In G.C. Ulmer and H.L. Barnes (Eds.), *Hydrothermal Experimental Techniques*. pp. 61-99, John Wiley & Sons Ltd., New York.

**Cuney, M., Marignac C., Weisbrod, A., 1992.** The Beauvoir topaz-lepidolite albite granite (Massif Central, France): The disseminated magmatic Sn-Li-Ta-Nb-Be mineralization. *Economic Geology* 87, 1766-1794.

**Daubrée, A., 1841.** Sur le gisement la constitution et l'origine des amade mineraux d'étain. *Ann. des Mines 3e Series* 20, 65-112.

**De Beaumont, E., 1847.** Note sur les emanations volcaniques et métallifères. *Bulletin de la Soc. Géol. De France, 2e Series IV*, 1249-1333.

**Dingwell, D.B., 1985.** The structure and properties of fluorine-rich silicate melts: Implications for granite petrogenesis (abstr.). In R.P. Taylor and D.F. Strong (Eds.), *Granite related Mineral Deposits*. pp. 72-81, Can. Inst. Mining Extended Abstr. of Conf. On Granite-Related Mineral Deposits, Halifax.

**Durasova, N.A., Barsukov, V.L., Ryabchikov, I.O., Khramov, D.A., Kravtsova, R.P., 1984.** The valency states of tin in basalts at various oxygen fugacities. *Geochemistry International* 21, 7-8.

**Dickinson, Jr. J.E., Hess, P.C., 1985.** Rutile solubility and titanium coordination in silicate melts. *Geochimica et Cosmochimica Acta* 49, 2289-2296.

**Dubessy, J., 1987.** Physical and chemical controls ( $fO_2$ , T, pH) of the opposite behaviour of U and Sn-W as exemplified by hydrothermal deposits in France and Great Britain, and solubility data. *Bull. Minéral.* 110, 261-281.

**Ellison, A.J., Hess, P.C., 1986.** Solution behavior of +4 cations in high silica melts: Petrological and geochemical implications. *Contributions to Mineralogy and Petrology* 94, 343-351.



- Ellison, A.J., Hess, P.C., Naski, G.C., 1998.** Cassiterite solubility in high-silica K<sub>2</sub>O-Al<sub>2</sub>O<sub>3</sub>-SiO<sub>2</sub> liquids. *Journal of the American Ceramic Society* 81, 3215-3220.
- Ertel, W., Pichavant, M., Scaillet, B., 1998.** Experimentally determined solubilities of Pt in a haplobasaltic melt under well constraint conditions of *f*O<sub>2</sub>, P, T, and H<sub>2</sub>O activity. Goldschmidt Conference, Toulouse. pp. 425.
- Ertel, W., O'Neill, H.St.C., Sylvester, P.J., Dingwell, D.B., 1999.** Solubilities of Pt and Rh in a haplobasaltic silicate melt at 1300°C. *Geochimica et Cosmochimica Acta* 63, 2439-2449.
- Eugster, H.P., 1985.** Granites and hydrothermal ore deposits: A geochemical framework. *Mineralogical Magazine* 49, 7-23.
- Eugster, H.P., 1986.** Minerals in hot water. *American Mineralogist* 71, 655-673.
- Farrow, C.E.G., Watkinson, D.H., 1992.** Alteration and the role of fluids in Ni, Cu and platinum-group element deposition, Sudbury Igneous Complex contact, Onaping-Levack area, Ontario. *Mineralogy and Petrology* 46, 67-83.
- Ferguson, H.G., Bateman, A.M., 1912.** Geologic features of tin deposits. *Economic Geology* 7, 209-262.
- Fleet, M.E., Wu, T.-W., 1993.** Volatile transport of platinum-group elements in sulfide-chloride assemblages at 1000°C. *Geochimica et Cosmochimica Acta* 57, 3519-3531.
- Gammons, C.H., 1996.** Experimental investigations of the hydrothermal geochemistry of platinum and palladium: V. Equilibria between platinum metal, Pt(II), and Pt(IV) chloride complexes at 25 to 300°C. *Geochimica et Cosmochimica Acta* 60, 1683-1694.
- Giordano, D., Romano, C., Dingwell, D.B., Poe, B., Behrens, H., 2004.** The combined effects of water and fluorine on the viscosity of silicic magmas. *Geochimica et Cosmochimica Acta* 68, 5159-5168.
- Glasstone, S., Laidler, K.J., Eyring, H., 1941.** The theory of rate processes. McGraw-Hill. Gmelin, 1986. In R. Keim (Ed.), *Handbook of Inorganic and Organometallic Chemistry*. Pt, Supplement Volume A 1, Technology. Springer-Verlag.
- Groves, D.I., 1972.** The geochemical evolution of tin-bearing granites in the Blue Tier batholith, Tasmania. *Economic Geology* 67, 445-457.
- Groves, D.I., 1974.** Geochemical variation within tin-bearing granites, Blue Tier batholith, NE Tasmania. In M. Štemprok (Ed.), *Metallization associated with acid magmatism*. pp. 154-158, John Wiley & Sons Ltd, New York.

- Groves, D.I., Martin, E.L., Murchie, H.M., Welington, H.K., 1972.** A century of tin mining at Mount Bishoff, 1871-1971. Tasmania Department of Mines, geological Survey Bulletin 54, p. 310.
- Groves, D.I., McCarthy, T.S., 1978.** Fractional crystallization and origin of tin deposits in granitoids. *Mineralium Deposita* 13, 11-26.
- Haapala, I., Thomas, R., 2000.** Melt inclusions in quartz and topaz of the topaz granite from Eurajoki, Finland. *Journal of Czech Geological Society* 45, 149-154.
- Haendler, H.M., Bartram, S.F., Bernard, W.J., Kippax, D., 1954.** The reaction of fluoride with tin, its oxides and sulfides. *Journal of American Chemical Society* 76, 2179-2180.
- Harris, D.M., Anderson, A.T., 1984.** Volatiles H<sub>2</sub>O, CO<sub>2</sub>, and Cl in a subduction related basalt. *Contributions to Mineralogy and Petrology* 87, 120-128.
- Harrison, T.M., Watson, E.B., 1983.** Kinetics of zircon dissolution and zirconium diffusion in granitic melts of variable water content. *Contributions to Mineralogy and Petrology* 84, 66-72.
- Hedenquist, J.W., Lowenstern, J.B., 1994.** The role of magmas in the formation of hydrothermal ore deposits. *Nature* 370, 519-527.
- Heinrich, C.A., 1990.** The chemistry of hydrothermal tin (-tungsten) ore depositions. *Economic Geology* 85, 457-481.
- Hesp, W.R., Rigby, D., 1972.** The transport tin in acid igneous rocks. *Pac. Geol.* 4, 135-152.
- Hess, F.L., Graton, L.C., 1905.** The occurrence and distribution of tin. United States Geological Survey. Bulletin No. 260, 161-187.
- Hill, R.E.T., 1984.** Experiental study of phase relations at 600°C in a portion of the Fe-Ni-Cu-S system and its application to natural sulphide assemblages. In Eds. D.L. Buchanan and M.L. Jones, *Sulphide Deposits in Mafic and Ultramafic Rocks*, pp. 14-21. Inst. Mining Metall.
- Holtz, F., Dingwell, D.B., Behrens, H., 1993.** Effects of F, B<sub>2</sub>O<sub>3</sub> and P<sub>2</sub>O<sub>5</sub> on the solubility of water in haplogranitic melts compared to natural silicate melts. *Contributions to Mineralogy and Petrology* 113, 492-501.

- Hosking, K.F.G., 1969.** Aspects of the geology of Southeast Asia. 2nd Tech. Conference on Tin, Bangkok. 1, International Tin Council, 41-80.
- Hosking, K.F.G., 1972.** The truth concerning Daubr e work on the genesis of cassiterite. Geological Society of Malaysia Newsletter No. 36, 6-7.
- Hosking, K.F.G., 1973.** Primary mineral deposits. In D.J. Gobett (Ed.), *Geology of the Malay Peninsula (West Malaysia and Singapore)*. pp. 335-390, John Wiley and Sons Ltd., New York.
- Hosking, K.F.G., 1974.** The search for deposits from which tin can be profitably recovered now and in the foreseeable future. 4th World Conference on Tin 1, International Tin Council, p. 21.83.
- Hsu, L.C., Lechler, P.J., Nelson, J.H., 1991.** Hydrothermal solubility of palladium in chloride solutions from 300° to 700°C: Preliminary experimental results. *Economic Geology* 86, 422-427.
- Jaireth, S., 1992.** The calculated solubility of platinum and gold in oxygen-saturated fluids and the genesis of platinum-palladium and gold mineralization in the unconformity-related uranium deposits. *Mineralium Deposita* 27, 42-54.
- Jackson, N.J., 1979.** Geology of Cornubian tinfield – a review. *Bulletin of Geological Society of Malaysia* 11, 209-237.
- Jackson, K.J., Helgeson, H.C., 1985.** Chemical and thermodynamic constraints on the hydrothermal transport and deposition of tin: I. Calculation of the solubility of cassiterite at high pressures and temperatures. *Geochimica et Cosmochimica Acta* 49, 1-22.
- Jambon, A., Deruelle, B., Dreibus, G., Pineau, F., 1995.** Chlorine and bromine abundance in MORB: contrasting behavior in the mid-Atlantic Ridge and East Pacific Rise and implications for a chlorine geodynamic cycle. *Chemical Geology* 126, 101-117.
- Jarrard, R.D., 2003.** Subduction fluxes of water, CO<sub>2</sub>, chlorine, and potassium. *Geochim. Geophys. Geosystem*. DOI 10, 1029/2002GC000392.
- Jiang, S.Y., Yu, J.M., Lu, J.J., 2004.** Trace and rare earth element geochemistry in tourmaline and cassiterite from the Yunlong tin deposit, Yunnan, China: implication for migmatitic – hydrothermal fluid evolution and ore genesis. *Chemical Geology* 209, 193-213.

- Johan, Z., Ohnenstetter, M., Slansky, E., Barron, L.M., Suppel, D., 1989.** Platinum mineralization in the Alaskan-type intrusive complexes near Fifield, New South Wales, Australia. Part 1. Platinum-group minerals in clinopyroxinites of the Kelvin Grove prospect, Owendale intrusion. *Mineralogy and Petrology* 40, 289-309.
- Johnston, D.A., 1980.** Volcanic contribution of chlorine to the stratosphere: more significant to ozone than previously estimated? *Science* 209, 491-493.
- Kelly, W.C., Turneaure, F.S., 1970.** Mineralogy paragenesis and geochemistry of the tin and tungsten deposits of the eastern Andes, Bolivia. *Economic Geology* 65, 609-680.
- Keppler, H., 1993.** Influence of fluorine on the enrichment of high field strength trace elements in granitic rocks. *Contributions to Mineralogy and Petrology* 114, 479-488.
- Keppler, H., Wyllie, P.J., 1989.** Partitioning of Mo, W, U, Cu and Sn between granitic melt and fluid phase. *EOS* 70, 1403.
- Keppler, H., Wyllie P.J., 1991.** Partitioning of Cu, Sn, Mo, W, U and thorium between melts and aqueous fluid in the systems haplogranite-H<sub>2</sub>O – HCl and haplogranite- H<sub>2</sub>O – HF. *Contributions to Mineralogy and Petrology* 109, 139-150.
- Kontak, D., 1990.** The East Kemptville topaz-muscovite leucogranite, Nova Scotia. I. Geological setting and whole rock geochemistry. *Canadian Mineralogist* 28, 787-825.
- Kontak, D. J., Clark, A. H., 2002.** Genesis of the giant, bonanza San Rafael lode tin deposit, Peru; origin and significance of pervasive alteration. *Economic Geology* 97, 1741-7717.
- Kovalenko, V.I., Legeydo, V.A., Petrov, L.L., Popolitov, E.I., 1968.** Tin and beryllium in alkali granitoids. *Geochemistry International* 5, 883-892.
- Kovalenko, N. I., Ryzhenko, B. N., Barsukov, V. L., 1996.** Experimental and computer modeling of greisenization in the system granite-SnO<sub>2</sub>-H<sub>2</sub>O-HCl. *Geochemistry International* 34, 483-495.
- Kovalenko, V.I., Tsaryeva, G.M., Naumov, V.B., Hervig, R.L., Newman, S., 1996.** Magma of pegmatites from Volhynia: Composition and crystallization parameters determined by magmatic inclusion studies. *Petrologiya* 4, 277-290.
- Kravchuk, I.F., Keppler, H., 1994.** Distribution of chlorine between aqueous fluids and felsic melts at 2 kbar and 800°C. *European Journal of Mineralogy* 6, 913-923.
- Lehmann, B., 1982.** Metallogeny of tin: Magmatic differentiation versus geochemical

heritage. *Economic Geology* 77, 50-59.

**Lehmann, B., 1990.** *Metallogeny of Tin*. Springer.

**Lemmlein, G.G., Klija, M.O., Ostrovski, I.A., 1962.** Conditions of formation of minerals in pegmatites according to studies of primary inclusions in topaz. *Dokl. Akad. Nauk. SSSR* 142, 81-83. (in Russian).

**Lenharo, S. L. R., Pollard, P. J., Born, H., 2003.** Petrology and textural evolution of granites associated with tin and rare-metals mineralization at the Pitinga mine, Amazonas, Brazil. *Lithos* 66, 37-61.

**Lessiter, J.C., Hauri, E.H., 2001.** Constraints on melt/lithosphere and melt/hydrosphere interactions from the volatile budgets of melt inclusions from the Austral Islands. Abs. 3639, LPI Contribution No. 1088, Lunar and Planetary Institute, Houston, (CD-ROM).

**Linnen, R.L., 1998a.** Depth of emplacement, fluid provenance and metallogeny in granitic terrains: A comparison of western Thailand with other Sn-W belts. *Mineralium Deposita* 33, 461-476.

**Linnen, R.L., 1998b.** The solubility of Nb-Ta-Zr-Hf-W in granitic melts with Li+F: constraints for mineralisation in rare metal granites and pegmatites. *Economic Geology* 93, 1013-1025.

**Linnen, R.L., Pichavant, M., Holtz, F., Burgess, S., 1995.** The effect of  $fO_2$  on the solubility, diffusion, and speciation of tin in haplogranitic melt at 850°C and 2 kbar. *Geochimica et Cosmochimica Acta* 59, 1579-1588.

**Linnen, R.L., Pichavant, M., Holtz, F., 1996.** The combined affect of  $fO_2$  and melt composition on  $SnO_2$  solubility and tin diffusivity in haplogranitic melts. *Geochimica et Cosmochimica Acta* 60, 4965-4976.

**Linnen, R.L., William-Jones, A.E., 1993.** The evolution of pegmatite-hosted tin-tungsten mineralization at Nong Sua, Thailand. Evidence from fluid inclusions and stable isotopes. *Geochimica et Cosmochimica Acta* 57, 735-747.

**Linnen, R.L., William-Jones, A.E., Martin, R.F., 1992.** Evidence of magmatic cassiterite mineralization at the Nong Sua Aplite-Pegmatite Complex, Thailand. *Canadian Mineralogist* 30, 739-761.

**London, D., 1987.** Internal differentiation of rare-element pegmatites: Effects of boron, phosphorous, and fluorine. *Geochimica et Cosmochimica Acta* 51, 403-420.

- London, D., 1992.** Phosphorus in S-type magmas: The P<sub>2</sub>O<sub>5</sub> content of feldspars from peraluminous granites, pegmatites, and rhyolites. *American Mineralogist* 77, 126-145.
- London, D., 1997.** Estimating abundances of volatile and other mobile components in evolved silicic melts through mineral-melt equilibria. *Journal of Petrology* 38, 1691-1706.
- London, D., 2004.** Granitic pegmatites: An assessment of current concepts and directions for the future. *Lithos* (*in press*).
- London, D., Morgan, G.B., Babb, H.A., Loomis, J.L., 1993.** Behavior and effects of phosphorus in the system Na<sub>2</sub>O – K<sub>2</sub>O – Al<sub>2</sub>O<sub>3</sub> – SiO<sub>2</sub> – P<sub>2</sub>O<sub>5</sub> – H<sub>2</sub>O at 200 MPa (H<sub>2</sub>O). *Contributions to Mineralogy and Petrology* 113, 450-465.
- London, D., Spooner, E.T.C., Roedder, E., 1982.** Fluid-solid inclusions in spodumene from the Tanco pegmatite, Bernic Lake, Manitoba. *Carnegie Institute of Washington Yearbook* 81, 334-339.
- Lowenstern, J.D., 1994.** Chlorine, fluid immisibility, and degassing in peralkaline magmas from Pantelleria, Italy. *American Mineralogist* 79, 353-369.
- Lowenstern, J.B., 1995.** Applications of silicate melt inclusions to the study of magmatic volatiles. In J.F.H. Thompson (Ed.), *Magmas, Fluids, and Ore Deposits*. pp. 71-99, Mineralogical Association of Canada 23.
- Lugov, S.F., 1965a.** Geological Characteristics of Tin-Tungsten Mineralization of Chukotka and prospecting Problems. Nedra Press, p. 336.
- Lugov, S.F., 1965b.** Genetic types and economic value of tin and tungsten deposits in Chukotka. *International Geological Reviews* 7, 621-630.
- Lukkari S., Holtz F., 2000.** Phase relations on F-enriched leucogranitic melts at 200 MPa: an Experimental investigation. IGCP Project 373 Field Conference in southern Finland, July 3-7, 2000, Excursion Guide and Abstracts, p. 43.
- Maier, W.D., Barnes, S.-J., 2003.** Platinum-group elements in the Boulder Bed, western Bushveld Complex, South Africa. *Mineralium Deposita* 38, 370-380.
- Manning, D.A.C., 1981.** The effect of fluorine on liquidus phase relations in the system Qz-Ab-Or with excess water at 1 kb. *Contributions to Mineralogy and Petrology* 76, 206-215.
- Marcantonio, A.J., Reisberg, L., Zindler, A., Hulbert, L.J., England, J. Wyman, D.A., 1994.** An isotopic study of the Ni-Cu-PGE-rich Wallgreen intrusion of the Wrangellia

Terrane: Evidence for Hydrothermal mobilization of rhenium osmium. *Geochimica et Cosmochimica Acta* 58, 1007-1017.

**Matthews, W., Linnen, Robert L., Guo, Q., 2003.** A filler-rod technique for controlling redox conditions in cold-seal pressure vessels. *American Mineralogist* 88, 701-707.

**Mathez, E.A., Dietrich, V.J., Holloway, J.R., Boudreau, A.E., 1989.** Carbon distribution in the Stillwater Complex and evolution of vapor during crystallization of Stillwater and Bishveld magmas. *Journal of Petrology* 30, 153-173.

**McCallum, M.E., Loucks, R.R., Carlson, R.R., Cooley, E.F., Doerge, T.A., 1976.** Platinum metals associated with hydrothermal copper ores of the New Rambler mine, Medicine Bow Mountains, Wyoming. *Economic Geology* 71, 1429-1450.

**Metrich, N., Rutherford, M.J., 1992.** Experimental study of chlorine behaviour in hydrous silicic melts. *Geochimica et Cosmochimica Acta* 56, 607-616.

**Mlynarczyk, M. S. J., Sherlock, R. L., Williams-Jones, A. E., 2003.** San Rafael, Peru; geology and structure of the worlds richest tin lode. *Mineralium Deposita* 38, 555-567.

**Mogessie, A., Stumpfl, E.F., Weiblen, P.W., 1991.** The role of fluids in the formation of platinum-group minerals, Duluth Complex, Minnesota: Mineralogic, textural and chemical evidence. *Economic Geology* 86, 1506-1518.

**Morgan, G. B. VI, London, D., 1999.** Crystallization of the Little Three layered pegmatite-aplite dike, Ramona District, California. *Contributions to Mineralogy and Petrology* 136, 310-330.

**Mountain, B.W., Wood, S.A., 1988.** Chemical controls on the solubility, transport and deposition of platinum and palladium in hydrothermal solutions: A thermodynamic approach. *Economic Geology* 83, 492-510.

**Muller, B., Frischknecht, R., Seward, T. M., Heinrich, C. A., Camargo, G., 2001.** A fluid inclusion reconnaissance study of the Huanuni tin deposit (Bolivia), using LA-ICP-MS micro-analysis. *Mineralium Deposita* 36, 680-688.

**Nekrasov, I.Y., 1984.** Tin in magmatic and postmagmatic processes. *Doklady Akademii Nauk SSSR, Izdanja Nauka, Moscow*, pp. 238 (in Russian).

**Nekrasov, I. Y., Epelbaum, M.B., Sobolev, V. P., 1980.** Partitioning of tin between melt and chloride fluid in the granite-SnO-SnO<sub>2</sub>-fluid system. *Doklady Earth Science* 252, 165-168.

- Nyman, M.W., Sheets, R.W., Bodnar, R.J., 1990.** Fluid inclusion evidence for the physical and chemical conditions associated with intermediate-temperature PGE mineralization at the New Rambler deposit, southeastern Wyoming. *Canadian Mineralogist* 28, 629-638.
- Ohlhorst, S., Behrens, H., Holtz, F., 2001.** Compositional dependence of molar absorptivities of near-infrared OH- and H<sub>2</sub>O bands in rhyolitic to basaltic glasses. *Chemical Geology* 174, 5-20.
- Ohnenstetter, M., 1992.** Platinum group elements enrichment in the upper mantle peridotites of the Monte Maggiore Ophiolitic Massif (Corsica, France): Mineralogical evidence for one fluid metasomatism. *Mineralogy and Petrology* 46, 85-107.
- Paparoni, G., 2000.** Tin in silicate melts. Ph.D. dissertation. Columbia University, New York.
- Patterson, D.J., 1977.** The hydrothermal transport and deposition of tin. 2<sup>nd</sup> Australian Geological Convocation, Melbourne, 68 (abstract).
- Pichavant, M., Herrera, J.V., Boulmier, S., Briquieu, L., Joron, J., Juteau, J., Marin, L., Michard, A., Sheppard, S.M.F., Treuil, M., Vernet, M., 1987.** The Macusani glasses, SE Peru: evidence of chemical fractionation in peraluminous magmas. In B.O. Mysen (Ed.), *Magmatic Processes: Physicochemical Principles*. pp. 359-373, Special Publication 1, Geochemical Society, University Park, Pennsylvania.
- Pollard, P.J., Pichavant, M., Charoy, B., 1987.** Contrasting evolution of fluorine – and boron – rich tin systems. *Mineralium Deposita* 22, 315-321.
- Raia, F., Webster, J.D., De Vivo, B., 2000.** Preruptive volatile contents of Vesuvius magmas: constraints on eruptive history and behavior. I- the medieval and modern interplinian activities. *European Journal of Mineralogy* 12, 179-193.
- Raia, F., Webster, J.D., De Vivo, B., Belkin, H.E., 1997.** Pre-eruptive volatile and trace element contents of Vesuvius magma (abstract). *EOS* 78, F779.
- Raimbault, L., Cuney, M., Azencott, C., Duthou, J.L., Joron, J.L., 1995.** Geochemical evidence for a multistage magmatic genesis of Ta-Sn-Li mineralization in the granite at Beauvoir, French Massif Central. *Economic Geology* 90, 548-576.
- Razin, L.V., 1968.** Problem of the origin of platinum metallization of forsterite dunite. *International Geology Reviews* 13, 776-788.



- Reyf, F.G., 1973.** Inclusions of melt in quartz of postorogenic granites of central Buryatiya and the pressures and temperatures accompanying their formation. Dokl. Akad. Nauk. SSSR 213, 918-921. (in Russian).
- Rivas, S., 1979.** Geology of the principal tin deposits of Bolivia. Bulletin of Geological Society of Malaysia 11, 161-180.
- Ryabchikov, I.D., Durasova, N.A., Barsukov, V.I., Laputina, I.P., Efimov, A.S., 1978a.** Role of volatiles for the mobilization of tin from granitic magmas. In: Štemprok, M., Burnol, L., Tischendorf, B. (Eds.), Metallization associated with acid magmatism 3. pp. 94-109, John Wiley & Sons Ltd, New York.
- Ryabchikov, I.D., Durasova, N.A., Barsukov, V.I., Efimov, A.S., 1978b.** Oxidation reduction potential as a factor of an ore-bearing capacity of acid magmas. Geokhimiya 8, 832-834 (in Russian).
- Sainte-Claire Deville, H., 1861.** De la reproduction de l'étain oxydé et du rutile. L'Acad. Des Sci., Paris, Comptes Rendus 53, 161-164.
- Sassani, D.C., Shock, E.L., 1990.** Speciation and solubility of palladium in aqueous magmatic-hydrothermal solutions. Geology 18, 925-928.
- Sassani, D.C., Shock, E.L., 1998.** Solubility and transport of platinum-group elements in super critical fluids: Summary and estimates of thermodynamic properties for ruthenium, rhodium, palladium, and platinum solids, aqueous ions, and complexes to 1000°C and 5 kbar. Geochimica et Cosmochimica Acta 62, 2643-2672.
- Scambelluri, M., Phillipot, P., 2001.** Deep fluids in subduction zones. Lithos 55, 213-227.
- Scambelluri, M., Piccardo, G.B., Phillipot, P., Robbiano, A., Negretti, L., 1997.** High salinity fluid inclusions formed from recycled seawater in deeply subducted Alpine serpentine. Earth and Planetary Science Letters 148, 485-499.
- Schröcke, H., 1954.** Zur Paragenese erzgebirgischer Zinnlagerstätten. Neues Jahrb. Mineral. Abh. 87, 611-624.
- Schuiling, R.D., 1967.** Tin belts on the continents around the Atlantic Ocean. Economic Geology 62, 540-550.
- Schwartz, M.O., Rajah, S.S., Askury, A.K., Putthapiban, P., Djaswadi, S., 1995.** The Southeast Asian Tin Belt. Earth Science Reviews 38, Elsevier, p. 95-293.

- Seltmann, R., 1994.** Sub-volcanic minor intrusions in the Altenberg Caldera and their metallogeny. In (Ed.), *Metallogeny of Collosional Orogens*. pp. 198-206, Czech Geological Survey.
- Shcherba, G.N., 1970.** Greisens. *International Geol. Reviews* 12, 114-150.
- Shinohara, H., 1994.** Exsolution of immiscible vapor and liquid phases from a crystallizing silicate melt: Implications for chlorine and metal transport. *Geochimica et Cosmochimica Acta* 58, 5215-5221.
- Shinohara, H., Iiyama, J.T., Matsuo, S., 1989.** Partition of chlorine compounds between silicate melt and hydrothermal solutions. *Geochimica et Cosmochimica Acta* 53, 2617-2630.
- Sillitoe, R.H., 1974.** Tin mineralization above mantle hot spots. *Nature* 248, 497-499.
- Sillitoe, R.H., Halls, C., Grant, J.N., 1975.** Porphyry tin deposits in Bolivia. *Economic Geology* 70, 913-977.
- Singewald, J.T. Jr., 1912.** Some genetic relations of tin deposits. *Economic Geology* 7, 263-279.
- Sisson, T.W., Layne, G.D., 1993.** H<sub>2</sub>O in basalt and basaltic andesite glass inclusions from four subduction-related volcanoes. *Earth and Planetary Science Letters* 117, 619-635.
- Skryabin, V.Y., 1976.** Melt inclusions in granites of the Voronezh massif. *COFFI* 10, 265 (abstract).
- Štemprok, M., 1969.** Geochemical association of tin. 2nd Tech. Conference on Tin, Bangkok. 1, International Tin Council, p. 159-176.
- Štemprok, M., 1971.** Petrochemical features of tin-bearing granites in Krušné Hory Mountains, Czechoslovakia. *Society of Mining Geologists of Japan Special Issue 2 (Proc IMA-IAGOD Meeting)*, pp. 112-118.
- Štemprok, M., 1982.** Tin-fluorine relationship in ore bearing assemblage. In A.M. Evans (Ed.), *Metallization associated with acid magmatism*. pp. 321-338, John Wiley & Sons Ltd., New York.
- Štemprok, M., 1990a.** Intrusion sequences with ore-bearing granitoid plutons. *Geol. J.* 25, 413-417.
- Štemprok, M., 1990b.** Solubility of tin, tungsten, and molybdenum oxides in felsic magmas. *Mineralium Deposita* 25, 205-212.
- Štemprok, M., Skvor, P., 1974.** Composition of tin-bearing granites from the Krusne hory

- metallogenic province of Czechoslovakia. *Sbornik Geologických Vied-Rad* 6, 7-83.
- Štemprok, M., Voldán, J., 1978.** Solubility of tin oxide in dry sodium rich granite melts: Mineralogical criteria for the relationship between magmatism and ore mineralization. Proceedings of the XI General Meeting of the International Mineralogical Association, Novosibirsk 4-10, September 1970. Izd. Nauka, Leningrad, pp. 125-133.
- Stone, W.E., Crocket, J.H., Fleet, M.E., 1994.** Light-rare earth element-rich minerals associated with platinum-group element mineralization in the Archean Boston Creek Flow, Ontario. *Mineralogy and Petrology* 51, 85-109.
- Stumpfl, A.M., Weiblen, P.W., 1991.** The role of fluids in the formation of Platinum-Group Minerals, Duluth Complex, Minnesota: mineralogical, Textural, and chemical evidence. *Economic Geology* 86, 1506-1518.
- Svensen, H., Jamtveit, B., Yardley, B., Engvik, A., Austrheim, H., Broman, K., 1999.** Lead and bromine enrichment in eclogite-facies fluids: Extreme fractionation during lower crustal hydration. *Geology* 27, 467-470.
- Symonds, R.B., Rose, W.I., Gerlach, T.M., Briggs, P.H., Harmon, R.S., 1990.** Evaluation of gases, condensates, and SO<sub>2</sub> emissions from Augustine volcano, Alaska: the degassing of Cl-rich volcanic system. *Bulletin of Volcanology* 52, 355-374.
- Symonds, R.B., Reed, M.H., Rose, W.I., 1992.** Origin, speciation, and fluxes of trace-element gases at Augustine volcano, Alaska: Insights into magma degassing and fumarolic processes. *Geochimica et Cosmochimica Acta* 56, 633-657.
- Tauson, L.V., 1968.** Distribution regularities of trace elements in granitoid intrusions of the batholith and hypabyssal types. In L.H. Ahrens (Ed.), *Origin and distribution of elements*. pp. 629-639, Pergamon, Oxford.
- Tauson, L.V., 1974.** The geochemical types of granitoids. In M. Štemprok (Ed.), *Metallization associated with acid magmatism*. pp. 221-227, John Wiley & Sons Ltd, New York.
- Taylor, J.R.P., 1988.** Experimental studies on tin in magmatic-hydrothermal systems. Ph.D. Thesis, Monash University, Australia.
- Taylor, R.G., 1979a.** *Geology of tin deposits*. Elsevier, Amsterdam.
- Taylor, R.G., 1979b.** Some observations upon the primary tin deposits of Australia. *Bulletin of Geological Society, Malaysia* 11, 181-207.

- Taylor, J.R., Wall, V.J., 1992.** The behavior of tin in granitoid magmas. *Economic Geology* 87, 403-420.
- Taylor, J. R., Wall, V. J., 1993.** Cassiterite solubility, tin speciation, and transport in a magmatic aqueous phase. *Economic Geology* 88, 437-460.
- Taylor, J.R., Wall, V.J., Pownceby, M.I., 1992.** The calibration and application of accurate redox sensors. *American Mineralogist* 77, 284-295.
- Thomas, R., 1989.** Investigations of melt inclusions and their application to the solution of various problems of deposit geology and petrology. Dissertation B, Bergakademie Freiberg. (in German).
- Thomas, R., 1994.** Fluid evolution in relation to the emplacement of the Variscan granites in the Erzgebirge region: A review of the melt and fluid inclusion evidence. In R. Seltrmann et al. (Eds.), *Metallogeny of Collisional Orogens*. pp. 70-81, Czech Geological Survey.
- Thomas, R., Klemm, W., 1997.** Microthermometric study of silicate melt inclusions in Variscan granites from SE Germany: Volatile contents and entrapment conditions. *Journal of Petrology* 38, 1753-1765.
- Thomas, R., Webster, J. D., 2000.** Strong tin enrichment in a pegmatite-forming melt. *Mineralium Deposita* 35, 570-582.
- Thomas, R., Webster, J.D., Heinrich, W., 2000.** Melt inclusions in pegmatite quartz: complete miscibility between silicate melts and hydrous fluids at low pressure. *Contributions to Mineralogy and petrology* 139, 394-401.
- Tischendorf, G., 1977.** Geochemical and petrographic characteristics of silicate magmatic rocks associated with rare-element mineralisation. In: Štemprok, M., Burnol, L., Tischendorf, G. (Eds.), *Metallization associated with acidic magmatism*. pp. 41-96, John Wiley & Sons Ltd, New York.
- Tischendorf, G., Forster, H.-J., 1990.** Acid magmatism and related metallogenesis in the Erzgebirge. *Geology Journal* 25, 443-454.
- Touret, J.L.R., 2001.** Fluids in metamorphic rocks. *Lithos* 55, 1-25.
- Turek, A., Riddle, C., Cozens, B.J., Tetley, N.W., 1976.** Determination of chemical water in rock analysis by Karl-Fischer titration. *Chemical Geology* 17, 261-267.
- Turneure, G.S., 1960.** A comparative study of major ore deposits of Central Bolivia. *Economic Geology* 55, 217-254.

- Vogt, J.H.L., 1895.** Der durch Pneumatolyse entstanden Erzvorkommen. *Zeit. Prak. Geol.* 465-484.
- Webber, K. L., Simmons, W. B., Falster, A. U., Foord, E. E., 1999.** Cooling rates and crystallization dynamics of shallow level pegmatite-aplite dikes, San Diego County, California. *American Mineralogist* 84, 708-717.
- Webster, J.D., 1997.** Exsolution of magmatic volatile phases from Cl-enriched mineralizing granitic magmas and implications for ore metal transport. *Geochimica et Cosmochimica Acta* 61, 1017-1029.
- Webster, J.D., Burt, D.M., Duffield, W.A., Nash, W.P., Gavigan, T., Augillon, R.A., 1991.** Constraints from glass inclusions in tin/topaz rhyolites on magma evolution, volatile element degassing, and mineralization. *Geological Society of America Abstracts with Programs* 23, A46.
- Webster, J.D., De Vivo, B., 2002.** Experimental and modeled solubilities of chlorine in aluminosilicate melts, consequences of magma evolution, and implications for exsolution of hydrous chloride melt at Mt. Somma-Vesuvius. *American Mineralogist* 87, 1046-1061.
- Webster, J.D., De Vivo, B., Tappen, C., 2003b.** Volatiles, magmatic degassing, and eruptions of Mt. Somma-Vesuvius: constraints from silicate melt inclusions, solubility experiments and modeling. In: Bodnar, R.J., De Vivo, B. (Eds.), *Melt inclusions in volcanic systems*. *Development in Volcanology* 5, pp. 207-226, Elsevier, Amsterdam.
- Webster, J.D., Duffield, W.A., 1991.** Volatiles and lithophile elements in Taylor Creek Rhyolite: Constraints from glass inclusion analysis. *American Mineralogist* 76, 1628-1645.
- Webster, J.D., Duffield, W.A., 1994.** Extreme halogen abundances in tin-rich magmas of the Taylor Creek Rhyolite, New Mexico. *Economic Geology* 89, 840-850.
- Webster, J.D., Holloway, J.R., 1988.** Experimental constraints on the partitioning Cl between topaz rhyolite and H<sub>2</sub>O and H<sub>2</sub>O+CO<sub>2</sub> fluids: New implications for granitic differentiation and ore deposition. *Geochimica et Cosmochimica Acta* 52, 2091-2105.
- Webster, J.D., Kinzler, R.J., Mathez, E.A., 1999.** Chloride and water solubility in basalt and andesite melts and implications for magmatic degassing. *Geochimica et Cosmochimica Acta* 63, 729-738.
- Webster, J.D., Raia, F., Tappen, C., De Vivo, B., 2003a.** Pre-eruptive geochemistry of

the ignimbrite-forming magmas of the Campanian volcanic zone, southern Italy, determined from silicate melt inclusions. *Mineralogy and Petrology* 79, 99-125.

**Webster, J.D., Rebbert, C.R., 2001.** The geochemical signature of fluid-saturated magma determined from silicate melt inclusions in Ascension Island granite xenoliths. *Geochimica et Cosmochimica Acta* 65, 123-136.

**Webster, J. D., Thomas, R., Foerster, H.-J., Seltmann, R., Tappen, C., 2004.** Geochemical evolution of halogen-enriched granite magmas and mineralizing fluids of the Zinnwald tin-tungsten mining district, Erzgebirge, Germany. *Mineralium Deposita* 39, 452-472.

**Webster, J.D., Thomas, R., Rhede, D., Forster, H.-J., Seltmann, R., 1997.** Melt inclusions in quartz from an evolved peraluminous pegmatite: Geochemical evidence for strong tin enrichment in fluorine-rich and phosphorous-rich residual liquids. *Geochimica et Cosmochimica Acta* 61, 2589-2604.

**Willmore, C.C., Boudreau, A.E., Kruger, F.J., 2000.** The halogen geochemistry of the Bushveld Complex, Republic of South Africa: Implications for chalcophile element distribution in the Lower and Critical Zones. *Journal of Petrology* 41, 1517-1539.

**Wilson, G.A., Eugster, H.P., Neiva, A.R., Coteló Neiva, J.M., Wang, S.Y., Chang, C.K., 1983.** Tin-tungsten deposition in silicate and carbonate rocks: A comparison of a Portuguese with a Chinese deposit (an abstract). *Geological Association of Canada, Program with Abstracts* 8, A-74.

**Wyllie, P.J., Tuttle, O.F., 1961.** Experimental investigation of silicate systems containing two volatile components. Part II. The effects of NH<sub>3</sub> and HF, in addition to H<sub>2</sub>O on the melting temperatures of albite and granite. *American Journal of Science* 259, 128-143.

**Yamashita, S., Kitamura, T., Kusakabe, M., 1997.** Infrared spectroscopy of hydrous glasses of arc magma compositions. *Geochemical Journal* 31, 169-174.

# LEBENS LAUF / CURRICULUM VITAE

## PARAS BHALLA

### PERSÖNLICHE ANGABEN:

- Anschrift: 225, Am Papehof 10, 30459 Hannover
- Geburtstag: 25. Mai 1977
- Geburtsort: Sundernagar (Himachal Pradesh), Indien
- Familienstand: ledig
- Staatsangehörigkeit: indisch

### AUSBILDUNG/BERUF

---

1982 - 1987 Primary Schooling Ropar (Punjab), Indien

---

1989 - 1990 Middle Class Ropar (Punjab), Indien

---

1991 - 1992 Higher Secondary (10<sup>th</sup> Standard) Ropar (Punjab), Indien

1992 - 1994 Senior Secondary (12<sup>th</sup> Standard) Chandigarh, Indien

---

1995 - 1998 Bachelor of Science in Geology, Panjab University,  
Chandigarh, Indien

---

1998 - 2000 Master of Science (H.S.) in Geologie, Panjab University,  
Chandigarh, Indien

---

15/04/2001-31/03/2002 Wissenschaftlicher Mitarbeiter (FB  
Geowissenschaften) Uni Hannover, Hannover, Deutschland

---

01/04/2002 – 31/03/2005 Stipendium von der Promotionsprogramm „Neue  
Materialien mit Maßgeschneiderten Eigenschaften“ finanziert vom Land  
Niedersachsen (Deutschland) eingerichtet vom ZFM (Zentrum für  
Festkörperchemie und Neue Materialien)